

GEOLOGY AND GEOCHEMISTRY OF MAGNESITE
OCCURRENCES, AKAMAS AREA, NORTHWEST CYPRUS

CENTRE FOR NEWFOUNDLAND STUDIES

**TOTAL OF 10 PAGES ONLY
MAY BE XEROXED**

(Without Author's Permission)

JAMES RONALD BRYDIE



**GEOLOGY AND GEOCHEMISTRY OF MAGNESITE OCCURRENCES,
AKAMAS AREA, NORTHWEST CYPRUS.**

by

© James Ronald Brydie

**A thesis submitted to the
School of Graduate Studies
in partial fulfilment of the
requirements for the degree of
Master of Science**

**Department of Earth Science
Memorial University of Newfoundland**

September 1995

St. John's

Newfoundland



National Library
of Canada

Acquisitions and
Bibliographic Services Branch

395 Wellington Street
Ottawa, Ontario
K1A 0N4

Bibliothèque nationale
du Canada

Direction des acquisitions et
des services bibliographiques

395, rue Wellington
Ottawa (Ontario)
K1A 0N4

Your file Votre référence

Our file Notre référence

The author has granted an irrevocable non-exclusive licence allowing the National Library of Canada to reproduce, loan, distribute or sell copies of his/her thesis by any means and in any form or format, making this thesis available to interested persons.

L'auteur a accordé une licence irrévocable et non exclusive permettant à la Bibliothèque nationale du Canada de reproduire, prêter, distribuer ou vendre des copies de sa thèse de quelque manière et sous quelque forme que ce soit pour mettre des exemplaires de cette thèse à la disposition des personnes intéressées.

The author retains ownership of the copyright in his/her thesis. Neither the thesis nor substantial extracts from it may be printed or otherwise reproduced without his/her permission.

L'auteur conserve la propriété du droit d'auteur qui protège sa thèse. Ni la thèse ni des extraits substantiels de celle-ci ne doivent être imprimés ou autrement reproduits sans son autorisation.

ISBN 0-612-13882-8

Canada

ABSTRACT

A complex Late Cretaceous suture zone between two distinct geological terranes is preserved in southern Cyprus in a series of erosional windows through Tertiary-Recent cover sediments. The two terranes are the Mamonia and Troodos Complexes, and the suture zone contains evidence of two major contractional tectonic events :- primary north-northeast- and secondary west-southwest-directed thrusting. Delamination of the Mamonia Complex during juxtaposition against the Troodos Complex resulted in Mamonia rocks being thrust beneath and over the Troodos Complex. Later west-southwest-directed back-thrusting resulted in imbrication of the Troodos Complex and also Mamonia rocks being thrust over Troodos rocks (Malpas et al., 1993). The serpentinite sheet containing magnesite mineralisation was tectonically emplaced from east to west over sheeted diabase dykes and lower- and upper pillow lavas during this latter contractional tectonic episode.

Magnesite deposits are found in a large sheet of serpentinitised harzburgite in the Akamas Peninsula and trend north-south along a 5km line adjacent to Tertiary limestone cover. The largest magnesite occurrence, the Magnisia mine, exhibits many clues to magnesite vein genesis prior to, and during, the tectonic emplacement of the serpentinite. Several temporally and spatially related generations of magnesite are identified. The magnesite deposits contain two distinct styles of mineralisation within the serpentinite, and have been divided into Zones I and II. Zone I encompasses veins and stockwork magnesite and Zone II contains nodular magnesite. Antitaxial magnesite veins have mineralised serpentinite along planes of weakness, encapsulating serpentinite fragments and exhibiting classic features associated with vein minerals formed in active shear zones, i.e. well developed median lines in veins, comb textures, brecciated veins recemented by further mineralisation and spalled wallrock lying parallel to the edges of vein walls. These

veins are interpreted as having formed during emplacement of the serpentinite, and define the main phase of magnesite mineralisation. The magnesite veins and stockworks define Zone I style mineralisation. Voids within these magnesite veins have subsequently been filled by epigenetic calcite and dolomite, probably derived from solutions passing through the limestone cover above the deposits. A later generation of magnesite is present within sheared serpentinite above the veins and stockworks. This carbonate is present as a replacement style of mineralisation with magnesite nodules prominent in a sheared, carbonatised serpentinite matrix. This magnesite defines mineralisation of the Zone II type.

Petrographic examination and chemical analyses of magnesite and associated lithologies provides further clues to magnesite genesis in the Akamas area. Stable isotope analyses of magnesite, calcite and dolomite show two distinct populations of magnesite with a singular source of carbon, one precipitated around 165°C (veins and stockworks) and the other around 40°C (nodular magnesite). Calcite and dolomite from overlying karst sediments lie in an isotopic field comparable with typical marine carbonates. Trace element analyses of magnesite, calcite, dolomite, serpentinite and organic-rich sandstone samples indicate calcite, dolomite and serpentinite to be unlikely sources of carbon present within the magnesite. From isotope and trace element data, the source of carbon within the magnesite is likely decarboxylation of organic material.

A suggested model for magnesite formation would be as follows. Magnesite veins were formed during the initial disruption of the serpentinite, probably initiated by the production of CO₂ upon decarboxylation of organic-rich sediments underthrust beneath the serpentinite. The earliest magnesite veins were then brecciated by continued compressional tectonism and cemented by further cryptocrystalline magnesite precipitation. The serpentinite (including magnesite veins and stockworks) was eventually emplaced westward over gabbro and sheeted diabase dykes resulting in the formation of a

prominent c-s shear fabric present at the base of the serpentinite. Thrusting also resulted in the formation of an intra-serpentinite shear zone which was mineralised by nodular magnesite, defining a later generation of magnesite formation. No magnesite veins are present in this shear zone. Isotope data suggest a similar source of carbon for both veins and nodules but veins were precipitated at elevated temperatures, while nodules were formed at lower temperatures. The magnesite nodules are most likely a result of remobilisation of vein material followed by precipitation as nodules in the overlying shear zone

Recent precipitates of magnesite and dolomite around the study area may be the continuance of magnesite mineralisation.

TABLE OF CONTENTS

	Page
Abstract	ii
List of Figures	ix
List of Tables	xii
List of Plates	xiii
Acknowledgements	xviii
1.0 INTRODUCTION	
1.1 Introduction	1
1.2 Topography and Exposure in the study area	5
1.3 Previous Work	6
1.4 Present Study	8
2.0 REGIONAL AND LOCAL GEOLOGY	
2.1 Introduction	16
2.2 Regional Stratigraphy of Southwest Cyprus	16
2.2.1 Mamonia Complex Rocks in Southwest Cyprus	17
2.2.2 Troodos Complex Rocks in Southwest Cyprus	18
2.2.3 Post-collisional Sediments	19
2.3 General Structure of Southwest Cyprus	20
2.4 Geological Relationships in the Field Area	23
2.4.1 Stratigraphy	23

2.4.1.1	The Mamonia Complex	23
2.4.1.2	The Troodos Complex	27
2.4.1.3	Tertiary Cover Sediments	39
2.4.2	Structure	30
3.0	STRUCTURAL FEATURES OF MINERALISATION	
3.1	Introduction	41
3.2	Styles of Magnesite Mineralisation	41
3.2.1	Zone I Type Mineralisation	42
3.2.2	Zone II Type Mineralisation	45
3.3	Other Carbonate Precipitates	47
3.3.1	Carbonate Precipitates in Serpentinite	47
3.3.2	Carbonate Mineralisation in Footwall of BST	48
4.0	PETROGRAPHY	
4.1	Introduction	64
4.2	Description	64
4.2.1	Zone I Magnesite	65
4.2.2	Zone II Magnesite	67
4.2.3	Other Carbonates	67
4.2.4	Recent Precipitates	69
4.3	Summary	70

5.0 GEOCHEMISTRY

5.1	Introduction	85
5.2	X-Ray Diffraction (XRD) Study	85
5.2.1	Results	85
5.3	Background for Stable Isotope Study	85
5.3.1	Stable Isotope Study of Akamas Magnesite	88
5.3.2	Analytical Procedures	89
5.3.3	Results	92
5.3.4	Discussion	95
5.4	Trace Element Study	98
5.4.1	Present Study	100
5.4.2	Analytical Technique	101
5.4.3	Results	101
5.4.4	Discussion	105
5.4.5	Comparison of Trace Element and Isotope Data	109

6.0 SUMMARY AND CONCLUSIONS

6.1	Regional Geological setting	125
6.2	Local Geological Setting of the Magnesite Deposits	126
6.3	Chemistry	130
6.4	Model for Magnesite Formation	134

REFERENCES	141
APPENDICES I - V	146...

LIST OF FIGURES

Figure	Description	Page
Figure 1.1	Location of Cyprus in the eastern Mediterranean showing relative positions of Troodos, Mamonia and other ophiolite-related lithologies (Taken from Malpas et al., 1993).	10
Figure 1.2	a) Diagram showing the two main areas of magnesite mineralisation; 1 - Akamas Peninsula, 2 - Limassol Forrest. b) Location of study area (After Malpas et al., 1993)	11
Figure 2.1	Schematic reconstruction of Mamonia and Troodos terranes during Middle-Late Cretaceous times (Malpas et al., 1993).	32
Figure 2.2	General geological map of southwest Cyprus (taken from Malpas et al., 1993).	33
Figure 2.3a	Stratigraphic relations within southwest Cyprus. Most of these lithologies are present in the study area, with the few exceptions described in the text.	34
Figure 2.3b	Stratigraphy and lithology of the supra-ophiolite sediments (After Roberston et al., 1990)	35
Figure 2.4a	Geological map of the Akamas area.	Separate
Figure 2.4b	Cross section through the study area illustrating the structural position of the magnesite mineralisation	Separate
Figure 2.4c	Legend for Figures 2.4a & b.	Separate
Figure 2.5	Schematic illustration of the structure of the western part of the Polis Graben.	36
Figure 3.1	Schematic illustration of Zones I and II within serpentinite. All deposits exhibit mineralisation of Zone I-type, Zone II-type, or both.	50

Figure	Description	Page
Figure 3.2	Diagram showing borehole logs from the Magnisia site. Data were obtained from the Hellenic Mining Co., Nicosia, Cyprus.	51
Figure 3.3	Schematic cross section through the Magnisia deposit	52
Figure 3.4a	The relationship between kinematic indicators within the Basal Serpentine Thrust (BST) and carbonate veins associated with the mineralisation.	53
Figure 3.4b	a) Stereoplot of c-planes, s-planes and lineations on c-planes, b) Stereoplot showing the orientation of large magnesite veins and groove lineations on those veins.	54
Figure 5.1	Diagram showing the ranges in isotopic composition of carbon within several reservoirs (Schwarcz, 1969; Deines, 1980; Hoefs, 1980).	112
Figure 5.2	Common stable isotope ratios (carbon and oxygen) of different genetic types of magnesite deposits (Moller, 1989).	113
Figure 5.3	Carbon vs. Oxygen crossplot for magnesite (m), calcite (c) and dolomite (d).	115
Figure 5.4.1	Trace element compositions of two samples of serpentinite; one taken from the Magnisia locality, the other from an unmineralised area.	116
Figure 5.4.2	Trace element compositions of five samples of calcite taken from the Magnisia locality.	117
Figure 5.4.3	Trace element signatures of calcite samples, Elements vs. ppm / chondrite.	118
Figure 5.4.4	Trace element compositions of three samples of dolomite taken from the Magnisia locality.	119
Figure 5.4.5	Trace element signatures of dolomite samples, Elements vs. ppm / chondrite.	120

Figure	Description	Page
Figure 5.4.6	Trace element compositions of four samples of sandstone taken from an area outside the mineralisation	121
Figure 5.4.7	Trace element compositions of four samples of vein magnesite taken from the Magnisia locality	122
Figure 5.4.8	Trace element compositions of four samples of nodular magnesite taken from the Magnisia locality	123
Figure 5.4.9	Trace element signatures of nodular magnesite samples. Elements vs. ppm / chondrite.	124
Figure 6.1	The proposed sequence of mineralisation events in relation to timing and processes affecting the hosting serpentinite	138
Figure 6.2	Sequence of cartoons illustrating the genetic model proposed for the Akamas magnesite deposits.	139
Figure 6.2 (Continued)	Sequence of cartoons illustrating the genetic model proposed for the Akamas magnesite deposits.	140

LIST OF TABLES

Table	Description	Page
Table 1 1	Types of important and potentially economic magnesite deposits	12
Table 1 2	a) Akamas magnesite major element composition (Gass, 1960), b) Akamas magnesite major element composition (Ilich and Maliotis, 1984), and c) Trace element composition of Akamas magnesite (Ilich and Maliotis, 1984).	13
Table 5 1	Results of X-Ray Diffraction analyses for Akamas samples. M = Magnesite, C = Calcite, D = Dolomite, Cl = Clay, S = Serpentine, T = Tenorite, and G = Gypsum.	111
Table 5 2	Carbon and oxygen isotope values for 26 Akamas carbonate samples including magnesite, calcite and dolomite.	114

LIST OF PLATES

Plate	Description	Page
Plate 1.1	Vein magnesite at the base of the deposits	14
Plate 1.2	Nodular magnesite found throughout the upper portions of the serpentinite	14
Plate 1.3	100% exposure along the shore section at Loutra tis Aphroditis.	15
Plate 1.4	Road cut with sheeted diabase dykes.	15
Plate 2.1	Small klippe of Mamonia mudstone in serpentinite This outcrop marks the base of the Mamonia thrust sheets which were emplaced from east to west at a shallow angle. Lens cap for scale.	37
Plate 2.2	Moderately dipping (50°E) thrust contact between serpentinite and gabbro with limestone lying unconformably on serpentinite in the background. Photograph taken facing due south. Jeep for scale	38
Plate 2.3	Outcrop of serpentinitized harzburgite. Bastite serpentinite after orthopyroxene is common. Coin for scale.	38
Plate 2.4	Lefkara chalk overlain conformably by 10m of Tera limestone 500m east of Neokhorio village. Moped for scale.	41
Plate 2.5	Shore section along the northern boundary of the study area. Serpentinite on the shoreline is unconformably overlain by calcarenite. Bush in foreground approximately 1.5m high.	40
Plate 2.6	Light-blue carbonatised serpentinite of the ISSZ. Mudstones of the Mamonia Complex are present within the shear zone. Lens cap for scale	40

Plate	Description	Page
Plate 3.1	Large cryptocrystalline magnesite vein within Zone I of the Piana locality. Lens cap for scale.	55
Plate 3.2	Sample of vein magnesite taken from the base of the Magnisia locality. Coin for scale (diameter 10mm).	56
Plate 3.3	Photomicrograph of brecciated vein material which has been cemented by further magnesite precipitation. Plane-polarised light. Field of view is 5mm.	56
Plate 3.4	Close view of BST showing strongly developed shear fabric. BST is 20cm thick at this point. View to north. Key for scale.	57
Plate 3.5	Sheared, carbonatised serpentinite of the ISSZ which has incorporated Mamonia mudstones, gabbro and diabase.	58
Plate 3.6	Nodular magnesite within a mining adit in Zone II of the Magnisia deposit. Nodule size varies from millimetre to metre scale. Hammer for scale.	58
Plate 3.7	Large magnesite nodule within Zone II of the Magnisia locality. This nodule is approximately 1.5m in diameter. Hard hat for scale.	59
Plate 3.8	Hand specimen of nodular magnesite. Finger for scale.	59
Plate 3.9	A sample of the high-magnesium calcite/magnesite precipitate found on the walls of mining adits in the Magnisia area.	60
Plate 3.10	Outcrop of laminar precipitate found precipitating within a small cave in serpentinite. Lens cap for scale	61
Plate 3.11	Hand specimen of laminar dolomite. Coin for scale	62
Plate 3.12	Calcite veins precipitated within fractured gabbro, just below the BST. Veins are an average thickness of 3cm.	62
Plate 3.13	Close view of calcite veins in gabbro. Key for scale.	63

Plate	Description	Page
Plate 4.1	Dilational calcite veins in the c-s fabric. Quartz-sensitive plate was used to illustrate orientation of crystal fibres. Serpentine groundmass is sheared. Note the well developed median lines. Cross-polarised light. Field of view 5mm.	73
Plate 4.2	Well developed c-s fabric of the Basal Serpentine Thrust (BST). Calcite veins enhance the serpentine shear fabric. Key is 3cm long	74
Plate 4.3	Thin-section of dilational calcite veins with well developed median lines in serpentine shear fabric. Cross-polarised light. Field of view 5mm.	74
Plate 4.4	Cryptocrystalline magnesite veining in serpentinised harzburgite. Note the brecciated texture of the wallrock. Plane-polarised light. Field of view 5mm.	75
Plate 4.5	Same view as above, but in cross-polarised light. Magnesite veining in serpentine fragments is clearer here. Note overall brecciated appearance of wallrock. Field of view 5mm.	75
Plate 4.6	Magnesite precipitated in competent serpentine. Magnesite has been precipitated within voids and fractures. Cross-polarised light. Field of view 3mm.	76
Plate 4.7	Inclusion of serpentine minerals from the wallrock within magnesite veining. Cross-polarised light. Field of view 3mm.	76
Plate 4.8	Magnesite vein within serpentinised harzburgite showing brittle deformation. Note specifically cataclastic shear of vein in left bottom quarter of picture. Cross-polarised light. Field of view 3mm.	77

Plate	Description	Page
Plate 4.9	Same view as above but in plane-polarised light. Field of view 3mm.	77
Plate 4.10	Fine-grained nodular magnesite in thin-section. Plane-polarised light. Field of view 5mm.	78
Plate 4.11	Same view as Plate 4.10, but in cross-polarised light. Field of view 5mm.	78
Plate 4.12	Two magnesite nodules overprinting sheared serpentinite. Cross-polarised light. Field of view 1cm.	79
Plate 4.13	Same view as 4.12, but in plane-polarised light. Field of view 1cm.	79
Plate 4.14	Cryptocrystalline magnesite nodule overgrowing sheared serpentinite. Plane-polarised light. Field of view 1cm.	80
Plate 4.15	Same as Plate 4.14, but in cross-polarised light. Some nodules follow shear fabric but are themselves unsheared. Field of view 1cm.	80
Plate 4.16	Epigenetic calcite precipitated perpendicular to a fracture wall within a magnesite vein. Field of view 1cm.	81
Plate 4.17	Serpentinised harzburgite showing several successive veining episodes. Epigenetic calcite was precipitated last. Cross-polarised light. Field of view 5mm.	81
Plate 4.18	Rugose coral fragment in limestone. Micrite cement with minor magnesite. Cross-polarised light. Field of view 3mm.	82
Plate 4.19	Rounded clasts of coral and serpentinite are cemented by fine-grained calcite. Cross-polarised light. Field of view is 5mm.	82
Plate 4.20	Carbonate cave precipitate found within a small cave on the shore section near Loutra tis Aphroditis. Small specks in carbonate are sedimentary clasts. Coin diameter 2cm.	83

Plate	Description	Page
Plate 4.21	Laminar growth of high-magnesium calcite showing radial growth. Cross-polarised light. Field of view 3mm.	83
Plate 4.22	Hand specimen of calcite/dolomite 'adit precipitate' found within the vicinity of mineralisation (below the water table) in the study area.	84
Plate 4.23	Section showing laminar precipitates of dolomite between clasts of micro-crystalline magnesite. Brown bands denote ferroan dolomite. Cross-polarised light. Field of view 5mm.	84

ACKNOWLEDGMENTS

I would like to thank the following people for the invaluable help they provided during the course of this project. My supervisor, Dr. John Malpas for help, guidance, friendship and the opportunities for extensive travel. Dr. Tom Calon for inspiration and encouragement in the field. Dr. Costas Xenophontos for maps, help, advice, brandy sours and various barbecued animals. Andreas and Tony from the Axiothea Hotel (Paphos) for friendship and a second home. Thanks to Mark Wilson, Adrian Timbal, Henry Longeridge, Ali Aksu, Beverly Chapman and Darryl Clarke for help with analytical work and the staff of the Lapidary Shop for excellent work.

Special thanks is given to Darryl Williams, Kevin Deveau, Jeff Saunders, Gary Thompson, Nurdan & Adnan Aydin and Stuart Deveau for making Newfoundland an unforgettable experience. Thanks to Laurel McDonald for support and encouragement. Thanks to Euan McGookin for proof-reading this thesis.

I would also like to thank the Department of Earth Sciences and Department of Graduate Studies for financial support throughout this study.

1.0 INTRODUCTION

1.1 Introduction

The aim of this study is to use field observations and geochemical means to obtain as detailed a picture as possible of magnesite mineralisation within serpentinites of the Akamas Peninsula, northwest Cyprus (Figures 1.1 and 1.2). Carbonate genesis, structural setting and timing of mineralisation are addressed as the main points of interest.

On a global scale, porcellaneous cryptocrystalline vein and stockwork magnesite (MgCO_3) occurs in several geological environments including sabkha, lagoon and coral reef settings, but is most frequently associated with mafic and ultramafic portions of ophiolite complexes found within orogenic zones (Pohl, 1989). Notable deposits are located along Tethyan micro-plate boundaries in countries such as Serbia, Bosnia, Greece, Turkey and Oman within wholly or almost completely serpentinised parts of ophiolite suites (Figure 1.1).

There are four main classifications of magnesite deposit (Pohl, 1989). These are i) Bela-Stena, ii) Greiner, iii) Veitsch and iv) Kraubath type deposits (Table 1.1).

i) Bela-Stena Type (Ilich 1968)

Magnesite may be found in freshwater lacustrine sediments nearby, or overlying, ultramafic rocks. Its concentration is usually the result of surface weathering and deposition of magnesite-rich sediments derived from magnesite mineralisation present in the ultramafic rocks.

ii) **Greiner Type (Redlich, 1909)**

These lensoid-shaped deposits are found in metamorphosed ultramafic rocks where auto-metasomatism results in magnesite formation. The mineralisation tends to contain nets of siliceous veining associated with the magnesite and is usually restricted to weathering zones toward the surface of the serpentinite.

iii) **Veitsch Type (Redlich, 1909)**

Veitsch Type deposits are found within layered lacustrine and lagoonal sediments. Such magnesite deposits tend to exhibit lesser degrees of mineralogical purity than their vein and stockwork counterparts in ultramafic complexes due to marine-derived contaminants such as porcellaneous silica and traces of boron (Pohl, 1989). This stratabound magnesite occurs as euhedral crystals and may be fibrous or sparry.

iv) **Kraubath Type (Redlich, 1909)**

These magnesite deposits form at low temperatures at shallow crustal levels in mafic and ultramafic complexes and are made up of veins and stockworks which are usually associated with fractured and faulted serpentinite. The deposits usually exhibit large veins which grade into stockworks near the top of the mineralisation.

Akamas Deposit Classification

Magnesite deposits (containing minor calcite, dolomite, siderite and amorphous silica) in the Akamas area of northwestern Cyprus are associated with ultramafic lithologies (Figure 1.2; Figure 2.4a). They occur in the form of 0.5-1m thick veins at the base, grading into stockworks at higher levels (Plate 1.1). The deposits form an arcuate line in serpentinitised harzburgite close to the contact with unconformably overlying

Tertiary marine limestone, and vary in magnitude from several hundred to several thousand tonnes. The aerial extent of each deposit varies between 250m and 350m. Typically, the mineralisation is located between surface level and perceived depths of no more than 100m. Depth estimates are limited due to terrain layout, extensive cover sediments above the deposits and limited exploratory drilling to depths greater than 100m. Veins and stockworks infill shear zones and open fractures, and impregnate serpentinite along planes of weakness. Other features of the magnesite deposits are serpentinite fragments trapped within the vein magnesite and iron hydroxide which is ubiquitous and, in many places, dendritic. The most frequently documented mineral assemblage in this study is calcite, dolomite, magnesite, serpentine (lizardite) and iron hydroxide, the calcite and dolomite appearing as epigenetic vein-fill within the magnesite (Ilich and Mahotis, 1984). Nodular magnesite is present at the top of the serpentinite sheet within sheared serpentinite (Plate 1.2)

It is therefore suggested that Akamas magnesite mineralisation should be classified as being mainly of the Kraubath-type of deposit. Some features of the deposits, such as nodular precipitates in sheared serpentinite, are more consistent with the Greiner type of magnesite deposits (Redlich, 1909).

Magnesite Genesis

Fluid inclusions within magnesite often provide a means of establishing the temperature of formation. Also, coexisting minerals precipitated in equilibrium with mineralising solutions may be present such as talc-magnesite or quartz-magnesite, and these may also allow calculation of pressure and temperature conditions during mineral

formation (Morteani, 1989; Bone, 1983). In the case of Akamas magnesite, however, the carbonate is cryptocrystalline and contains no measurable fluid inclusions or co-existing equilibrium mineral assemblages. Therefore petrographic examination, along with isotope and trace element data, are the best tools to study carbonate genesis

Other magnesite deposits are present in southern Cyprus, but are of marginal economic significance. These deposits are found in serpentinised dunite in the Amyrou Church locality (Limassol Forest), approximately 40km north of Limassol (Figure 1.2), and differ in many respects from the typical veins and stockworks of the Akamas area. Amyrou Church magnesite is not cryptocrystalline but is soft, powdery and is less dense, i.e. specific gravity of 1.7 as opposed to 2.5 in Akamas samples (Ilich and Maliotis, 1984).

Industrial Use of Magnesite

Once extracted, usually by opencast or shallow adit methods, the magnesite is heated, reducing it to periclase (MgO). In this form the mineral may be used industrially as a refractory component during the manufacture of heat-resistant plastics and textiles. It is also utilized as paper-filler, as a supplement to animal foodstuffs and in the pharmaceuticals industry. Due to stringent purity requirements magnesite is often produced artificially in industrial countries using seawater, calcined limestone and dolomite. Usually "dressing methods" are used to reduce quantities of surface-borne impurities. Unfortunately, no such cleansing methods exist for the removal of contaminants substituting for magnesium ions within the carbonate structure. It is for this reason that the majority of 'natural magnesite' used for commercial purposes is obtained from vein and stockwork sources

1.2 Topography and Exposure in the Study Area

The study area is situated on the western flank of the north-south trending Polis graben. Elevation ranges from sea level to a height of 331m. Hills are surrounded by steep river-cut valleys, some of which are partially filled by sedimentary deposits. In the north, the area is bounded by a coastline from Loutra tis Aphroditis to Fontana Amorosa, with cliffs descending dramatically into the sea affording several decametres of excellent exposure. Up to 10m of limestone unconformably overlie serpentinite, older sedimentary lithologies and the mineralised zones, providing a karstic cap over approximately 30% of the study area. Good exposure is therefore provided on hillsides, in river valleys, road sections and along the extensive coastal cliff section (Plate 1.3, Plate 1.4).

Solid rock outcrop is common in the area, but beach and river-derived deposits also occur. Cobble beaches are present along most of the coastal section, apart from a few small stretches of sand in the northeast of the study area.

Vegetation in the area varies, not surprisingly, with substrate lithology. Over karst (limestone) topography there are generally small bushes and shrubs growing in a very fertile soil which is deep red/brown in colour. These bushes and shrubs are usually less than a metre in height and are not a problem for fieldwork. In river valleys and gullies, however, vegetation tends to be of a dense structure and grows large, has aggressively protruding thorns, and obscures the better rock outcrops. In places, cultivated arable land also obscures solid rock outcrop, making accessibility difficult.

1.3 Previous Work

As an aid to commercial exploration, it is useful to establish the physical distribution of ore within any particular deposit, and the geological processes that operated during magnesite formation. This provides a genetic model and hence an aid in finding similar deposits elsewhere where comparable geological processes have been identified. The mode of magnesite formation has usually been studied almost completely by geochemical means using major-, trace- element data as well as stable isotope analyses (Moller, 1989; Kralik *et al.*, 1989). This has been done for many magnesite bodies worldwide (Greece - Dabitzias, 1980; Turkey - Zedef, 1994; Serbia & Bosnia - Fallick *et al.*, 1991).

In the Akamas area of northwest Cyprus, the deposit of Magnisia is the largest and has been the most exploited. Early investigations during the period 1923-24 established the size, grade, distribution of ore and possible genetic mechanisms involved in its formation (Haralambides Mining Company, 1923). Extracted magnesite was used industrially for its refractive properties. It was not until 1960 that the first chemical analyses were performed on vein carbonates from the Akamas area. These deposits were studied in particular as they were considered to be of more economic value than the carbonate mineralisation in the Limassol Forest area. Analysis of magnesite veins from the Magnisia deposit provided the mineralogy of the ore (Table 1.2). Results of chemical analyses were fairly consistent throughout the deposits and are comparable to similar Kraubath-type magnesite mineralisation elsewhere (Pohl, 1989).

Active extraction of the magnesite ceased in 1970 until the period 1982-84, when investigations were carried out by the Hellenic Mining Company Ltd. who re-initiated a series of exploratory steps including geological mapping, drilling boreholes through limestone cover into serpentinite around Magnisia, and driving a number of shallow adits and pits. During this period of study, the carbonates were further tested for their major element compositions, which proved consistent with earlier results (Gass, 1960). Trace elements patterns for the magnesite and unmineralised serpentinitised harzburgite showed concentrations of boron and lead within the magnesite which were not detected in the serpentinite (Ilich and Maliotis, 1984) (Table 1.2). These results, coupled with the morphology and classification of the deposits, led to the suggestion of a possible hydrothermal source for the vein and stockwork mineralisation. The mines have been in disuse since 1986.

More recently an aspect previously untouched upon was studied using samples taken from the Magnisia mine (Brydie *et al.*, 1993). This study involved preliminary isotope analyses of carbonates. Stable isotope carbon and oxygen data from samples of magnesite, calcite and dolomite were obtained. A possible genetic model was produced to explain the geochemical signature of carbonates present. This study was however somewhat rudimentary and proposed only basic indications of potential source reservoirs of elements present within the magnesite, and possible compositions of mineralising solutions. It was proposed that mineralising solutions were derived from isotopically exchanged, circulating meteoric waters during the Cretaceous period (Brydie *et al.*, 1993).

1.4 Present Study

This study concentrates on two main aspects of the mineralisation, field relationships and geochemistry. The distribution of ore within the magnesite deposits, classification of the various styles of magnesite mineralisation and the orientation of shear zones and faulted serpentinite has been established by re-mapping the study area. The presence of shallow thrust faults and dip-slip graben-related faults was established during mapping, and these have been added to update the existing geological map of the area (Malpas and Xenophontos, 1992). Some thrust klippen of Mamonia sediments have also been added to this existing map, which aid in the overall interpretation of structure in the area (see Figures 2.4a,b,c). Observations of dip-slip fault traces, and measurement of thickness of limestone around the serpentinite-limestone contact resulted in the construction of a block diagram showing how graben-related faulting has affected the study area (Figure 2.5).

Depth-down-hole data from three cores, supplied by the Hellenic Mining Co. Ltd., were correlated with deposit-scale surface geology to extrapolate the mineralisation beneath the limestone cover sediments. Detailed field observations include shear zone fabric orientation measurements and orientation data of shear zone structures such as slickenside lineations (grooves and fibrous minerals), etc.

Samples of magnesite and associated lithologies from the environs of the magnesite deposits were taken for stable isotope and trace element analyses. Isotope data provide clues to the provenance of carbonate ions and source characteristics of mineralising solutions (Kralik *et al.*, 1989), while Rare Earth Element distributions and

other trace element data are useful for determining the source of magnesium within the magnesite. Magnesium, it is assumed, is obtained directly from the serpentinite, while carbon and oxygen are derived from the mineralising solutions. Temperature of carbonate formation may be calculated from oxygen isotopic data (Aharon, 1988)

Within the scope of this project, an attempt has been made to provide a viable genetic model for the mineralisation, and potentially to clarify some features of the local, and to some extent, the regional geology of the Akamas area such as the extent of Mamonia thrusting and effects of the Polis Graben faulting. This project adds stable isotope data (carbon and oxygen) to the existing database for samples taken systematically from the variety of styles of magnesite mineralisation present in the Akamas occurrences. All samples analysed for their isotopic composition have also been analysed for their trace element composition. Certain lithologies within the study area are organic-rich and may have contributed carbon to the magnesite. Although it is not possible to isotopically relate one of these carbon sources to the carbon in the carbonate, due to unknown isotopic fractionation within the source organic material, there is the possibility of linking carbonate veins with possible organic-containing lithologies by way of trace element couplets or sequences. Each potential donor of carbon within the area has a distinctive trace element signature and so it may be possible to identify which signature has been preserved within the magnesite, hence indicating the probable source(s) of carbon.

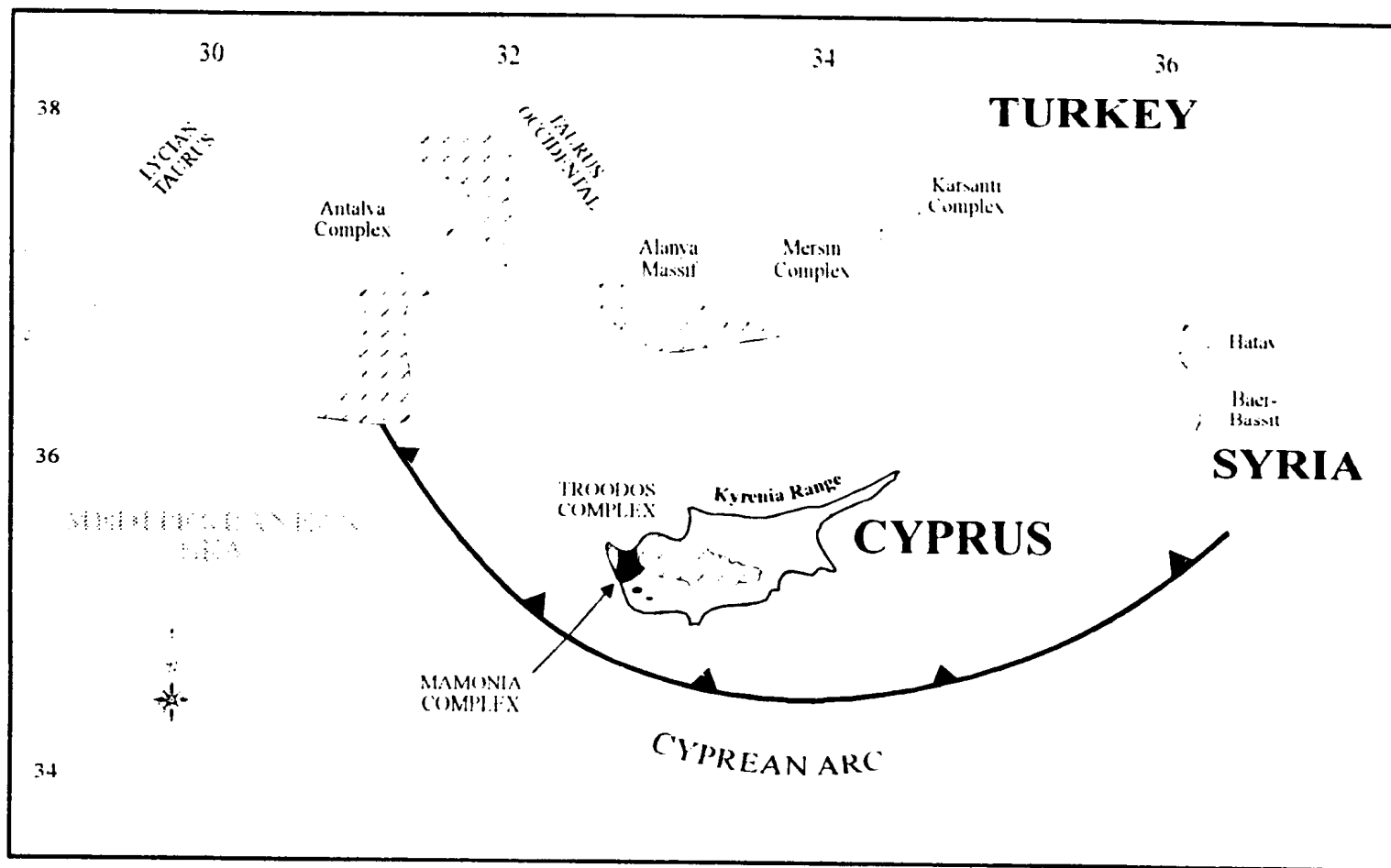


Figure 1.1 Location of Cyprus in the eastern Mediterranean showing relative positions of Troodos, Mamonia and other ophiolite-related complexes (Taken from Malpas et al., 1993).

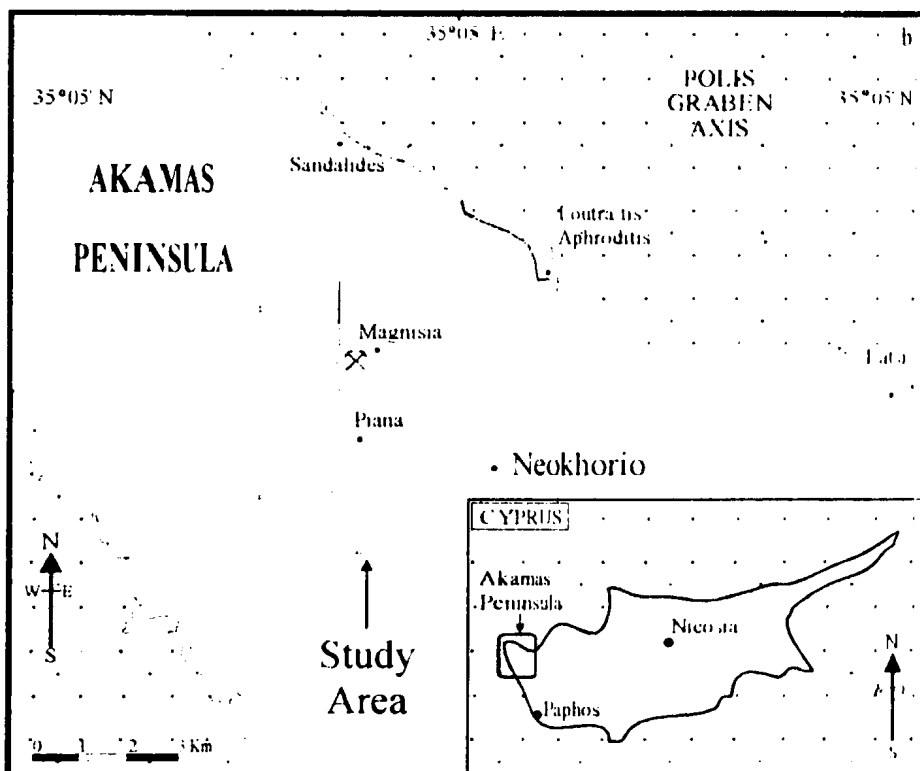
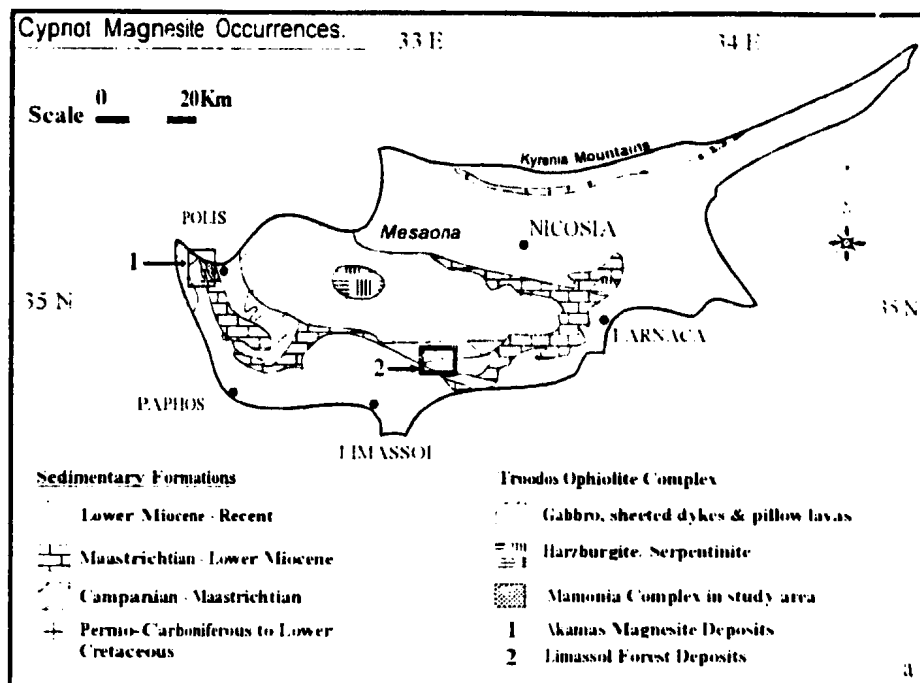


Figure 1.2 a) Diagram showing the two main areas of magnesite mineralisation; 1 - Akamas Peninsula, 2 - Limassol Forest, b) Location of study area.

Table 1.1 Types of important and potentially economic magnesite deposits

Author	Redlich (1909)	Bain (1924)	Ilich (1968)	Main descriptive features	Examples
	Descriptive, genetic interpretation	Genetic	Genetic		
	Veitsch Type	Limestone replacement	Endogenic-hydrothermal/metasomatic	Sugary to coarse-grained sparry magnesite in thick, nearly monomineralic lenses and irregular bodies within marine carbonate/clastic shelf suites; metasomatic relations to enveloping dolomite very characteristic	Austria, Brazil, Czechoslovakia, India, Korea, Manchuria, Spain, Tasmania, and USSR
	Kraubath Type	Serpentinite alteration (hypogene?)	Endogenic-hydrothermal veins	Very fine-grained, microcrystalline bone magnesite in veins and stockworks within dunite and peridotite (or serpentinite); structural control and proximity to erosion surface typical	Austria, Australia, California, Greece, Turkey, and USSR
			Bela-Stena Type	Fine-grained banded or massive magnesite sinter associated with hydromagnesite, huntite, sepiolite etc. in freshwater lakes; coincidence with ultramafic basement, large faults, and volcanism	Servia (Greece), Bozkurt (Turkey), and Bela Stena (Yugoslavia)
	Greiner Type			Magnesite or breunnerite in talc-carbonate masses derived from ultramafic rocks, usually in a metamorphic environment	Austria, Timmins (Ontario, Canada)

Table 1.2 a) Akamas magnesite major element composition (Gass, 1960), b) Akamas magnesite major element composition (Ilich and Maliotis, 1984), and c) Trace element composition of Akamas magnesite (Ilich & Maliotis, 1984).

a)

	Components (weight %)						TOTAL
	SiO ₂	Fe ₂ O ₃	Al ₂ O ₃	CaO	MgO	CO ₂	
Sample 1	0.14	trace	trace	2.73	46.07	51.41	<u>100.35</u>
Sample 2	0.24	trace	0.30	3.23	45.10	51.27	<u>97.14</u>

b)

	Components (weight %)						IGNITION LOSS
	SiO ₂	Al ₂ O ₃	Fe ₂ O ₃	CaO	MgO		
Sample 1	0.65	0.03	0.08	4.93	45.58	48.73	
Sample 2	0.70	0.07	0.16	4.44	46.23	48.40	
Sample 3	0.82	0.04	0.16	4.48	44.90	49.60	
Sample 4	0.33	0.02	0.08	7.89	41.28	50.40	
Sample 5	2.49	0.71	0.64	4.93	42.97	48.26	
Sample 6	1.47	0.04	0.32	5.37	43.94	48.86	
Sample 7	1.10	0.07	0.10	2.05	46.76	49.92	
Sample 8	0.72	0.03	0.10	4.20	44.23	50.72	

c)

Specimens 1 - 9 :- magnesite, 10 :- dolomite vein within magnesite, 11 :- serpentine within a magnesite vein, & 12 :- serpentinitised harburgite sampled away from mineralisation.
ND :- Not Detected.

SAMPLE #	1	2	3	4	5	6	7	8	9	10	11	12
LEAD (ppm)	25	ND	ND	ND	15	7	3	3	3	12	3	ND
BORON (ppm)	20	10	10	10	40	10	25	10	10	ND	18	ND



Plate 1.1 Vein magnesite at the base of the deposits.



Plate 1.2 Nodular magnesite found throughout the upper portions of the serpentinite.



Plate 1.3 100% exposure along the shore section at Loutra tis Aphroditis.



Plate 1.4 Road cut with sheeted diabase dykes.

2.0 REGIONAL AND LOCAL GEOLOGY

2.1 Introduction

The geology of southwest Cyprus has been well documented, and was most recently described by Malpas *et al.* (1993). Below, the general features are presented first and then the specific stratigraphy and structure of the study area are discussed.

2.2 Regional Stratigraphy of Southwest Cyprus

The geology of the island of Cyprus is dominated by ophiolitic rocks. In the Troodos range, which forms the core of the island rising to a height of 1951m on Mount Olympus, an intact, complete ophiolite suite is preserved. This ophiolite was produced above a subducted slab of the Neotethys Ocean in late Cretaceous times. Further subduction along this zone resulted in the juxtaposition of two distinct geological terranes derived from either side of the convergent plate margin (Figure 2.1). In southwest Cyprus, evidence of this late Mesozoic collision is well preserved in a series of erosional windows through Tertiary sedimentary cover sequences (Figure 2.2; Figure 1.2).

The two juxtaposed terranes are the Mamonia Complex and the Troodos Complex. Their collision was clearly along a structurally complicated zone, the tectonic style of which is dominated by a combination of thrust- and strike-slip faults. The northern margin of the suture zone lies on a line through the villages of Statos and Kannaviou and the zone extends toward the Limassol area (Figures 2.1, 2.2). Its southern limit is likely concordant with the main Cyprian Arc, some 40km offshore (Figure 1.1). The suture zone, as exposed in the erosional windows, is marked by a 60km long arcuate line of serpentinite bodies lying between the Akamas Peninsula and Petra tou Romiou running

through Akamas, Mavrokolymbos, Ayia Varvara, and Phasoula. These serpentinite bodies are now mapped as a series of thrust sheets associated in some places with other Troodos ophiolitic lithologies such as gabbros, diabase and pillow lavas.

2.2.1 Mamonia Complex Rocks in Southwest Cyprus

Rocks of the Mamonia Complex occur in west and southwest Cyprus, where they are generally covered by a blanket of late Cretaceous to Quaternary sediments (Figure 2.3a). Sporadic outcrops are also present in the southeast and east of the island, and similar rock types are associated with the Baer Bassit ophiolite in Syria (Figure 1.1). The Mamonia Complex, a deformed late Triassic to mid-Cretaceous volcano-sedimentary terrane, represents a highly tectonized and collapsed passive margin sequence, which formed within Neotethys. The sedimentary rocks from the Mesozoic continental margin are collectively known as the Ayios Photios Group. The volcanic rocks, forming part of the Dhiarizos Group, are remnants of Upper Triassic volcanism, and are most recently interpreted as old ocean crust with associated seamounts developed along the northern margin of Gondwana (Malpas *et al.*, 1992).

The Ayios Photios Group can be further subdivided into the Vambouras, Marona and Episkopi formations, which comprise a variety of siliciclastics, calcareous and siliceous lutites, arenites and rudites. The Dhiarizos Group includes pillow lavas and volcanoclastic sandstones of the Phasoula and Loutra tis Aphroditis formations, and carbonates and mudstones of the Petra tou Romiou and Mavrokolymbos formations respectively.

Metamorphic rocks including psammitic and pelitic schists and amphibolites are found in association with serpentinites and, in this region, are known as the Ayia Varvara Formation (Swarbrick and Robertson, 1980; Malpas *et al.*, 1992)

2.2.2 Troodos Complex Rocks in Southwest Cyprus

In general terms the Troodos Complex comprises a complete ophiolite suite disposed in a domal structure forming the core of the island of Cyprus. However, the southern portion of the massif, both in the Limassol Forest Complex and further to the west where the ophiolite is juxtaposed with the Mamonia Complex, does not display a characteristic ophiolite stratigraphy. Rather, a sequence of intercalated lavas and breccias, not found elsewhere in the Troodos Massif, is here interpreted to have formed in a transtensional transform fault system (Simonian and Gass, 1978; Murton, 1990; MacLeod, 1990; MacLeod and Murton, 1993). This Southern Troodos Transform Fault Zone (STTFZ) is underlain by a series of ultramafic and gabbroic intrusions that were emplaced at a shallow crustal level and were, in part, exposed on the seafloor. In the eastern part of the STTFZ, MacLeod (1990) has recognized oceanic crust produced at an 'anti-Troodos ridge' (the Limassol Forest Complex) and has inferred dextral movement along the transform which he interprets as a late reactivation of the zone in response to anticlockwise movement of the Troodos Complex in latest Cretaceous time. In contrast to this, Malpas *et al.* (1992) recognize the Limassol Forest Complex as an integral part of the transform fault zone itself.

Within the Mamonia-Troodos suture zone, the Troodos Complex is represented by volcanic rocks and serpentinites with only sparse gabbros and diabase dykes. In contrast to

southwestern Cyprus, diabase dykes are common in the Akamas area. The volcanic rocks, and locally the serpentinites, are overlain in places by volcanogenic sandstones and bentonitic clays of the Campanian to Maastrichtian Kannaviou Formation.

2.2.3 Post-Collisional Sediments

Locally, notably in the Ayia Varvara erosional window (Figure 2.2), rocks of the upper portion of the Kannaviou Formation are interbedded with sedimentary melange consisting of a red mudstone matrix with variably sized clasts (up to 2m) of volcanic rocks derived from both the Troodos Complex and the Dhiarizos Group, as well as cherts, sandstones and recrystallized limestones of obvious Mamonia Complex provenance (Malpas *et al.*, 1993). This depositional sequence can be correlated with the Moni Melange (Figure 2.3a) that lies in a trough along the southern margin of the STTFZ in the Limassol Forest (Robertson, 1977). Because the Moni Melange transgresses both terranes, it is the first indication of the proximity of the advancing Mamonia continental margin to the Troodos ophiolite.

A slightly younger olistostromal unit, the Maastrichtian Kathikas Melange, also seals structural contacts within the Mamonia Complex, as well as the fundamental suture between the two terranes. This unit consists of variably sized clasts of Mamonia rocks and rarer blocks of Troodos material arranged chaotically in a red argillaceous matrix. It appears undeformed and is post-orogenic for the most part. The melange passes upwards into deep water limestones of the Tertiary Lefkara Formation, or is directly overlain by younger units of the cover sequence (Swarbrick and Robertson, 1986).

A sequence of marine carbonates, calcarenites, sandstones, and marls covers much of southwest Cyprus. The carbonates are divided into two main formations, the Lefkara and Pakhna formations, which have each been subdivided further on the basis of distinct lithological characteristics (Robertson *et al.*, 1990).

The Lefkara Formation is made up of three deep-water pelagic carbonate units, the Lower, Middle and Upper Lefkara sediments, and the boundary between each unit appears, from field relationships, to be diachronous (Gass, 1960) (Figure 2.3b). The Lower-, Middle- and Upper Lefkara Formation sediments are Maastrichtian, Palaeocene-Oligocene and Oligocene in age, respectively. The lower contact of the Lefkara Formation with Mamonia and/or Troodos lithologies is defined by a basal conglomerate containing rounded clasts of serpentinite, gabbro, diabase, chert and sandstone (Robertson and Hudson, 1974).

The Pakhna Formation is composed of marls, chalks and calcarenites which, in most places, conformably overlie Lefkara sediments; locally, however, the Pakhna marls and chalks unconformably overlie the Lefkara Formation (Robertson and Hudson, 1974). Lateral facies variations are common within the Pakhna Formation. The Pakhna sediments are thought to have been deposited within a shelf environment, as indicated by faunal assemblages and the composition and texture of the limestones and marls (Robertson *et al.*, 1990).

2.3 General Structure of Southwest Cyprus

Along the suture zone, evidence is preserved of i) an early period of extensional tectonism which occurred during the formation of the ophiolitic rocks related to an

extensional forearc setting adjacent to, or part of, a major transform fault zone (Malpas *et al.*, 1993), ii) two main consecutive contractional tectonic episodes associated with terrane collision, and iii) a late extensional episode resulting from the Tertiary uplift of the Troodos Massif

i) Early extensional structures

The oldest megascopic structural features are extensional faults which are restricted to Troodos Complex rocks. These faults define narrow, linear horst and graben structures, with upthrown blocks occupied by serpentinites and gabbros, and downthrown blocks by volcanic rocks, sedimentary serpentinite breccias and Kannaviou Formation sandstones and clays (with locally interbedded Moni Melange). These extensional structures are best seen where preserved in Troodos rocks beneath the overthrust Mamonia Complex. Here, planar rotational and listric faults with steep to gentle dips define a geometrically complex master system which is linked by steep transfer faults. Kinematic indicators on fault surfaces and in shear zones show consistently normal sense dip-slip or oblique-slip (Malpas *et al.*, 1993).

ii) Contractional structures

Evidence of two major contractional events of late Cretaceous age is preserved in both Troodos and Mamonia rocks as apparently early north-northwest-directed thrusts, and later backthrusts towards the west and southwest which reorganized the early stacking sequence (Malpas *et al.*, 1993). Distinguishing criteria include small-scale kinematic indicators such as slip-plane fibres, c-s fabrics, shear bands in foliated rocks, cleavage orientation in mesoscopic shear zones and vergence of minor folds of bedding as well as

cleavage, all of which are common features in the lower portions of the thrust systems. The contractional fault systems clearly post-date the early extensional features described above, which acted as focal points for thrust ramping, i.e. structural relationships show that basal thrusts in the Mamonia Complex truncate lithological units and steep extensional structures in the underlying Troodos Complex. The relative timing of the two thrust systems is not well constrained, although several lines of evidence suggest that the structures recording north-directed emplacement are overprinted by the southwest-directed structures. North-directed, steeply inclined inversion structures in pillow lavas and Kannaviou Formation sediments in the northern graben of the Ayia Varvara window are truncated by serpentinite shear zones at the base of the south-directed system. Also, imbricates of the Ayios Photios Group in the south-directed systems of the Mavrokolymbos and Ayia Varvara windows display mesoscopic and macroscopic fold interference patterns which indicate that rare north-facing and verging folds are overprinted by ubiquitous south- or southwest-facing and verging folds. The resultant complicated tectono-stratigraphic sequence is best displayed in the eastern part of the Ayia Varvara window. Here, a basal zone of sheared serpentinite entraining blocks of metamorphic rocks of the Ayia Varvara Formation, is overlain by thrust sheets of the Dhiarizos Group which, in turn, are overlain by imbricate thrusts of the Ayios Photios Group. A similar stacking sequence emerges from restoration of geological cross sections within the Mavrokolymbos window (Malpas *et al.*, 1993).

iii) Late extensional structures

The youngest extensional fault system resulted in a number of major grabens formed during Tertiary uplift of the Troodos Massif (Robertson, 1990). In western Cyprus, regional extension of this age led to the development of the Polis Graben. This is situated directly west of the Troodos Massif, and bounding normal faults have downthrown the rocks of the suture zone (Mamonia Complex and Troodos Complex) as well as sedimentary cover, giving the graben an overall topographic relief of 200m. Graben master faults are oriented north-south, with a series of smaller east-west transfer faults (Figures 2.4, 2.5).

2.4 Geological Relationships in the Field Area

The following descriptions are based on field mapping which was carried out in order to relate the study area to the regional structure and stratigraphy. Features such as klippen of Mamonia thrust packages, dip-slip faults related to the Polis Graben, and the orientation of shear zones in the serpentinite body have been added to the existing geological map (Malpas and Xenophontos, 1992) and are shown in Figure 2.4a. An east-west geological cross-section through the area has also been drawn (Figure 2.4b).

2.4.1 Stratigraphy

Lithologies exposed in the study area include those of the Mamonia Complex, Troodos Complex and Tertiary cover sediments (Figure 2.3a, b).

2.4.1.1 The Mamonia Complex

Mamonia Complex rocks in the study area are mostly Ayios Photios Group sediments. Dhiairizos Group rocks are exposed in only one locality, on the northern

coastline. Here, the contact between the Ayios Photios Group and underlying Dhiarizos Group rocks is marked by a fine-grained grey cataclasite along a shallow thrust contact (Swarbrick, 1980). The base of the Dhiarizos Group is not seen in the area. For simplicity, the Ayios Photios and Dhiarizos groups are not differentiated on Figure 2-4a.

The Ayios Photios Group (Upper Triassic - Middle Cretaceous)

In the study area, the Ayios Photios Group crops out along the northern coastline and runs southward for approximately 5km. The western extent of Mamonía rocks occurs near Piana, and the easternmost occurrence lies near the town of Androlykou (see Figures 2-4a, b, c). The thrust contact with the underlying Dhiarizos Group is too small to be depicted on Figure 2-4a but occurs just to the east of Loutra tis Aphroditis. Further south, Ayios Photios rocks are also thrust directly over a large sheet of serpentinitised harzburgite belonging to the Troodos Complex. This serpentinite outcrops between Loutra tis Aphroditis and Piana, a distance of 3-4km, and the sub-horizontal tectonic contact with sediments is irregular, with Ayios Photios Group sediments occurring on top of the serpentinite as widespread thrust sheets in the east and as two small klippen in the west, one 1km west of Neokhorio (Plate 2.1) and the other close to the limestone cover sediments at Piana. These klippen are shown with somewhat exaggerated size on Figure 2-4a.

The Ayios Photios Group is dissected internally by a complex of low-angle, easterly dipping thrust faults and displays west-verging and west-facing asymmetric folds. The thrusts and folds both indicate an overall westward displacement of the Ayios Photios Group.

The Vlamboiros Formation crops out in the south of the study area and consists of grey-green, medium- to coarse-grained sandstone intercalated with subordinate silt- and mudstone. Organic material is present in the form of vascular plant remains. Repeated cycles of upward-fining quartz-rich sand layers, intercalated with silt- and clay-rich layers, display slump structures and lateral facies changes indicating their deposition from turbidity flows. The base of this unit is not seen in the area and the upper contact is marked by a conformable gradation into red mudstones and chert bands of the Episkopi Formation. Total thickness of the Vlamboiros Formation is estimated at approximately 50m (Swarbrick and Robertson, 1980), but from more recent mapping during this project, the formation appears to be thicker than 100m in places. The Vlamboiros Formation has been dated as Triassic in age, from foraminifera contained in associated sediments (Swarbrick and Robertson, 1980).

The Episkopi Formation crops out in the centre of the study area and along the coastline to the north, and comprises well-bedded radiolarian mudstones with intercalated cherts and siltstones. At the top of this unit is an unconformable contact with marine chalks and limestones of the Cretaceous to Palaeocene-Eocene Lefkara Formation. Thick-bedded (2m) sandstone layers are present (the Akamas Member) at certain horizons within the radiolarian sediments and represent occasional influxes of terrestrial sediment into a deep water marine environment (Swarbrick and Robertson, 1980). The Episkopi Formation was dated using radiolaria from the cherts and mudstones and is of Jurassic to late Cretaceous age (Swarbrick and Robertson, 1980).

The Dhiarizos Group (Middle Triassic-Lower Cretaceous)

Within the study area, the occurrence of the Dhiarizos Group is restricted to the shore section in the vicinity of Loutra tis Aphroditis. The lower contact, between Dhiarizos and Troodos (?) rocks, is not seen in outcrop. The upper contact is a low angle thrust with overlying Ayios Photios rocks. The Loutra tis Aphroditis Formation consists of breccia containing small angular clasts of siltstone and larger (5-10cm) coarse-grained sandstone cobbles. Minor quantities of volcanic glass are also seen within the tuffaceous matrix of the breccia. In the study area, the only outcrop of Loutra tis Aphroditis Formation is a single block near Loutra tis Aphroditis. The bottom of this block is not seen but lateral contacts with surrounding Ayios Photios cherts and mudstones are high angle faults. Groove lineations on the faces of the block indicate that the most recent relative movement between the block and surrounding rocks was almost vertical.

Petra tou Romiou Formation limestone is present as isolated blocks suspended within Mamonias sediments. The best outcrops are a series of blocks or 'knockers' on the shore section close to Loutra tis Aphroditis. These blocks are silicified (ooliths and coral fragments replaced by silica) and are interpreted as remnants of carbonate reefs formed on seamounts upon Triassic ocean floor. The blocks probably became silicified after sinking beneath the carbonate compensation depth at some time before exhumation during terrane collision (Swarbrick and Robertson, 1980).

The Ayia Varvara Formation (Upper Cretaceous)

This formation has been discussed by Malpas *et al.* (1992), and is thought to be the metamorphosed remnants of Triassic ocean crust and associated volcanic seamounts.

and sediments preserved within the subduction (accretion) melange. Metamorphism most likely occurred during subduction. Chemistry of the amphibolites is indicative of both tholeiitic basalt (MORB) and ocean island basalt (OIB), unlike any lavas associated with the Troodos ophiolite (Malpas *et al.*, 1993).

Amphibolites, quartz-mica schists and blocks of recrystallised chert are found along the shore section near Loutra tis Aphroditis, and amphibolites are present within serpentinite approximately 1km west of the town of Neokhorio (Figure 2.4a).

The **Mavrokolymbos** and **Phasoula formations** are not seen in the area.

2.4.1.2 The Troodos Complex

Serpentinised harzburgite

Serpentinised harzburgite crops out over an area of approximately 9km² (extending south from Loutra tis Aphroditis) and is interpreted as an allochthonous sheet emplaced from east to west over gabbro and sheeted diabase dykes (Malpas and Xenophontos, 1992; Murton, 1990) (Plate 2.2). Extensive serpentinite exposure occurs on the shoreline adjacent to Loutra tis Aphroditis. Bastite (after orthopyroxene) serpentine is common (Plate 2.3).

The degree of serpentinisation is not uniform throughout the ultramafic body, and is more pronounced towards the margins of the serpentinite mass and along the numerous internal zones of sheared and shattered material. The serpentinite is highly weathered and degraded where shearing and brecciation have occurred.

Gabbroic rocks

Variably-sized plutonic bodies occur as sporadic intrusions within the sheeted diabase dyke complex. The largest of these lies immediately below the large serpentinite sheet (Plate 2.2). The gabbroic rocks are mostly vari-textured and include a range of lithologies from gabbros(ss), olivine-gabbros, quartz-gabbros, diorites to rare plagiogranites.

Sheeted diabase dyke complex

An extensive sheeted diabase dyke complex crops out in the west of the area, where it is thrust over volcanic rocks. The dykes are themselves overthrust by the serpentinite. They are aphyric to sparsely phyric basalts and basaltic andesites with equigranular, fine-grained ophitic, sub-ophitic and intergranular textures (Gass, 1960). These dykes are chemically similar to those diabase dykes found in the southern part of the Troodos Massif, with which they are therefore correlated (Gass, 1960).

For the most part, the complex has been tectonically disrupted and dykes now dip at 40° eastward (Plate 1.4). It is not clear whether these dykes, which were presumably originally intruded vertically, were disrupted during thrusting or as a result of back-rotation of faulted blocks during formation of the Polis Graben.

Lower and Upper Lava Series

Volcanic rocks belonging to the Troodos Complex include an extrusive sequence of tholeiitic pillow- and sheet flow-basalts, intercalated with deep water sediments, lying structurally below the sheeted diabase dykes (Malpas and Xenophontos, 1992). Way-up

indicators suggest that the lavas are upright and therefore must occur in discrete thrust slices.

2.4.1.3 Tertiary Cover Sediments

In the Akamas area, chalks, marls and limestones of the Lefkara and Pakhna formations are well exposed and cover approximately 40% of the study area (Figure 2.4a, Plate 2.4).

The Lefkara Formation unconformably overlies Mamonia and Troodos rocks (Plate 2.2) and consists of chalk with chert bands, grading upwards into massive chalk. The Pakhna Formation is a series of chalks, marls and calcarenites which conformably overlies the Lefkara Formation (Plate 2.4). Over most of the study area, however, the Pakhna Formation directly unconformably overlies basement rocks (Troodos and Mamonia complexes). It is capped by the Tera Limestone, a coralline limestone containing reef talus and reworked calcareous sediment. Therefore, on many of the graben footwall blocks, there exists a considerable stratigraphic hiatus.

A series of Recent conglomerates, fanglomerates, sandstones, marls and calcareous arenites are present in the north and east of the study area (Plate 2.5), they are particularly well developed along the axis of the Polis Graben.

2.4.2 Structure

Early extensional tectonic features are preserved within the serpentinite and occur in the form of small grabens and half-graben faults. Sedimentary serpentinite breccia, interpreted as fault talus, is found at the base of graben-bounding faults. The small grabens vary from 10 to 30m wide and show relative displacements in the order of 5-10m.

Kinematic indicators on fault surfaces and within shear zones consistently show normal slip sense. Normal faults (half-graben bounding faults?) are present in a few localities in the south of the area near Piana and along the coastline just below the limestone cover to the west of Loutra tis Aphroditis. Similar features have been described in the Mavrokolymbos and Ayia Varvara Windows, 40 to 60 km to the south. These features are interpreted as being formed as a result of an early period of extensional tectonism which occurred during the formation of the ophiolitic rocks presumably in an extensional forearc setting adjacent to, or part of, a major transform fault zone (Malpas *et al.*, 1993).

Low- to moderate-angle, eastward-dipping thrust faults are the dominant structures in the study area (Figures 2.4a-c). These faults appear to be related to the regional west-southwest thrusting of Mamonia and Troodos rocks, although the thrusting is directed more to the west than at the Ayia Varvara and Mavrokolymbos windows (Malpas *et al.*, 1993).

In the study area, a large sheet of serpentinite is thrust over gabbro and sheeted diabase. This thrust is referred to as the basal serpentinite thrust (BST) and contains structural features relevant to the magnesite mineralisation which is discussed later (Chapter 3). A shear zone, the intra-serpentinite shear zone (ISSZ) is present higher up in the harzburgite thrust sheet. The ISSZ is essentially a carbonatised serpentinite shear zone which outcrops a few metres below the carbonate cover sediments. Small clasts of Ayios Photios Group cherts, mudstones and gabbro are present in this shear zone (Plate 2.6).

Folding is seen on a variety of scales within the Mamonia Complex; asymmetric anticlines are common throughout the area, particularly within thrust packages where

competent sandstone beds are intercalated with siltstones and mudstones. Tightly folded layers of chert and mudstone (with minor sandstone horizons) are common along the shoreline and are well exposed along road cuts and in river valleys. All folds are westward verging and are best developed within the Episkopi Formation.

Miocene extensional faulting, related to the formation of the Polis Graben, has downthrown large blocks of both Troodos and Manonia rocks. The study of sediment deposition in the graben and the onset, and age span, of extensional tectonics (Robertson et al., 1990) conform to the geometry of the cross section through the area (Figure 2.4b). Graben faults are rarely seen in outcrop due to extensive Tertiary carbonate cover. Fault attitudes and the magnitude of normal fault displacement must therefore be inferred from stratigraphic relationships (e.g. Figures 2.4a-c), changes in topography and the relative thickness of carbonate cover on the downthrown side of the fault (Figure 2.5). Around the perimeter of the serpentinite for example, the thickness of the syntectonically deposited limestone cover has been used to identify areas of fault activity. Only normal faults are shown in Figure 2.5. The dip and dip-direction of these faults were inferred from the attitudes of sheared serpentinite and the presence of slumped limestone sediments on the downthrown side of the faults. Fault traces are seen to run beneath the limestone cover in directions consistently east-west and north-south. These faults can then be followed by a corresponding change in topography. This gives the Pakhna sediments a terraced appearance in places.

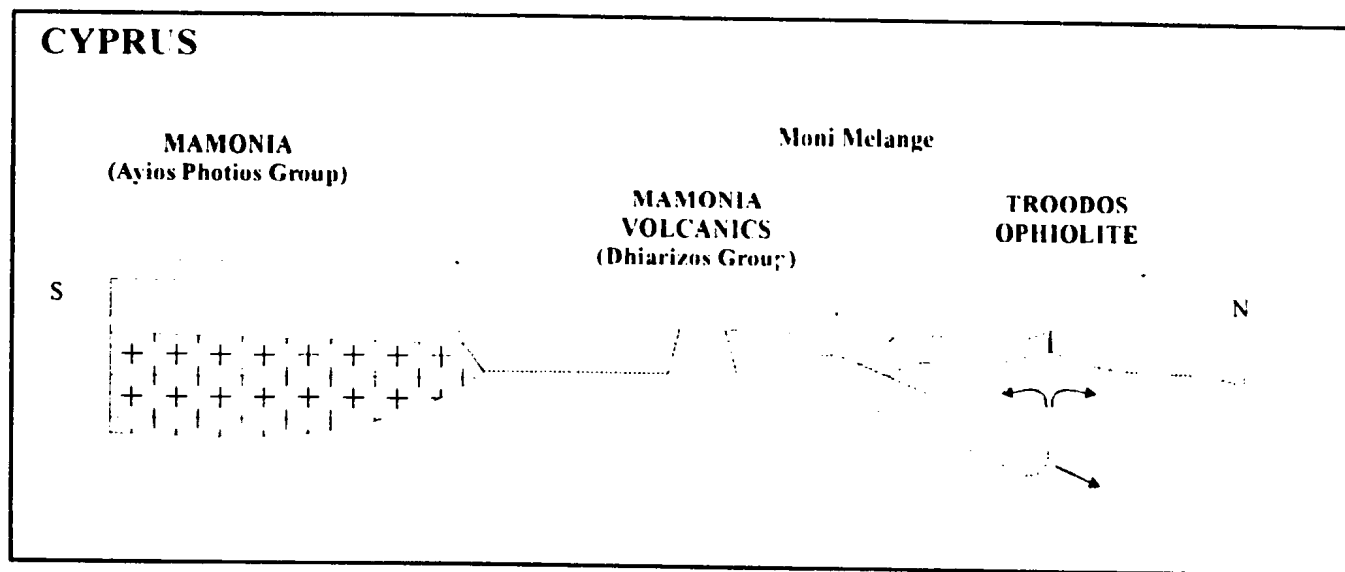


Figure 2.1 Schematic reconstruction of Mamonia and Troodos terranes during Middle-Late Cretaceous times (Malpas et al., 1993).

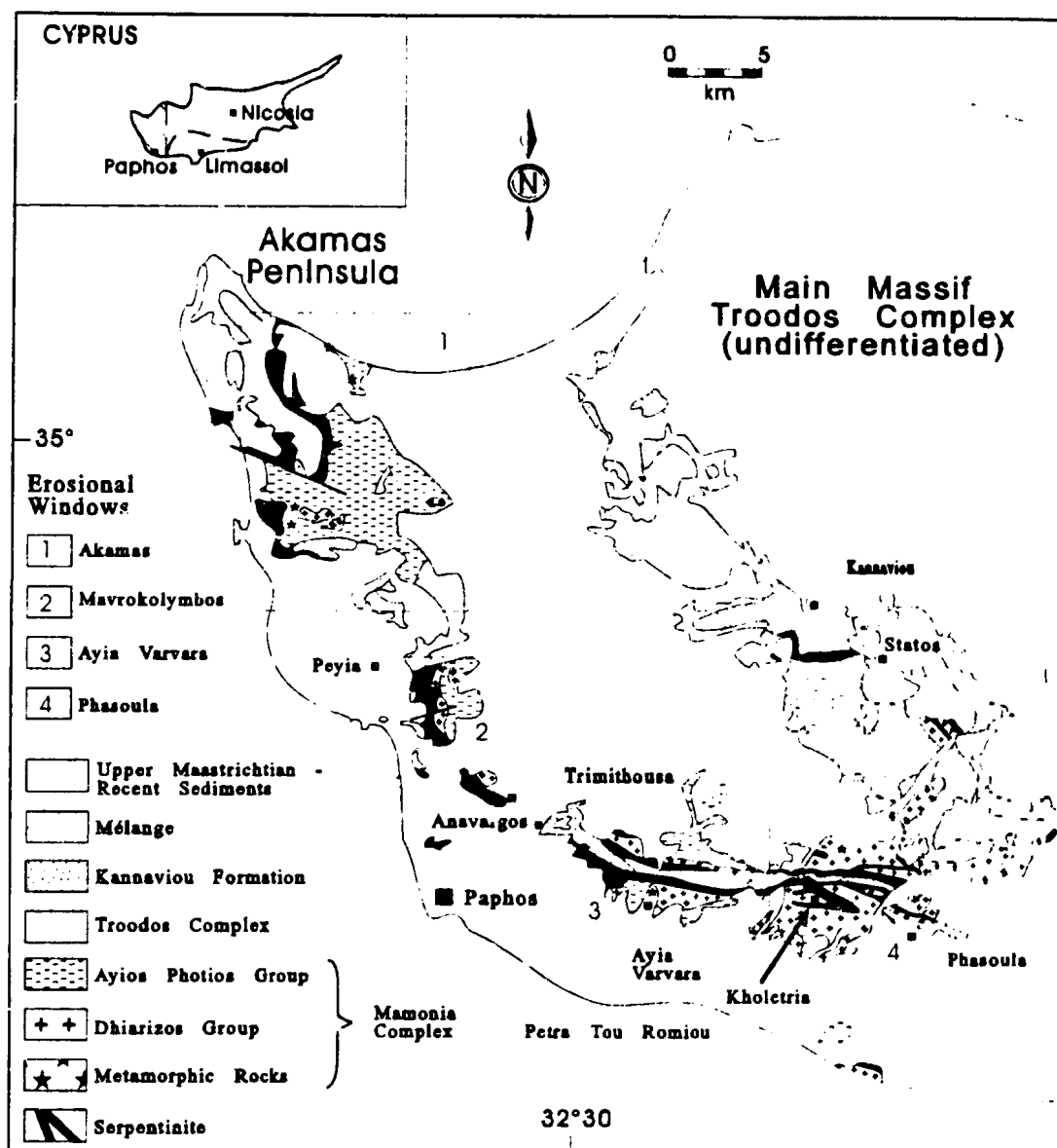


Figure 2.2 General geological map of southwest Cyprus (taken from Malpas et al., 1993).

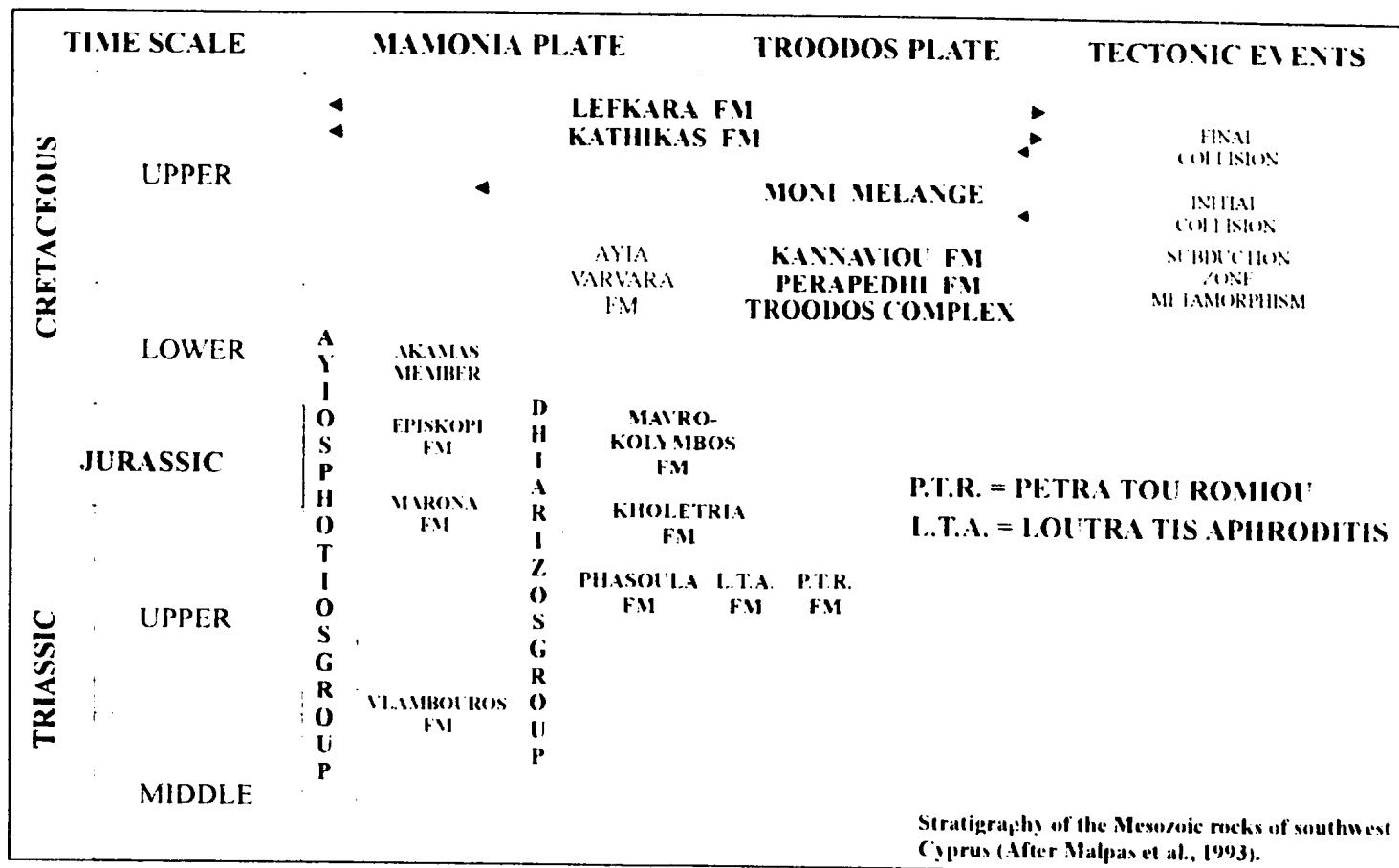


Figure 2.3a Stratigraphic relations within southwest Cyprus. Most of these lithologies are present in the study area, with the few exceptions described in the text.

Age (Ma)		Formation	Lithology
2.0	Pleistocene	Fanglomerate	Conglomerates and sandstones
		Apalos	Calcarenite, sandstone and conglomerate
		Kakkaristra	
5.2	Pliocene	Athalassa	
		Nicosia	Marls, silts, muds, sandstone, conglomerate
		Kalavassos	Evaporites
		Koronia Member	Reefal and bioclastic limestone
23.3	Miocene	Pakhna	Pelagic chalks, marls, calcarenites, conglomerates
		Tera Member	Reefal and bioclastic limestone
35.4	Oligocene		Pelagic chalks and marls
56.5	Oligocene	Middle Lefkara	Massive pelagic chalks
65.0	Palaeocene		Pelagic chalks, replacement chert
74.0	Maastrichtian	Lower Lefkara	Pelagic chalks
83.0	Campanian	Kannaviou	Volcanic sandstone, bentonitic clays
90.4	Turonian	Perapedhi	Umbers and radiolarites

Figure 2.3b Stratigraphy and lithology of the autochthonous supra-ophiolite sediments (After Robertson et al., 1990)

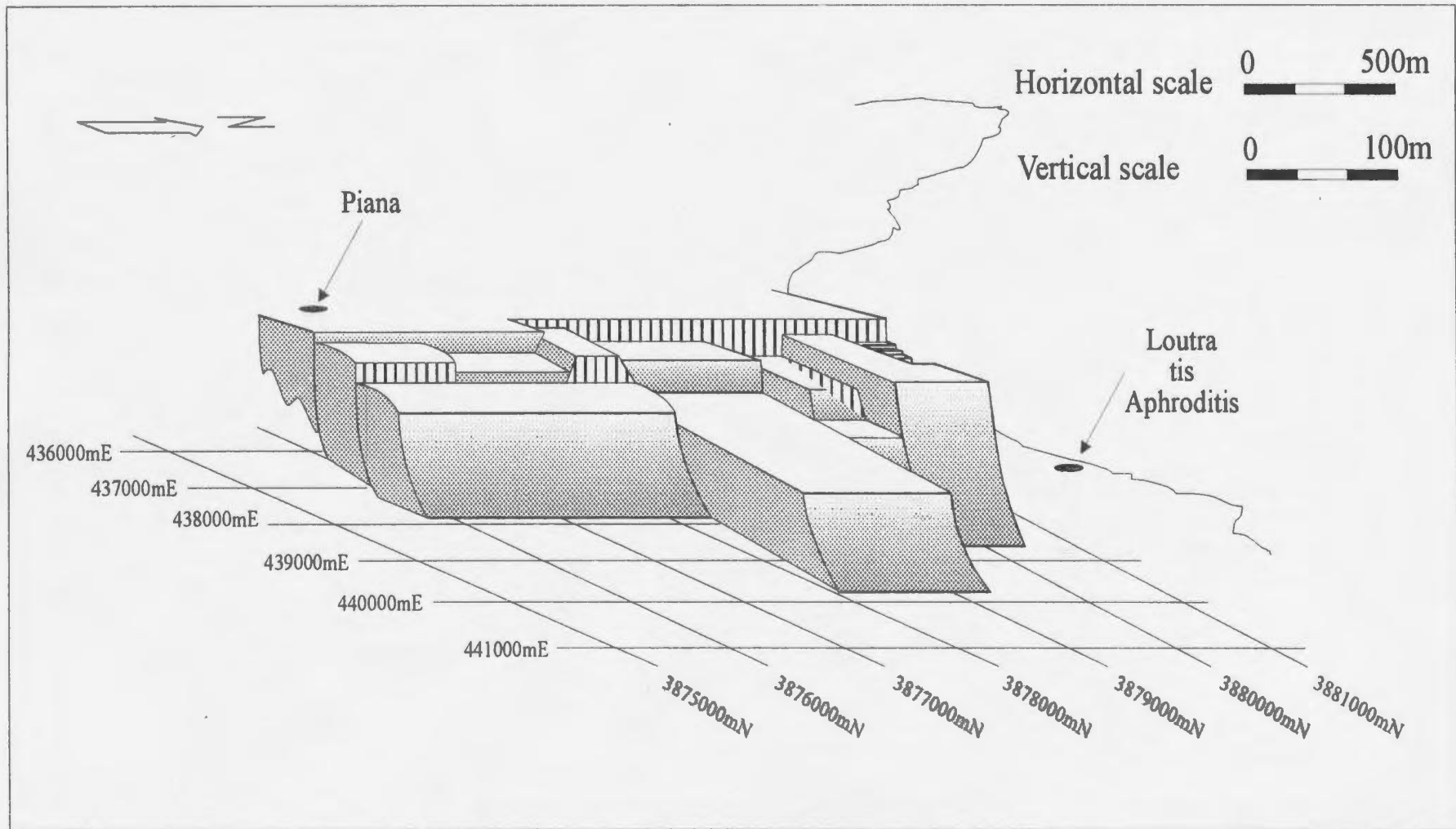


Figure 2.5 a) Schematic illustration of the structure of the western part of the Polis Graben, and b) Photograph taken looking eastward into the graben.



Plate 2.1 Small klippe of Mamonia mudstone on serpentinite located 1km west of Neokhorio. This outcrop marks the base of the Mamonia thrust sheets which were emplaced from east to west at a shallow angle. Lens cap for scale.



Plate 2.2 Moderately dipping (50°E) thrust contact between serpentinite in hanging wall and gabbro with limestone lying unconformably on serpentinite in the background. Photograph taken facing due south. Jeep for scale.



Plate 2.3 Outcrop of serpentinitised harzburgite. Bastite serpentinite after orthopyroxene is common. Coin for scale.



Plate 2.4 Lefkara chalk overlain conformably by 10m of Tera limestone 500m east of Neokhorio village. Moped for scale.



Plate 2.5 Shore section along the northern boundary of the study area. Serpentinite on the shoreline is unconformably overlain by calcarenite.



Plate 2.6 Light-blue carbonatised serpentinite of the ISSZ. Mudstones of the Mamonia Complex are present as clasts within the shear zone. Lens cap for scale.

3.0 STRUCTURAL FEATURES OF MINERALISATION

3.1 Introduction

Structural features in the serpentinised harzburgite and within the magnesite deposits provide information concerning the relative timing of, and physical conditions prevalent during, carbonate mineralisation in this area. Two styles of magnesite mineralisation are clearly discernible which are interpreted as belonging to different genetic episodes. Each style appears within distinct structural settings in the serpentinite. Examination of features within the magnesite and serpentinite indicate that the earliest magnesite veins were precipitated during contractional tectonism and so this style of mineralisation is associated with the emplacement of the serpentinite. Nodular precipitates appear to have formed later, after all contractional tectonism had ceased.

3.2 Styles of Magnesite Mineralisation.

The mineralisation has been categorized, based upon field relationships and magnesite distribution, into two zones; 'ZONE I' and 'ZONE II' (Figure 3.1). These two zones are recognized within each of the magnesite deposits in the study area, but are best seen in the Magnisia mine (Figures 3.2, 3.3). Each 'zone' where magnesite is present contains significant information regarding structural and mineralisation processes involved in each stage of carbonate formation. Zones I and II are described separately in the following section paying attention to structurally significant features. These two zones constitute the main styles of magnesite mineralisation present in the Akamas area.

3.2.1 Zone I Type Mineralisation

Mineralisation of this type is hosted by extensive vein networks, which are particularly well developed in the lower portion of the serpentinite thrust sheet (Figure 3.1). Large veins occur at the bases of the deposits (Plate 3.1) and grade upwards into a diffuse stockwork consisting of variably oriented smaller veins.

The magnesite in the large veins is for the most part a hard, white, cryptocrystalline material (Plate 3.2) with dendritic iron hydroxide (limonite) upon vein surfaces. The veins have been injected into sheared and shattered serpentinite as well as along existing anisotropies, including shear zone fabrics. In surrounding serpentinites, shear zone structures such as c-s planes and slickenside lineations defined by both fibrous minerals as well as grooves are abundantly present both in outcrop and many samples. Slickensided surfaces with lineations are particularly common on the walls of sizable veins (>10cm in thickness). The large magnesite veins are oriented almost vertically and show well developed features associated with dilational vein system development (Hodgson, 1989). These features are spalled wallrock fragments now included in the veins in zones parallel to wallrock within the outer borders of the veins, "comb" textures within some large veins, internal "ladder vein" textures, median-lines within veins and hydraulic brecciation and re-cementation of vein material (Plate 3.3). Groove lineations along slickensided surfaces on the walls of veins indicate displacement after vein formation with some reworking of the shear fabric. The large magnesite veins are dilational and antitaxial in nature and interpreted to have formed during a syn-kinematic stage.

Zone 1 magnesite veins grade upwards into small veinlets and stockwork mineralisation which are present in most exploited sites. The transition between these two forms of magnesite is not uniform but, where well exposed, commonly occurs over a vertical interval of approximately 3-4m. Stockworks everywhere lie above the large magnesite veins. The lower and upper limits of this zone are the Basal Serpentinite Thrust (BST) separating serpentinite from gabbro/diabase, and the Intra-Serpentinite Shear Zone (ISSZ) near the top of the serpentinite sheet (Figures 3.1, 3.3). Above the BST the sheared serpentinite grades upwards into a more common massive-blocky texture.

Where magnesite veins are common, the serpentinitised harzburgite is a dark olive-green colour with relatively little evidence of associated carbonatisation of the ultramafic material. Where stockworking is well developed however, the host rock is a light mottled green-white due to extensive carbonate alteration. At the Magnisia and Piana localities (Figure 1.2), weathering and alteration is severe and has resulted not only in extensive degradation of the serpentinite, but also in the formation of calcite and dolomite veins, especially in close proximity to the marine limestone which unconformably overlies the magnesite deposits. Petrographic examination indicates that the majority of this calcite and dolomite is epigenetic in nature, infilling fractures and voids within the magnesite veins and surrounding serpentinite (see chapter 4).

Zone 1 structural features

Zone 1 varies in apparent thickness between 10 and 40m along the line of magnesite deposits, and is at its thickest at the Magnisia locality. Lateral thickness and continuity of Zone 1 mineralisation underground outside Magnisia is not easily constrained.

due to extensive overlying Tertiary marine limestone cover (Figures 2-4a-c) and lack of exploratory adits. Boreholes from two sites within the vicinity of the Magnisia mineralisation do not intersect magnesite mineralisation (and/or extensive calcite or dolomite precipitates) below depths of 80m within serpentinite (Figures 3-2, 3-3). Boreholes AK2 and AK3 do not intersect the BST. It is uncertain exactly how deep the magnesite occurs but, assuming magnesite mineralisation remains restricted to serpentinite at depth, best estimates from field mapping indicate thickness of Zone I magnesite occurrence to be no greater than 80m (Lich and Maliotis, 1984).

Orientation of shear zone structures

The BST is marked by a 10-20cm thick shear zone developed in serpentinite, which exhibits a well defined contractional c-s fabric implying emplacement of serpentinite over gabbro and sheeted diabase dykes (Figures 3-4a,b, Plate 3-4, see also Plate 4-2). A few high-magnesian calcite veins, known to be genetically related to the magnesite mineralisation (see chapter 5), are present within the c-s fabric of the BST (Plate 4-2). When plotted on a lower hemisphere, equal area projection, poles to the c-planes and s-planes of the shear zone fabric lie in orientations which define a moderately east-dipping contractional shear zone with movement of the harzburgite hanging wall directed toward the west-northwest (Figure 3-4b). Groove lineations and fibrous packages of calcite on the walls of the calcite veins, which enhance the c-planes of the BST shear fabric, are oriented with a maximum statistical azimuth-plunge of 108/50°, the point maximum lies at approximately 90° to the intersection lineation defined by the c- and s-planes. These

grooves are therefore oriented in a direction consistent with the overall shear direction inferred for the BST

Large magnesite veins situated at various sites around Piana and Magnisia, lying structurally above the BST (Figure 3.2), also show groove lineations upon their vein walls. The veins are oriented with a north-south strike and with dips between 85°E and 90°, almost parallel to BST s-plane orientations (Figure 3.4b). Grooves upon these veins, affecting both magnesite fragments and the cryptocrystalline matrix, formed during relative displacement of the serpentinite and have azimuth-plunge orientations of 090/85°, which indicates a comparable displacement direction on these veins to the shear direction for the c-s fabric of the BST (Figure 3.4a,b).

3.2.2 Zone II Type Mineralisation

Zone II occurs throughout the large magnesite deposits in the area and is separated from Zone I by a low angle, eastward-dipping shear zone within the serpentinite above the magnesite veins and stockworks (Figures 3.1, 3.3). This intra-serpentinite shear zone (ISSZ) is characterized by a very fine-grained, light-blue, friable, sheared serpentinite which has been extensively carbonatised (Plates 2.6, 3.5). It occurs approximately 10m below the upper limit of the serpentinite sheet, varies from 2m to 7m in thickness and is interpreted as a shallow shear zone which formed during the main phase of contractional tectonism affecting the serpentinite. Sheared serpentinite in places grades upwards into uncarbonatised blocky serpentinite. Nodular magnesite has been precipitated mostly within this sheared serpentinite (ISSZ) (Plates 3.6, 3.7, 3.8), but is also present in the blocky serpentinite above the shear zone. A single small klippe of Ayios Photios Group sediments

at the top of the serpentinite sheet, at the base of the Limestone cover at the top of Zone II, contains small quantities of nodular magnesite precipitated in fractures and voids.

Nodular magnesite, which overgrows all shear fabrics in the serpentinite host rock, is definitive of Zone II mineralisation and belongs to a later magnesite forming episode (see chapter 4).

Zone II Structural Features

The lower and upper limits of the nodular precipitates are marked by the base of the ISSZ and the unconformable contact separating serpentinite from overlying marine limestone respectively (Figure 3.3). At the Magnisia mine the projection of the ISSZ at depth is constrained by the presence of sheared serpentinite containing nodular magnesite with small magnesite veinlets at depths from surface between 46m and 78m in borehole AK2, and between 62m to 67m in AK1 (Figure 3.2), as well as the distribution of nodular magnesite in the mine workings of Magnisia (Figure 3.3). The absolute limit of Zone II mineralisation at depth is unknown due to limited access, extensive carbonate cover sediments and lack of borehole data. The bluish colour of the carbonatised ultramafic rock is distinctive and the zone can be followed throughout an area which encompasses all the magnesite deposits (between Sandalides and Piana).

Kinematic indicators are present within the ISSZ in the form of c-s fabrics, but are less well developed than in the BST. The shear fabric of the ISSZ lies at a shallow angle with an inferred dip direction of $\sim 155^\circ$. At the Magnisia locality, the ISSZ lies at a shallow angle ($358/10^\circ\text{E}$) and horizontally dissects the magnesite deposit (when viewed from west in the main mine workings). The lower half of this deposit clearly shows Zone I type

mineralisation, while the upper half contains the nodular material typical of Zone II (Figure 3.3).

Unlike the veins and stockworks, magnesite within the ISSZ formed subsequent to any active tectonism affecting the serpentinite, and is seen to have nucleated within and subsequently overgrown the shear fabric. Magnesite nodules vary in diameter from centimetre scale up to 2m across (Plate 3.7). There are no sheared nodules present in the area.

No magnesite veins have been precipitated within the ISSZ, and the sheared serpentinite in Zone II contains no vein or stockwork material.

3.3 Other Carbonate Precipitates

3.3.1 Carbonate Precipitates in Serpentinite

Within this category are carbonate precipitates found overprinting magnesite mineralisation throughout the serpentinite which are far less pure than either magnesite veins or nodules. These recent precipitates form a 10cm thick carbonate crust and are comprised of cryptocrystalline 'chunks' of magnesium carbonate and high-magnesium calcite in a soft calcite matrix on the walls of adits (Plate 3.9). Dendritic iron hydroxide is present throughout the carbonate matrix. The more open structure of these precipitates may be due to formation upon a free surface (adit walls), as opposed to precipitation within sheared serpentinite. Such precipitates have formed within the past ten years as a result of the opening of the adits and are generally best developed at sites below the water table, 150-200m above sea level. The best occurrence of this type of carbonate formation is found in the small test adits at the base of the Magnisia mine. Similar occurrences are

noted from the north of the area near Sandalides (Figures 2.4a-c, 3.2). Blocks of marine limestone in and around the mineral deposits have been cemented together by relatively recent botryoidal magnesite precipitates.

Within brecciated fault zones in marine limestone above the magnesite deposits are small areas where breccia has been cemented together by cryptocrystalline carbonate precipitation. Small blocks of limestone which have fallen downhill onto outcropping serpentinite appear to have been cemented onto the substrate by botryoidal magnesite. The blocks of limestone lie on the exposed serpentinite hillside and so were probably cemented recently.

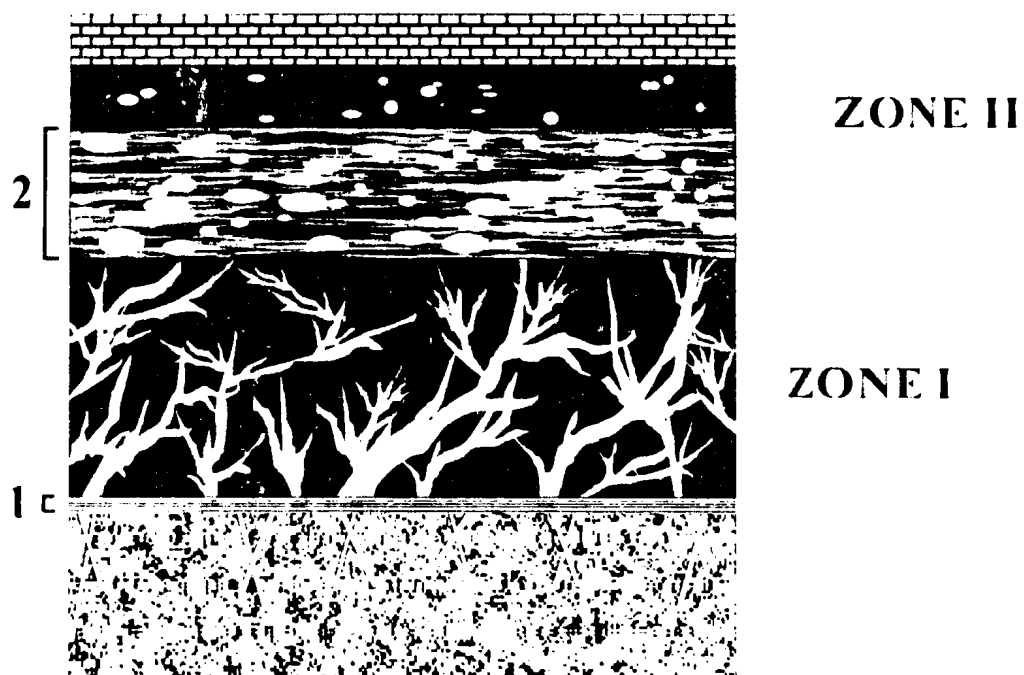
In one locality, circulating groundwater is precipitating fine laminar sheets of carbonate on the sides of a small cave within the serpentinite (Plates 3.10, 3.11). This material, from petrographic examination, is an Fe-rich dolomite, a very unusual occurrence for such a site. Usually one might expect travertine or a calcite tufa (Barnes and O'Neil, 1969, Gribble and Hall, 1985).

The process of carbonate mineralisation in this area is therefore of a continuous nature.



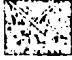
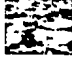

3.3.2 Carbonate Mineralisation in Footwall of BST

Calcite veining is developed within a set of conjugate shear fractures in gabbro which lies immediately beneath the serpentinite body containing magnesite mineralisation (Plates 3.12 & 3.13). These veins terminate against the thrust plane between the gabbro and serpentinite. Grooves on the veins indicate relative dip-slip displacement along the conjugate shear fractures in the gabbro subsequent to vein precipitation, possibly induced

by either vertical loading during thrusting, or unloading due to extension in the Polis Graben. The veins show marked similarities to some magnesite and high-magnesium calcite veins of Zone I mineralisation such as well developed median-lines along veins and "comb" textures (see chapter 4). It is unsure whether these calcite veins are syngenetic with Zone I mineralisation. Detailed vein orientation data and lineation orientations, relative to the serpentinite shear zone above the calcite veins and graben-related faulting, would be required to link the formation of these veins to either thrusting or extensional tectonism.



Legend

-  Unconformable marine limestone
-  Serpentinite with magnesite veining
-  Gabbro with calcite veining
-  Sheared serpentinite with magnesite nodules
-  Sheared serpentinite with calcite veining

1:- Basal Serpentinite Thrust (BST)

2:- Intra Serpentinite Shear Zone (ISSZ)

Figure 3.1 Schematic illustration of Zones I and II within serpentinite. All deposits exhibit mineralisation of Zone I-type, Zone II-type, or both.

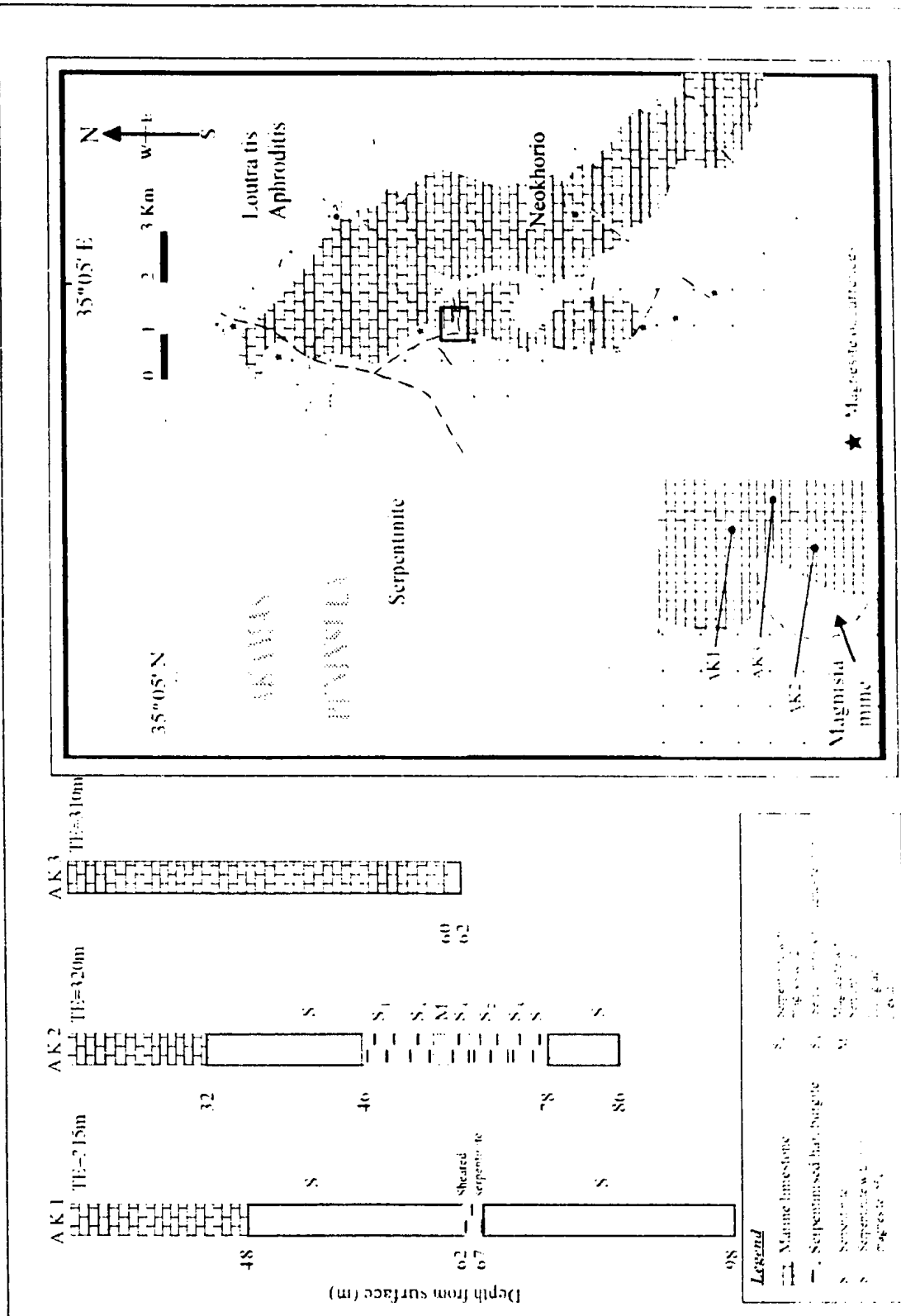
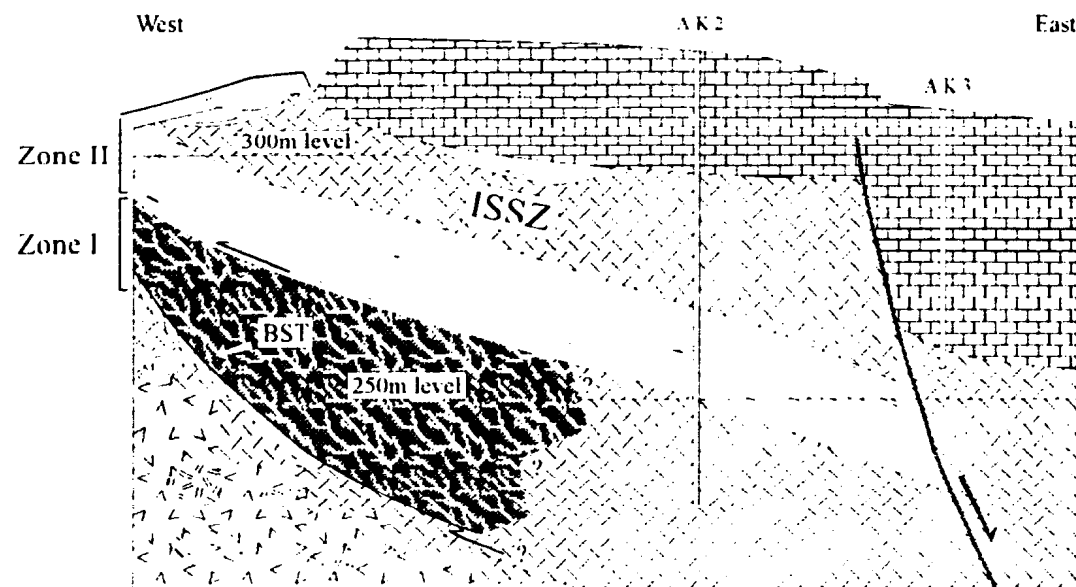


Figure 3.2 Diagram showing borehole logs from the Magnisia site. Data were obtained from the Hellenic Mining Co., Nicosia, Cyprus.



Legend

- | | |
|-----------------------------|-----------------------------|
| Marine limestone | Mamonia rocks |
| Serpentinised harzburgite | Vari-textured gabbro |
| Highly sheared serpentinite | Thrust fault / normal fault |
| Sheeted diabase dykes | C-S shear fabric |

0 50m
Vertical / horizontal scale

Figure 3.3 Schematic cross section through the Magnisia deposit

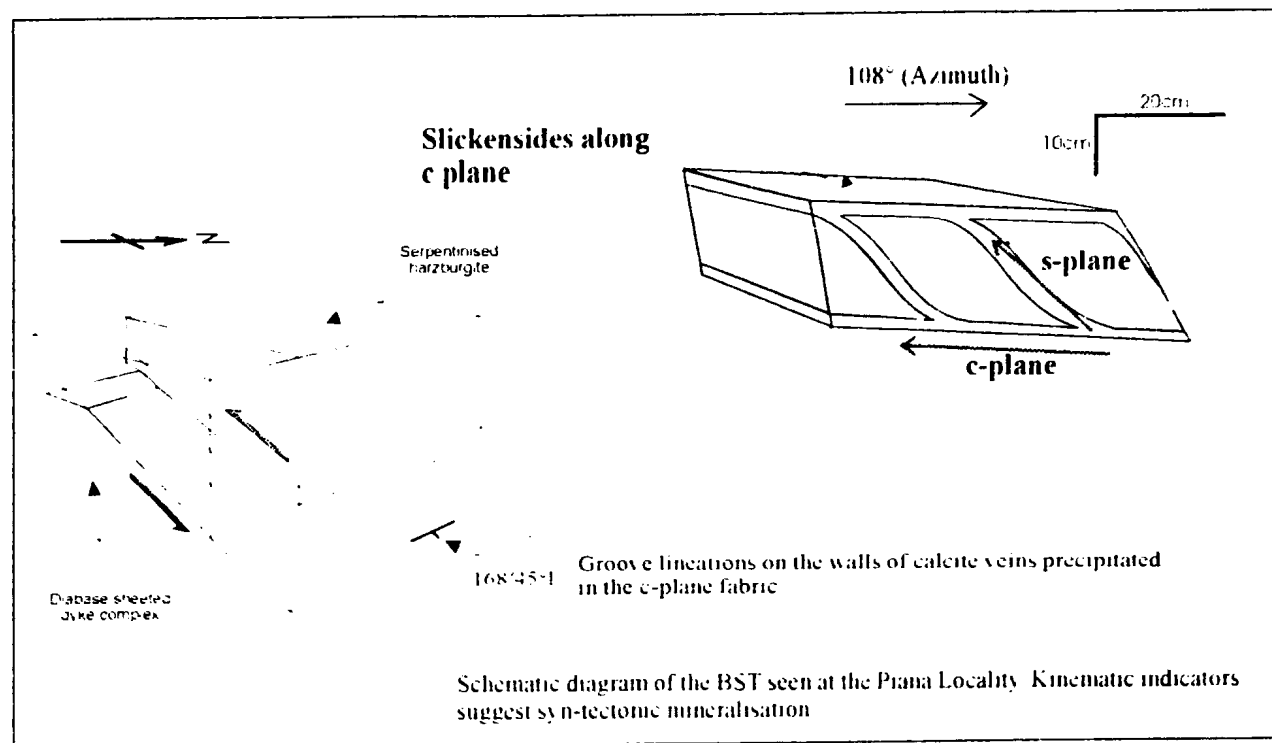
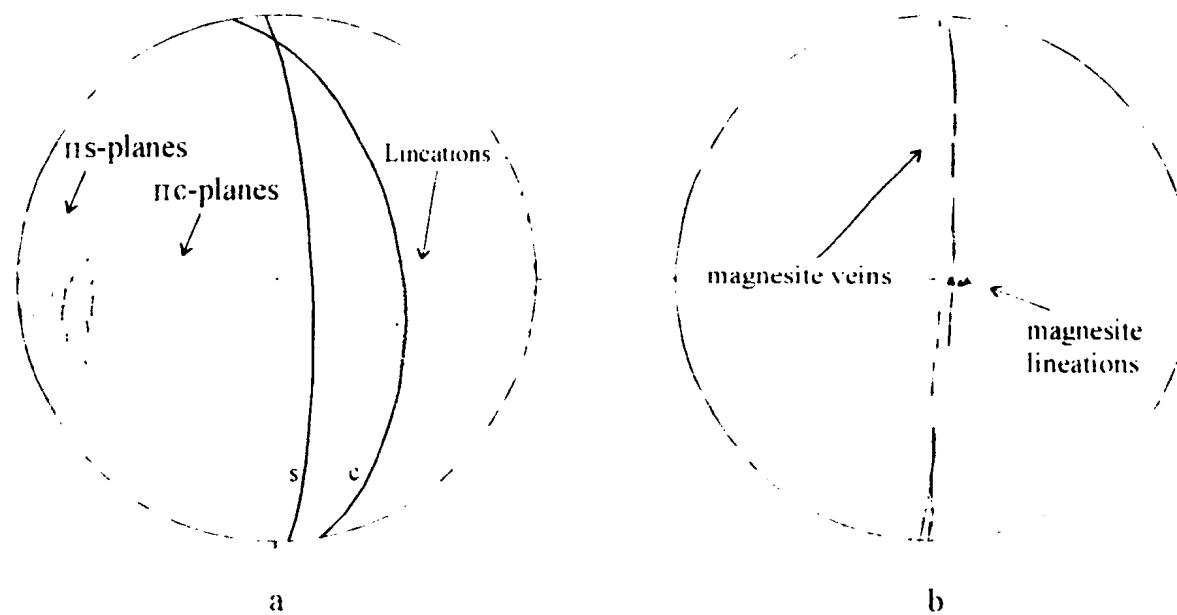


Figure 3 4a The relationship between kinematic indicators within the Basal Serpentine Thrust (BST) and carbonate veins associated with mineralisation

Equal area lower hemispherical projections of magnesite data.



Contours: 1 10 20 30 40 50 60 70 80 times uniform distribution

Figure 3.4b a) Stereoplot of c-planes, s-planes and lineations measured on c-planes,
b) Stereoplot showing the orientation of large magnesite veins and groove lineations
on those veins



Plate 3.1 Large cryptocrystalline magnesite vein within Zone I of the Piana locality. Lens cap for scale.



Plate 3.2 Sample of vein magnesite taken from the base of the Magnisia locality. Coin for scale (diameter 10mm).

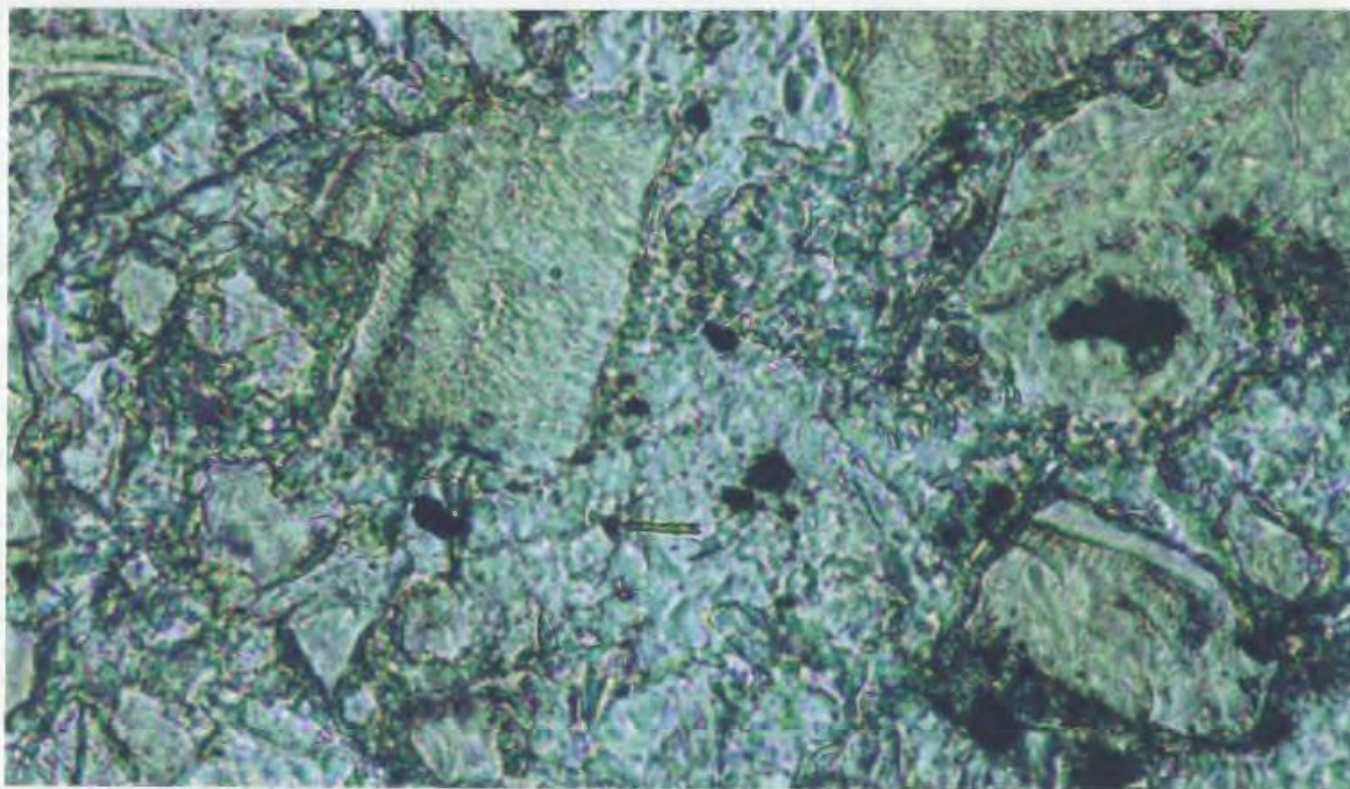


Plate 3.3 Photomicrograph of brecciated vein material which has been cemented by further magnesite precipitation. Plane-polarised light. Field of view is 5mm.



Plate 3.4 Close view of BST showing strongly developed shear fabric. BST is 20cm thick at this point. Gabbro in footwall. View to north. Key for scale.

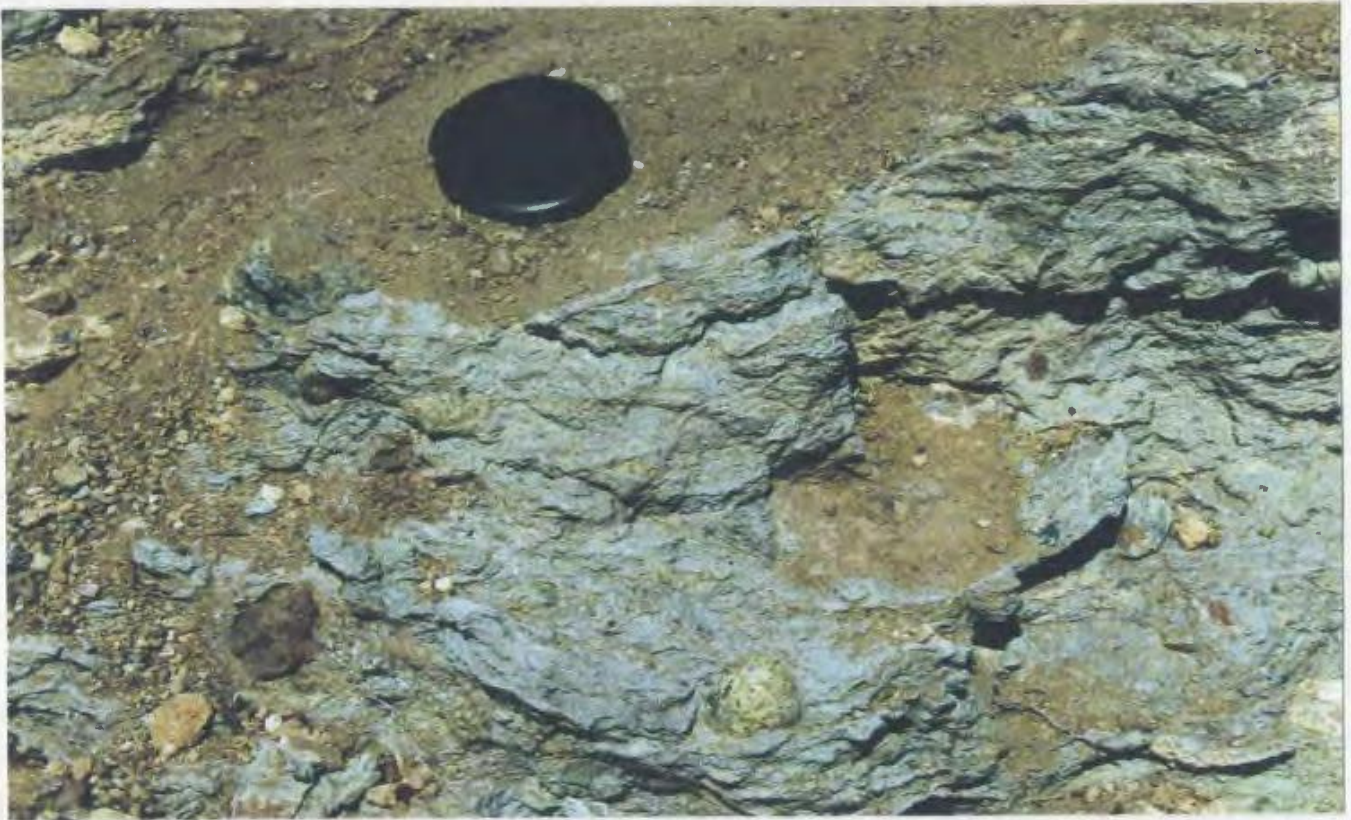


Plate 3.5 Sheared, carbonatised serpentinite of the ISSZ which has incorporated Mamonia mudstones, gabbro and diabase.

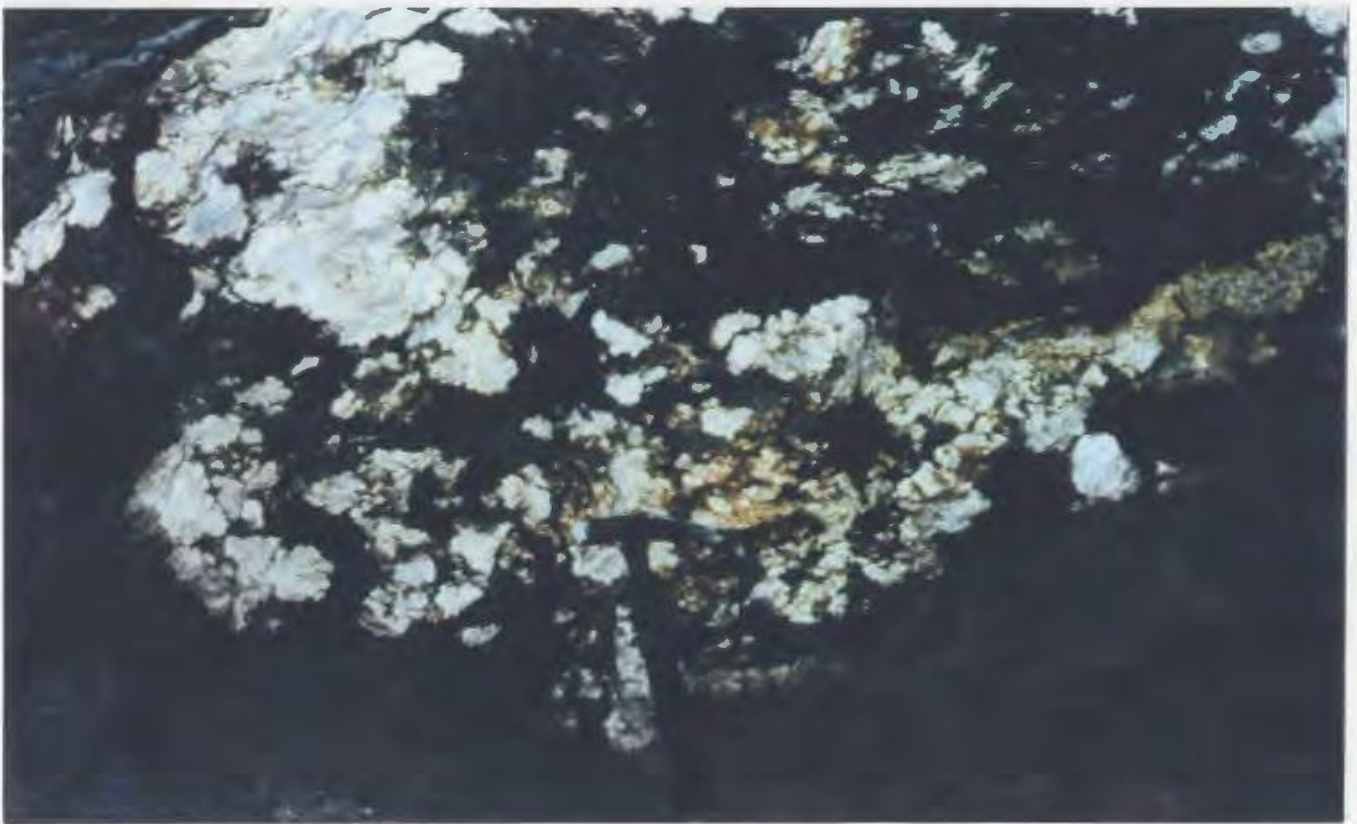


Plate 3.6 Nodular magnesite within a mining adit in Zone II of the Magnisia deposit. Nodule size varies from millimetre to metre scale. Hammer for scale.

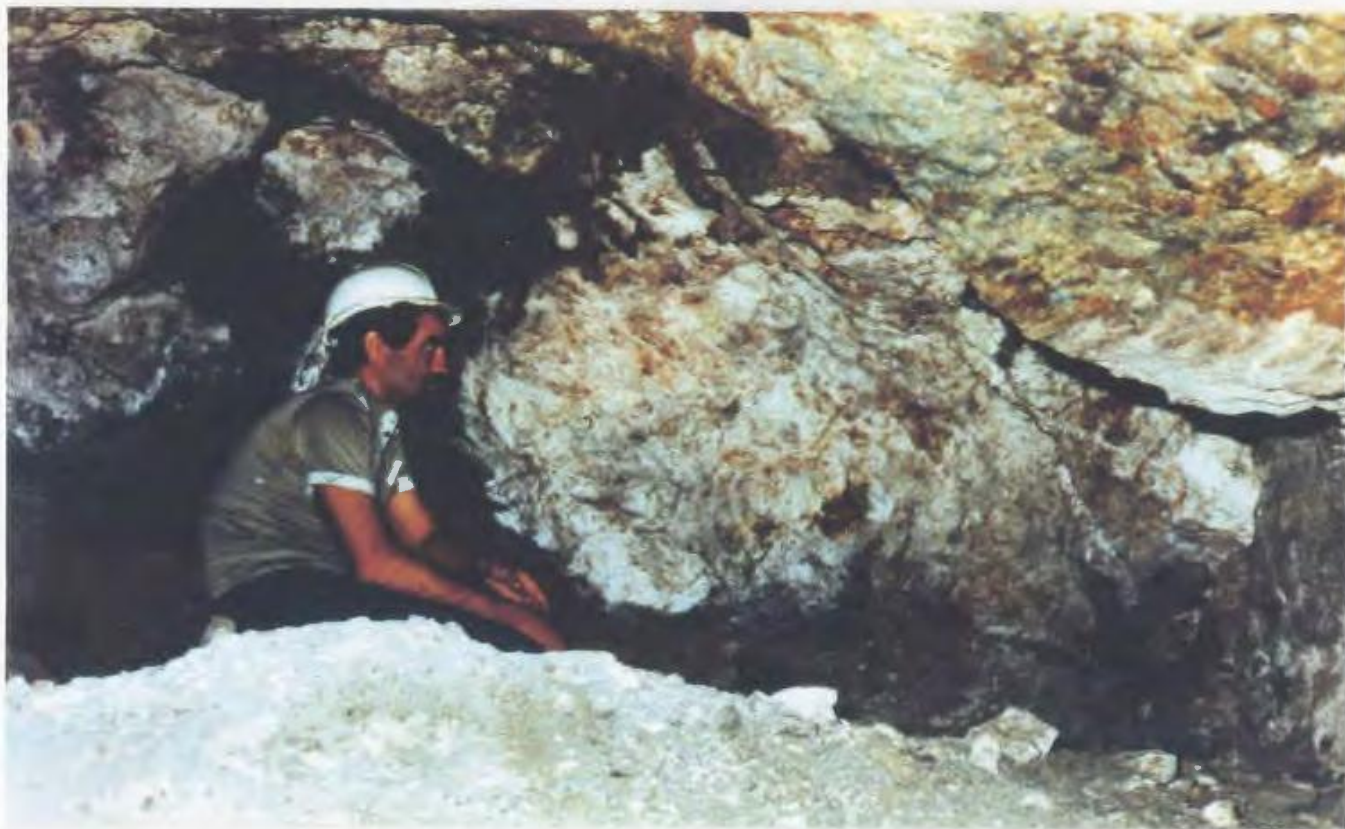


Plate 3.7 Large magnesite nodule within Zone II of the Magnisia locality. This nodule is approximately 1.5m in diameter. Hard hat for scale.



Plate 3.8 Hand specimen of nodular magnesite. Finger for scale.

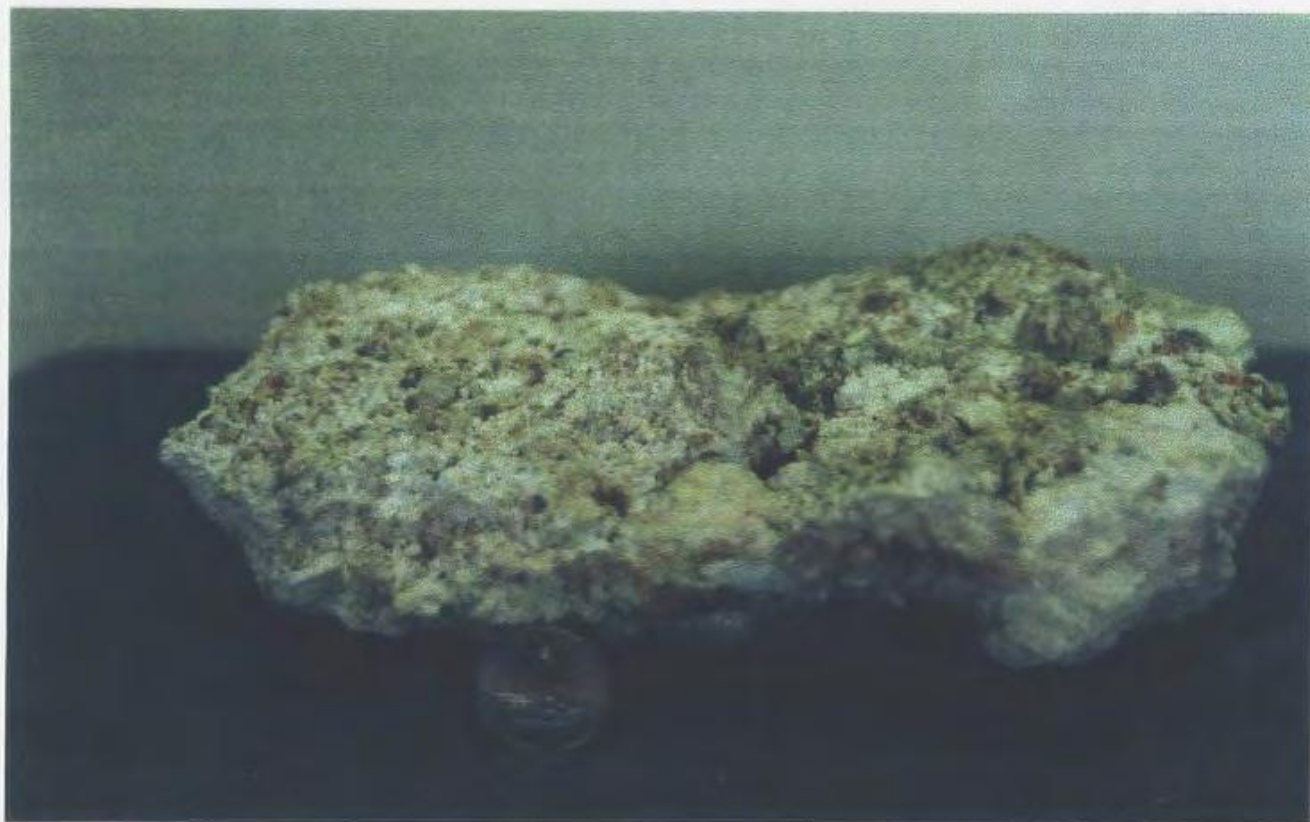


Plate 3.9 A sample of the high-magnesium calcite/magnesite precipitate found on the walls of mining adits in the Magnisia area. Coin for scale.



Plate 3.10 Outcrop of laminar precipitate found precipitating within a small cave in serpentinite. Lens cap for scale.



Plate 3.11 Hand specimen of laminar dolomite. Coin for scale.



Plate 3.12 Calcite veins precipitated within fractured gabbro, just below the BST. Veins are an average thickness of ~3cm.



Plate 3.13 Close view of calcite veins in gabbro. Key for scale.

4.0 PETROGRAPHY

4.1 Introduction

A petrographic study of ore minerals (magnesite from Zones I and II) and other vein precipitates, serpentinite and spatially-related lithologies in the area of interest was undertaken in order to establish the relationship between the magnesite mineralisation and the serpentinite in which it is found. The same samples used for petrographic examination were subsequently used for isotope and trace element analyses.

It is clear from chapter three that Zone I calcite veins precipitated in the shear fabric of the Basal Serpentinite Thrust (BST) during contractional tectonism. For this reason these veins were examined for evidence of syntectonic precipitation. Vein magnesite (consisting of re-cemented fragments of cryptocrystalline magnesite) within Zone I was examined for evidence of a multiple precipitation history. Magnesite-cemented limestone clasts and cryptocrystalline magnesite found in voids within overthrust Mamonia mudstones (at the top of Zone II) were also studied petrographically.

Relative timing of mineralisation, as well as the presence of several generations of magnesite, was established in the field and was verified petrographically.

4.2 Description

The following section will deal with magnesite samples and other related lithologies. Many magnesites were examined but certain ones appear representative of each zone

4.2.1 Zone I Magnesite

All Zone I magnesite samples exhibit vein magnesite within fractured and brecciated serpentinite. This section deals with vein magnesite taken from the Magnisia deposit.

Sample c-s (BST fabric)

In hand specimen, calcite veins are present along both c- and s-planes within the c-s shear fabric of the BST. They range in thickness between 3mm and 0.5cm, and are continuous throughout the fabric (see section 3.2, chapter 3). These veins show lineations such as grooves and fibrous calcite packages where the vein walls are in contact with wallrock, particularly along the c-plane (Plates 4.1, 4.2, 4.3). The veins themselves are made of material not present in the immediate wallrock and so are presumed to be antitaxial in nature.

Petrographically, in plane-polarised light, the calcite veins appear light in colour with medium relief and are surrounded by light-brown, sheared serpentinite. Under cross-polarised light, veins are highly birefringent. For the most part, the veins show well developed fibrous mineral growth ("comb texture" (Hodgson, 1989)) perpendicular to the c- and s-planes developed in the wallrock. Median lines, enhanced by the presence of iron hydroxides along the length of the veins, are ubiquitous in veins thicker than 2mm (Plates 4.1, 4.3). Small fragments of spalled wallrock are found in zones in the outer borders of veins, and are aligned parallel to the vein-wallrock contact. In some localities, well developed "ladder vein" networks are common (Hodgson, 1989) (Plates 4.4, 4.5).

Rarely, calcite veins present in the c- and s-planes of the shear zone exhibit angular extinction relative to the vein edge. Calcite extinction is inclined anticlockwise from base to top of each vein in the fabric. It is along the contact surfaces of these veins with wallrock that grooves occur. Also, some veins show stretched fibres and are fractured, indicating minor reworking after formation.

Sample 2C15 (magnesite veining in serpentinite)

Sample 2C15 is magnesite taken from a large vein in Zone I of the Magnisia locality. This sample clearly shows the relationship between magnesite veins and serpentinite where magnesite comes into contact with the ultramafic wallrock.

Magnesite is present throughout the sample and has pervasively mineralised wallrock utilizing any fractures and planes of weakness present in the ultramafic material (Plates 4.4, 4.5). Magnesite mineralisation here has the appearance of a typical "ladder vein network" (Hodgson, 1989). Fragments of serpentinite and serpentine minerals (lizardite and chrysotile) are found enclosed within the cryptocrystalline magnesite (Plates 4.6, 4.7). Certain of these enclosed serpentinite fragments contain micro-veins of magnesite (on less than a millimetre scale) which have apparently been physically separated by magnesite formation. Some magnesite veins in more competent serpentinite, up to a few millimetres in thickness, are brecciated and displaced (Plates 4.8, 4.9).

Sample mx (re-cemented magnesite vein)

Sample 'mx' is made up of a number of angular, cryptocrystalline magnesite clasts which are supported in a matrix of fine-grained magnesite (Plate 3.3). The early, blocky fragments have a characteristic comb texture preserved. These brecciated pieces of

magnesite show evidence of fracturing and displacement and are therefore suggested to be the result of the brecciation of magnesite vein material, with subsequent cementation of the fragments during further magnesite formation.

4.2.2 Zone II Magnesite

This section describes nodular magnesite taken from the centre of the ISSZ in Zone II (Plates 4.10, 4.11). Sample JBN1 was taken to be most representative of Zone II mineralisation.

Sample JBN1 (nodular magnesite in sheared serpentinite)

Sample JBN1 is characteristic of Zone II mineralisation as nodules are seen to overgrow the sheared serpentinite (Plates 4.12, 4.13, 4.14, 4.15). Petrographically, the serpentinite shows abrupt termination without any other distortion of serpentinite at the edges of the nodular magnesite (botryoidal). Opaque minerals (e.g. iron hydroxide) are precipitated as dendrites throughout the nodules.

These observations indicate formation of nodular magnesite after any active displacement of serpentinite in the shear zone. The magnesite nodules of Zone II therefore define a generation of magnesite formation later than that of Zone I magnesite.

4.2.3 Other Carbonates

Sample X14 (calcite veining in gabbro)

Sample X14 is calcite which was precipitated as veins in conjugate fractures in gabbro (lying immediately beneath the BST). In hand specimen the walls of these calcite veins are grooved adjacent to wallrock, but show no evidence of internal shearing (Plates 3.12, 3.13).

In thin-section, the sample illustrates fibrous calcite growth from the edges of fracture walls perpendicular to the walls, with a gap of up to 1mm at the centre of each vein. Iron-hydroxide is present as layers within the veins (parallel to wallrock) and appears to have been formed periodically during repeated stages of dilation and calcite fibre growth, i.e. crack-seal mechanism (Hodgson, 1989, Sibson, 1990). The vein texture and microstructure of these calcite veins are similar to the calcite veins present in the c-s fabric described in section 4.2.1 (Plates 4.1-4.3).

Sample 2C12 (calcite and dolomite within magnesite veining)

Calcite and dolomite have nucleated upon fine-grained magnesite and are precipitated in radial fashion from the edges of voids and fractures within the magnesite veins of Zone I, serpentinite and mudstone (Plates 4.16, 4.17).

This feature is found throughout all of the samples taken from Zone I, and is most pronounced close to the contact with overlying marine limestone. Thus the calcite and dolomite are believed to be epigenetic in nature, probably derived through dissolution of the marine limestone above the deposits.

Fossiliferous marine limestone

This limestone exhibits many rugose coral fragments cemented by a mixture of fine-grained calcite, dolomite and minor magnesite (Plates 4.18, 4.19). Voids inside corals have been filled by calcite precipitation.

A basal conglomerate associated with this limestone (Sample "cong1") contains small rounded clasts of serpentinite, mudstone, diabase and coral fragments.

4.2.4 Recent Precipitates

Sample PPT1 (cave precipitate)

A 5cm thick laminar precipitate of high-magnesium calcite/dolomite was collected from a small cave within serpentinite, where carbonate was found precipitating from circulating groundwaters (Plates 4.20, 4.21). The cave lies in Zone I of the magnesite mineralisation, below the water table. The calcite tufa is layered and reaches a maximum thickness of 7cm, with each carbonate layer being approximately 1.3mm thick.

In thin-section, the calcite is seen to have radial extinction and has precipitated perpendicular to the serpentinite substrate (Plate 4.21). Various small clasts consisting of serpentinite, chert, limestone, diabase and mudstone are enclosed within successive calcite layers. These clasts probably adhered to the surface of the carbonate during its formation. Where clastic material has been trapped, later tufa growth is perpendicular to the outer edges of each clast (in radial fashion).

Distinct layers occur throughout the tufa and are marked by a brown opaque material. Above these layers, new calcite growth is initiated as at the base (upon serpentinite), and so they are identified as erosional surfaces formed during times of no calcite precipitation.

Sample PPT2 (Chunky precipitate)

Carbonate precipitated on the walls of mining adits contains chunks of cryptocrystalline magnesite cemented by a matrix of soft, friable, fine-grained calcite and interlaced with dendritic iron hydroxide (Plate 4.22). This precipitate is fissile and mantles the adit below the water table, reaching a thickness of 10-15cm. This carbonate material is

not considered merely waste magnesite fragments, which have adhered to wet adit walls during mining, because they are petrographically distinct from either Zone I or Zone II magnesite samples

In cross-polarised light the carbonate chunks appear dark brown, with lighter patches of fine-grained calcite (Plate 4.23). Some early "carbonate chunks" appear to have nucleated upon the serpentinite substrate, while later chunks formed within voids in the carbonate crust. All chunks are rich in iron-hydroxide which is present at various stages throughout the growth of each piece of magnesite. This opaque mineral reveals the growth pattern of the chunky material to be laminar in nature. Many interfering growth patterns are seen between neighbouring chunks.

4.3 Summary

From petrographic examination, the relationship between magnesite and all other lithologies and minerals within the magnesite deposits is clear. Samples from Zone I show pervasive magnesite vein mineralisation of fractured and brecciated serpentinite. Injection along planes of weakness is common. Field observations show the same relationship between magnesite and serpentinite on a larger scale.

From the physical distribution of calcite veins in the Basal Serpentinite Thrust, lineations on these calcite veins, the orientation of large magnesite veins, and isotopic evidence relating calcite veins to magnesite mineralisation (see chapter 3, Figures 3.4a, b; chapter 5, section 5.3.4), it is likely the formation of the calcite veins and magnesite mineralisation are genetically linked. These calcite veins show well defined dilatancy and fracturing of the serpentinite with associated precipitation of veins along both c- and s-

planes of the shear fabric. The veins have "comb textures" and include serpentinite wallrock fragments. Some of these veins show a limited amount of stretching after formation. One sample of vein magnesite (mx) contains angular fragments of cryptocrystalline magnesite, ranging in size between 0.5mm and 1cm, which are supported in a matrix of cryptocrystalline magnesite.

Zone II magnesite nodules clearly overprint sheared serpentinite within the ISSZ. Nodular magnesite (in places) also overprints some magnesite veins, but this is restricted to the upper reaches of Zone I. Texturally, magnesite nodules are clearly related to nucleation with the serpentinite, as opposed to replacement of previous concretions. Zone II magnesite has overgrown sheared, carbonatised serpentinite, and no nodules examined show deformation or evidence of shearing. It is unknown when the nodular magnesite began to form, only that it must have been after all tectonic activity affecting the serpentinite had ceased. In contrast to the dilatant, antitaxial nature of veins injected into the serpentinite of zone I, nodular magnesite in Zone II is, overall, a replacement style of mineralisation within the serpentinite shear zone. These nodules therefore define a younger generation of magnesite growth compared to the veins and stockworks.

The formation of Recent carbonates as crusts on adit walls in the study area (magnesite, calcite and dolomite) may signify either the latest phase of carbonate mineralisation, or the continuance of Zone II-type carbonate formation.

Calcite and dolomite in fractured magnesite veins, serpentinite and mudstone are epigenetic in nature and are most likely the result of dissolution of the overlying marine

limestone by circulating groundwaters as these epigenetic carbonates are most pronounced close to the limestone.

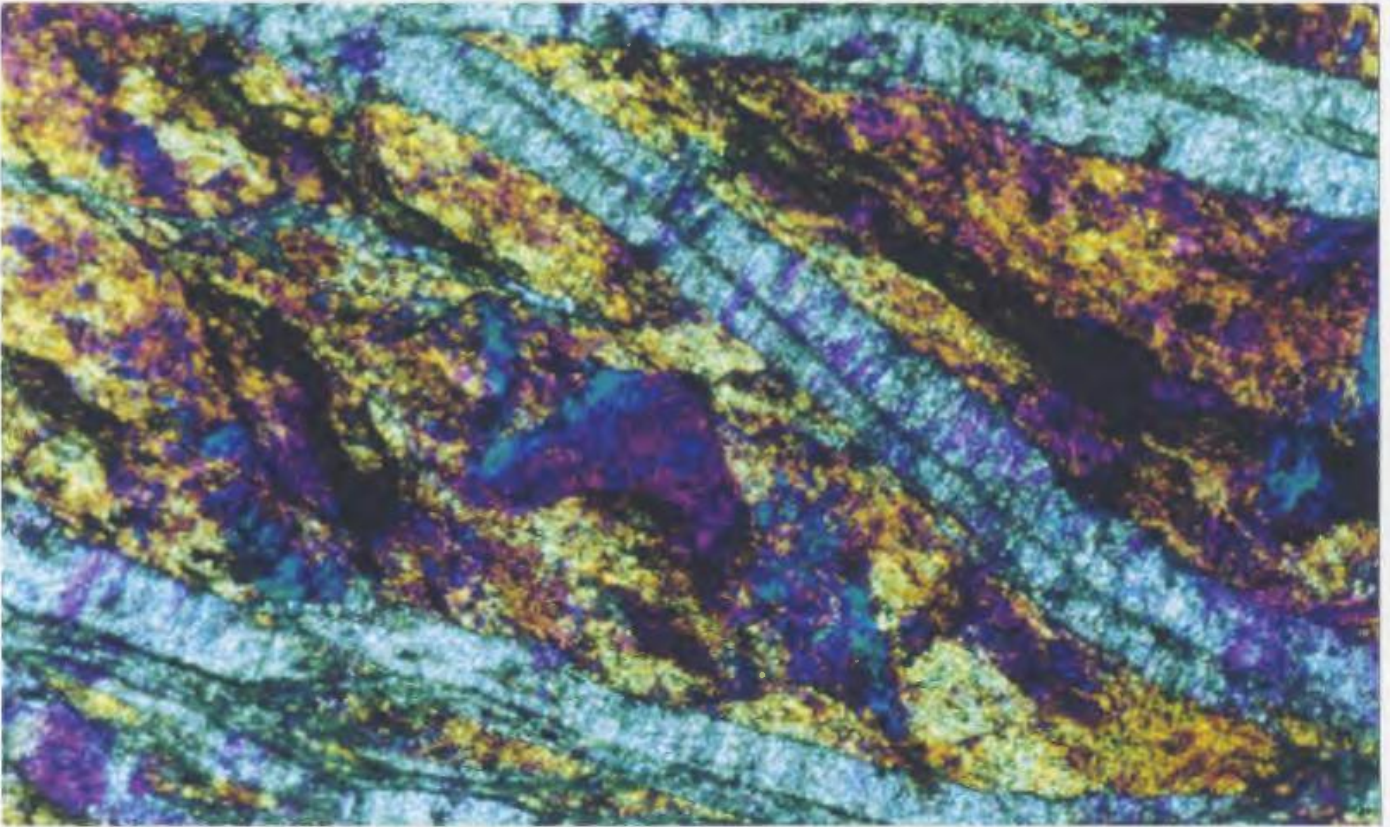


Plate 4.1 Dilational calcite veins in the c-s fabric. Quartz-sensitive plate was used to illustrate orientation of crystal fibres. Serpentinite groundmass is sheared. Note the well developed median lines. Cross-polarised light. Field of view 5mm.

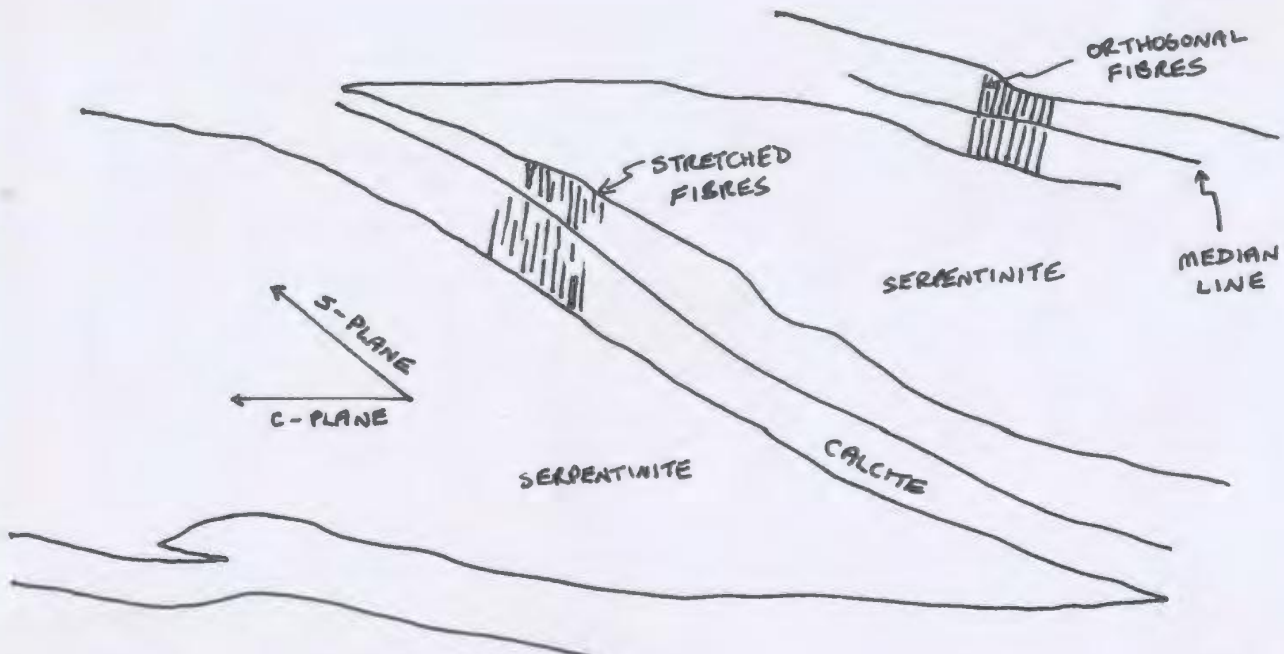




Plate 4.2 Well developed c-s fabric of the Basal Serpentinite Thrust (BST). Calcite veins enhance the serpentinite shear fabric. Key is 3cm long.



Plate 4.3 Thin-section of dilational calcite veins with well developed median lines in serpentinite shear fabric. Cross-polarised light. Field of view 5mm.

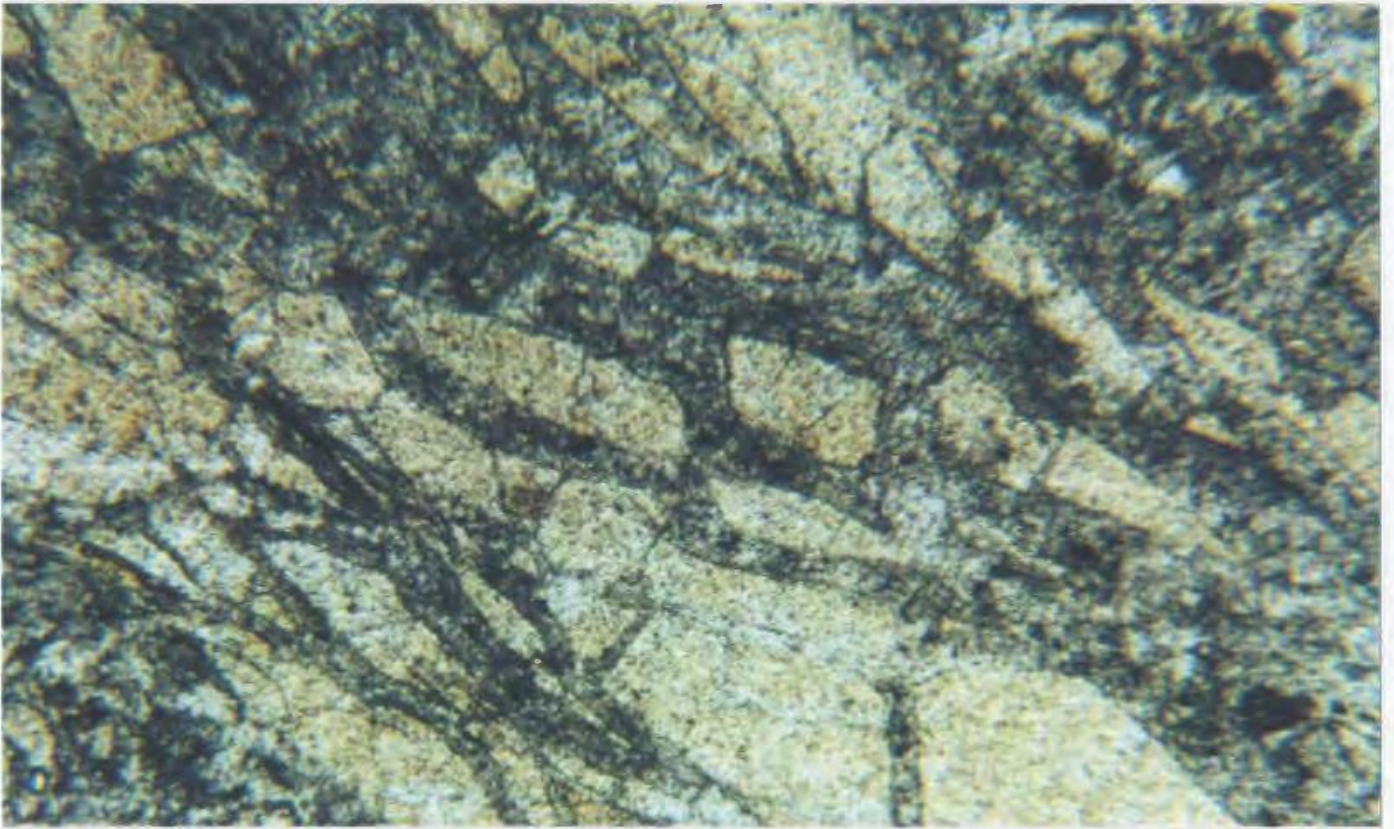


Plate 4.4 Cryptocrystalline magnesite veining in serpentinitised harzburgite. Note the brecciated texture of the wallrock. Plane-polarised light. Field of view 5mm.

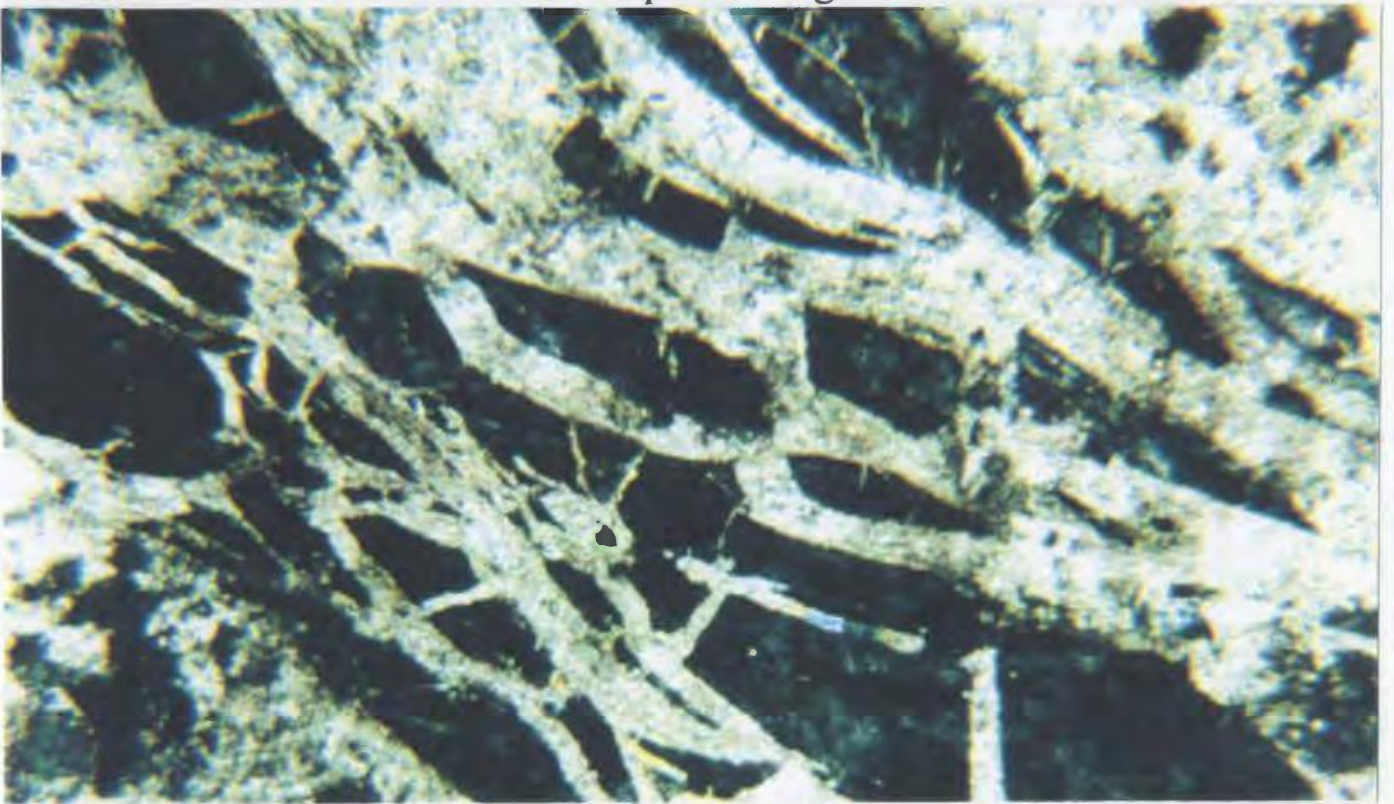


Plate 4.5 Same view as above, but in cross-polarised light. Magnesite veining in serpentinite fragments is clearer here. Note overall brecciated appearance of wallrock. Field of view 5mm.

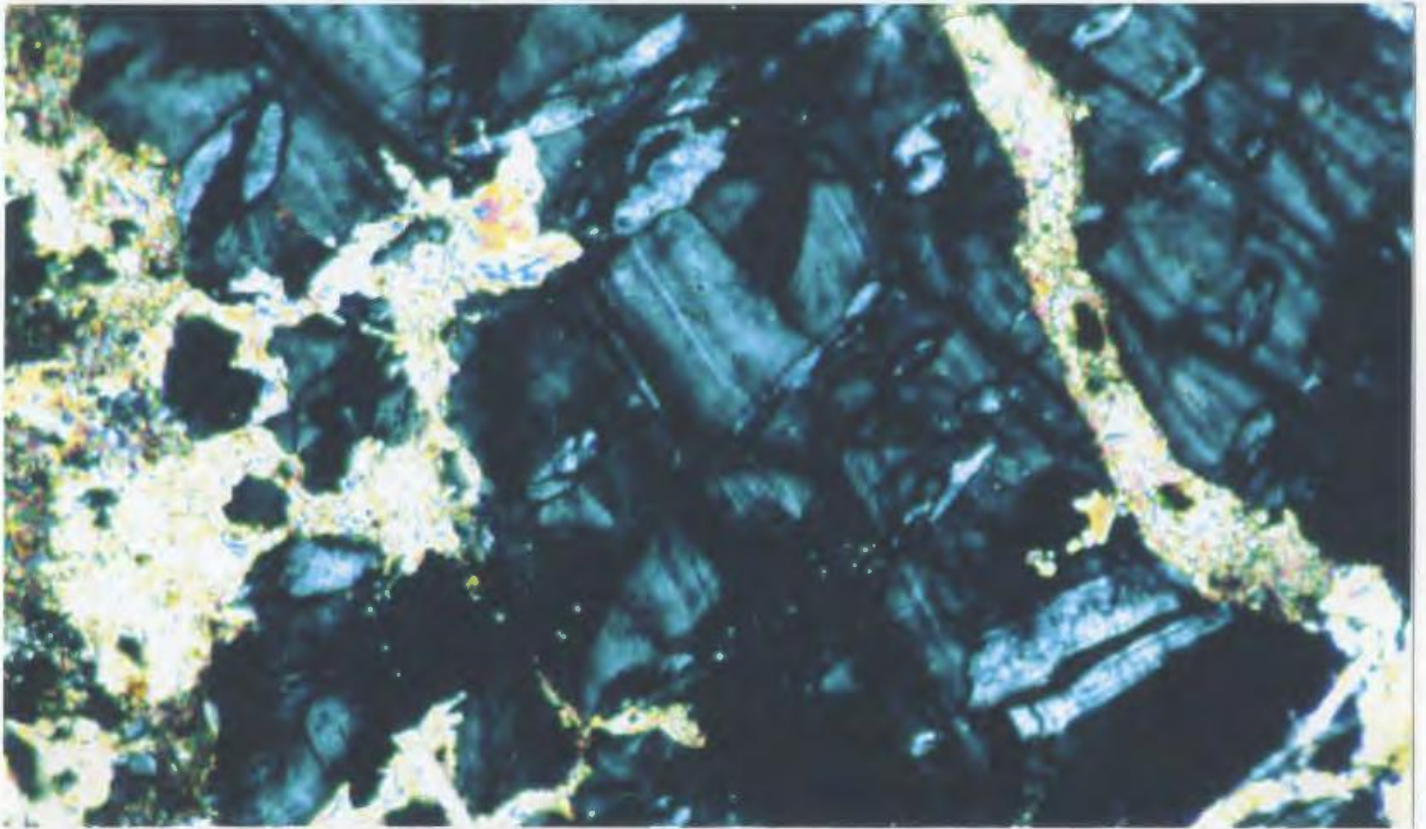


Plate 4.6 Magnesite precipitated in competent serpentinite. Magnesite has been precipitated within voids and fractures. Cross-polarised light. Field of view 3mm.

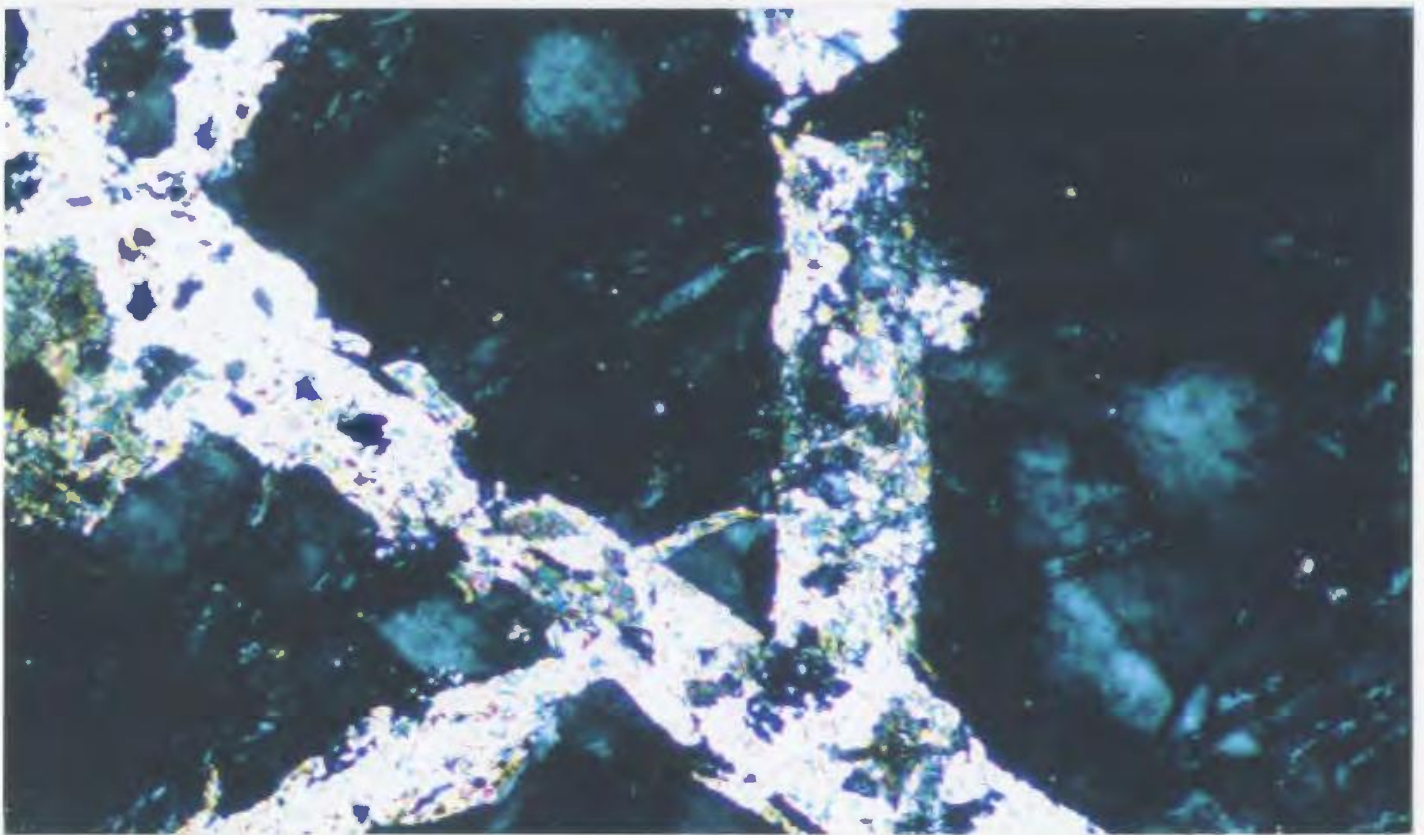


Plate 4.7 Inclusion of serpentine minerals from the wallrock within magnesite veins. Cross-polarised light. Field of view 3mm.

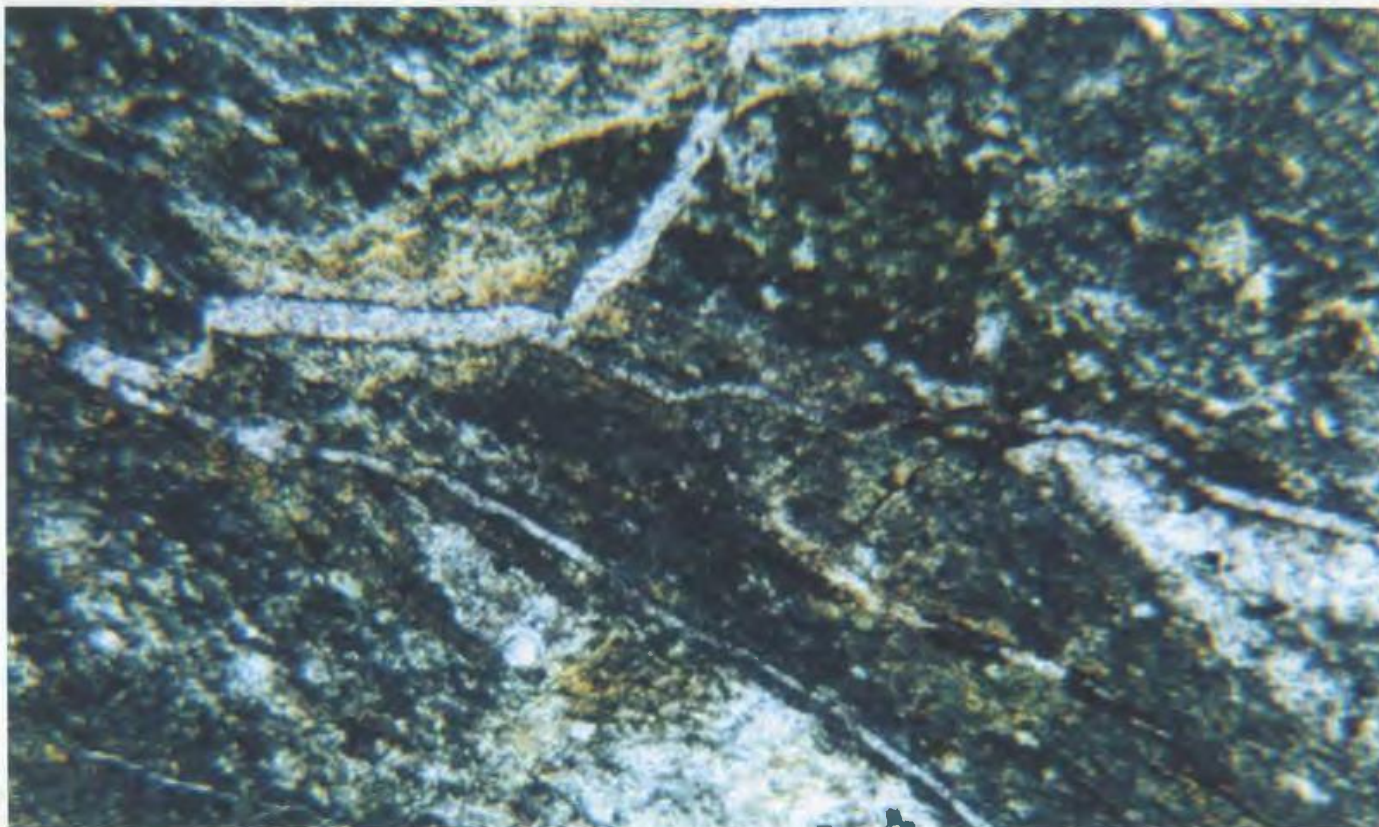


Plate 4.8 Magnesite vein within serpentinised harzburgite showing brittle deformation. Note specifically cataclastic shear of vein in left bottom quarter of picture. Cross-polarised light. Field of view 3mm.

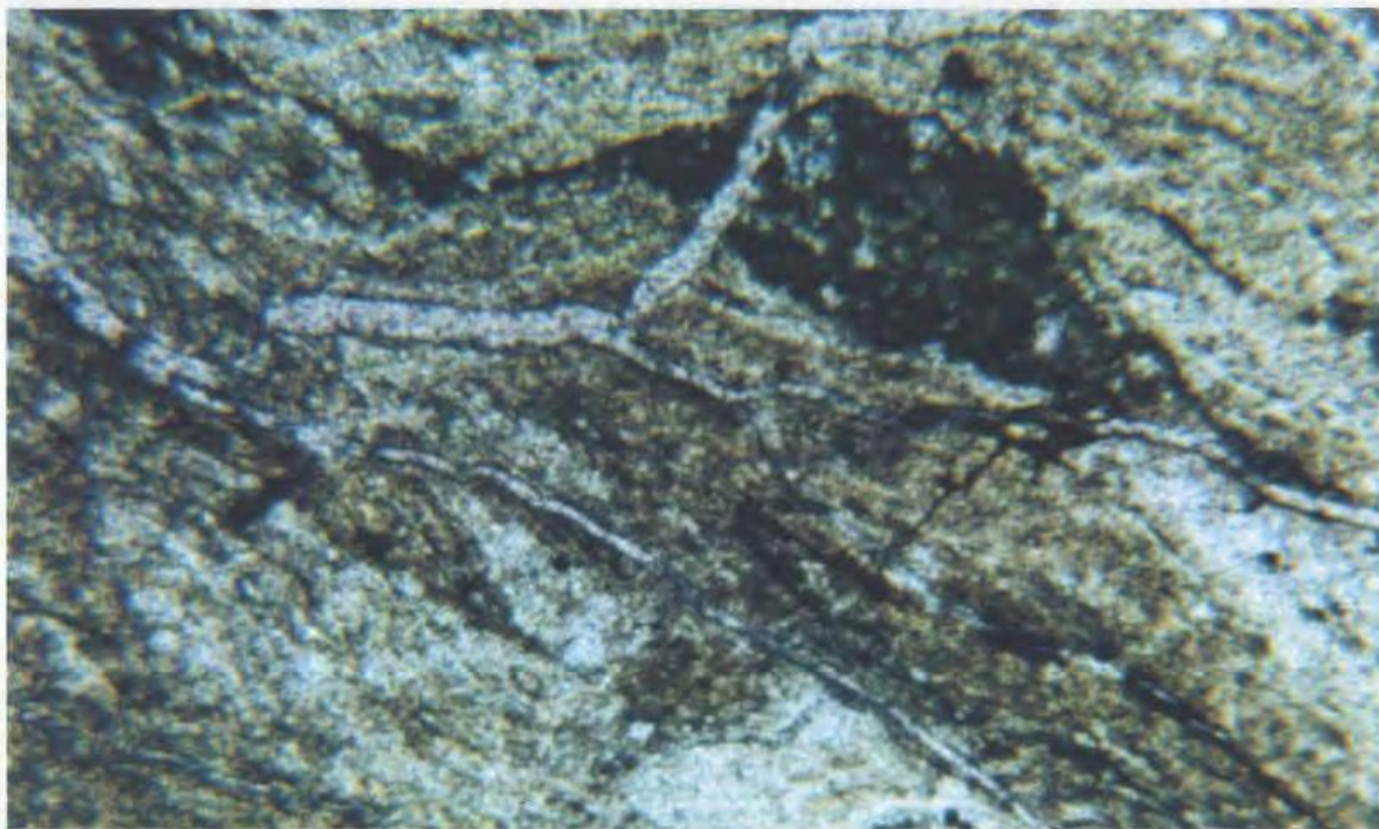


Plate 4.9 Same view as above but in plane-polarised light. Field of view 3mm.

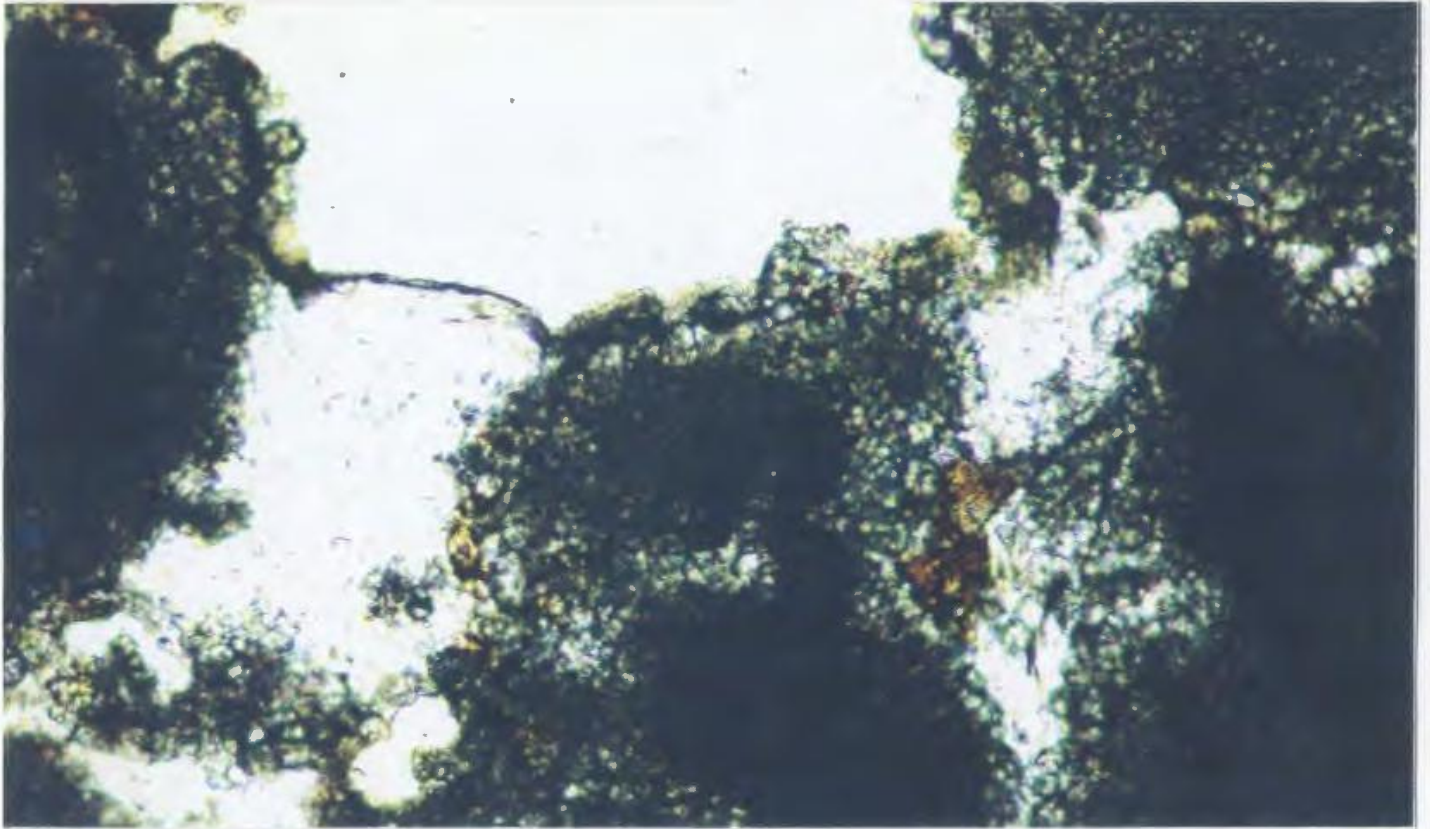


Plate 4.10 Fine-grained nodular magnesite in thin-section. Plane-polarised light. Field of view 5mm.

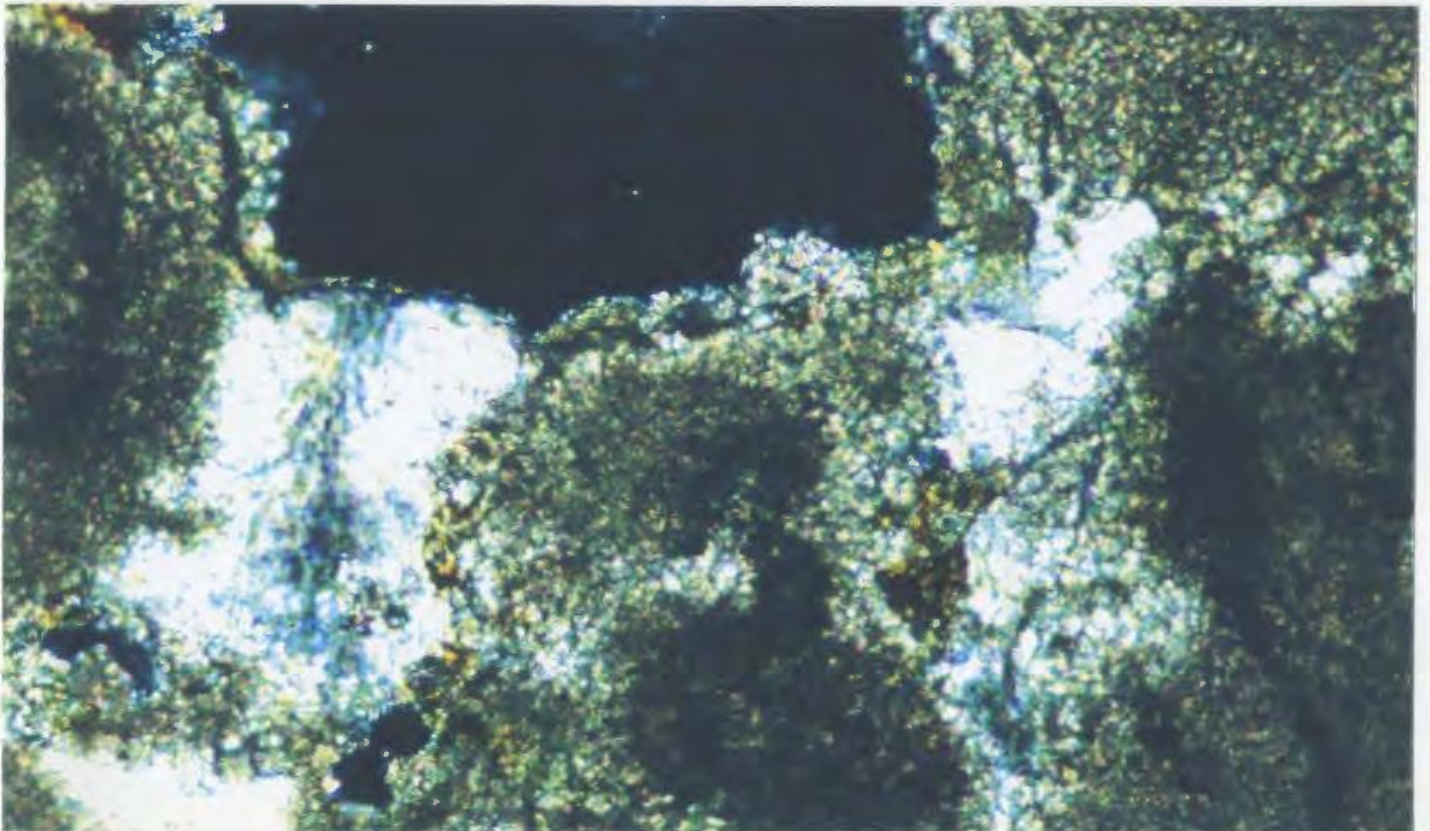


Plate 4.11 Same view as Plate 4.10, but in cross-polarised light. Field of view 5mm.

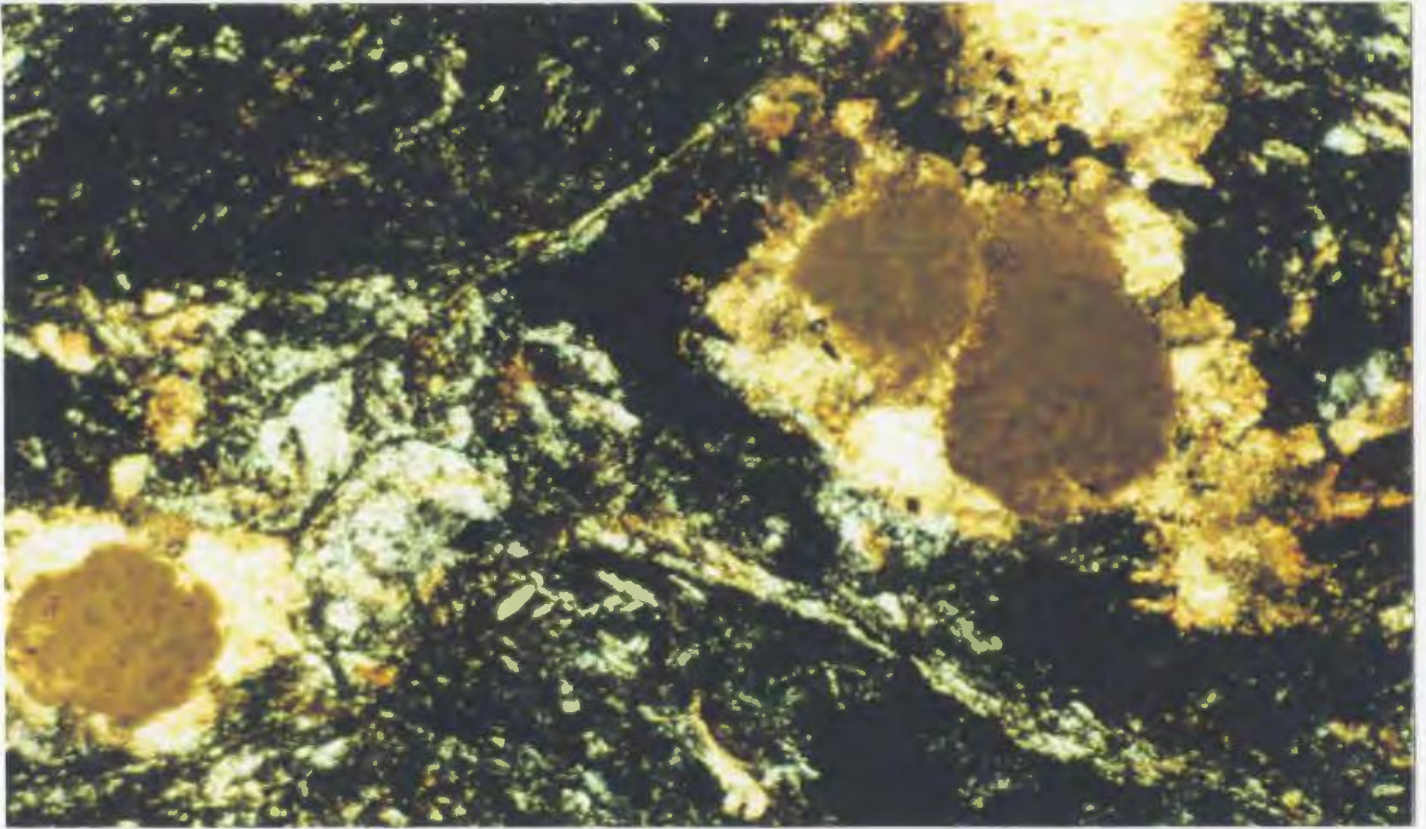


Plate 4.12 Two magnesite nodules overprinting sheared serpentinite. Cross-polarised light. Field of view 1cm.

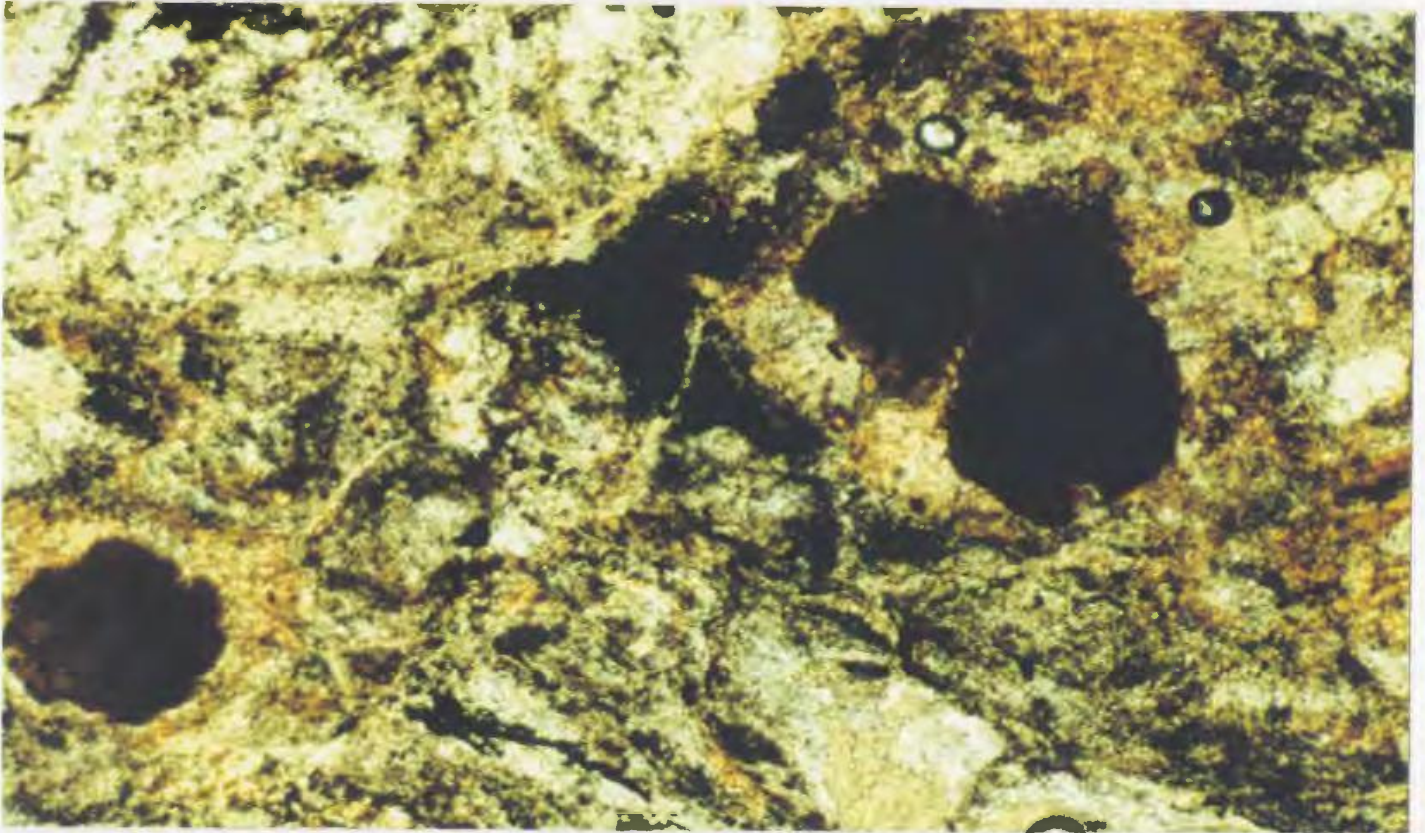


Plate 4.13 Same view as 4.12, but in plane-polarised light. Field of view 1cm.

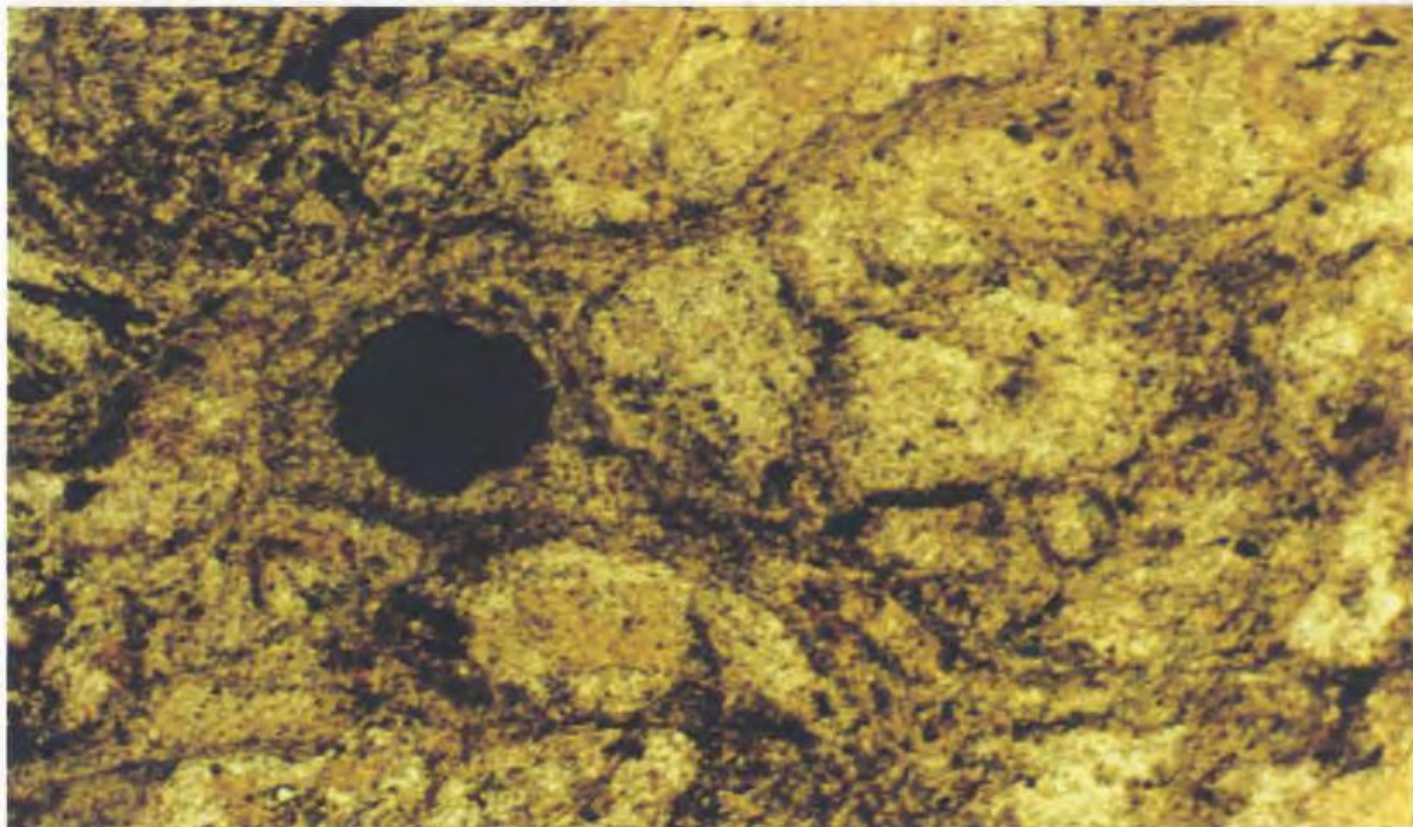


Plate 4.14 Cryptocrystalline magnesite nodule overgrowing sheared serpentinite. Plane-polarised light. Field of view 1cm.

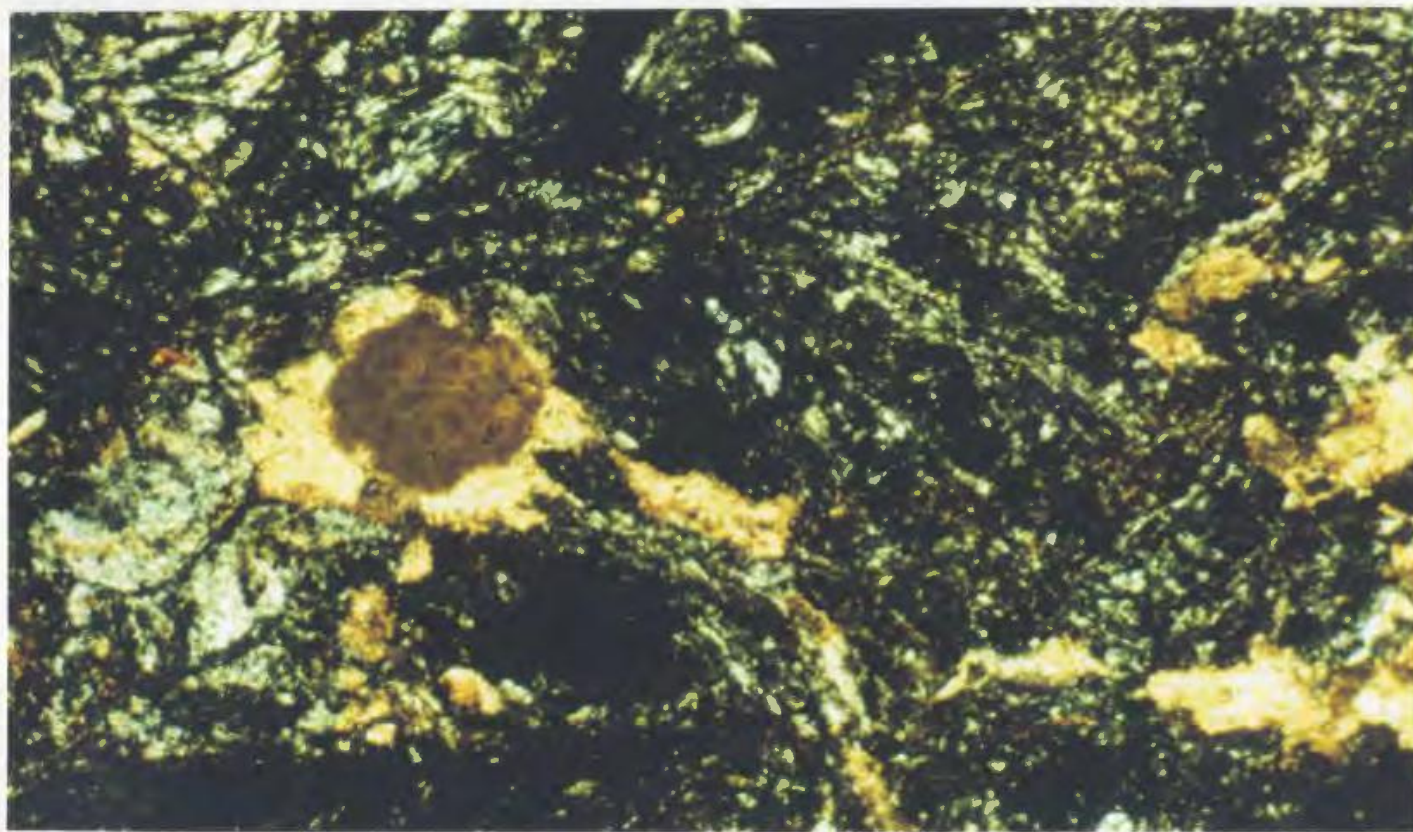


Plate 4.15 Same as Plate 4.14, but in cross-polarised light. Some nodules follow shear fabric but are themselves unsheared. Field of view 1cm.

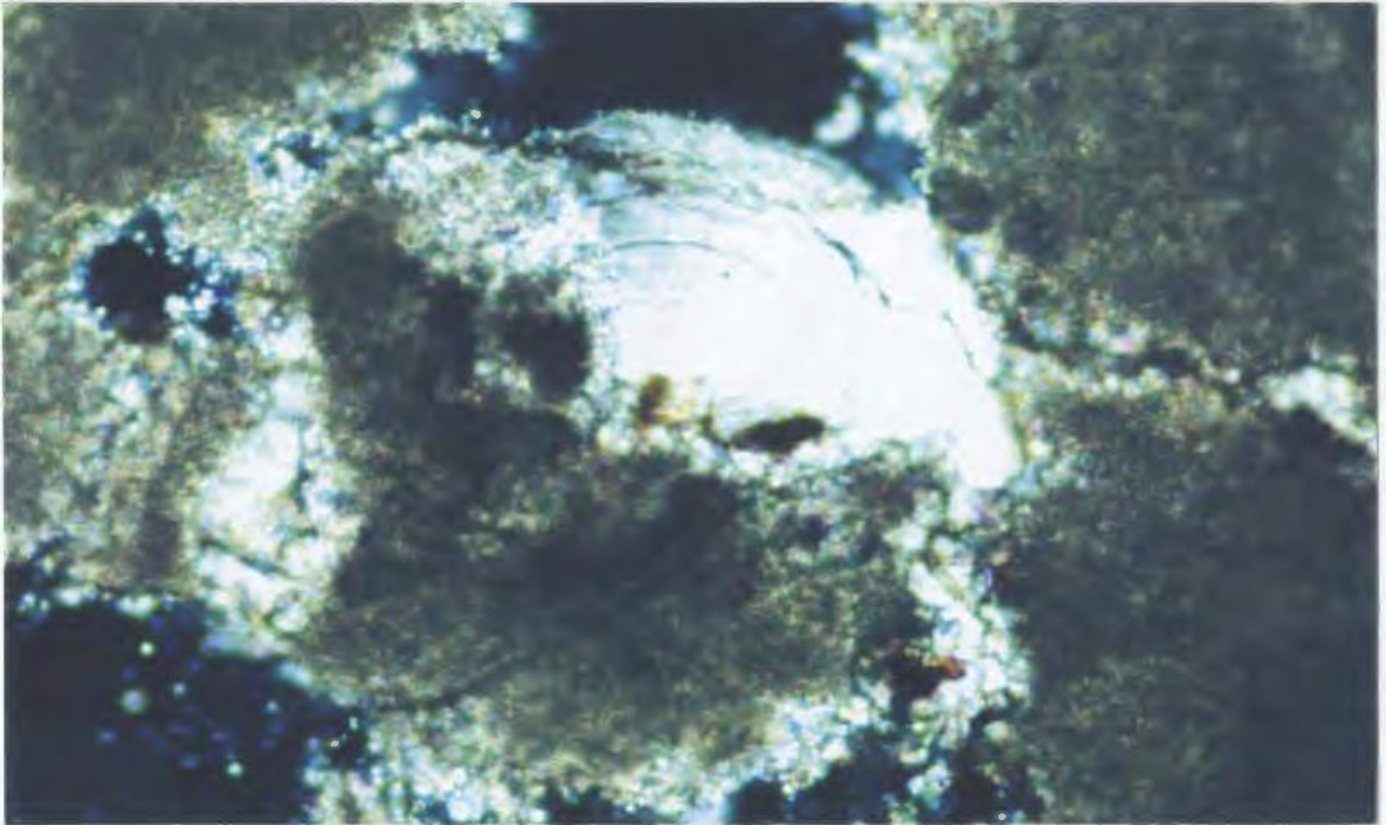


Plate 4.16 Epigenetic calcite precipitated perpendicular to a fracture wall within a magnesite vein. Field of view 1cm..

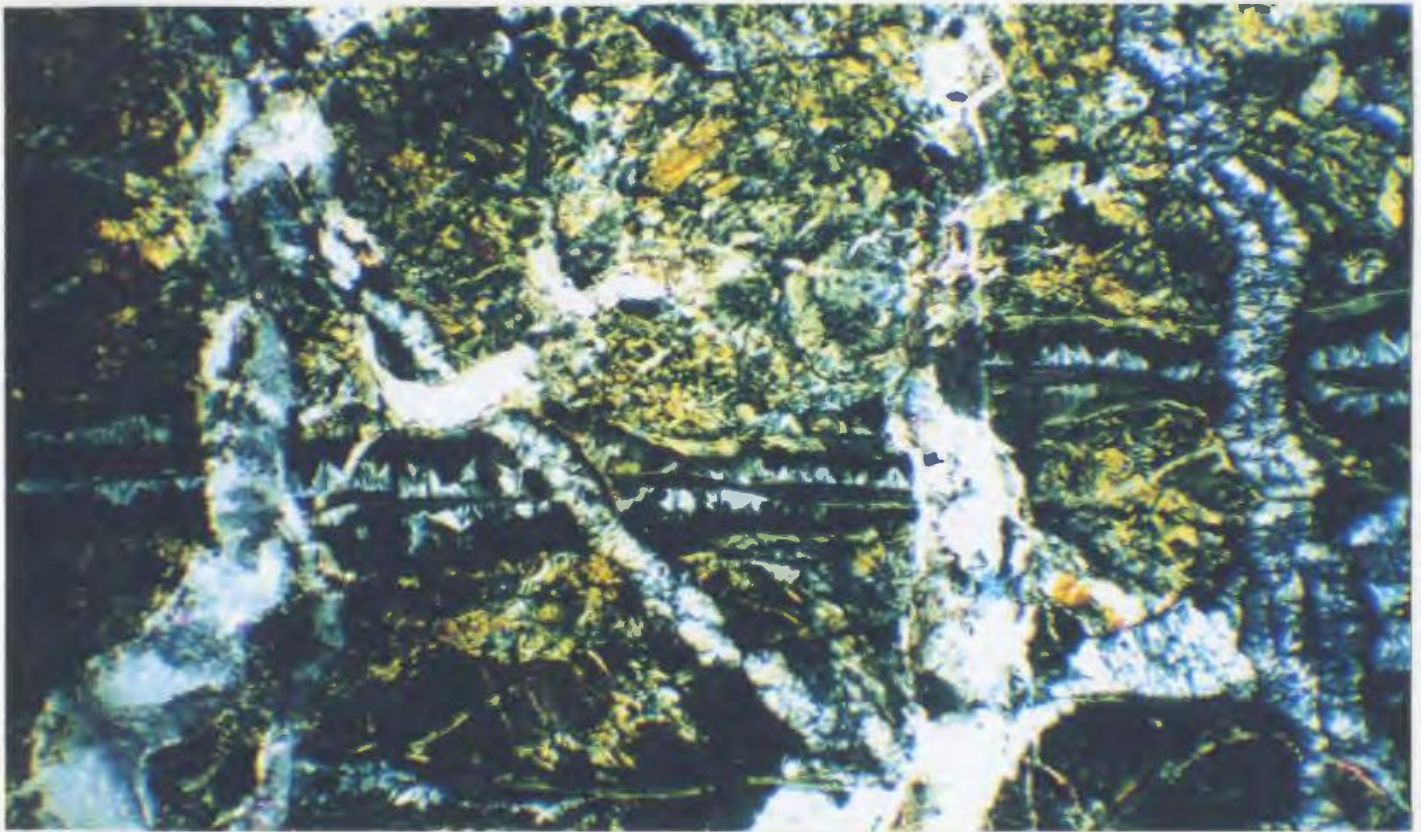


Plate 4.17 Serpentinised harzburgite showing several successive veining episodes. Epigenetic calcite was precipitated last. Cross-polarised light. Field of view 5mm.

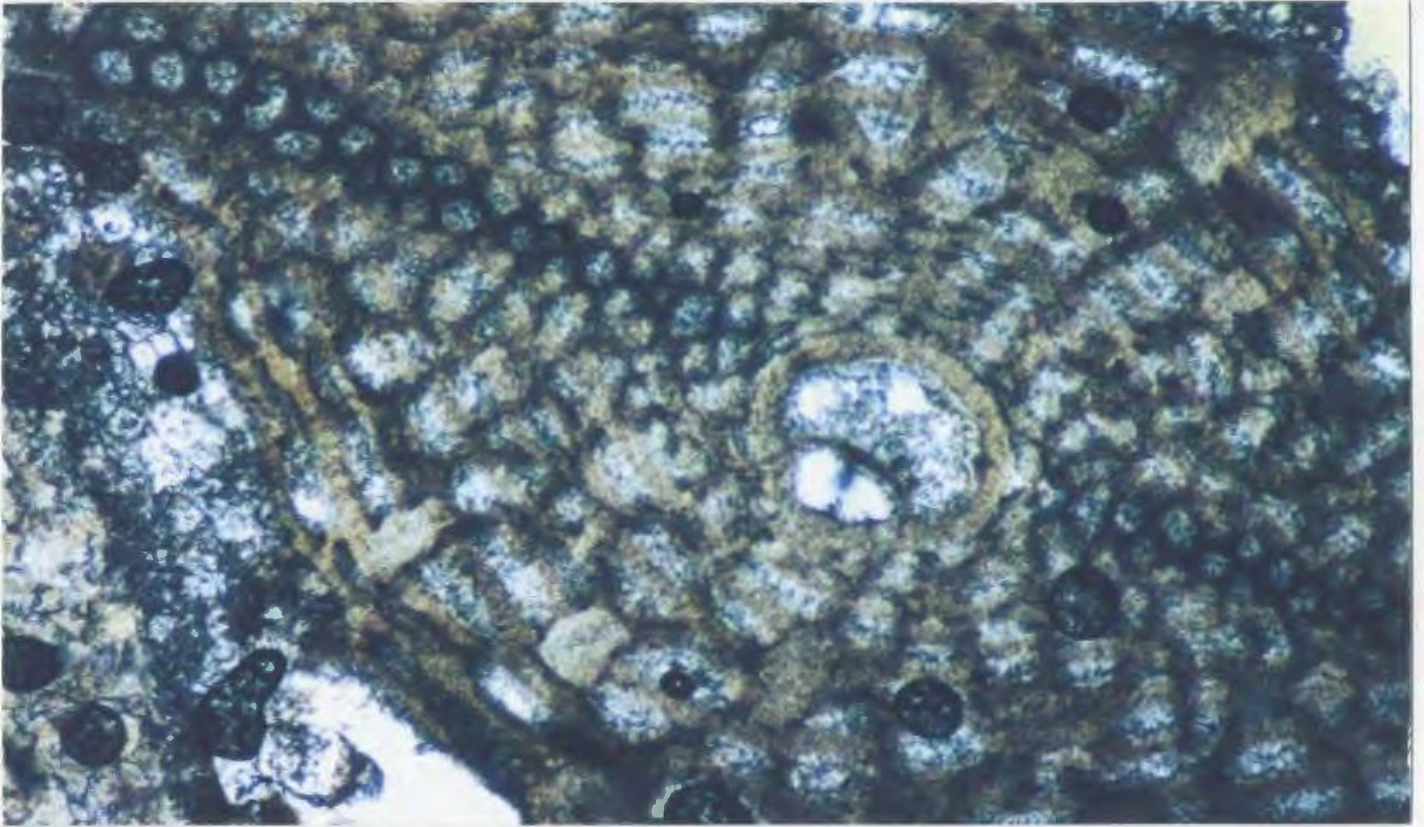


Plate 4.18 Rugose coral fragment in limestone. Micrite cement with minor magnesite. Cross-polarised light. Field of view 3mm.

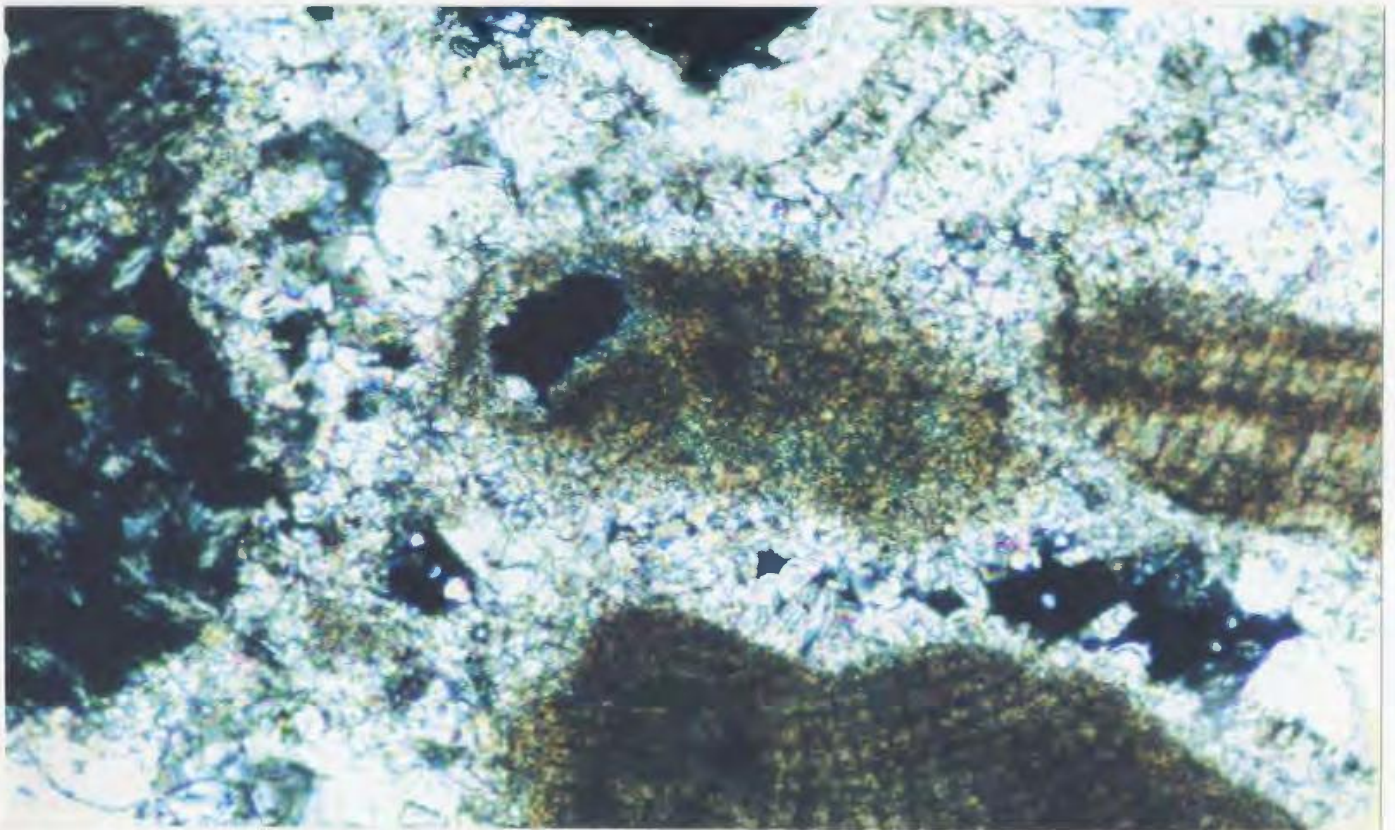


Plate 4.19 Rounded clasts of coral and serpentinite are cemented by fine-grained calcite. Cross-polarised light. Field of view is 5mm.



Plate 4.20 Carbonate cave precipitate found within a small cave on the shore section near Loutra tis Aphroditis. Small specks in carbonate are sedimentary clasts. Coin diameter 2cm.

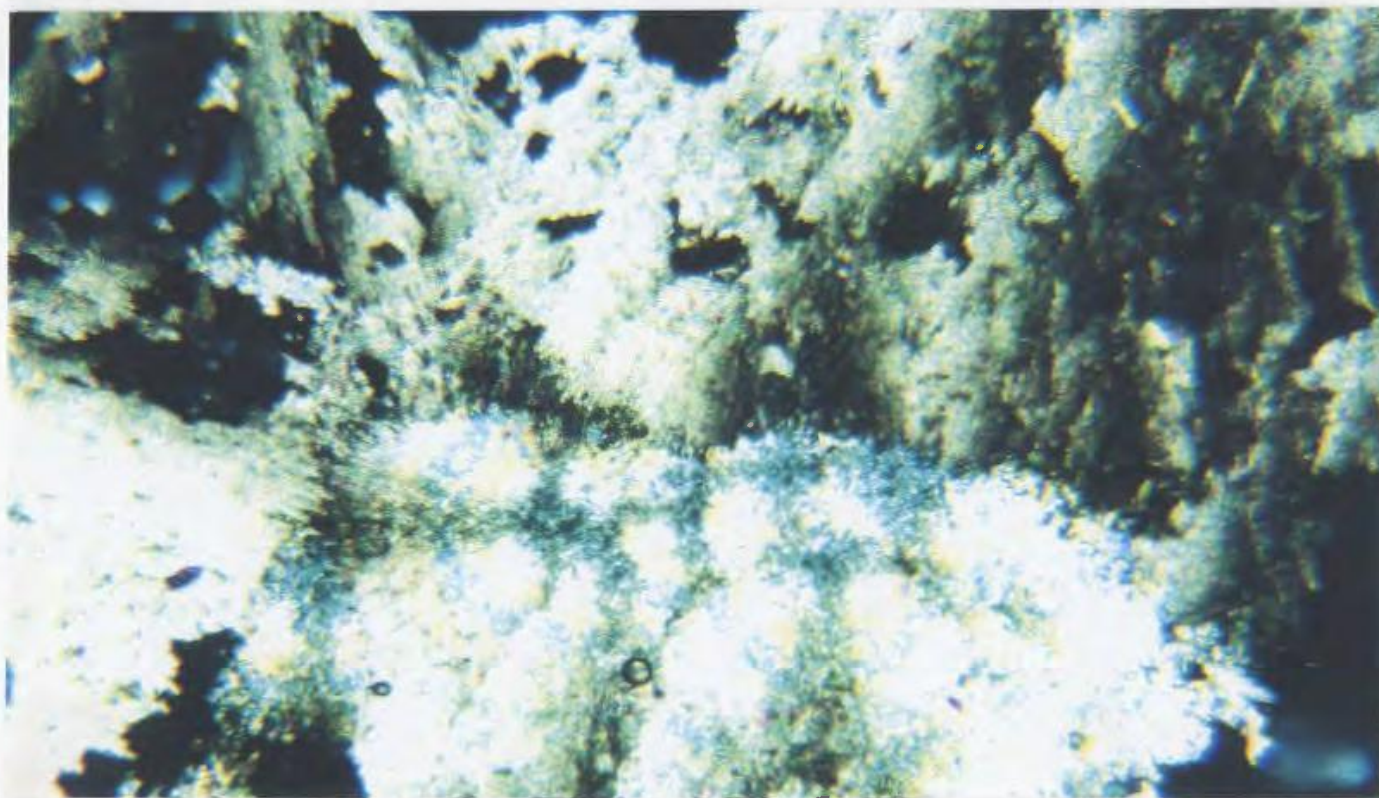


Plate 4.21 Laminar growth of high-magnesium calcite showing radial growth. Cross-polarised light. Field of view 3mm.

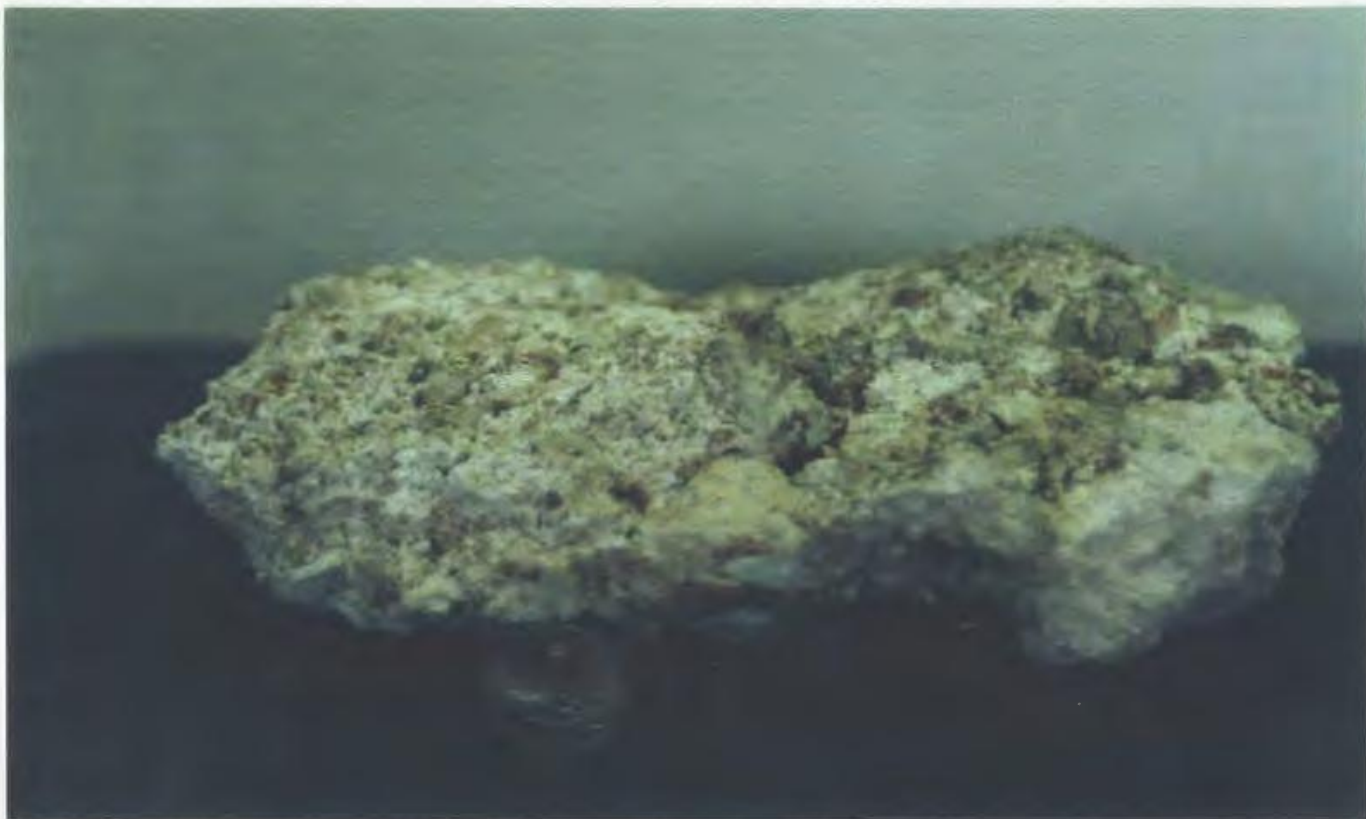


Plate 4.22 Hand specimen of calcite/dolomite 'adit precipitate' found within the vicinity of mineralisation (below the water table) in the study area.

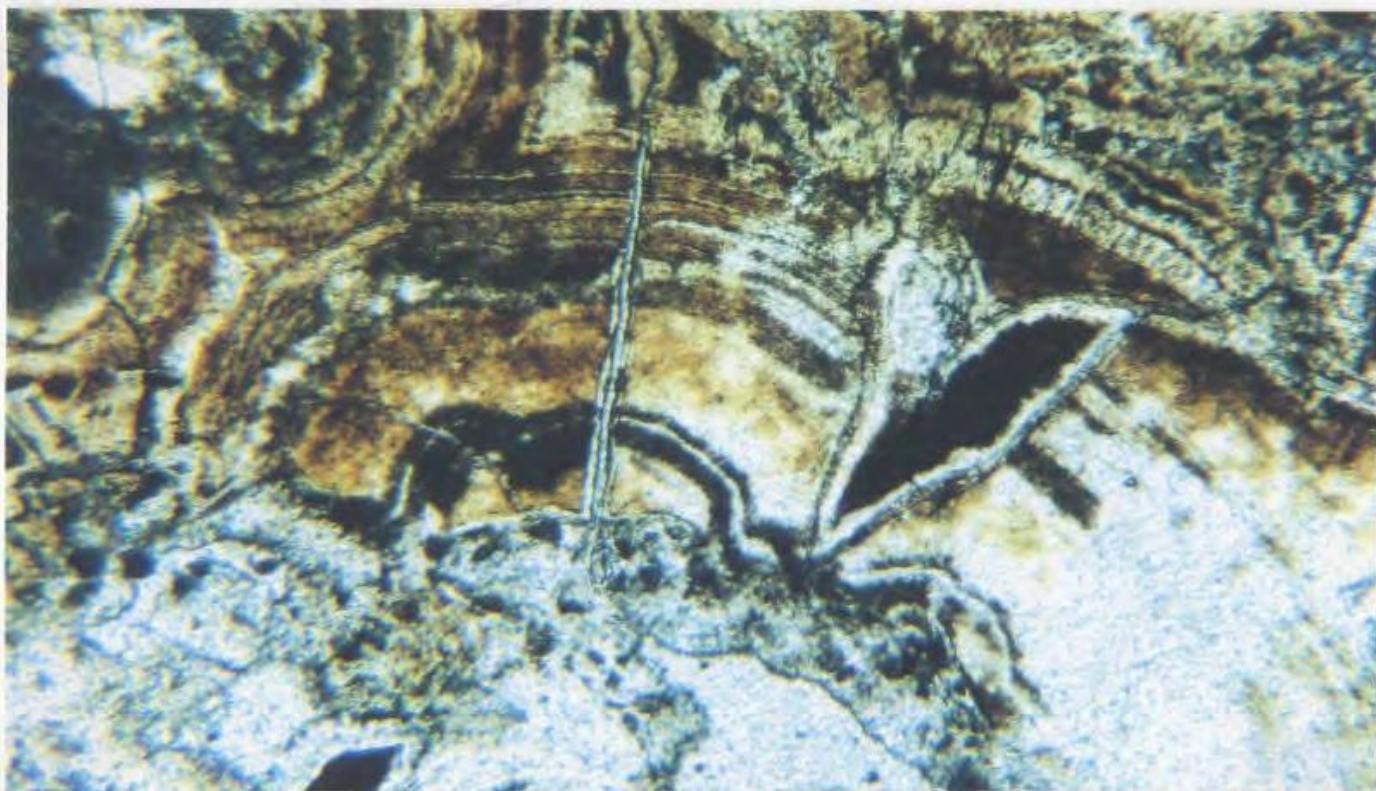


Plate 4.23 Section showing laminar precipitates of dolomite between clasts of microcrystalline magnesite. Brown bands denote ferroan dolomite. Cross-polarised light. Field of view 5mm.

5.0 GEOCHEMISTRY

5.1 Introduction

This chapter deals with various analytical techniques and results of mineral identification for carbonates, serpentinite and sedimentary lithologies including sandstones and radiolarian mudstones. Three separate studies were undertaken; i) an X Ray Diffraction (XRD) study in order to qualitatively identify mineralogy, ii) a stable isotope study of carbonate samples from Zones I and II, marine limestone and dolomite, and iii) a trace element study of magnesite, serpentinite, and sedimentary lithologies within the environs of the mineralisation.

The XRD study was carried out in order to identify samples to be used in the succeeding isotope and trace element studies. The aim of isotope and trace element analyses was to understand certain features of the magnesite mineralisation which are not apparent from field observation, in particular features such as the temperature of formation, chemical composition of mineralising solutions, and the nature of probable source reservoirs of magnesium (Mg), carbon (C) and oxygen (O).

Each study is described separately with an introduction, analytical procedures, results and brief discussion. An overall summary section is then provided which links the three studies together.

5.2 X-Ray Diffraction (XRD) Study

X-Ray Diffraction (XRD) analyses were performed on 27 samples; 24 carbonates including calcite, dolomite and magnesite and 3 samples of serpentinite. These samples, particularly the carbonates, were collected specifically from Zones I and II of the

magnesite mineralisation in order to measure their carbon and oxygen isotopic compositions, as well as their trace element compositions. A qualitative measure of the mineralogical purity of each sample was required before performing chemical analyses. Pure samples (>97% pure) are easily tested for their isotopic composition, but less pure samples (usually mixtures of minerals such as calcite, dolomite, and magnesite) need to be separated to leave only magnesite. Separation may be done physically and/or chemically. Ideally, once separation is complete, the remaining sample should again be X-rayed to determine whether or not further separation is required.

5.2.1 Results

Many of the carbonates tested were identified as calcite, dolomite or magnesite confirming field observations. Samples were identified with relative ease using only the three most intense peaks seen on the XRD trace. The option of using more peaks is available but usually, for monomineralic samples, three are sufficient. Some sample searches resulted in a small list of possible minerals, but in each case, the true identification was made using a combination of XRD and petrographic examination. Table 5.1 shows the main results obtained, and detailed data are given for those minerals identified in the appendices.

5.3 Background for Stable Isotope Study

Introduction

Stable isotopes have been used in the study of cryptocrystalline magnesite deposits throughout the world (Kralik *et al.*, 1989) to determine possible genetic mechanisms associated with magnesite mineralisation. Probable sources of carbon and oxygen are

identified by comparison of magnesite data with known isotope ratios from common carbon and oxygen isotope reservoirs.

Carbon isotope data indicate that each magnesite occurrence usually contains carbon derived from a single source (i.e. organic, atmospheric, juvenile, metamorphic, ...etc.) (Figure 5.1), and it has been suggested that the availability of this carbon is the only restriction placed upon the extent of magnesite mineralisation (Kralik *et al.*, 1989). Isotope data for different types of magnesite deposits (Veitsch, Kraubath, Bela Stena and Greiner) fall into internally consistent isotopic fields. For example, cryptocrystalline magnesite within ultramafic complexes (Kraubath Type) usually contains carbon derived from an organic source (Zachmann and Johannes, 1989).

The oxygen isotopic composition of magnesite, as with any mineral, is highly variable and is dependent upon several factors including temperature of formation, kinetic fractionation between precipitated minerals and mineralising solutions, and the composition of the isotopic reservoir sampled (O'Neil, 1977; O'Neil and Barnes, 1979). Marine limestones, fresh water carbonates and hydrothermal veins fall into isotopically distinct fields, making identification of the isotopic source straightforward (Brownlow, 1979). Oxygen isotopes are particularly useful as palaeo-thermometers (McCrea, 1950), as well as indicating the oxygen isotopic composition of mineralising solutions. Temperature of carbonate formation, and fluid isotopic composition may be calculated from the isotopic composition of minerals using the following equation provided by Aharon (1988) :-

$$10^3 \ln \alpha_{ab} = \Delta_{ab} = (A \times 10^6) \cdot T^{-2} + B \quad \text{..... (Equation 1)}$$

Where A and B are experimentally determined constants which vary for calcite, dolomite and magnesite. Δ = difference in delta values, a, b = different phases.

A crossplot of $^{13}\text{C}/^{12}\text{C}$ (PeeDee Belemnite) vs. $^{18}\text{O}/^{16}\text{O}$ (Standard Mean Ocean Water) (see section 5.3.2) is most often used for comparison of magnesite and other carbonates. Marine limestone has a value of $\sim 0\text{‰}$ (Hoefs, 1973). Isotopic fields of $^{13}\text{C}/^{12}\text{C}$ for some common materials are shown in Figure 5.1. Many stable isotope magnesite ratios from comparable types of deposits (Kraubath, Bela Stena, Veitsch, and Greiner Types) fall into separate and consistent fields. Kraubath Type magnesite deposits for example have a mean carbon isotopic ratio between -11 and -13‰ (PDB) (Zachmann and Johannes, 1989).

5.3.1 Stable Isotope Study of Akamas Magnesite

Structural relationships in Akamas deposits have indicated that magnesite belonging to several generations of mineralisation is preserved in distinct structural settings within the serpentinite. Within this study, samples were collected from various locations within Zone I (carbonate veining (calcite +/- magnesite) within the BST, large magnesite veins), and from Zone II (nodular magnesite), in order to investigate isotopic differences between the two zones. Recent precipitates of carbonate crust were also sampled from the walls of adits and within a small cave in the vicinity of the mineralisation.

Previous carbon and oxygen isotope data for magnesite from the Magnisia deposit indicate an organic source for the carbon within the magnesite, and a meteoric water signature for the oxygen present (Brydie *et al.*, 1993). A large portion of this data was

obtained from Zone II nodular magnesite, the remaining samples being vein magnesite from Zone I, resulting in a poor representative sample set.

One of the purposes of this study is to determine the isotopic provenance of carbon and oxygen within the magnesite. Temperature of formation of minerals is calculated, and comparisons are drawn between mineralisation from Zones I and II.

5.3.2 Analytical Procedures

The analysis of carbonate material for its isotopic composition has been well documented by McCrea (1950) using the standard extraction of carbon dioxide by 103% phosphoric acid dissolution, extraction *in vacuo*, and analysis of the gas using mass spectrometry. Aharon (1988) lists a series of fractionation factors calculated from empirical measurements of calcite and dolomite, and extrapolates for use with magnesite.

Isotopic fractionation of the phosphoric acid used in analyses is well documented and a universally accepted correction factor is applied to all data (Aharon, 1988). Equations are available which allow calculation of the isotopic composition of fluids in equilibrium with precipitated minerals (Faure, 1986). This is useful when it comes to calculation of the isotopic composition of mineralising solutions.

All samples were identified by XRD analysis and certain veins were found to contain calcite (with minor dolomite) in fractures within the vein material. This was identified (petrographically) as being epigenetic in nature, both calcite and dolomite having been precipitated in laminar and radial fashion upon vein fracture surfaces. This calcite and dolomite was easily removed by treatment with 10% hydrochloric (HCl) acid. Other samples were also found to contain a high proportion of calcite and had to be treated in a

similar manner. In particular, nodular precipitates tend to contain calcite to varying degrees, from 1-2 weight % up to 20 weight % CaCO_3 . In such cases, the nodular magnesite (including calcite) was powdered and mixed with 10% HCl for one hour, or until all effervescence had ceased. Usually, all reaction of calcite with acid was complete within ten minutes. The sample was then rinsed in distilled water several times, and placed in an oven (in vacuo) for twenty four hours to dry. This follows the procedure outlined by Al-Aasm et al. (1990) with regard to the fine crushing of carbonates containing more than one phase (magnesite-calcite) before acidification. The use of hydrochloric acid, as opposed to the phosphoric acid used by Al-Aasm (1990), was found to provide good results in less than five hours. It was found that the calcite from an initial mixture of calcite and magnesite reacted within the first 20 minutes. Washing and re-acidification was then performed on the remaining sample. The epigenetic calcite and dolomite occurs in fractures and voids, while the calcite related to magnesite formation either occurs in the sheared serpentinite fabrics or is intergrown with magnesite.

Samples were crushed, weighed and flame sealed in vacuo in a pyrex vile with acid (the acid separated from the powdered sample). After heating the vile to 100°C , the vile was upturned and the acid-carbonate reaction initiated. The vile was then placed in the oven for 24 hours, after which the CO_2 obtained from the carbonate-acid reaction was extracted via a series of pumps and run through a mass spectrometer. Complete transfer of all CO_2 during extraction was ensured in order to decrease the chances of isotopic fractionation.

Analytical Standard

The carbonate standard used in these experiments has been used in previous studies of magnesite (sample 142C, Timbal, A., pers. comm. 1994) and is a pure magnesium carbonate of known isotopic composition. Oxygen isotopic ratios are reported relative to Standard Mean Ocean Water (SMOW), and carbon values are reported relative to the Pee Dee Belemnite (PDB) universal standard. Average isotopic values for this standard, derived from a series of approximately 10 separate determinations, were found to be -11.9 ‰ (PDB) and 13.5 ‰ (SMOW), for carbon and oxygen respectively. These values were repeatable to within 0.1 ‰ for both carbon and oxygen.

The same standard was analysed a further 9 times during this study and most carbon and oxygen isotopic ratios fell within 0.1-0.2 per mil of expected values. Although the first three analyses were 0.4 ‰, 0.5 ‰ and 0.4 ‰ lighter with respect to oxygen than expected, values obtained after this were consistently within accepted limits. Results obtained using this technique for reaction and extraction of gas seem reliable and are repeatable to a high degree of precision. It was concluded that the first three results deviated from the 'accepted standard value' due to inconsistent analytical technique. For example, the transfer of the carbon dioxide sample between storage receptacles may cause isotopic fractionation, mainly loss of the heavier isotopes ^{13}C and ^{18}O , if the sample is not pumped sufficiently (McCrea, 1950; Cornides and Kukasabe, 1977).

A sample analysed elsewhere (Brydie *et al.*, 1993) was also re-tested and provided results of similar accuracy to that of the standard. A previously obtained value of -10.1 ‰ (PDB) for carbon, and 25.6 ‰ (SMOW) for oxygen was found tested as -10.0 ‰ and

25.6‰ (for carbon and oxygen isotope values respectively) in this study. It is likely, therefore, that results obtained for the other carbonates tested during this study are reliable and self consistent.

5.3.3 Results

Carbon and oxygen isotope values for Akamas carbonates occupy very different fields. Magnesites have carbon values between -7.8 and -12.7‰, and oxygen values between 12.2 and 30‰. Marine limestone samples from the Tera Limestone lie between -2.7 and -0.1‰ (carbon) and 26.3 to 27.5‰ (oxygen). Magnesite veins and nodules occupy a range of carbon isotope values usually restricted to organically derived carbon species. The limestone is within acceptable limits of typical marine carbonates and the single sample of dolomite is thought to have derived carbon and oxygen in the form of carbon dioxide directly from the atmosphere. One sample of magnesite lies away from the main body of samples with a similar carbon value (-9‰) but with distinctly lower oxygen (24‰). The reason for this difference is not known, but probably reflects a difference in the temperature of formation of this magnesite. Data are shown in Figure 5.3 and Table 5.2. These are considered below.

Carbon Isotope Results

i) Magnesite

Carbon, usually present only in small quantities within any particular geochemical reservoir, was found to vary between -12.7‰ and -7.8‰ for all magnesite samples. This includes both veins and nodules.

ii) Calcite

Samples of calcite taken from the overlying limestone, both near and distant to areas of significant mineralisation, show values close to those expected for typical marine carbonates, i.e. approximately 0‰. Values obtained vary between -0.13 and -0.11‰. These values are close to those found previously for similar samples within the study area.

Four samples of vein calcite associated with Zone II of the magnesite mineralisation have carbon isotope values between -13.8 and -8.9‰. Two small calcite veins sampled close to the Limestone cover sediments had carbon values of -2.5 and -2.7‰.

iii) Dolomite

A single sample of dolomitised limestone, taken from close to the contact with serpentinite, exhibits a carbon value of -9.6‰. Samples within fault zones show similar values to this dolomite. Dolomite precipitating within a cave in the karst limestone has a carbon value of +2.4‰.

Oxygen Isotope Results

The results obtained for oxygen are highly variable, ranging from 12.2‰ to 30.0‰ for magnesite, calcite and dolomite. A single sample with an isotope value of 34.3‰ was recorded for dolomite within a small cave in the study area (close to the main area of mineralisation). Results for different carbonates are reported separately below.

i) Magnesite vein samples

Vein magnesite, taken from very pure large veins at the base of Magnisia have $^{18}\text{O}/^{16}\text{O}$ values ranging from 12.2‰ to 15.4‰. An average oxygen value for these veins would be 13.8‰.

ii) Magnesite nodules

Nodular magnesites have values between 23.6‰ and 30.0‰. The difference of approximately 6.4‰ between veins and nodular precipitates defines two isotopically distinct fields for magnesite samples, the difference being between 'early' (veins) and 'late' (nodules) magnesite generations. The 'early' veins provide the more isotopically depleted population, while the 'late' precipitates are enriched with respect to ^{18}O .

iii) Calcite

The marine limestone deposited unconformably over the serpentinite and Mamonia sediments, is found to have an oxygen isotope composition similar to other marine-derived sediments of this type, i.e. approximately 27‰.

iv) Dolomite (dolomitised limestone)

Areas of limestone appear to have been dolomitised adjacent to, and within, faulted and brecciated zones. This dolomite has an isotope value of 26.6‰. Other samples were taken from positions close to the contact with serpentinite and up through the section into fresh unaltered limestone. No clear trend is seen from the analysis of these samples.

5.3.4 Discussion

It is clear from extensive studies of serpentinisation in mafic and ultramafic complexes (Wenner and Taylor, 1973) that various types of waters are responsible for the alteration of most mafic igneous rocks. These waters include seawater, meteoric, connate, juvenile, metamorphic and a combination of these. However, in most continental ophiolite complexes, it is noted that the action of seawater is usually negligible and that a combination of hot, exchanged meteoric waters, mixed magmatic-meteoric waters and mixed connate-meteoric waters are usually responsible for the major part of the serpentinisation process. Also, from oxygen isotope studies of serpentinite and serpentine minerals from the Troodos ophiolite (Wenner and Taylor, 1973), it is clear that meteoric water (-2‰ (SMOW)) was responsible for the serpentinisation of this ultramafic complex. Calculations in the present study therefore assume exchanged meteoric waters with a value of -2‰ for the oxygen isotopic composition of the mineralising fluids.

It is clear from the crossplot of carbon and oxygen (for magnesite, calcite and dolomite) that there are several distinct populations of carbonates which occupy very different fields. The isotopic fields in which metamorphic-, juvenile-, and atmospheric- CO_2 are usually found (Faure, 1986, Hoefs, 1973) are completely separate and different to values obtained for magnesite from Zones I and II (Figure 5.2). Carbon isotope values of these veins suggest an organic source comparable to similar deposits in Serbia and Bosnia (Fallick *et al.*, 1991). Two main magnesite populations are present (Figure 5.3), one defining an elevated magnesite formation temperature corresponding to the large veins of Zone I ($^{13}\text{C}/^{12}\text{C}$ values from -7.8‰ to -12.7‰ (PDB), and $^{18}\text{O}/^{16}\text{O}$ values from 12.3‰

to 15.4‰ (SMOW)), the other indicating a lower temperature of nodule formation (40°C) within Zone II ($^{13}\text{C}/^{12}\text{C}$ values from -11.1‰ to -7.8‰ (PDB), and $^{18}\text{O}/^{16}\text{O}$ values from 23.6‰ to 30.0‰ (SMOW)). Isotope results for Zone II magnesite are in accordance with values obtained previously. However, vein magnesite occupies the most ^{18}O -depleted magnesite field on the crossplot, completely revising previous work. Three magnesite vein samples taken from Zone I lie within a field which is distinct from any other carbonate population. Temperature of formation for carbonate is calculated as being approximately 165° (+/-10°C) for the largest of veins sampled (see Appendix V).

Zone II magnesite appears to have formed at temperatures as low as 40°C. The source of carbon within the nodules is similar to that of the vein magnesite, with a slightly wider spread of data. Oxygen isotope values are quite different from veins with a positive shift of 9‰. From field evidence it is clear that 'vein magnesite' was precipitated before 'nodular magnesite', possibly during emplacement of the serpentinite. Nodular magnesites did not form until after all of the contractional tectonism had ceased, yet these two different types of magnesite are similar with respect to the source of carbon. Considering the spatial relationship between these two styles of magnesite mineralisation (see chapter 3), it is likely that vein material was remobilized during, and/or subsequent to, the formation of the ISSZ and was re-precipitated within Zone II.

Two samples of calcite taken from marine limestone above the Magnisia deposit have isotopic values indicative of marine carbonates, but appear a little light in carbon

(-2‰, as opposed to ~0‰ (PDB)), and a little heavy with respect to oxygen (up to 27.5‰) This shift in isotopic composition may be due to diagenetic effects, or may be a direct result of the interaction of marine limestone with the mineralising solutions.

Two small calcite veins sampled within serpentinite, from just below the serpentinite- limestone contact, have isotopic compositions between that of Zone II magnesites and marine limestone. These calcite veins may have been precipitated from mineralising solutions and have subsequently re-equilibrated with carbonate-rich groundwaters within the karst limestone. The veins may also be the result of epigenetic calcite precipitated from circulating groundwaters which has been diagenetically altered by fluids passing through the magnesite deposits.

The origin of carbon within Akamas magnesite is of particular interest, as there are several possible sources within the vicinity of the mineralisation. These sources are i) atmospheric carbon dioxide, ii) oxidation of plant material, iii) dissolution of the limestone above the deposits, with precipitation of magnesite from reaction of carbonated waters with mafic minerals within serpentinite, iv) decarbonation of metamorphosed marine limestone, v) decarboxylation of organic-rich sediments underthrust beneath the serpentinite and vi) mantle carbon (Hoefs, 1973; Faure, 1986; Zachmann and Johannes, 1989).

Metamorphism of limestone (Petra tou Romiou Formation) may be dismissed as a source of carbon upon the premise that there are relatively few blocks of this limestone in the study area, and each block of limestone was silicified during the Triassic (well before magnesite mineralisation) (Swarbrick and Robertson, 1980). Metamorphism of the Tera

Limestone is not an option as it is much younger than the magnesite mineralisation (Swarbrick and Robertson, 1980). The remaining sources of carbon can be discriminated isotopically. The isotope field occupied by the magnesite is very different to either metamorphic or juvenile carbon and so it is apparent that carbon within the magnesite was not derived from either the decarbonation of marine limestone or by the introduction of juvenile carbon.

Atmospheric carbon dioxide and carbonate-rich waters derived through dissolution of the overlying limestone may also be dismissed as carbon donors, as neither of these fields is situated near the magnesite isotope field. Of the two sources remaining, the oxidation of higher plant material is a possibility, but seems unlikely due to the requirement for substantial quantities of organic material to have undergone oxidation (at the surface) during ophiolite emplacement. This leaves decarboxylation of organic material after burial as the most likely carbon source.

It is also noted that, in the majority of low temperature vein and stockwork magnesite deposits worldwide, the source of carbon is organic. Akamas magnesites contain carbon and oxygen isotope signatures similar to these other deposits

5.4 Trace Element Study

Introduction

Many studies have attempted to classify magnesite deposits (Veitsch, Kraubath, Bela Stena and Greiner types) using the trace element signatures of magnesite from each deposit type (Morteani *et al.*, 1983). These studies have shown that the Rare Earth Element (REE) patterns of magnesites may be employed to determine genetic features of

the mineralisation, e.g. metasomatism of serpentinite during the hydrothermal precipitation of minerals as opposed to the formation of magnesite during weathering and degradation of the serpentinite (Ilich, 1968; Martiny and Rojkovic, 1977). Usually, the concentration of REE's (and other trace elements in magnesite) is relatively low (0.01 - 0.1 ppm). Where elevated values do occur, it is usually the result of the inclusion of trace mineral phases within the carbonate such as serpentine or clay minerals (Morteani *et al.*, 1983). Certain trace elements are known to substitute for the Mg^{2+} ion in the magnesite structure (Cr, Ni, Co, Cu being most common) in low concentrations. Other elements are also found such as Fe, Hg, Mn, Sr, Ba, B and heavy REE's which may be captured by magnesite, or which are present within the trace mineral phases (Maksimovic and Dangic, 1974).

Previous work indicates that magnesite from the Akamas area contains measurable amounts of trace elements, in particular Cr, Cu, Ni, Pb and B (Gass, 1960; Ilich and Maliotis, 1984). Of these elements, Cr, Cu and Ni are ubiquitous within the serpentinite, being released from mafic minerals (such as serpentine minerals and brucite) and either substituted for Mg^{2+} (in magnesite), or captured in the cryptocrystalline magnesite during precipitation. Trace elements present in the mineralising solutions may also be introduced to hydrothermally altered wallrock during mineralisation. Lead (Pb) and Boron (B) are not present within unmineralised serpentinitised harzburgite, suggesting a hydrothermal origin for the magnesite deposits which obtained anomalous trace element concentrations (Pb and B) from solutions originating elsewhere, other than the ultramafic complex (Ilich and Maliotis, 1984).

5.4.1 Present Study

In the present study, the trace element compositions of magnesite samples from Zones I and II have been used to relate carbon present within the magnesite to possible sources of carbon within the study area. It was presumed that the trace element composition of the carbonates, when used with the isotope data, would provide further insight into chemical processes prevalent during magnesite formation. Trace elements present within magnesite may be inherited from the mineralising solutions (either within trace mineral phases, or directly substituted into the magnesite), possibly indicating the trace element compositions of lithologies through which solutions have passed (Maksimovic and Dangic, 1974). These phases provide chemical information about their own source and conditions of formation and so may be useful as indicators of the overall magnesitisation processes.

Rigorous sampling of key structural sites and analysis of magnesite from Zones I and II, serpentinite, marine limestone and organic-rich sandstone has resulted in an overall view of trace element distribution within the magnesite deposits and associated lithologies. The following samples were analysed, four samples of vein magnesite, four nodular magnesites, four organic-rich sandstones, two samples of serpentinitised harzburgite (one taken 5km from any obvious magnesite mineralisation, the other from within the main deposit), four samples of dolomite (three samples from the base of the limestone cover above the deposits, and one sample from a small cave in serpentinite) and four samples of calcite (two within mineralisation and two from wholly karstic marine sediment above the deposit of Magnisia). These samples were chosen specifically in the hope of chemically

linking the magnesite with carbon-bearing lithologies within the vicinity of the magnesite deposits, thought to be possible carbon-donors during mineralisation.

5.4.2 Analytical Technique

The analysis of rock and mineral samples was performed using Inductively Coupled Mass Spectrometry (ICP-MS). Sample preparation is described separately in Appendix III. Elements measured in the trace element analytical package include :- Li, Rb, Sr, Y, Zr, Nb, Mo, Cs, Ba, La, Ce, Pr, Nd, Sm, Eu, Gd, Tb, Dy, Ho, Er, Tm, Yb, Lu, Hf, Ta, Ti, Pb, Bi, Th and U. Limits of detection are indicated in Appendix IV, and are defined as being "equal to three times the background concentrations for each element (within the blank)" (Taylor and McLennan, 1985).

5.4.3 Results

Results for each sample type will be reported separately, followed by a brief comparison and discussion. All concentrations are reported relative to chondritic ratios (Taylor and McLennan, 1985), i.e. $\text{ppm}(\text{sample}) / \text{ppm}(\text{chondrite})$. Where elements are "undetected", this implies the 'absolute' value of that particular element is below the limit of detection of the ICP MS.

i) Serpentinite

Two samples of serpentinite were analysed, one from within a few centimetres of a 50cm-wide magnesite vein within Zone I of the Magnisia locality (s4), the other from a site approximately 5 km due west of the Magnisia deposit (away from any carbonate mineralisation) in blocky serpentinised harzburgite (1c16). The two samples contain very different trace element compositions (Figure 5.4.1).

Analysis of unmineralised serpentinite (1c16) reveals ten elements to be below the limit of detection, including Y, Nd, Eu, Tb, Dy, Hf, Ta and U. Elements present in highest concentrations are Li, Sr, Ba and Eu which occur in relative concentrations from 0.1 to 10. Notable in this serpentinite sample is the relative quantity of Ba, not commonly present within serpentinitised ultramafic rocks (Deer *et al.*, 1962). Both light and heavy REE's are present, but Nd, Gd, Tb and Ho reduce to practically zero after results are normalized to chondrite.

The serpentinitised harzburgite sample taken from within the mineralised zone (s4) contains more trace elements within detection limits. Elements not seen after normalization are Cs, Nd, Sm, Eu, Tb, Ta and Ti. The elements Tm, Yb, Lu, Pb, Th and U are present in chondrite normalized concentrations which are elevated with respect to apparently unmineralised serpentinite (0.05-1ppm/chondrite). Previous studies within the Magnisia deposit also show enrichment of trace elements associated with magnesite veins and stockworks, but less noticeable trace element signatures when progressively less mineralised serpentinite is tested (Ilich and Maliotis, 1984).

ii) **Calcite**

Calcite samples were taken from various locations within and proximal to the magnesite mineralisation. Three calcite veins were sampled approximately 10cm away from a large, massive magnesite outcrop within the Magnisia mine (1c8, 1c10 and 1c21). Two samples were taken from the coraliferous marine limestone unconformably overlying the deposits, from approximately 10m and 2m above the unconformity with serpentinite

(1c20 and 1c19 respectively). Trace element signatures show certain differences in relative concentration and distribution depending on location sampled (Figure 5.4.2).

Samples '1c19' and '1c20' have trace element signatures similar to those expected for marine carbonates, and both appear fairly similar when concentration (normalized to chondrite) is plotted for elements present. Most elements appear in relative concentrations between 0.04 and 100. Tb lies below the detection limit in sample 1c20, and neither Tb nor Ta are detected in sample 1c19. Samples 1c8, 1c10 and 1c21 contain all elements within the package except for Y, Nd, Sm, Tb and Ho which were not detected. REE's are present in appreciable concentrations (~1ppm/chondrite) in samples 1c19 and 1c20 (Figure 5.4.3).

Elements which are present in highest concentrations are Li, Sr, Ba and U, particularly in samples 1c19, 1c20 and 1c21 which were taken from, or close to, the marine limestone.

iii) Dolomite Samples

Samples 1c22 and mx show typical marine carbonate signatures, exhibiting a full range of 30 trace elements (Figure 5.4.4). Peaks are found for Sr, Ba, REE's, Pb, Th and U, between values of 1 and 50 x chondrite. 1c22 was sampled approximately 5m above any magnesite mineralisation, sample 'mx' 3m above the dolomitised marine limestone-serpentinite contact, and sample '1c6' close to the dolomite-serpentinite boundary. Sample 1c6 is not characteristic of a typical marine sediment of this type and has a signature more similar to that of the serpentinite with Y, U and REE's in the dolomite effectively disappearing upon normalization to chondrite (Figure 5.4.5).

iv) Sandstone

Four samples of sandstone (D1-D4) contain remarkably consistent trace element concentrations and distributions with only Mo, Ta, Pb, and U differing significantly in concentration relative to chondrite (Figure 5.4.6). Of these elements, Mo is low with values of 0.1-0.3 and Ta varies in concentration between 40 and 100. The average value for all elements plotted lies around 20-30. Pb is present in concentrations of 3-10. U occurs in concentrations relative to chondrite of 100-2000. There appears to be a W-shaped pattern between elements Lu and U which seems characteristic of the trace element distribution within all of the sandstone samples. REE's are present in all samples, with a small negative Eu anomaly, characteristic of terrestrial sediments of this type (Pohl, 1989)

v) Zone I magnesite (vein samples)

Trace element patterns for samples taken from the main workings at Magnisia (2c13, 2c14, SM and X6) are somewhat erratic and cover most of the spectrum of analysed elements (Figure 5.4.7).

Some samples contain more trace elements within detection limits than others but, overall, quantities of Li, Sr, Nb, Ba, Tb, Hf, Ta, Pb, and U occur in concentrations ranging from 0.1 to 50. Samples X6, 2c13, and SM exhibit low concentrations of Mo (0.01)

Samples were taken from massive carbonate toward the centre of large veins within Zone I mineralisation, 20m above the base and approximately 1m below the stockwork magnesite zone (sample 2c13, 2c14 and X6 respectively) Sample 2c14 contains a full suite of elements, with peaks at Li, Sr, Ba, Nd, Tb, Ta, Bi and U. X6 is similar apart from Y, Eu, Gd, Tb, Er and Ti which are below detection limits. Sample

2c13 contains 21 elements with peaks at Li, Sr, Ba, Th and U. However, Y, Sm, Eu, Gd, Tb, Dy, Ho, Er and Lu are below detection limits.

vi) Zone II (nodules)

Nodular magnesites (1c9, 1c17, 2c12, and m5) contain certain measured trace elements in concentrations of 0.1 to 100 (Figure 5.4.8). Peaks appear to follow similar patterns to those seen in some vein samples (Li, Sr, Ba, and U). However, Li, Sr, Zr, Ba, Hf, Ta, Th and U and Pb do not appear above values of 0.04. Elements not detected within the magnesite nodules, but which do occur within vein samples, are Y, Tb and Dy (Figure 5.4.9).

5.4.4 Discussion

The distribution of trace elements within the magnesite and within lithologies in the vicinity of the deposits has certain implications regarding the trace element composition of both mineralising fluids and source reservoirs of elements now residing within the magnesite of Zones I and II. Each sample type analysed (magnesite, serpentinite, limestone, dolomitised limestone, and sandstone) has a distinct and characteristic trace element signature. It is assumed that the trace element composition of the magnesite reflects (at least in part) the trace element composition of mineralising solutions (Maksimovic and Danjic, 1974). Even if few trace elements are present within the magnesite itself, either by inclusion or by replacement of Mg^{2+} ions, included silicate phases should provide a trace element signature of solutions causing mineralisation. Since these phases are enclosed within the cryptocrystalline magnesite (with low porosity and

permeability), then presumably they have remained generally unaltered since the time of mineralisation.

Serpentinite

Close to large magnesite veins in Zone I, the trace element signature of serpentinite resembles that of magnesite vein signatures. Altered serpentinite in close proximity to magnesite mineralisation contains some trace elements peculiar to the mineralisation (such as Li, Th and U), while serpentinite sampled away from any magnesite mineralisation has a quite different trace element signature. This indicates the introduction of trace elements from a source outside the ultramafics which may be related to the mineralisation process.

Unmineralised serpentinite contains elevated levels of Ba, which are not usually found within ultramafic rocks (Deer *et al.*, 1962). This Ba may have been derived from circulating meteoric waters responsible for the serpentinisation of the harzburgite minerals, but perhaps more likely is that the Ba was introduced by mineralising solutions which are known to contain elevated levels of Ba. Ilich and Maliotis also report elevated trace element contents of the serpentinite in the area surrounding magnesite mineralisation (Ilich and Maliotis, 1984).

Calcite

Trace element signatures of marine limestone differ from those of magnesite veins and nodules, suggesting the limestone as an unlikely source of carbonate within the magnesite. This is in agreement with isotope data (see previous section). It is noticeable when comparing various trace element plots, (magnesites, calcites and dolomites) that

relative elemental abundances are variable in samples taken from sites close to mineralisation. Close to the serpentinite-limestone boundary, trace element compositions of calcite (and dolomite) resemble serpentinite and/or magnesite in that they contain anomalous amounts of trace elements which are common to the serpentinite and/or magnesite. Further away from the contact (higher in the limestone outcrop) calcite samples contain far smaller amounts of trace elements characteristic of serpentinite and magnesite, and are more typical of common marine carbonates (Bathurst, 1971).

Dolomite

Samples of dolomite (1c6, mx, 1c22) taken from a single vertical section over a distance of 20m above the Magnisia deposit, have trace element signatures ranging from serpentinite-type upwards to more typically marine carbonate signatures. Overall, sample 1c6 exhibits trace element qualities very similar to that of unmineralised serpentinite, mx shows higher quantities of Pb, Tm, Yb and Eu, and sample 1c22 contains a full suite of elements with elevated concentrations of Sr, Nb, Ba, Ce, Ta and U. Mo, Tb, and Bi are notably depleted in all three samples. Sample 'mx' has a similar trace element distribution pattern to 1c22, but with higher Pb and Ba contents. Dolomite samples indicate dolomitisation of limestone due to close proximity with serpentinite. Samples taken from progressively higher levels (over a vertical distance of 5-6m) from dolomite in contact with serpentinite into marine limestone, show progressively less of these trace element features.

Magnesite veins

Certain trace elements within Akamas magnesite vein samples such as Pb, Hf, Ta, U, Th, and Sm, are not commonly substituted into the magnesite structure (Pohl, 1989), and so it must be assumed these are present within minor silicate phases included throughout the cryptocrystalline magnesite vein material. These phases, either clay (smectite) or serpentine, are however, only detectable by XRD or petrographic examination in very small quantities. Pb and Ba, which are not usually detected within serpentinite, are found in measurable concentrations within the magnesite. These elements are particularly interesting as they are usually restricted to felsic igneous rocks and terrestrial sediments. In the absence of large amounts of clay minerals in the deposits, this possibly indicates the interaction of mineralising solutions with felsic lithologies.

Trace element distributions and concentrations in magnesite from the Magnisia mine area show some trace element features similar to serpentinite samples (both fresh and mineralised). However, the presence of chemically mobile trace elements in the magnesite, which are not detected in the serpentinite or limestone, indicate that magnesite has been precipitated by solutions introduced into the serpentinite from elsewhere. Some features appear to have been inherited from serpentinite (peaks at Li, Eu, and Nb), particularly where samples have been taken from Zone 1. Some elemental abundance patterns, particularly with respect to Ba, La, Ce, U, and Th, are comparable to the trace element patterns obtained for the sandstone samples. These particular trace elements are present in lower abundances than in other lithologies tested.

Trace elements present in magnesite (which are more common in the limestone) may be present due to the physical nature of the magnesite veins. For example many magnesite veins contain epigenetic calcite and dolomite precipitated in fractures and voids in the magnesite. Serpentinite fragments (wallrock) and serpentine minerals are also present in the magnesite which were captured during magnesite formation. Allowing for the presence of calcite, dolomite, and serpentine in the magnesite veins, it is reasonable to suggest the trace element composition of a whole-rock sample may reflect trace element characteristics from each mineral present.

Magnesite nodules

Close to the serpentinite-limestone contact, magnesite nodules take on some of the characteristics of the marine limestone. Some of the Rare Earth Elements found within the nodules which are common to the limestone are present in magnesite nodules, but at lower concentrations. The presence of these elements in the magnesite may be due to diagenesis with remobilisation of trace elements, as the change in trace element distribution patterns is only seen in nodules sampled close to the contact with the limestone.

Nodules show marked similarities to the vein sample trace element signatures. This would be expected if the two different styles of mineralisation were initially derived from the same solutions.

5.4.5 Comparison of Trace Element and Isotope Data

Isotopic evidence suggests an organic source for the carbon within the magnesite veins and nodules ($\delta^{13}\text{C} = -10\text{‰}$ (PDB)), probably derived from decarboxylating organic material within sediments during emplacement of the serpentinite (Fallick *et al.*, 1991).

This being the case, then one possible candidate for such an organic source (within the vicinity of mineralisation) is an organic-rich sandstone formation belonging to the Mamonia Complex. If carbon was derived from an organic component in sedimentary material, then a chemical (trace element) link exists between magnesite and sandstone in the form of similar relative concentrations (normalized) and trace element distribution patterns. Dissolution and reprecipitation of magnesite veins as nodules is indicated as the trace element patterns of both Zone I and Zone II magnesite are similar. This is consistent with stable isotope data for Zones I and II.

Table 5-1 Results of X-Ray Diffraction analyses for Akamas samples. M = Magnesite, C = Calcite, D = Dolomite, Cl = Clay, S = Serpentinite, T = Tenorite, and G = Gypsum

Sample name	Sample #	Mineralogy	Comments
M1	Z11600.RAW	M	
M2	Z11596.RAW	M	
M3	Z11619.RAW	M	
M4	Z11488.RAW	M/T	MAGNESITE/TENORITE
M5	Z11599.RAW	M	
M6	Z11500.RAW	M/T	MAGNESITE/TENORITE
M7	Z11618.RAW	M	
M9	Z11487.RAW	C	
M12	Z11616.RAW	S	
M13	Z11625.RAW	M	
M14	Z11501.RAW	M	
M15	Z11501a.RAW	M	
D1	Z11626.RAW	D	FERROAN
D2	Z11621.RAW	C	
D3	Z11620.RAW	C	
L1	Z11629.RAW	C	
L2	Z11624.RAW	C/G	
S1	Z11628.RAW	S	CLINOCHRYSTOTILE
S3	Z11627.RAW	S	CLINOCHRYSTOTILE
S4	Z11485.RAW	S	CLINOCHRYSTOTILE
BOA	Z11622.RAW	Cl	
Ai	Z11623.RAW	M	
Aii	Z11493.RAW	M	
Aiii	Z11492.RAW	Cl	MONTMORILLONITE
Aiv	Z11490.RAW	M	
Av	Z11617.RAW	C	
A5b	Z11499.RAW	Cl	MONTMORILLONITE
A5b(v)	Z11598.RAW		

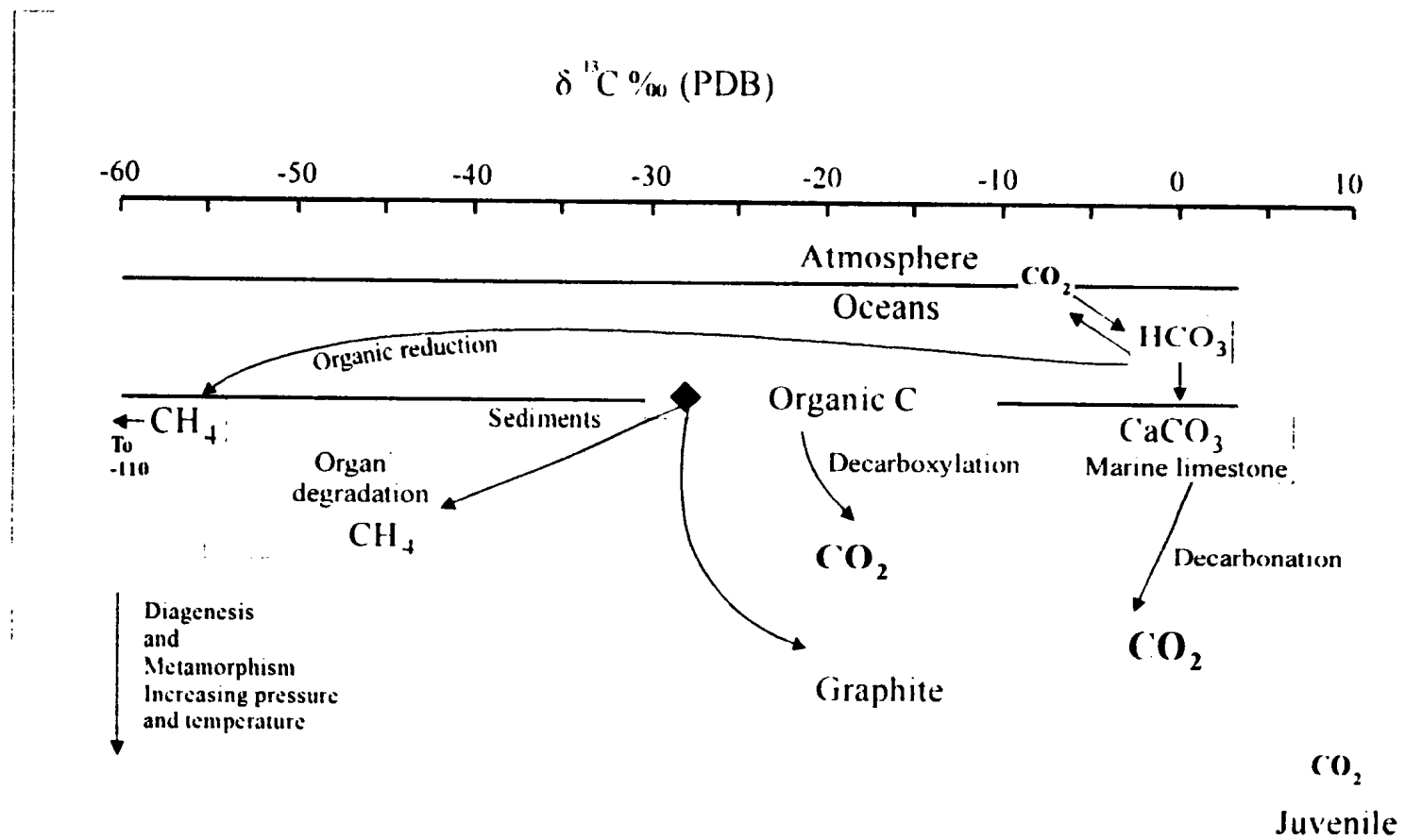


Figure 5.1 Diagram showing ranges in isotopic composition of carbon within several reservoirs (Faure, 1986; Hoefs, 1973)

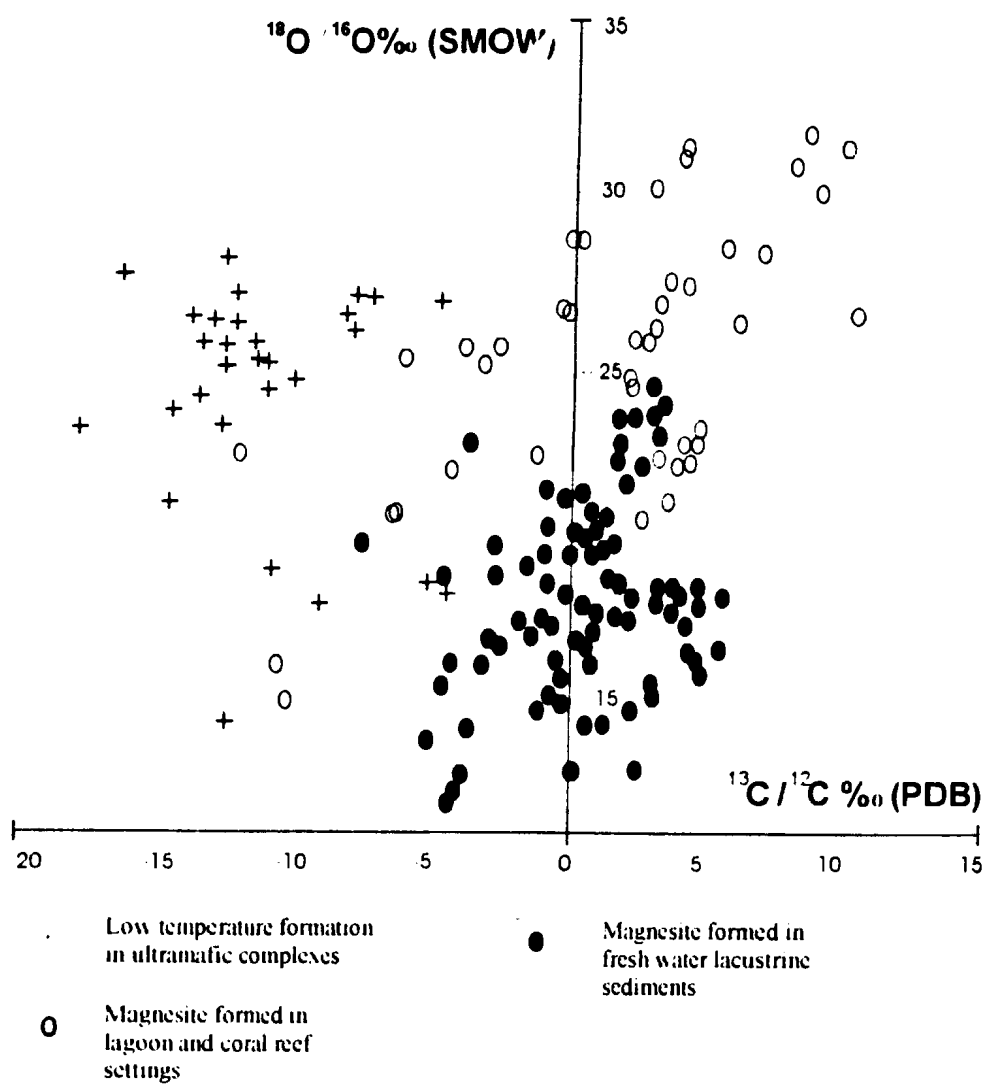


Figure 5.2 Common stable isotope ratios (carbon and oxygen) of different genetic types of magnesite deposits (Moller, 1991).

Table 5.2 Carbon and oxygen isotopic values for Akamas carbonate samples including magnesite, calcite and dolomite

Carbonate	Carbon (PDB)	Oxygen (SMOW)	Morphology	Mineralogy
1c12	-10.5	29.3	Nodule	Magnesite
2c12	-10.2	27.3	Nodule	Magnesite
1c9	-9.1	23.6	Nodule	Magnesite
2c15	-9.8	29.5	Nodule	Magnesite
s1	-9.5	29.7	Nodule	Magnesite
s9	-10.4	30.0	Nodule	Magnesite
s10	-9.8	29.1	Nodule	Magnesite
x4	-10.0	26.5	Nodule	Magnesite
m1	-9.8	26.3	Nodule	Magnesite
m4	-11.1	27.7	Nodule	Magnesite
x14	-9.4	26.0	Nodule	Magnesite
m5	-9.4	27.2	Nodule	Magnesite
2c14	-10.4	28.1	Vein	Magnesite
x6	-9.4	14.5	Vein	Magnesite
2c13	-10.8	26.6	Vein	Magnesite
10x	-7.8	15.4	Vein	Magnesite
sm	-12.7	12.2	Vein	Magnesite
1c8	-9.6	25.5	Karst	Calcite
1c10	-11.4	26.8	Karst	Calcite
1c19	-1.1	26.3	Karst	Calcite
1c20	-0.1	27.5	Vein Fill	Calcite
1c21	-8.9	26.4	Vein Fill	Calcite
1c23	-2.5	26.3	Vein	Calcite
1c24	-2.7	26.1	Vein	Calcite
c-s	-13.8	29.4	Vein	Calcite
1c22	2.4	34.3	Laminar ppt	Dolomite
1c6	-9.6	26.6	Vein	Dolomite

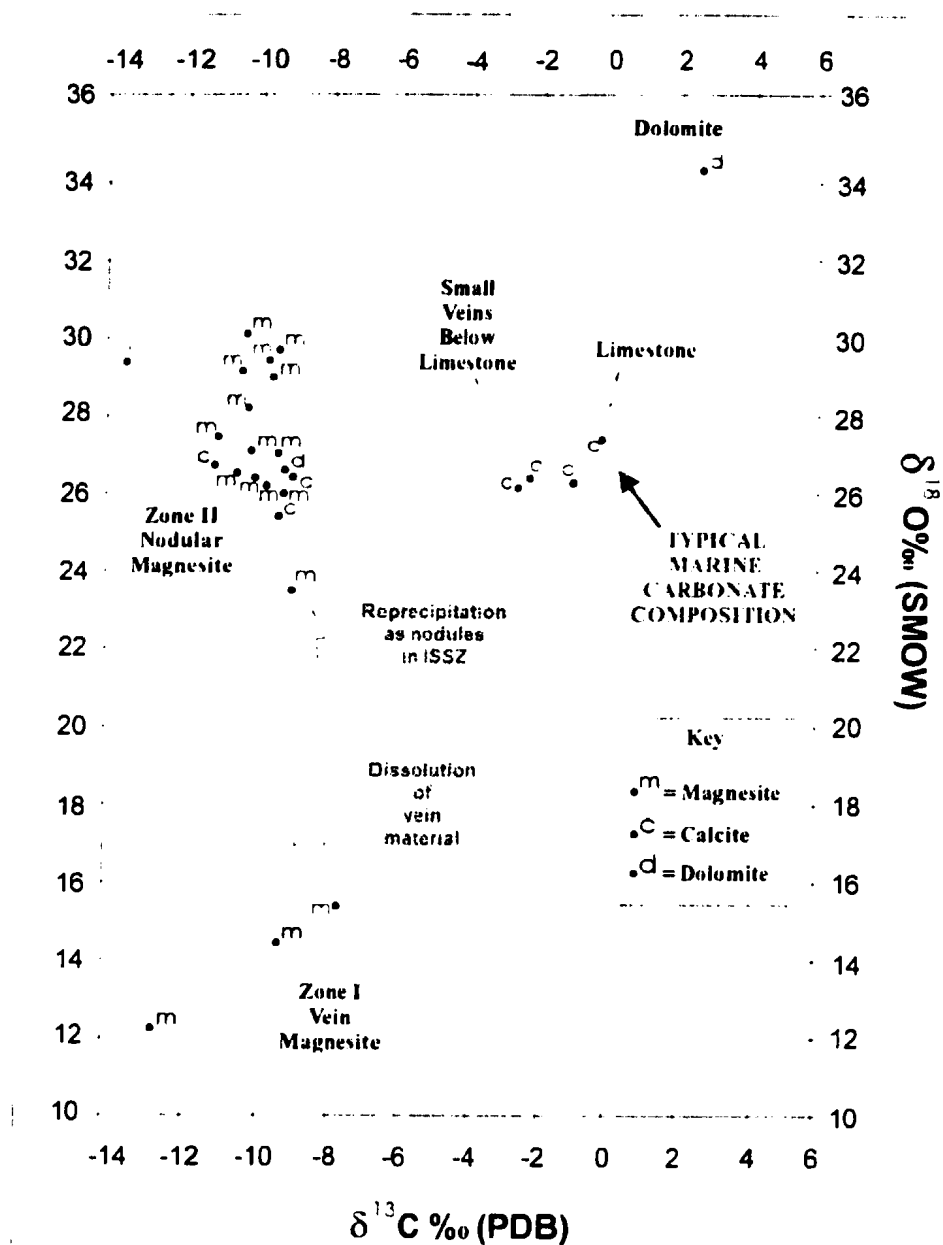


Figure 5.3 Carbon vs. Oxygen Crossplot for magnesite (m), calcite (c) and dolomite (d).

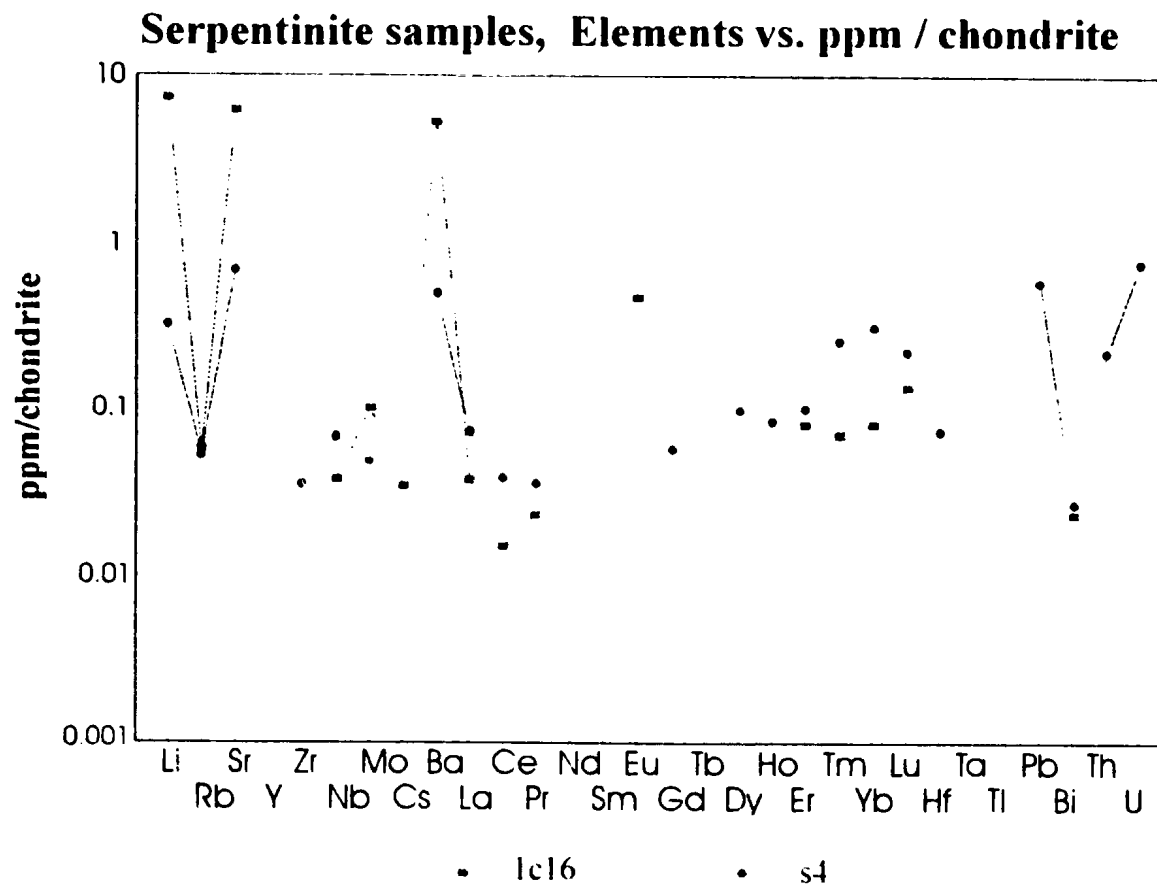


Figure 5-4-1 Trace element compositions of two samples of serpentinite, one taken from the Magnisia Locality, the other from an unmineralised area (see text for explanation)

Calcite samples, Elements vs. ppm / chondrite

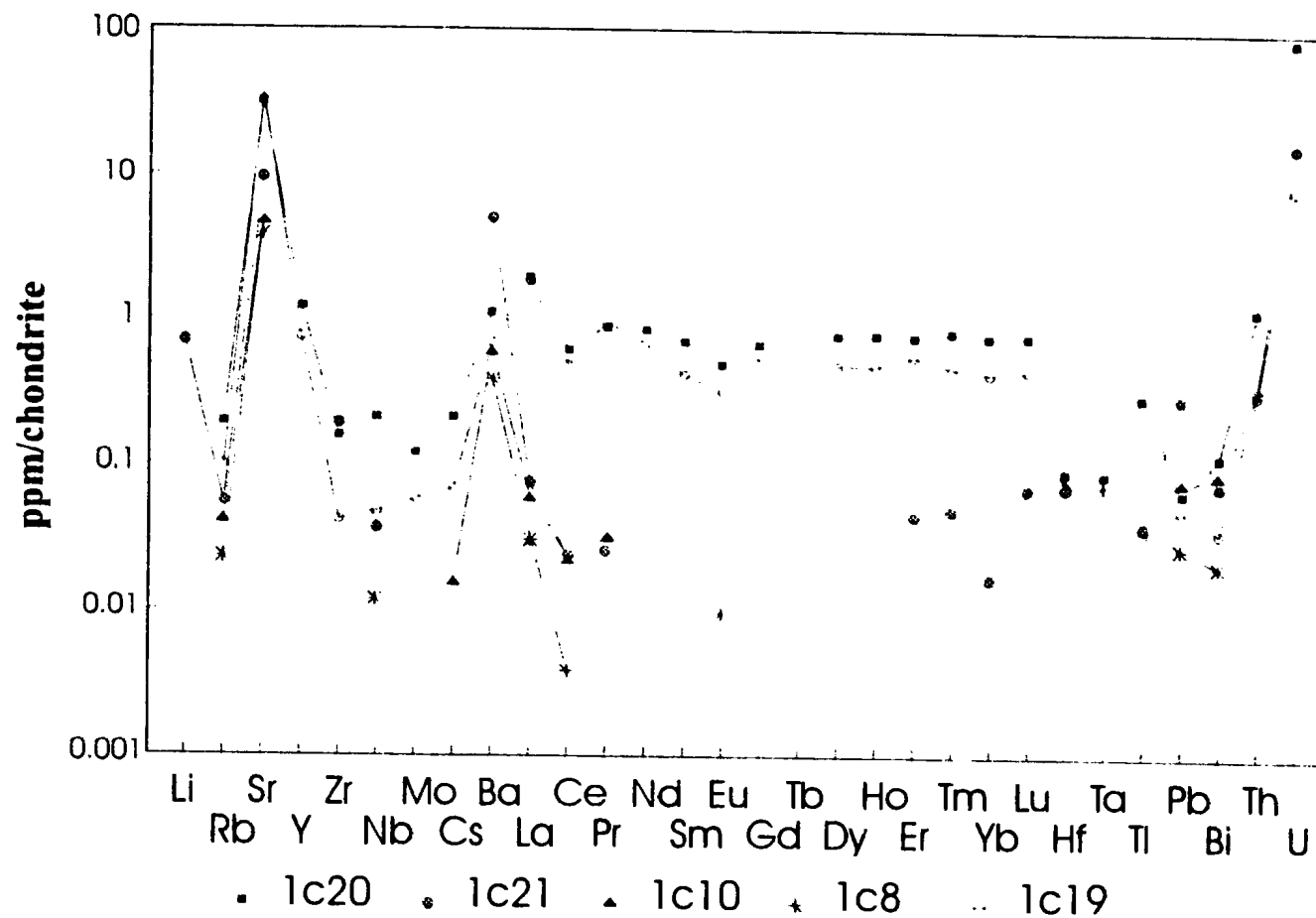


Figure 5.4.2 Trace element compositions of five samples of calcite taken from the Magnisia Locality.

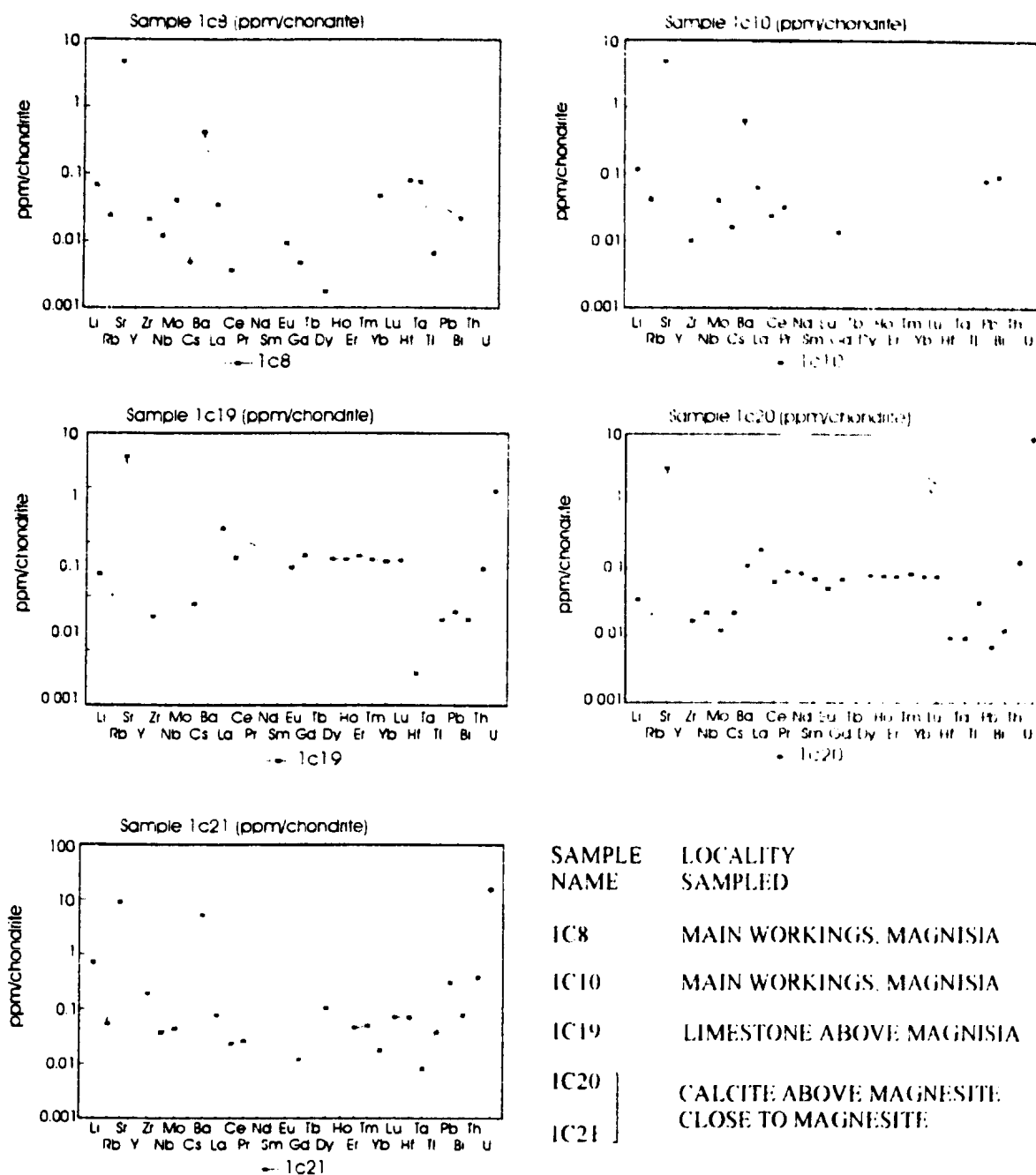


Figure 5.4.3 Trace element signatures of calcite samples, Elements vs. ppm / chondrite

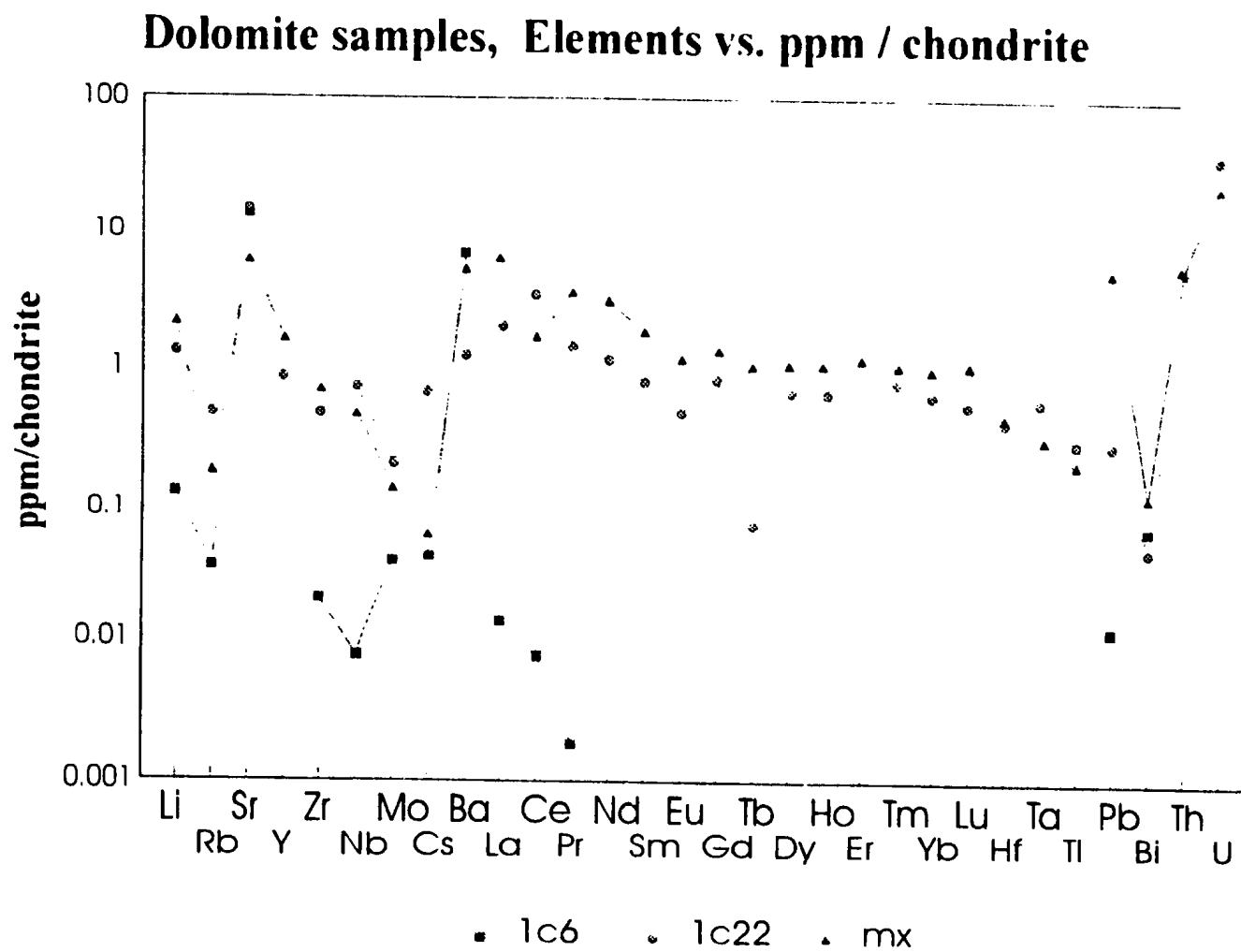


Figure 5.4.4 Trace element compositions of three samples of dolomite taken from the Magnisia Locality

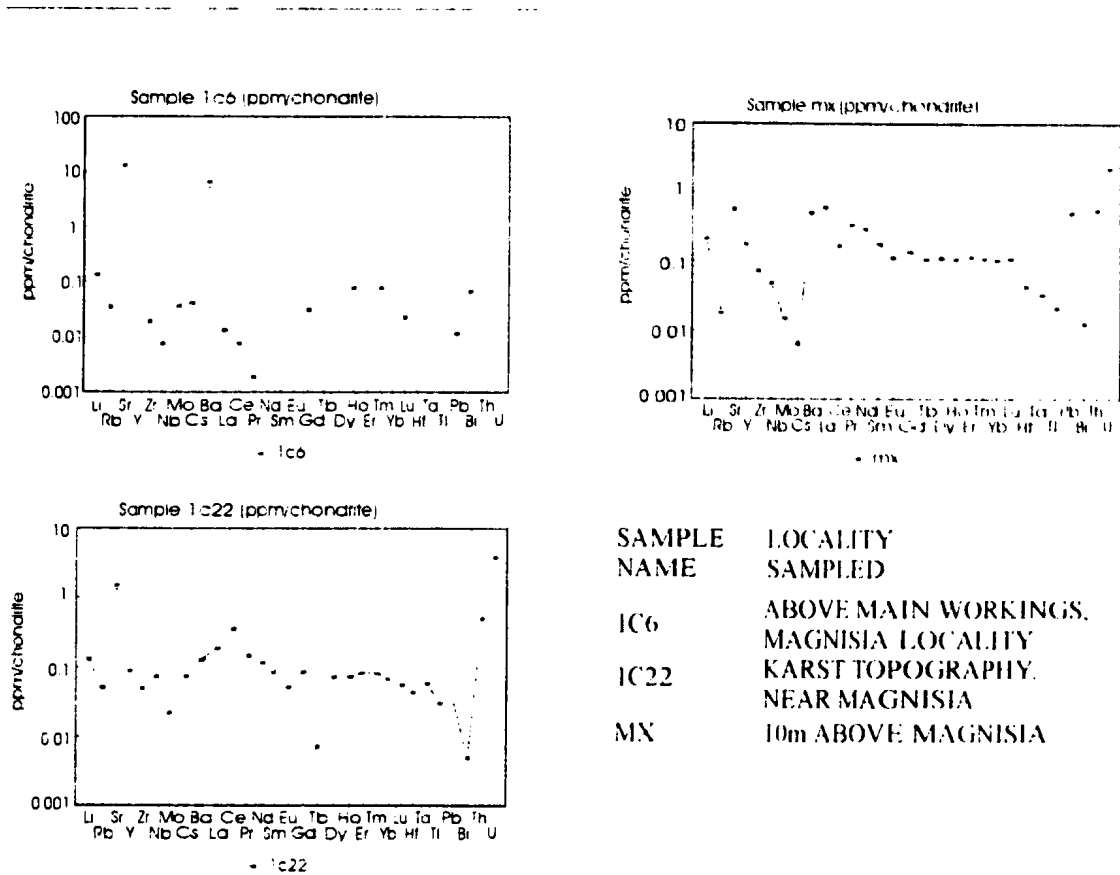
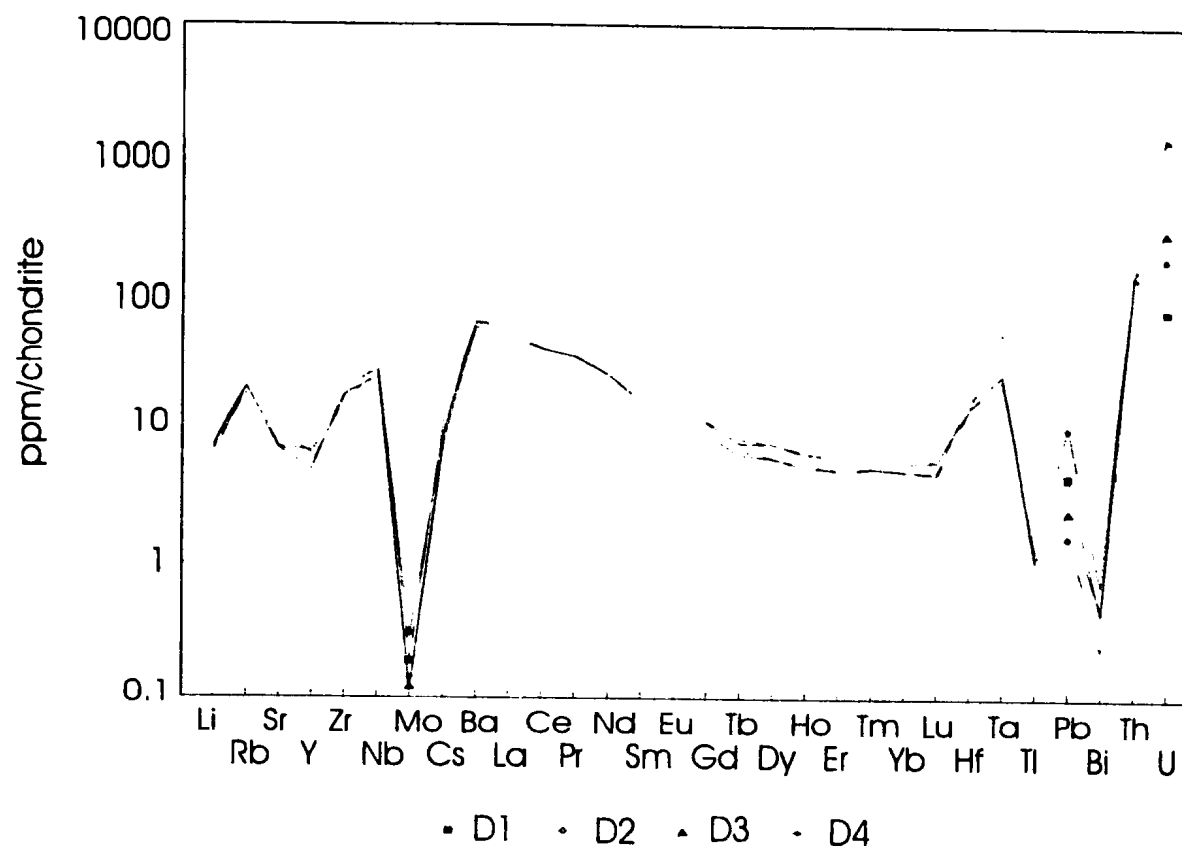


Figure 5.4.5 Trace element signatures of dolomite samples, Element vs ppm/chondrite

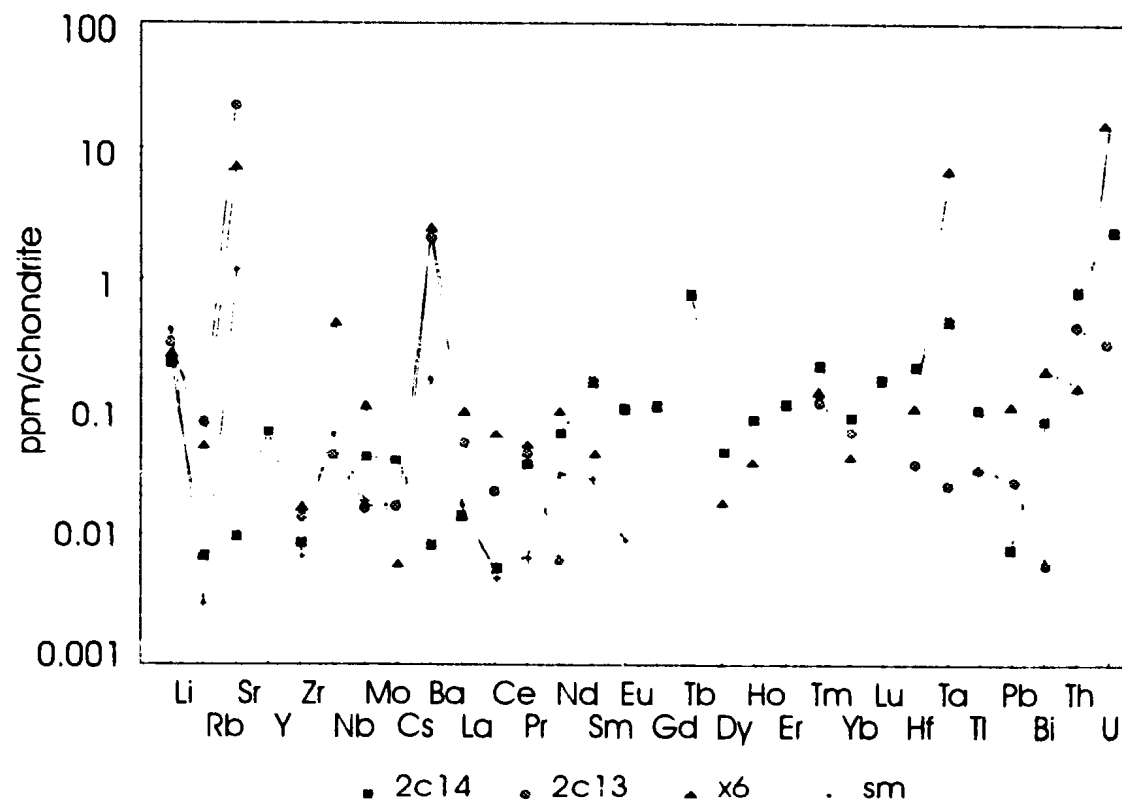
Sandstone samples, Elements vs. ppm / chondrite



BREAKS IN EACH LINE INDICATE ELEMENTS WHICH ARE BELOW THE LIMIT OF DETECTION AFTER NORMALISATION.

Figure 5.4.6 Trace element compositions of four samples of sandstone taken from an area outside the mineralisation.

Magnesite vein samples, Elements vs. ppm / chondrite



BREAKS IN EACH LINE INDICATE ELEMENTS WHICH ARE BELOW THE LIMIT OF DETECTION AFTER NORMALISATION

Figure 5.4.7 Trace element compositions of four samples of vein magnesite taken from the Magnisia Locality.

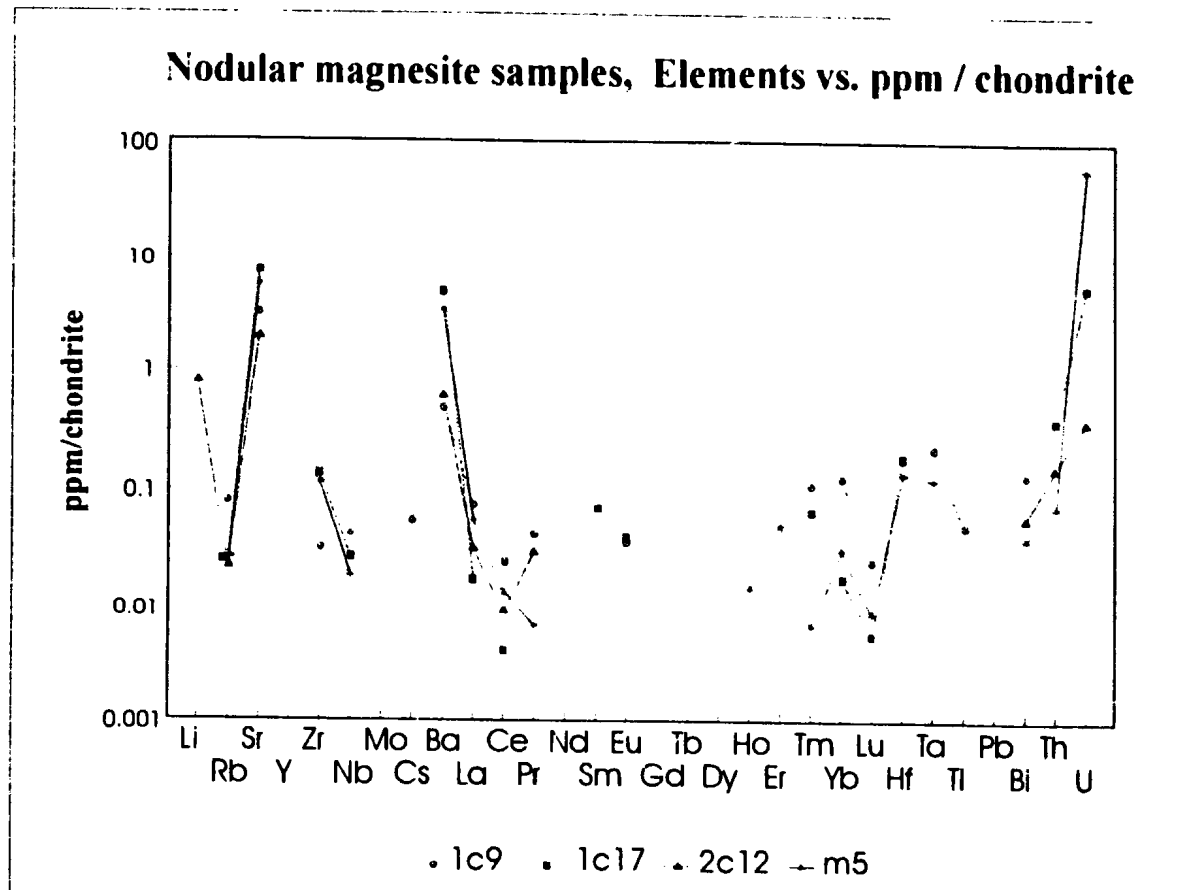
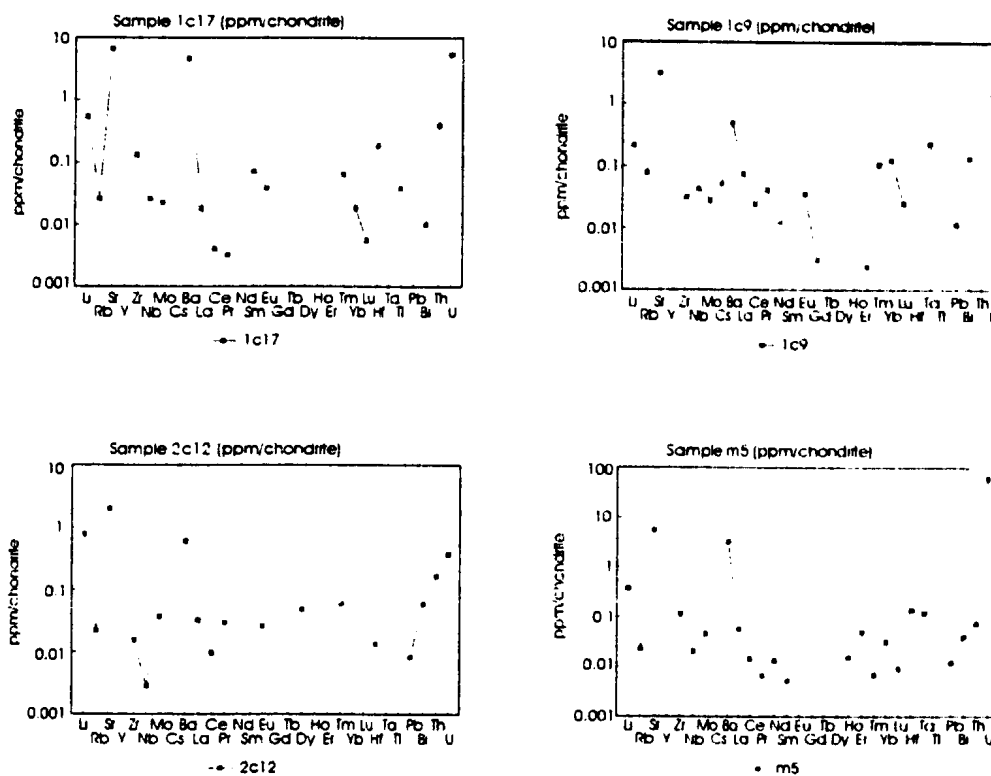


Figure 5.4.8 Trace element compositions of four samples of nodular magnesite taken from the Magnisia Locality.



<u>SAMPLE NAME</u>	<u>LOCALITY SAMPLED</u>
1C9	MAIN WORKINGS, MAGNISIA LOCALITY
1C17	MAIN WORKINGS, MAGNISIA LOCALITY
2C12	MAIN WORKINGS, MAGNISIA LOCALITY
M5	MAIN WORKINGS, MAGNISIA LOCALITY

Figure 5.4.9 Trace element signatures of nodular magnesite samples, Elements vs ppm / chondrite.

6.0 SUMMARY AND CONCLUSIONS

6.1 Regional Geological Setting

Cyprus exhibits a complex geological history which records tectonic processes associated with a long period of interaction of several lithospheric micro-plates in the eastern Mediterranean. The results of this interaction during the late Cretaceous are preserved in the rocks of southwest Cyprus. Two major juxtaposed terranes, the Mamonia Complex consisting of Triassic ocean floor, seamounts and passive margin sediments, and the Troodos Complex consisting of ophiolitic rocks formed in a supra-subduction zone environment, were juxtaposed at this time along an intricate suture zone (Figure 2.2). The suturing process was complex and involved thin-skinned delamination of the Mamonia terrane and both overthrusting and underthrusting of the Troodos ophiolite by Mamonia rocks. Rocks belonging to the Mamonia Complex are therefore not only likely to be found at depth beneath the Troodos Complex, but have also been thrust over ophiolitic rocks during back-thrusting in the late Cretaceous.

Plutonic, volcanic and sedimentary rocks of the Troodos and Mamonia Complexes crop out in erosional windows through Tertiary-Recent marine carbonate cover sequences. Geological features resulting from a complex series of tectonic events, both contractional and extensional, are preserved. Two main contractional tectonic episodes are evident, a primary north- and northwest-directed thrusting, and a secondary west- and southwest-directed thrusting episode. The second contractional episode is better preserved in the study area than the first.

6.2 Local Geological Setting of the magnesite deposits

The Akamas Window contains rocks which belong to the Troodos and Mamonia complexes. The magnesite mineralisation in this window is set within a large allochthonous sheet of serpentinitised harzburgite belonging to the Troodos ophiolite which has been emplaced from east to west and is thrust over sheeted diabase dykes (with minor gabbro stocks) which are, in turn, thrust over upper and lower pillow lavas. Rocks of the Mamonia Complex, namely radiolarian mudstones and cherts of the Ayios Photios Group, are thrust over the serpentinite.

The magnesite deposits are situated on the western flank of the Neogene Polis Graben where rocks of the Mamonia and Troodos complexes, as well as Tertiary carbonate cover sequences have been downthrown to the east in step-like fashion. Deposits are not continuous, but are spaced at intervals of a few hundred metres along a line between Sandalides and Piana, a distance of approximately 5km (Ilich and Maliotis, 1984). The largest of the magnesite deposits is Magnisia mine, which has been the most exploited but still shows many of the features characteristic of the mineralisation throughout the whole area.

Magnesite Mineralisation

Field mapping of shear zones and magnesite vein orientations in the fractured and serpentinitised harzburgite host rock, and observation of styles of magnesite mineralisation allow the formulation of an overall model for magnesite formation in this area.

On the deposit scale, two distinct zones of magnesite mineralisation are defined within the serpentinite, Zone I at the base of the deposits and Zone II at higher structural

levels. Zone I includes a network of large magnesite veins and stockworks. At the bottom of Zone I, a Basal Serpentine Thrust (BST) occurs as a 10-20cm thick shear zone separating serpentinite from underlying diabase and gabbro. Zone II consists of nodular magnesite formed as a replacement style of mineralisation in the Intra-Serpentine Shear Zone (ISSZ). The division of the mineralisation into zones, and the constraints on timing of magnesite formation, are based upon field relations.

Zone I

Zone I magnesite mineralisation is associated with the development of a dilational (antitaxial) vein system. Magnesite and high magnesium calcite veins show features such as "comb" textures, median lines and spalled wallrock included in veins. The vein system is hosted by a regional east-dipping contractional shear zone developed in serpentinite with well defined features such as c-s shear fabrics, grooves and fibrous mineral package lineations. The overall shear direction is west-northwest. The magnesite vein system has typically developed along pre-existing anisotropies which formed relatively early in the shear zone deformation. Carbonate veins precipitated along c- and s-planes of the shear zone fabric (particularly along the Basal Serpentine Thrust). Increased pore fluid pressures, presumably developed during periods of relaxation in the contractional tectonism, resulted in hydraulic fracturing of serpentinite and associated opening and mineralisation of the existing shear zone anisotropies. Large magnesite veins are aligned with the steep anisotropy common to the s-plane of the serpentinite shear fabric (Figure 3.4b). It is likely that mineralising fluids utilized these planar elements of the shear zone fabric during periods of magnesite vein formation due to their inherent mechanical

weakness (i.e. fissility of the serpentinite schistosity). Continued contractional tectonism after formation of the large magnesite veins is recorded as groove lineations at the edges of veins in contact with wallrock. The orientation of these lineations is consistent with the overall shear direction of the serpentinite sheet. In the large magnesite veins, angular fragments of magnesite (some of which preserve 'comb' textures) are apparently brecciated vein material which were displaced and cemented by later magnesite precipitation. It is suggested that early dilational magnesite veins were disrupted by hydraulic brecciation of magnesite and serpentinite during later phases of magnesite mineralisation. These features, when considered with the groove lineations upon calcite veins in c-planes and bull veins in s-planes, indicate vein formation during quiescent periods between active displacement of the surrounding serpentinite (Friedman, 1964; Hodgson, 1989; Coli and Sani, 1990). 'Ladder vein networks' are indicative of mineralisation of an "incompetent unit in a ductile matrix under extension" (Hodgson, 1989).

The structural control on the Zone I type mineralisation is therefore visualized as hydraulic fracturing in an already evolving regional shear zone structure. Fracturing was probably induced by high pore fluid pressures, possibly during periods of reduced slip or sticking on the shear zone, followed by renewed slip (Sibson, 1990). Vein formation is envisaged as being a cyclic process of active shear, relaxation of shear stress, build-up of pore-fluid pressure, reduction of effective normal stress and consequently jacking open (dilation) of existing anisotropies, mineralisation, and finally back to active shear as a result of the mechanical weakening of the shear zone. This model is the same as that

described by Sibson (1990) where active faulting and fluid flow are related to mineralisation of various types. Zone I magnesite vein formation is therefore syn-tectonic in nature.

Zone II

Zone II overlies Zone I and is separated from it by the Intra-Serpentine Shear Zone (ISSZ) which contains magnesite nodules. The ISSZ is a 5-10m thick zone near the top of the serpentinite body and contains a fabric which indicates displacement in a similar westerly thrusting direction to the BST. Whereas the BST exhibits a well defined c-s fabric, as well as sheared and shattered serpentinite suggesting both brittle and ductile deformation, the ISSZ lies at a much shallower angle than the BST and exhibits wholly brittle deformation in the form of cataclastically sheared serpentinite. The inclusion of clasts of Mamonia mudstones and chert within the ISSZ indicate a shallower level thrust system incorporating Mamonia rocks in the serpentinite shear zone. This shear zone is probably part of the floor thrust that emplaced the Mamonia thrust sheets westwards over the Troodos rocks (i.e. harzburgite). The presence of a small klippe of Ayios Photios Group mudstones and chert structurally above the ISSZ is consistent with this interpretation.

Zone II encompasses the ISSZ and the blocky magnesite up to the contact with the overlying Tertiary marine limestone. Magnesite nodules have been precipitated within the shear fabric of the ISSZ and to a certain extent within the serpentinite above this shear zone. The nodules are best developed at the Magnisia locality, but may also be seen elsewhere along the line of deposits.

All magnesite precipitation within Zone II occurred after the cessation of serpentinite thrusting, because nodules of magnesite have clearly overgrown all shear fabrics in the ISSZ. The ISSZ itself probably formed contemporaneously with the BST. It is possible that the ISSZ formed an impermeable layer at the top of Zone I which allowed ponding of mineralising solutions and the formation of vein and stockwork magnesite during the phase of Zone I type mineralisation. The sheared, carbonatised serpentinite within Zone II (ISSZ) therefore contains mineralisation which is later than that of Zone I. Later, after the regional thrusting, this shear zone would likely relax resulting in the development secondary permeability allowing mineralising solutions to access the shear zone and hence form the magnesite nodules. It is also possible that vein magnesite may have been remobilized by circulating solutions within Zone I, and deposited as nodules in Zone II.

6.3 Chemistry

The chemistry, both isotopic- and trace element compositions of magnesite, serpentinite, limestone, dolomite and organic sandstones support the field evidence, and provides an insight into petrogenetic aspects of the magnesite formation process

The dolomite along the walls of the Magnisia mine adits, along with microcrystalline magnesite, calcite, are recognized as recent precipitates and are seen in places to overprint the mineralisation in Zones I & II.

Samples were taken from Zones I & II of the magnesite deposits for chemical analyses. Carbonates, such as the marine limestone which unconformably overlies the deposits, and dolomite from a small cave in serpentinite (which is precipitating from

circulating groundwater at present) in the vicinity of the magnesite deposits, were sampled for comparison of isotope compositions.

Stable Isotope Study

The detailed investigation of field relationships in and around the magnesite deposits, and strategic sampling of Zones I & II for isotope analyses, provide new results which significantly revise genetic models for magnesite formation in the Akamas area. Most of the samples tested previously were taken from nodular magnesite in Zone II of the Magnisia deposit. A new isotope field is recognized for Zone I vein magnesite. Carbon isotope values are very similar to Zone II nodular magnesite, but the oxygen isotopes are notably different; vein and nodule populations inhabit completely different fields. Both vein and nodular magnesite have an average carbon isotope value of approximately -10‰ (PDB). Vein magnesite has an average oxygen isotope value of 14‰ (SMOW) while nodular magnesite have an average oxygen isotope value of 28‰ (SMOW).

The stable isotope study of the magnesite and other carbonates within the vicinity of the mineralisation was undertaken in order to identify probable source reservoirs of carbon and oxygen. Marine limestone has an isotopic signature quite different to either magnesite veins or nodules ($^{13}\text{C} \sim -2$ to 0‰ (PDB)) and is therefore unlikely to have provided the carbon now present in the magnesite. The same is true for juvenile-, metamorphic-, and atmospheric-carbon sources which lie in fields completely separate from either Zone I or Zone II magnesite.

Vein magnesite from Zone I occupies a field with mean carbon and oxygen isotopic values of -10‰ (PDB) and $+14\text{‰}$ (SMOW), while nodular magnesite from Zone

II has mean carbon and oxygen isotopic values of -10‰ (PDB) and 26‰ (SMOW). Calculations performed using mineral isotope ratios and an assumed isotopic value for mineralising solutions, indicate that Zone I magnesite veins were formed at an approximate temperature of 165°C , while Zone II magnesite nodules formed at an average temperature of 40°C . Carbon reservoirs during mineralisation are usually limited (Moller, 1989), making the probability of two separate carbon sources with identical carbon isotope ratios, unlikely. The similarity in carbon isotopic compositions for both magnesite veins and nodules indicates a similar source for the carbon in the magnesite of Zones I & II. As the carbon for both zones appears similar, then it is probable that vein material has been remobilized and has subsequently been precipitated in the shear zone (ISSZ) of Zone II. This process must have begun after the formation of the ISSZ.

Isotope results therefore support a genetic model for magnesite in which veins are precipitated from hydrothermal solutions during, or prior to, thrusting of the serpentinite (at elevated temperatures), with nodules forming later (at lower temperatures), either from the tail end of the mineralising solutions responsible for the veins, and/or by remobilisation of the vein material of Zone I.

The carbon and oxygen isotope ratios of calcite taken from the BST shear fabric are -13.87‰ (PDB) and $+29.42\text{‰}$ (SMOW). This calcite sample lies within the same field as the magnesite nodules of Zone II, and is therefore thought to be a low temperature carbonate formed during the final stages of the emplacement of the serpentinite into its present position, probably precipitated from the mineralising solutions responsible for magnesite formation (at a temperature of approximately 40°C).

Recent precipitates exhibit the active formation of carbonates from circulating CO₂-rich solutions. It is not clear whether these carbonates are a continuation of Zone II nodular formation, or whether they are entirely separate genetically. Recent precipitates have a carbon and oxygen isotopic composition of +2.43‰ and +34.34‰ respectively, and formed at temperatures around 10°C, reflecting the ambient air temperature inside serpentinite caves.

Isotope compositions of marine limestone, and some veins associated with the mineralisation of Zone II, indicate either mixing of mineralising fluids with limestone or diagenetic shifting of ¹³C/¹²C of ratios of marine calcite toward the nodular magnesite isotope field. Isotopic compositions of small veinlets within Zone II, close to the marine limestone cover, lie between the isotope fields of magnesite nodules and limestone. These veins are probably the result of re-equilibration of magnesite mineralisation with solutions derived from the limestone. Samples of calcite taken from the base of the limestone (several centimetres above the serpentinite-limestone contact) show a slight deviation toward the isotopic field for the mineralisation. Diagenetic effects are also likely responsible for this isotopic shift.

Trace Element Study

The trace element study was undertaken in an attempt to link carbon present within the magnesite to possible carbon sources in the study area, such as marine limestone, dolomite and organic sandstone.

Some of the trace elements present in magnesite samples are not present within any of the surrounding lithologies (such as Pb, U, Th, and Ce), lending support to the proposal for a hydrothermal provenance of mineralising solutions.

Trace element compositions of the magnesite veins are similar in many respects to the composition of the nodules, and both show certain common features with respect to trace elements present and relative elemental abundances of these elements. This supports the idea of the remobilisation of magnesite vein material, and reprecipitation in Zone II as magnesite nodules. Trace element signatures of the marine limestone and the dolomite just above the serpentinite are very different to those of the magnesite, suggesting that the magnesite carbon was derived from elsewhere (other than the limestone or dolomite). Similarities are noted in trace element signatures of the organic sandstones tested, and the magnesite mineralisation. Since the carbon isotopes suggest an organic source for the carbon in the magnesite, it is proposed that the carbon within the magnesite may have been derived through decarboxylation of organic material. The source and provenance of this organic material is not clear, but some portion may have been contained within the organic sandstones inferred to lie structurally beneath the serpentinite (Malpas et al., 1993).

6.4 Model for Magnesite Formation

A model for magnesite mineralisation has been formulated from field relations, petrography, and chemical analyses of magnesite, serpentinite, and associated lithologies (marine limestone, dolomite, sediments) and is summarized in Figure 6.1. Figure 6.2 depicts important aspects at relevant stages during the process magnesite formation.

The earliest magnesite was precipitated as veins during initial disruption of the serpentinite body. It is most likely that the first magnesite was formed after the initiation of obduction, as the isotope evidence suggests an organic source for the carbon within the magnesite. Recent re-interpretation of the regional geology of SW Cyprus (Malpas *et al.*, 1993) implies both overthrusting and underthrusting of Mamonia rocks in the Mamonia-Troodos suture zone, allowing Mamonia sediments to lie structurally beneath the serpentinite containing magnesite mineralisation. The presence of Mamonia sedimentary thrust sheets below the Troodos Complex in the Akamas Peninsula however, is not established (Malpas *et al.*, 1993). Carbon within the magnesite is probably derived from the decarboxylation of organic-rich sediments such as the organic-rich Vlambouros Sandstone belonging to the Ayios Photios Group. This could have provided CO₂ during the regional thrusting, thus initiating magnesite formation.

The earliest-formed magnesite was then brecciated, probably by active thrusting, and the brecciated pieces were cemented together by later cryptocrystalline magnesite formation. Such vein magnesite was formed at temperatures of around 165°C suggesting moderate burial depths for the mineralisation, in the range of 4 to 6km for normal geothermal gradients in zones of plate convergence. Further displacement of the serpentinite produced slickensides in this material, affecting both magnesite breccia and the cementing magnesite matrix. At some later stage, probably within the same contractional tectonic regime, the serpentinite (now containing the large magnesite veins and stockworks of Zone I) was emplaced into its present position with the formation of the BST, and precipitation of calcite within the c-s fabric. This calcite was formed at

temperatures around 40°C and has an isotopic signature similar to that of the magnesite nodules. It is suggested that this calcite was formed by the tail end of vein forming solutions during thrusting of the serpentinite.

The ISSZ, which is now carbonatised, is host to much of the magnesite mineralisation of Zone II. This mineralisation is in the form of magnesite nodules which were precipitated by remobilisation of vein material of Zone I as indicated by the results from the isotopic and trace element studies. It is noted that there is a relatively large temperature difference suggested for the two styles of magnesite mineralisation, veins having formed at temperatures of ~165°C and nodules at a lower temperature of ~40°C. Magnesite nodules may have formed at any time after active contractional tectonism affecting the serpentinite, but likely before the deposition of the overlying Tertiary marine limestone due to the limited degree of dolomitisation of this limestone. Magnesite nodules were probably formed in the earliest Tertiary.

Trace element data support the incorporation of trace elements into the magnesite which are not detected in the serpentinite, limestone, or dolomite, and show elemental abundances and distributions similar to that of organic sandstones from the Mamonia. It is suggested that the process of magnesite mineralisation in the Akamas area is long lasting and continues to the Present. This is supported by the presence of recent magnesite, calcite and dolomite precipitates on the walls of adits and within a small serpentinite cave on the shore section at Loutra tis Aphroditis. Adit precipitates of cryptocrystalline calcite, magnesite and dolomite have formed most recently, within the past few decades, and may be remnants of the mineralisation process which formed the nodules. Nodular magnesite is

also seen cementing limestone erratics on a serpentinite hillside, and is present within faulted limestone above the serpentinite.

TIME	LITHOLOGICAL AGE CONSTRAINTS	MINERALISATION EVENT	TECTONIC EVENTS
Recent	Age of marine terrace deposits (Swarbrick and Robertson, 1980)	PRECIPITATION OF MAGNESITE AND DOLOMITE IN MINING ADITS AND CAVES	CONTINUED EXTENSION
Middle Tertiary			EXTENSIONAL REGIME - GRABEN FORMATION
Early Tertiary	Age of Tera Limestone deposited during Polis graben formation (after magnesite vein formation)	NODULAR PRECIPITATES FORMED WITHIN UPPER THRUST ZONE (ISSZ)	
	Final emplacement of ophiolite (Swarbrick and Robertson, 1980)	MAGNESITE VEINS PRECIPITATED IN BSI	RELAXATION OF ZONE II AND FORMATION OF SECONDARY PERMEABILITY
		MAIN VEIN AND STOCKWORK MINERALISATION	FORMATION OF BSI AND ISSZ AND FINAL EMBLACEMENT OF SERPENTINITE
		BRECCIATION OF EARLY MAGNESITE AND FURTHER MAGNESITE FORMATION	
Late Cretaceous	Ophiolite generation (Robertson & Dixon, 1984)	INITIAL FORMATION OF MAGNESITE VEINS	INITIAL THRUSTING OF SERPENTINITE

Figure 6.1 The proposed sequence of mineralisation events in relation to timing and processes affecting the hosting serpentinite.

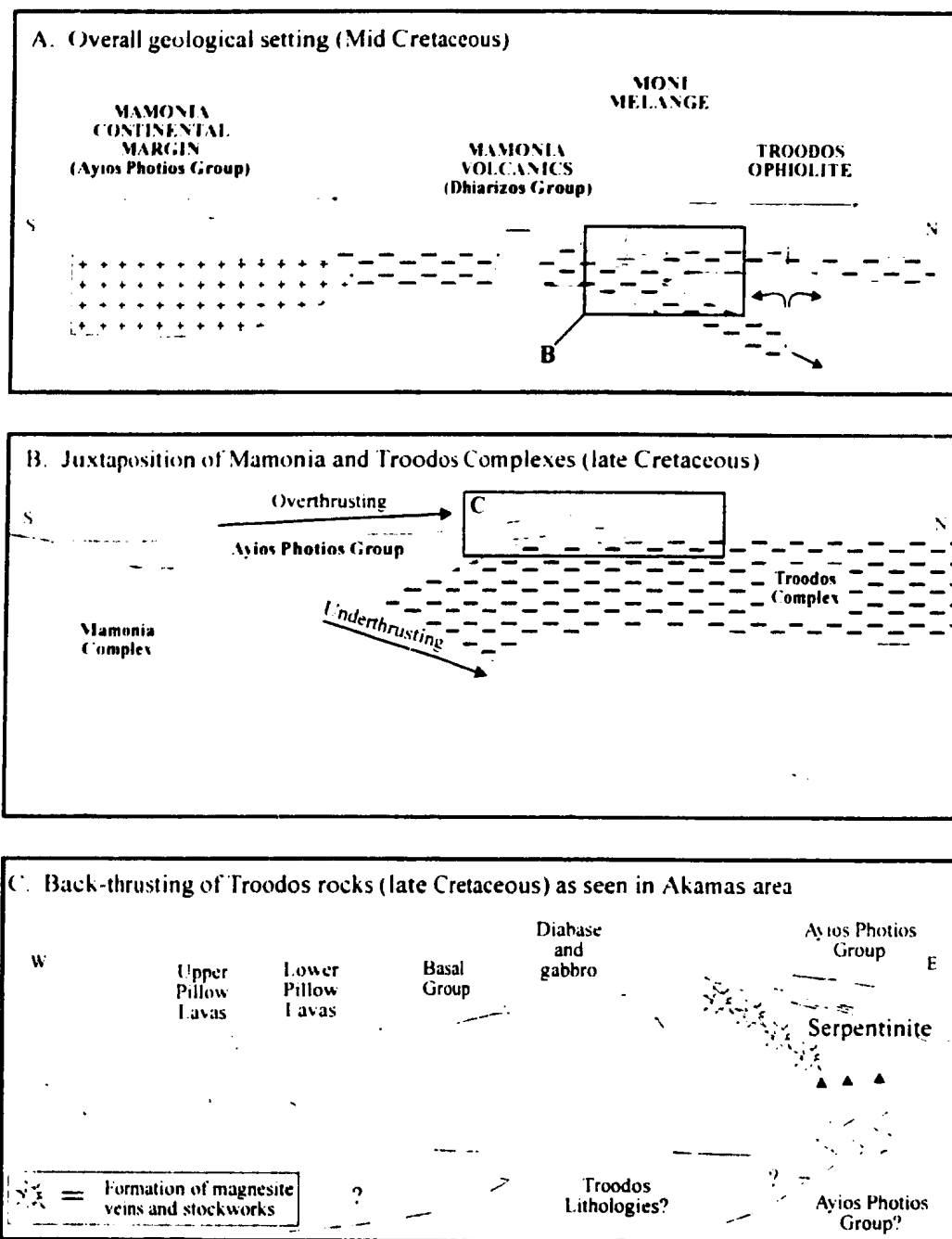


Figure 6.2 Sequence of cartoons illustrating the genetic model proposed for the Akamas magnesite deposits.

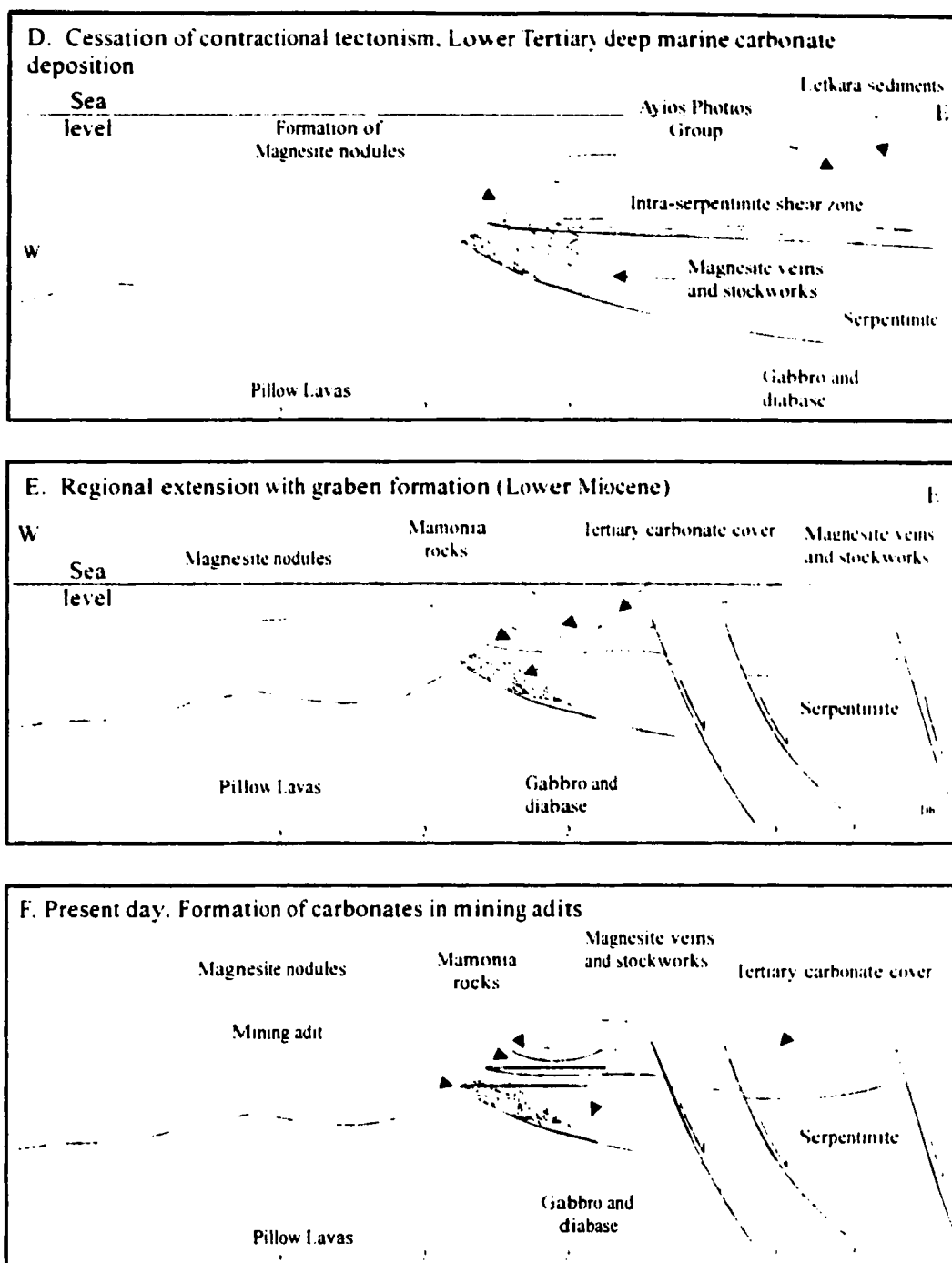


Figure 6.2 (continued) Sequence of cartoons illustrating the genetic model proposed for the Akamas magnesite deposits.

REFERENCES

- Aharon, P.** 1988. A stable isotope study of magnesite deposits from the Rum Jungle Uranium Field, Australia: Implications for the origin of strata-bound massive magnesites. In: *Chem. Geol.*, **69**, 127-145.
- Al-Aasm, I. S., Taylor, B. E. and South, B.** 1990. Stable isotope analysis of multiple carbonate samples using selective acid extraction. In: *Chem. Geol. (Isotope Geoscience Section)*, **80**, 119-125.
- Bain, G. W.** 1924. Types of Magnesite Deposits and their Origin. In: *Econ. Geol.*, **19**, 412-433.
- Barnes, I. and O'Neil, J. R.** 1969. The Relationship Between Fluids in some Fresh Alpine-Type Ultramafics and Possible Modern Serpentinisation, Western United States. In: *Bull. Geol. Soc. Am.*, **80**, 1947-1960.
- Barnes, I. and O'Neil, J. R.** 1971. Silica-carbonate alteration of serpentine: Wall rock interaction in mercury deposits of the California Coast Ranges. In: *Econ. Geol.*, **68**, 388-398.
- Bathurst, R. G. C.** 1971. Carbonate sediments and their diagenesis. -Elsevier, Amsterdam - New York.
- Bone, Y.** 1983. Interpretation of magnesites at Rum Jungle, N. T., using fluid inclusions. In: *J. Geol. Soc. Australia*, **30**(3).
- Brownlow, A.** 1979. Geochemistry. Englewood Cliffs, London, Prentice-Hall (Ed.).
- Brydie, J. R., Fallick, A. E., Ilich, M., Maliotis, G. and Russell, M. J.** 1993. Stable isotopic study of magnesite in Akamas area, northwest Cyprus. In: *Trans. Instn. Min. Metall. (Sect. B: Appl. earth sci.)*, **102**, B1-54.
- Coli, M. and Sani, F.** 1990. Vein distribution in a thrust zone: a case history from the Northern Apennines, Italy. In: Knipe, R. J. and Rutter, E. H. (Eds). 1990. Deformation Mechanisms, Rheology and Tectonics, Geological Society Special Publication No. 54, pp 475-482.
- Cornides, I. and Kukasabe, M.** 1977. Preparation of Carbon Dioxide from Magnesite for Isotopic Analysis. In: *Fresenius Z. Anal. Chem.*, **287**, 310-311.
- Dabitzias, S.G.** 1980. Petrology and Genesis of the Vavdos Cryptocrystalline Magnesite Deposits, Chalkidiki Peninsula, Northern Greece. In: *Econ. Geol.* **75**, 1138-1151.

Deer, A. G., Howie, R. A. and Zussmann, R. A. 1962. An introduction to the rock-forming minerals, 16th Edition (New York : Longman Scientific Technical, 1989), 528.

Fallick, A. E., Ilich, M. and Russell, M. J. A 1991. Stable Isotopic Study of the Magnesite deposits Associated with the Alpine-Type Ultramafic Rocks of Yugoslavia. In: *Econ. Geol.*, **86**, 847-861.

Faure, G. 1986. Principles of Isotope Geology 2nd ed., Wiley and Sons (eds), New York p491-512.

Follows, E. J. 1980. Ph.D thesis, Dept. of Earth Science, University of Edinburgh, Edinburgh, Scotland.

Friedman, G. M. 1964. Depositional environments in carbonate rocks: a symposium, Friedman, G. M. (ed). In: Soc. Econ. Palaeontologists and Mineralogists, 1969, Special Pub., **14**, 198pp.

Gass, I. G. 1960. The geology and mineral resources of the Dhali area. In: *Cyprus Geol. Surv. Mem.*, **4**, 116pp.

Gribble, C. D. and Hall, A. J. 1985. A Practical Introduction to Optical Mineralogy George, Allen & Unwin (publishers) Ltd., London, U.K.

Haralimbides Mining Company. 1923-24. Polis, Paphos District, Cyprus.

Hodgson, C. J. 1989. Patterns of Mineralization. In: Mineralization and Shear Zones Geological Association of Canada Short Course Notes, **6**, J. T. Bursnell (ed)

Hoefs, J. 1973. Stable Isotopes. Cambridge University Press. p38-59

Ilich, M. 1968. Problems of the Genesis and Genetic Classification of Magnesite Deposits. In: *Geologica Carpathica*, **19**, 149-160.

Ilich, M. and Maliotis, G. 1984. The magnesite deposits of the Akamas area (Cyprus). In: Hellenic Mining Co. Ltd. Files, Nicosia, Cyprus. 10pp.

Kralik, M., Aharon, P., Schroll, E. and Zachmann, D. 1989. Carbon and oxygen isotope systematics of magnesite: a review. In: Monograph Series on Mineral Deposits, **28**, 197-225; Gebruder Borntraeger, Berlin-Stuttgart.

MacCleod, C. J. 1990. Role of the Southern Troodos Transform Fault in the rotation of the Cyprus microplate: evidence from the Eastern Limassol Forest Complex. In: Malpas, J., Moores, E., Panayiotou, A. and Xenophontos, C. (eds), Ophiolites: Oceanic Crustal Analogues, Proc. 'Troodos 87' Symposium. *Cyprus Geol. Surv. Dept.*, 75-85.

Maksimovic, Z. and Dangic, A. 1974. The study of trace elements in magnesite deposits of different genetic types. In: Bogdanov, B. (Ed.) : problems of ore deposition. - Fourth Iagod Symposium, Varna., 2, 387-394.

Maliotis, G. 1977. A report on the magnesite occurrences in the Akamas Peninsula. In Hellenic Mining Co. Ltd. Files. Nicosia, Cyprus. 10 pp.

Malpas, J. and Xenophontos, C. 1992. Geological map of the Polis-Akamas area at 1:25,000 scale. Cyprus Geol. Surv. Dept.

Malpas, J. and Xenophontos, C. and Williams, D. 1992. The Ayia Varvara Formation of SW Cyprus: a product of complex collisional tectonics. In: Tectonophysics, **212**, 193-211.

Malpas, J., Calon, T. and Squires, G. 1993. The Development of a late Cretaceous microplate suture zone in S.W. Cyprus. In: Magmatic Processes and PLate Tectonics, Geol. Soc. Spec. Publ. No.76, 177-197.

Martiny, E. and Rojkovic, I. 1977. Trace elements in magnesites of Slovakia (Central West Carpathians). In: Geol. Zbor. Geol. Carpath., **28**, 311-322.

McCrea, J. M. 1950. The isotopic chemistry of carbonates and a palaeotemperature scale. In: J. Chem. Phys., **18**, 849-857.

Moller, P. 1989. Minor and trace elements in magnesite. In: Monograph Series on Mineral Deposits, **28**, 173-196; Gebruder Borntraeger, Berlin-Stuttgart.

Morteani, G. 1989. Fluid inclusions in magnesite. In: Monograph Series on Mineral Deposits, **28**, 237-241; Gebruder Borntraeger, Berlin-Stuttgart.

Morteani, G., Schley, F. and Moller, P. 1983. On the formation of magnesite. In: Schneider, H. J. (ed): Mineral Deposits of the Alpine Epoch in Europe. 106-116 Springer.

Mukasa, S. B. and Ludden, J. N. 1987. Uranium-Lead ages of plagiogranite from the Troodos ophiolite, Cyprus, and their tectonic significance. In: Geology, **15**, 825-828.

Murton, B. J. 1990. Was the Southern Troodos Transform Fault a victim of microplate rotation? In: Malpas, J., Moores, E., Panayiotou, A. and Xenophontos, C. (eds), Ophiolites. Oceanic Crustal Analogues, Proc. of the International Ophiolite Symposium. Cyprus, 1987. Cyprus Geological Survey Dept., Nicosia, Cyprus. p87-98.

O'Neil, J. R. 1977. Stable isotope Geochemistry: A Tribute to Samuel Epstein, Taylor, H. P., O'Neil, J. R., and Kaplan, I. R. (eds). Geochem. Soc. Special Pub., **3**, 516p.

O'Neil, J. R. and Barnes, I. 1977. $\delta^{13}\text{C}$ and $\delta^{18}\text{O}$ compositions in some freshwater carbonates associated with ultramafic rocks and serpentinites : Western United States. In *Geochim. Cosmochim. Acta.*, **35**, 687-697.

Pohl, W. 1989. Comparative geology of magnesite occurrences. In: *Monograph Series on Mineral Deposits*, **28**, 1-15; Gebruder Borntraeger, Berlin-Stuttgart

Pohl, W. and Siegl, W. 1986. Sediment Hosted Magnesite Deposits. In: Wolf, K. H. (Ed.): *Handbook of strata-bound and strataform ore deposits*, **14**, 223-310, Elsevier, Amsterdam.

Redlich, K. A. 1909. Die Typen der Magnesitlagerstätten. In: *Z. Prakt. Geol.*, **17**, 300-310, Berlin.

Robertson, A. H. F. 1977. Tertiary Uplift of the Troodos Massif, Cyprus. In: *Geol. Soc. Am. Bull.*, **88**, 1763-1772.

Robertson, A. H. F. 1990. Tectonic evolution of Cyprus. In: Malpas et al (Eds) *Ophiolites. Proceedings of the International Ophiolite Symposium, 1987, Cyprus*

Robertson, A. H. F. and Hudson, J.D. 1974. Pelagic sediments in the Cretaceous and Tertiary history of the Troodos Massif, Cyprus. In: *Spec. Publ. Internat. Assoc. Sedimentol.*, **1**, 403-436.

Robertson, A. H. F. and Dixon, J. E. 1984. The Geological Evolution of the Eastern Mediterranean. *Geol. Soc. Spec. Pub.*, **17**, 36-48.

Robertson, A. H. F. and Woodcock, M.H. 1979. Mamonia Complex, S.W. Cyprus. Evolution and emplacement of a Mesozoic continental margin. In: *Geol. Soc. of Amer. Bull.*, **90**, 651-665.

Robertson, A. H. F., Eaton, S., Follows, E. J. and McCallum, J. E. 1990. Role of tectonics versus sea-level change in the Neogene (Miocene-Pliocene) evolution of the Cyprus active margin. In: MacDonald, D. I. M. (ed). *Sedimentation, tectonics and eustasy: sea-level change at active plate margins. Spec. Publ. Int. Ass. Sedimentol.*, **12**

Sibson, R. H. 1990. Faulting and Fluid Flow. In: *Mineralogical Association of Canada Short Course on 'Crustal Fluids'*, Handbook Vol. **18**, Nesbitt B. E. (ed).

Simonian, K. O. and Gass, I. G. 1978. Arakapas fault belt, Cyprus. A fossil transform fault. In: *Bull. Geol. Soc. Amer.*, **89**, 1220-1230.

Swarbrick, R.E. and Robertson, A. H. F. 1980. Revised stratigraphy of the Mesozoic rocks of S.W. Cyprus. In: *Geological Magazine*, **117**, 547-621.

Taylor, H.P. and McClelland, J. R. 1985. *The Continental Crust : Its Composition and Evolution*. 178pp.

Timbal, A 1994. Pers. Comm. , Dept. of Earth Sciences, Memorial University of Newfoundland, Newfoundland, Canada.

Wenner, D. B. and Taylor, H. P. 1973. Oxygen and hydrogen isotope studies of the serpentinization of ultramafic rocks on oceanic environments and continental ophiolite complexes. In: *Am. J. Sci.*, **273**, 207-239.

Zachmann, D. W. and Johannes, W. 1989. Cryptocrystalline Magnesite. In: *Monograph Series on Mineral Deposits*, **28**, 16-29; Gebruder Borntraeger, Berlin-Stuttgart.

Zedef, V. 1994. Unpublished PhD thesis, Dept. of Geology and Applied Geology, Glasgow University, Scotland, U.K.

APPENDIX 1

This section deals with the sampling regime for this study and a list of samples obtained.

ZONE I Mineralisation

Magnesite samples.

Magnesite samples were collected from the structural base of deposits up to the very top. Large veins and stockworks were sampled as well as the nodular precipitates found above the vein carbonates. It was found that the majority of excavations have taken place within the nodular precipitates of carbonate.

Thrust zone carbonates : Basal Serpentinite Thrust (BST)

The calcite veins were too delicate to sample individually and so it was decided to sample a complete section thrust zone. A piece sheared serpentinite approximately 25cm in thickness, containing veins and kinematic indicators, was sampled in order to obtain thin sections of the thrust fabric (as well carbonate samples). Individual veins are ~0.1 to 1cm in thickness.

Large magnesite veins

Large magnesite veins making up the basal portions of the deposits were sampled from the lowest structural positions accessible. Samples were taken from massive vein material, both within the central portions of the veins and from the outer edges (close to the serpentinite).

ZONE II Mineralisation

Nodular magnesite

Nodules of magnesite were sampled in order to ascertain any chemical variations between this generation of carbonate and previous generations of carbonate (in the form of veins and stockworks).

Recent precipitates

Two carbonates found precipitated in interesting positions, one on the walls of a mining adit (Magnisia) and the other in a small cave (Loutra tis Aphroditis), were sampled as they appear similar (in hand specimen) to the magnesite in nearby adits.

Calcite veins in gabbro.

Small centimetre scale veins were taken from vari-textured gabbro immediately below the thrust contact with serpentinite. These veins are soft, friable, and appear to have been precipitated from the edges of the fractures. Epigenetic calcite is present within voids.

Limestone-dolomite samples.

Shallow marine limestone overlies most of the mineralisation and surrounding area and shows evidence of brecciation and dolomitisation at the serpentinite-limestone contact. Some magnesite is also present in zones of faulting and brecciation. It is noted that the degree of dolomitisation appears to be greater within the vicinity of the larger deposits.

Serpentinite samples.

Samples of serpentinised harzburgite were collected from within deposits and also several kilometres away from any magnesite occurrence in order to test the lithology for evidence of contamination and/or element transfer between mineralising solutions and the serpentinite.

Samples collected from Cyprus 1991, 1992 and 1993.

1991 All samples from Magnisia deposit

<u>Sample</u>	<u>Description</u>	<u>Comments</u>	<u>Extra Information</u>
1C12	Magnesite	Stockwork	
2C12	Magnesite	Vein	
2C13	Magnesite	Vein	
1C9	Magnesite	Vein	
2C14	Magnesite	Vein	
2C15	Magnesite	Stockwork	
S1	Magnesite	Stockwork	
S9	Magnesite	Stockwork	
S10	Magnesite	Stockwork	
1C22	Dolomite	Tufa	Ppt on cave wall
1C6	Dolomite	Vein	Epigenetic vein
1C8	Calcite	Stockwork	Epigenetic ppt
1C10	Calcite	Stockwork	Epigenetic ppt
1C19	Calcite	Karst	Lst above deposit
1C20	Calcite	Karst	Lst above deposit
1C21(l)	Calcite	Vein	Epigenetic ppt
1C23	Calcite	Vein	Epigenetic ppt
1C24	Calcite	Vein	Epigenetic ppt

1992 Samples taken from various locations in and around mineralisation.

<u>Sample</u>	<u>Description</u>	<u>Comments</u>	<u>Extra</u>
M1	Magnesite	Vein	
M2	Magnesite	Vein	
M3	Magnesite	Vein	
M4	Magnesite	Stockwork	
M5	Magnesite	Stockwork	

<u>Sample</u>	<u>Description</u>	<u>Comments</u>	<u>Extra</u>
M6	Magnesite	Vein	
M7	Magnesite	Vein	
M8	Magnesite	Vein	
M9	Magnesite	Stockwork	
M10	Magnesite	Vein	
M11	Magnesite	Vein	
M12	Magnesite	Vein	
M13	Magnesite	Vein (botryoidal)	
S1	Serpentinite	Unmineralised	
S2	Serpentinite	Vein in Htz	
S3	Serpentinite	Massive, just below cover	
S4	Serpentinite	Unmineralised	
L1	Calcite	Karst topography	
L2	Calcite	Karst topography	
D1	Dolomite	1m above serpentinite	
D2	Dolomite	3m above D1	
D3	Dolomite	5m above D2	

1993 Selected samples from several deposits including Magnisia.

<u>Sample</u>	<u>Description</u>	<u>Comments</u>	<u>Specific</u>
X1	Conglomerate Gabbro, diabase and carbonate sand		
X2	Magnesite	Vein	Magnisia
X3	Serp. & Mag.	Sheared serp	Magnisia
X4	Magnesite	Nodule	Magnisia
X5	Sediments	Mamonia	In sheared serp
X6	Magnesite	Vein	Magnisia
X7	Magnesite	Nodule	Magnisia
X8	Dolomite	Breccia	Fault, Magnisia
X9	Calcite	Karst	Limestone (Tera)
X10			

<u>Sample</u>	<u>Description</u>	<u>Comments</u>	<u>Specific</u>
X11	Magnesite		
X12	Magnesite		
X13	Magnesite	Nodular	In dunite
X14	Magnesite	Soft & friable	Nodular
X15			
X16	Dol. & Mag.		
X17	Magnesite		
Cave ppt	Mag., Cal., Dol		
10x	Magnesite	Vein	
x6	Magnesite	Vein	
sm	Magnesite	Vein	

Samples collected Spring 1994

<u>Sample #</u>	<u>Lithology</u>	<u>Location</u>
A1	Sandstone	Asprokremnos Reservoir
A2	Pelagic limestone	Between Reservoir & Dhiarizos River
A3	Calcareous sst	Between Reservoir & Dhiarizos River
A4	Petra tou Romiou Lst	Chapotami
A5	Radiolarite	Chapotami
D1	Sandstone	Dhiarizos River
D2	Sandstone (Organic)	Dhiarizos River
D3	Sandstone (Organic)	Dhiarizos River
D4	Sandstone (Organic)	Dhiarizos River
D5	Sandstones	Dhiarizos River

D6	Sandstone	Dhiarizos River
D7	Limestone with chert	Dhiarizos River
<u>Sample #</u>	<u>Lithology</u>	<u>Location</u>
D8	Pelagic limestone	Dhiarizos River
D9	Pelagic limestone	Dhiarizos River
D10	Sandstone	Dhiarizos River

APPENDIX II

Table containing structural measurements of c-, s-planes and lineations on these c-planes

c-plane orientations				s-plane orientations				lineations on c-planes	
346	44	002	44	349	80	355	79	109	45
356	52	350	55	344	85	356	78	113	48
352	50	353	54	349	86	358	74	108	50
349	48	346	54	349	85	362	77	112	51
347	48	348	46	340	81	359	76	106	48
349	50	339	50	349	84	358	80	110	50
346	46	345	56	351	87	351	82	116	49
348	49	344	50	350	85			109	47
350	50	342	58	349	80			115	51
348	64	354	52	344	80			112	49
347	46	352	56	2	78			111	50
348	52	346	55	353	83			114	48
352	48	356	40	346	84			107	46
356	52	341	42	350	86			106	49
350	52	351	50	349	85			105	50
353	50	337	52	355	74				
346	54	352	46	356	80				
348	54	349	52	358	84				
350	50	350	49	1	81				
348	48	354	54	358	80				
345	50	345	48	361	77				
352	48	348	50	359	79				
348	53	350	47	360	86				
355	46	354	49	360	83				
347	54	340	58	357	85				

Where s-plane measurements were taken, there was a clear relationship between c- and s-planes. All lineations were taken on c-planes. Measurements of planes are given as strike and dip using the right-hand-rule convention.

APPENDIX III

Isotopic Analyses : Analytical Procedure

The techniques involved in the preparation and extraction of carbon dioxide from the carbonate samples are simple and straightforward. The sample is first crushed to a fine powder, then identified using X-Ray Diffraction (XRD). Once identified, the sample may then be prepared for isotopic analysis. If a combination of minerals are present, for example calcite with magnesite, then the sample is reacted for an hour with 10% hydrochloric acid (HCl). The calcite-acid reaction is fast, but the magnesite-acid reaction is much slower, so once all of the calcite has reacted, the magnesite remains 'in residuum'. The sample may then be washed with distilled water and dried in a warm oven (85 °C) for 24 hours.

Pyrex vessels are used to contain the sample, along with acid in a smaller vessel within (in order to keep carbonate and acid separate until the reaction between them is desired). Pyrex tubing (9mm in diameter) is cut into 30cm lengths and flame sealed at one end. The vessel is then cleaned with distilled water, then methanol and dried in the oven for several hours until all moisture is expelled. A smaller pyrex vessel (6mm in diameter) is cut to around 4cm and again is flame sealed.

A small portion of carbonate is carefully weighed, usually 5 to 6mg, and is placed within the large vessel where it rests at the bottom. The smaller vessel is then filled with 103% phosphoric acid (50mg of acid) and also placed within the large vessel and then pumped using both electric pump and diffusion pump for 2 hours to obtain vacuum. Once a reasonable vacuum has been obtained ($T_c = 120-150$), the vessel is sealed at the top, forming a completely sealed vessel with acid and sample unreacted inside. The sample is then placed in an oven until it reaches a temperature of 100°C. This usually takes one to two hours. The sample may then be 'spilled' to allow the acid to flow out of the small vessel and react with the sample. This reaction occurs at 100°C for approximately 24 hours. It has been found that the reaction is complete after 15 hours, so 24 hours is more

than adequate. The carbon dioxide is now trapped inside the large vessel and may be stored there for extended periods of time without fear of leakage and/or contamination as the vessel is completely sealed.

Extraction of the gas involves a series of steps which culminate in the collection of carbon dioxide in a temporary vessel used for loading the sample into a mass spectrometer. A 'break-seal' is used to break the vessel containing the sample gas and process it 'in vacuo'. A gas extraction line is used to extract samples under vacuum conditions. The sample is released from the vessel by breaking it, allowing the gas to condense in a U tube by cooling the tube with liquid nitrogen. Any non-condensable gasses are then extracted and the sample is moved again into a glass finger where it can be measured by the use of a mercury manometer. This allows the quantity of gas produced by the sample-acid reaction to be measured, and an effective yield to be calculated which aids in the analysis of results. If a high yield is obtained, it is more likely that the gas measured is a true indication of the carbon dioxide produced, indicating that there has been no leakage of gas to the atmosphere. Low yields are found to be statistically poor and may give unreliable results. Once the yield has been measured, the sample is moved into the temporary storage vessel and labeled.

The sample is then analysed using mass spectrometry to measure the ratio of ^{13}C to ^{12}C , relative to a standard gas. A computer package makes a series of corrections (for the various fractionation factors involved with the extraction process), performs statistical analyses of the results and produces all of this data in a single output. The sample is tested 7 times while the standard gas is passed through the mass spectrometer. A standard deviation is taken for these seven results to observe how far results deviate from an average value. In all cases, the standard deviation calculated is low, and the result obtained considered to be accurate.

When the results are obtained and ratios of $^{13}\text{C}/^{12}\text{C}$ (PDB) and $^{18}\text{O}/^{16}\text{O}$ (SMOW) have been calculated, a further correction is applied to the raw data for oxygen. The carbon values are constant and need no further correction. This correction factor concerns the difference in magnesite fractionation from that of either calcite or dolomite upon reaction with the acid.

Analytical Difficulties Encountered

The analytical procedure for extraction of carbon dioxide from the samples proved troublesome, in some respects, in the early stages. The acid placed in the small vessel was continually found to contain large amounts of atmospheric gasses which were expelled upon pumping to create vacuum conditions. This expulsion of large bubbles (up to 5mm in diameter) caused the acid to spill out of the vessel and come into contact with the powdered sample. This caused premature reaction of acid and carbonate, and so the sample had to be prepared again. This occurred several times in succession, only finally being solved by pumping the acid by itself before placing inside a large vessel with the sample. Heating the vessel before pouring the acid also seemed to limit any acid outpourings. It was decided that heating the acid would allow it to become less viscous and any bubbles formed would rise easily through the column of acid. Concern arose however about the effect of changing the properties of the acid in any way, and so cold acid was used for all field samples. Some standards were tested with preheated acid, some with cold acid and there was a slight shift in oxygen values of around 0.5 per mil (SMOW), both above and below the average value of the standard. It was decided that the first three samples were not very accurate due to inconsistencies in technique. Once established however, the procedure seems accurate and results are reproducible.

X-RAY Diffraction analytical technique

The technique of X-Ray Diffractometry (XRD) was used to identify mineral samples, taken from the magnesite deposits for chemical analysis. This is a rapid technique, routinely used to determine the purity of a sample, was used for all samples tested for trace element and isotopic compositions. If two species of carbonate, for example hydrothermal magnesite with epigenetic vein calcite (within voids and fractures), then an average isotopic composition will be obtained during isotope analyses (which is useless when trying to identify source reservoirs of elements). Any magnesite samples which were found to contain epigenetic calcite and/or dolomite were treated in order to obtain pure magnesite prior to further chemical analysis. Once an XRD trace is obtained, identification of minerals is made easy by computer aided matching with standard mineral traces

Trace element analytical technique

Waters are analysed by ICP-MS using four internal standards which are variable in mass (^{45}Sc , ^{89}Y , ^{159}Tb and ^{232}Th) in order to correct for drift and matrix effects. Standards are used in all analyses which conform to United States Geological Survey (USGS) standard reference water samples (T-101, T-103, T-105, T-107 and T-109 for major constituents, M-108, M-110, M-112 for trace constituents). Results are reported in parts per billion (ppb) of each element. Certain interferences are of course present with certain elements such as C, Ca, Fe, Cr, Si and Ti, but the absolute abundances of these elements are not critical in this study, only their presence and relative distribution. Limits of detection are calculated (parts per billion) as three times the standard deviation of the blank count rates. Values reported as being below the limit of detection are reported thus ; "<value". Sample values may be less accurate close to the limit of detection, than where elements are present in abundance. Rock and mineral samples were prepared for ICP-MS analysis by acid dissolution. Sample material, approximately 0.1g, was digested using

boric and oxalic acids (HF/HNO_3). A second digestion procedure is followed for any undissolved sample using hydrochloric and oxalic acid (HCl/HNO_3). This process usually dissolves all material present. Any undissolved solid remaining, possibly graphite, chromite, ilmenite or other oxides, is removed by filtering. The sample was then analysed by ICP-MS using the 'standard addition' method to counteract matrix effects. Limits of detection are calculated, as for waters, as three standard deviations above the background blank value. Values and limits of detection are measured in parts per million (ppm). As an internal standard, two of the samples were run as duplicates. Also, standard geological reference materials were analysed, as well as the reagent blank. Standards used were a diabase - DNC-1 (USGS), and/or a gabbro - CCRMP MRG-1 (USGS). Reagent values are compared to values obtained for samples and are found to be insignificant with respect to sample values, and so are not subtracted from the final total received for sample plus reagent. Limit of detection values lie approximately at 10% of chondritic concentrations.

There are some element interferences noted from the ICP-MS analyses. This is particularly the case with Ta and/or Nb. Tungsten-carbide grinding equipment can cause contamination of the sample and so, for this reason, agate lined grinding and milling equipment was used throughout the sample preparation. Also, Bi concentrations up to 0.1ppm are said to be due to memory effects within the equipment, and so may be disregarded.

APPENDIX IV

TRACE ELEMENT RESULTS

Raw Data.

Results of analyses were separated into specific categories before any arithmetic normalisation procedures were carried out on the data. Sample groups were separated into first of all their constituent mineralogies and or lithologies, then further subdivided with respect to their position within the mineralisation. Vein magnesites were separated from nodular magnesites. Sandstones, calcites, dolomite and serpentinites were also segregated. Once this had been accomplished, the samples were normalised to chondritic ratios according to (Taylor and McLennan, 1985). It is possible to normalise sample data to a specific set of results within the sample set used for this study, but as there were a variety of different lithologies present (igneous, sedimentary and individual mineral samples), it was decided to normalize all data to chondritic ratios.

Table of values (ppm) used for trace element normalisation. Data taken from Taylor and McLennan (1985)

Li	Rb	Sr	Y	Zr	Nb	Mo	Cs
2.4	3.45	11.9	2.25	5.54	0.375	1.38	0.279
Ba	La	Ce	Pr	Nd	Sm	Eu	Gd
3.41	0.367	0.957	0.137	0.711	0.231	0.087	0.306
Tb	Dy	Ho	Er	Tm	Yb	Lu	Hf
0.058	0.381	0.0851	0.249	0.0356	0.248	0.0381	0.179
Ta	Tl	Pb	Bi	Th	U		
0.026	0.215	3.65	0.167	0.0425	0.0122		

Trace element data are provided in the next few pages. Data in both raw form, and normalised (to chondrite) are given. Any results with negative sign were treated as not detected and so appear as zero on the normalised data sheets.

Trace Element results for Cypriot Samples

PPM Rock

Run = 576

FileName = Jul15134

CALCULATED ON

Ames/Jenner/Brydie/Malpas/Hewa, Jul15134, RUN = 576

Sample	Mineralogy	SampleName	Li	Rb	Sr	Y	Zr	Nb	Mo	Cs
			0.595	0.023	0.11	0.157	0.045	0.007	0.058	0.011
1c20	Cal/dol	M07011P	0.821	0.676	377.31	2.747	0.897	0.082	0.162	0.060
1c17	Mag/cal	M07012L	1.275	0.091	86.23	-0.130	0.744	0.010	0.031	-0.002
1c9	Mag/cal	M07013H	0.504	0.267	36.89	-0.127	0.175	0.016	0.040	0.015
1c16	serp	M07014C	17.482	0.196	73.33	-0.059	0.142	0.014	0.140	0.010
2c12	Magnesite	M07015Y	1.897	0.077	24.57	-0.158	0.088	0.001	0.051	0.000
1c21	Calcite	M07016U	1.657	0.192	109.94	-0.076	1.050	0.014	0.060	0.000
1c6	Dolomite	M07017Q	0.321	0.123	161.09	-0.099	0.109	0.003	0.053	0.012
2c14	Dol/mag	M07018M	0.693	0.288	289.59	-0.140	0.084	0.017	0.022	0.005
1c10	calcite	M07019I	0.280	0.145	58.61	-0.149	0.056	0.008	0.058	0.005
1c22	Dolomite	M07020W	3.151	1.746	178.42	2.000	2.768	0.282	0.299	0.202
2c13	Cal/mag	M07021I.	0.803	0.185	87.94	-0.080	0.079	0.185	0.155	0.002
1c8	Calcite	M07022A	0.161	0.081	56.13	-0.143	0.115	0.005	0.056	0.001
1c19	Calcite	M07023P	0.660	0.340	433.14	1.704	0.232	0.018	0.082	0.020
s4	serpent	M07024E	0.754	0.188	7.90	0.125	0.199	0.026	0.068	-0.001
x6	Magnesite	M07025T	1.048	0.010	13.30	-0.143	0.041	0.026	0.025	-0.011
d4	sst	M07026I	13.472	65.763	79.28	14.307	109.471	9.813	0.414	2.311
d1	sst	M07027W	16.182	71.061	96.01	13.666	90.396	10.849	0.284	2.875
m12	Magnesite	M07028L	7.553	0.136	136.18	1.476	0.501	0.026	0.096	0.024
d2	sst	M07029A	15.073	59.284	77.26	10.392	94.214	8.662	0.171	1.967
d3	sst	M07030Z	15.703	66.701	79.96	11.291	85.842	9.221	0.175	2.264
sm	Magnesite	M07031H	0.760	0.121	41.10	-0.035	0.726	0.040	0.046	0.000
m5	Magnesite	M07032P	5.039	0.632	71.69	3.712	4.039	0.183	0.202	0.017
x14	Magnesite	M07033X	26.218	0.253	119.81	1.651	0.255	0.027	0.115	0.022
x14	Magnesite	M07033X*	26.509	0.247	117.72	1.718	0.283	0.037	0.095	0.017

m5	Magnesite	M07034F	0.869	0.078	66.46	-0.039	0.641	0.007	0.062	-0.006
m5	Magnesite	M07034F*	0.945	0.088	64.82	-0.044	0.123	0.007	0.087	-0.005

Trace Element results for Cypriot SamplesPPM

Run = 576

Ames/Jenner/Brydie/Malpas/Hewa, Jul15134, RUN = 576

FileName = Jul15134

Sample	Ba	La	Ce	Pr	Nd	Sm	Eu	Gd	Tb	Dy	Ho
Det limit	0.03	0.006	0.005	0.006	0.048	0.041	0.009	0.034	0.049	0.017	0.007
1c20	3.79	0.721	0.602	0.125	0.600	0.164	0.043	0.208	-0.008	0.298	0.067
1c17	15.86	0.007	0.004	0.000	-0.011	0.017	0.003	-0.002	-0.042	-0.007	-0.001
1c9	1.67	0.027	0.024	0.006	0.009	-0.011	0.003	0.001	-0.045	-0.011	-0.001
1c16	18.76	0.014	0.014	0.003	-0.053	0.001	0.040	-0.005	-0.046	0.030	0.000
2c12	2.08	0.012	0.009	0.004	-0.011	-0.003	0.002	-0.003	-0.044	0.016	-0.002
1c21	17.31	0.028	0.022	0.004	-0.007	-0.015	-0.004	0.003	-0.039	0.036	0.002
1c6	22.70	0.005	0.007	0.000	-0.026	-0.002	0.000	0.007	-0.041	-0.003	0.004
2c14	7.37	0.020	0.021	0.007	0.005	-0.010	0.002	-0.010	-0.044	-0.010	-0.003
1c10	2.12	0.023	0.023	0.004	-0.009	-0.001	-0.002	0.005	-0.043	-0.017	-0.002
1c22	4.52	0.704	3.398	0.201	0.846	0.196	0.044	0.264	0.004	0.280	0.063
2c13	8.14	0.040	0.064	0.007	0.072	0.010	-0.002	-0.010	-0.044	0.007	0.003
1c8	1.40	0.012	0.004	-0.001	-0.009	0.000	0.001	0.002	-0.038	0.001	-0.002
1c19	2.38	0.677	0.469	0.132	0.493	0.098	0.028	0.176	-0.011	0.188	0.042
s4	1.65	0.027	0.038	0.005	-0.005	-0.005	-0.003	0.013	-0.039	0.038	0.007
x6	0.60	0.006	0.005	0.001	0.021	0.006	0.001	-0.005	-0.043	-0.013	-0.004
d4	239.47	21.111	40.724	4.992	19.138	3.743	0.767	3.186	0.424	2.790	0.520
d1	233.61	23.520	45.933	5.514	21.037	4.141	0.816	3.275	0.453	2.759	0.544
m12	1.77	0.040	0.072	0.011	0.038	0.021	0.018	0.061	0.002	0.132	0.040
d2	210.91	18.835	38.527	4.711	17.387	3.363	0.616	2.590	0.353	2.177	0.451
d3	230.10	19.658	39.030	4.794	17.711	3.557	0.648	2.752	0.374	2.224	0.419
sm	8.29	0.035	0.075	0.009	0.024	-0.004	-0.002	0.010	-0.008	0.010	0.000
mx	17.35	2.255	1.641	0.474	2.144	0.425	0.100	0.424	0.062	0.421	0.093
x14	1.90	0.170	0.172	0.025	0.153	0.049	0.054	0.068	0.003	0.110	0.034
x14*	1.85	0.155	0.145	0.022	0.093	0.020	0.057	0.090	0.005	0.128	0.034
m5	11.18	0.020	0.013	0.001	0.010	0.001	-0.004	-0.002	-0.009	-0.001	0.001
m5*	10.89	0.018	0.009	0.002	-0.006	0.002	-0.001	0.004	-0.009	0.008	0.000

Trace Element results for Cypriot Samples PPM

Run = 576

Ames/Jenner/Brydie/Malpas/Hewa, Jul15134, RUN = 576

FileName = Jul15134

Sample	Er	Tm	Yb	Lu	Hf	Ta	Tl	Pb	Bi	Th	U
Det. limit	0.030	0.008	0.022	0.007	0.038	0.014	0.022	0.031	0.014	0.034	0.029
1c20	0.192	0.030	0.191	0.030	0.016	0.002	0.068	0.244	0.020	0.051	1.074
1c17	-0.002	0.002	0.005	0.000	0.034	-0.001	0.012	-0.002	0.002	0.017	0.067
1c9	0.001	0.004	0.031	0.001	-0.001	0.006	0.010	0.043	0.022	-0.008	0.019
1c16	0.020	0.003	0.020	0.005	-0.008	-0.005	-0.002	0.042	0.004	0.000	0.000
2c12	-0.010	0.002	-0.010	-0.004	0.004	-0.006	-0.008	0.030	0.010	0.007	0.005
1c21	0.011	0.002	0.004	0.003	0.013	0.000	0.008	1.120	0.013	0.015	0.196
1c6	-0.011	0.002	-0.001	0.001	-0.001	0.000	-0.001	0.044	0.011	-0.005	0.019
2c14	-0.014	0.005	0.017	0.000	0.006	0.001	0.007	0.095	0.001	0.019	0.004
1c10	-0.009	-0.001	-0.013	-0.001	-0.003	-0.002	-0.008	0.294	0.015	-0.003	-0.003
1c22	0.212	0.030	0.166	0.022	0.077	0.016	0.066	1.126	0.008	0.208	0.477
2c13	-0.010	0.005	0.010	-0.002	0.020	0.172	-0.009	0.425	0.035	0.007	0.191
1c8	-0.004	-0.001	0.014	-0.003	0.014	0.002	0.001	0.107	0.004	-0.006	-0.014
1c19	0.143	0.017	0.109	0.018	0.001	-0.003	0.008	0.188	0.006	0.014	0.105
s4	0.025	0.009	0.076	0.008	0.014	-0.001	0.000	2.059	0.005	0.009	0.009
x6	-0.020	-0.001	-0.018	-0.003	-0.011	0.075	-0.001	0.151	-0.001	-0.012	0.004
d4	1.558	0.256	1.481	0.214	2.484	1.502	0.278	35.897	0.122	6.416	19.411
d1	1.424	0.204	1.351	0.211	2.458	0.663	0.249	16.113	0.075	6.909	1.081
m12	0.125	0.022	0.177	0.030	0.028	0.004	-0.009	4.646	0.006	0.012	0.171
d2	1.164	0.177	1.179	0.180	2.887	0.638	0.234	6.143	0.044	6.362	2.468
d3	1.218	0.178	1.181	0.173	2.459	0.594	0.247	9.218	0.082	6.862	3.888
sm	-0.002	-0.001	-0.001	0.001	0.017	0.078	-0.016	0.113	0.004	0.010	0.014
mx	0.301	0.039	0.256	0.042	0.078	0.009	0.047	18.288	0.021	0.231	0.281
x14	0.115	0.018	0.133	0.024	0.018	0.003	0.003	4.855	0.009	0.010	0.032
x14*	0.113	0.018	0.105	0.021	0.019	0.004	0.007	3.796	0.006	0.006	0.025
m5	0.012	0.000	0.008	0.000	0.025	0.003	-0.006	0.044	0.007	0.003	0.736
m5*	0.000	0.001	0.016	-0.001	-0.001	0.000	0.000	0.074	0.008	-0.001	0.734

Trace Element results for Cypriot Samples PPM

Run = 576

Ames/Jenner/Brydie/Malpas/Hewa, Jul15134, RUN = 576

FileName = Jul15134

Sample	206Pb/207Pb	208Pb/207Pb	147Sm/144Nd	87Rb/86Sr	Nb/Ta	Dil(G/KG)
	b	b	Nd			
1c20	1.2407	2.8191	0.1671	0.0051	35.12	0.567
1c17	2.1834	-2.8878	-0.8823	0.0030	-7.50	0.574
1c9	-0.0753	2.7750	-0.7077	0.0205	2.69	0.573
1c16	0.8960	5.2323	-0.0161	0.0076	-2.78	0.561
2c12	-1.2940	-7.4912	0.1374	0.0090	-0.18	0.575
1c21	1.4239	2.8306	1.2669	0.0051	68.33	0.569
1c6	0.3311	0.8141	0.0587	0.0022	-13.96	0.614
2c14	0.7361	3.2572	-1.3005	0.0029	26.52	0.564
1c10	1.0022	2.8889	0.0858	0.0071	-4.65	0.564
1c22	1.2368	2.7891	0.1399	0.0282	17.66	0.567
2c13	1.2326	2.8403	0.0885	0.0060	1.07	0.577
1c8	1.7205	3.0308	0.0000	0.0042	2.28	0.578
1c19	1.7381	3.0238	0.1200	0.0023	-5.51	0.578
s4	1.3022	2.7159	0.6618	0.0683	-18.16	0.563
x6	1.4248	3.0181	0.1759	0.0021	0.34	0.577
d4	1.2811	2.5870	0.1157	2.3673	6.53	0.577
d1	1.2732	2.4627	0.1157	2.1599	16.37	0.564
m12	1.2295	2.4378	0.3398	0.0029	6.04	0.569
d2	1.2625	2.5338	0.1173	2.1895	13.58	0.570
d3	1.2310	2.4418	0.1218	2.4081	15.52	0.563
sm	1.0147	2.3327	-0.1058	0.0085	0.51	0.574
mx	1.1971	2.3692	0.1214	0.0256	21.09	0.572
x14	1.3046	2.5496	0.1952	0.0062	9.37	0.565
x14*	1.2003	2.3988	0.1315	0.0060	8.27	0.563
m5	1.1799	1.0886	0.0765	0.0034	2.30	0.567
m5*	1.5710	2.6037	-0.1903	0.0039	572.61	0.556

Calcite data normalised to chondrite (Taylor and McLennan, 1985)

		Li	Rb	Sr	Y	Zr	Nb	Mo	Cs
		0.595	0.023	0.11	0.157	0.045	0.007	0.058	0.011
1c20	Cal/dol	0.342031	0.195831	31.70659	1.220868	0.161871	0.217621	0.117565	0.214936
1c21	Calcite	0.690399	0.055623	9.238907	-0.033623	0.189462	0.037436	0.043453	-0.001509
1c10	calcite	0.11651	0.041906	4.925108	-0.066	0.010173	0.020501	0.041781	0.016221
1c8	Calcite	0.067046	0.023484	4.716594	-0.063432	0.020696	0.01215	0.040441	0.004884
1c19	Calcite	0.274889	0.098476	36.39805	0.757201	0.041845	0.048105	0.059463	0.070566
		Ba	La	Ce	Pr	Nd	Sm	Eu	Gd
		0.03	0.006	0.005	0.006	0.048	0.041	0.009	0.034
1c20	Cal/dol	1.112361	1.96395	0.629177	0.91439	0.844317	0.711122	0.498617	0.680557
1c21	Calcite	5.076632	0.076905	0.02347	0.026154	-0.009977	-0.063792	-0.043209	0.010743
1c10	calcite	0.620954	0.062892	0.023748	0.032002	-0.012929	-0.005667	-0.025698	0.015095
1c8	Calcite	0.409153	0.033683	0.003701	-0.005604	-0.012063	0	0.009595	0.004915
1c19	Calcite	0.699043	1.843617	0.489578	0.964062	0.693392	0.424034	0.326687	0.574871
		Tb	Dy	Ho	Er	Tm	Yb	Lu	Hf
		0.049	0.017	0.007	0.030	0.008	0.022	0.007	0.038
1c20	Cal.dol	-0.13251	0.782541	0.787994	0.7718	0.833902	0.770693	0.785685	0.091801
1c21	Calcite	-0.672693	0.093425	-0.023778	0.045131	0.050522	0.017605	0.072043	0.073075
1c10	calcite	-0.733363	-0.043907	-0.024137	-0.035368	-0.032672	-0.050464	-0.027687	-0.016395
1c8	Calcite	-0.659078	0.002402	-0.019469	-0.015309	-0.023691	0.054793	-0.073072	0.080284
1c19	Calcite	-0.190164	0.493698	0.489327	0.573229	0.480047	0.438772	0.460519	0.003955

Calcite data normalised to chondrite (Taylor and McClennan, 1985)

		Tl	Pb	Bi	Th	U
		0.022	0.031	0.014	0.034	0.029
lc20	Cal/dol	0.315831	0.066723	0.117418	1.202101	88.0135
lc21	Calcite	0.03849	0.306787	0.076277	0.343288	16.02523
lc10	Calcite	0	0.080552	0.090002	0	0
lc8	Calcite	0.006486	0.029279	0.021351	0	0
lc19	Calcite	0.035366	0.051629	0.036079	0.32618	8.577207

Dolomite data normalised to chondrite (Taylor and McLennan, 1985) : Negative values reduced to zero.

		Li	Rb	Sr	Y	Zr	Nb	Mo	Cs
		0.595	0.023	0.11	0.157	0.045	0.007	0.058	0.011
1c6	Dolomite	0.133741	0.035596	13.53731	0	0.019617	0.007774	0.038263	0.042014
1c22	Dolomite	1.313026	0.50597	14.99298	0.88881	0.499685	0.750994	0.216761	0.72312
mx	Dolomite	2.099514	0.183151	6.02478	1.649882	0.729052	0.488764	0.146097	0.061171
		Ba	La	Ce	Pr	Nd	Sm	Eu	Gd
		0.03	0.006	0.005	0.006	0.048	0.041	0.009	0.034
1c6	Dolomite	6.657653	0.013693	0.007681	0.001889	0	0	0	0.022643
1c22	Dolomite	1.324316	1.918276	3.551193	1.467579	1.189677	0.847786	0.507574	0.862972
mx	Dolomite	5.087697	6.143165	1.714952	3.460985	3.015683	1.837776	1.145905	1.385244
		Hf	Ta	Tl	Pb	Bi	Th	U	
		0.038	0.014	0.022	0.031	0.014	0.034	0.029	
1c6	Dolomite	0	0	0	0.011973	0.067326	0	1.544579	
1c22	Dolomite	0.428537	0.613511	0.307246	0.308591	0.048053	4.896517	39.12802	
mx	Dolomite	0.43775	0.334227	0.216445	5.010518	0.128335	5.444437	23.07232	

Serpentine data normalised to Chondrite (Taylor and McLennan, 1985) : Negative values reduced to zero.

		Li	Rb	Sr	Y	Zr	Nb	Mo	Cs
		0.595	0.023	0.11	0.157	0.045	0.007	0.058	0.011
1c16	Serp (liz)	7.284347	0.056842	6.162209	0	0.0256	0.038274	0.10135	0.035294
s4	Serp. Harz	0.314134	0.054548	0.663908	0.055355	0.035904	0.069128	0.049591	0
		Ba	La	Ce	Pr	Nd	Sm	Eu	Gd
		0.03	0.006	0.005	0.006	0.048	0.041	0.009	0.034
1c16	Serp (liz)	5.500706	0.037476	0.015043	0.024285	0	0.006022	0.455578	0
s4	Serp. Harz	0.484175	0.073444	0.039451	0.036539	0	0	0	0.043578
		Tb	Dy	Ho	Er	Tm	Yb	Lu	Hf
		0.049	0.017	0.007	0.030	0.008	0.022	0.007	0.038
1c16	Serp (liz)	0	0.077938	0	0.082189	0.071363	0.080965	0.13627	0
s4	Serp. Harz	0	0.098443	0.085226	0.100896	0.254703	0.306054	0.220892	0.075897
		Ta	Tl	Pb	Bi	Th	U		
		0.022	0.031	0.014	0.034	0.029			
1c16	Serp (liz)	0	0	0.011606	0.024139	0.011502	0		
s4	Serp. Harz	0	0	0.564209	0.027673	0.217389	0.7496		

Sandstone data normalised to chondrite (Taylor and McLennan, 1985) : Negative values reduced to zero.

		Li	Rb	Sr	Y	Zr	Nb	Mo	Cs
		0.595	0.023	0.11	0.157	0.045	0.007	0.058	0.011
d1	Organic sst.	6.742675	20.59727	8.06798	6.073743	16.31695	28.93012	0.20596	10.30614
d2	Organic sst.	6.280407	17.18366	6.492711	4.618466	17.00614	23.09818	0.123912	7.049428
d3	Organic sst.	6.542963	19.33365	6.719729	5.018354	15.49486	24.58859	0.126901	8.115742
d4	Organic sst.	5.613511	19.06186	6.662552	6.358504	19.76012	26.16889	0.300339	8.282342
		Ba	La	Ce	Pr	Nd	Sm	Eu	Gd
		0.03	0.006	0.005	0.006	0.048	0.041	0.009	0.034
d1	Organic sst.	68.50794	64.08841	47.99711	40.2481	29.58767	17.92831	9.374432	10.70335
d2	Organic sst.	61.8505	51.32095	40.25851	34.38536	24.45433	14.55972	7.086018	8.464747
d3	Organic sst.	67.47754	53.56413	40.78378	34.9953	24.91014	15.39898	7.450267	8.992843
d4	Organic sst.	70.22619	57.52207	42.55405	36.44141	26.91754	16.20141	8.819987	10.41054
		Tb	Dy	Ho	Er	Tm	Yb	Lu	Hf
		0.049	0.017	0.007	0.030	0.008	0.022	0.007	0.038
d1	Organic sst.	7.816027	7.241083	6.395522	5.717902	5.734243	5.447297	5.534631	13.73169
d2	Organic sst.	6.094779	5.713209	5.302061	4.672927	4.978376	4.752682	4.729014	16.13001
d3	Organic sst.	6.451407	5.838492	4.927456	4.890648	5.013221	4.762719	4.553037	13.73476
d4	Organic sst.	7.314009	7.323225	6.113012	6.257886	7.183455	5.971959	5.610172	13.87885

Sandstone data normalised to chondrite (Taylor and McLennan, 1985).

		Ta 0.014	Tl 0.022	Pb 0.031	Bi 0.014	Th 0.034	U 0.029
d1	Organic sst	25.48764	1.15977	4.414598	0.446734	162.5655	88.57969
d2	Organic sst	24.53543	1.087078	1.682915	0.261656	149.6872	202.3044
d3	Organic sst	22.84588	1.149394	2.525441	0.49109	161.4574	318.6523
d4	Organic sst	57.7771	1.290834	9.834698	0.729858	150.9581	1591.054

Magnesite vein data normalised to chondrite (Taylor and McLennan, 1985) : Negative values are reduced to zero.

		Li	Rb	Sr	Y	Zr	Nb	Mo	Cs
		0.595	0.023	0.11	0.157	0.045	0.007	0.058	0.011
2c14	Dol/mag	0.247949	0.006682	0.009558	0.069733	0.00815	0.017843	0.041855	0.038568
2c13	Cal/mag	0.288663	0.083365	24.33492	0	0.015197	0.044354	0.016128	0.016777
x6	Magnesite	0.334699	0.053572	7.38964	0	0.014263	0.493566	0.112284	0.005672
sm	Magnesite	0.43674	0.002844	1.117523	0	0.007463	0.068329	0.018025	0
		Ba	La	Ce	Pr	Nd	Sm	Eu	Gd
		0.03	0.006	0.005	0.006	0.048	0.041	0.009	0.034
2c14	Dol/mag	0.008098	0.01518	0.00554	0.040186	0.06736	0.175361	0.10862	0.112693
2c13	Cal/mag	2.160765	0.055609	0.021673	0.047762	0.00637	0	0.018264	0
x6	Magnesite	2.387889	0.108787	0.066413	0.050504	0.101789	0.044951	0	0
sm	Magnesite	0.177187	0.015756	0.005172	0.006657	0.029246	0.026389	0.009042	0
		Tb	Dy	Ho	Er	Tm	Yb	Lu	Hf
		0.049	0.017	0.007	0.030	0.008	0.022	0.007	0.038
2c14	Dol/mag	0.8452	0.044638	0.088129	0.120648	0.228542	0.089278	0.183606	0.213617
2c13	Cal/mag	0	0	0	0	0.126914	0.066727	0	0.036145
x6	Magnesite	0	0.017757	0.038597	0	0.142551	0.040684	0	0.113512
sm	Magnesite	0	0	0	0	0	0	0	0

Magnesite vein data normalised to chondrite (Taylor and McLennan, 1985).

		Ta	Tl	Pb	Bi	Th	U
		0.014	0.022	0.031	0.014	0.034	0.029
2c14	Dol/mag	0.52089	0.100282	0.008596	0.080865	0.807513	2.356167
2c13	Cal/mag	0.024122	0.032211	0.025972	0.006018	0.447816	0.320845
x6	Magnesite	6.633706	0	0.116316	0.207174	0.159166	15.69062
sm	Magnesite	2.880751	0	0.041336	0	0	0.366322

Magnesite nodule data normalised to chondrite (Taylor and McClennan, 1985) : Negative values are reduced to zero.

		Li	Rb	Sr	Y	Zr	Nb	Mo	Cs
		0.595	0.023	0.11	0.157	0.045	0.007	0.058	0.011
1c17	Mag/cal	0.531257	0.026245	7.246203	0	0.134318	0.026865	0.022481	0
1c9	Mag/cal	0.209999	0.077359	3.100386	0	0.03151	0.042862	0.02902	0.053662
2c12	Magnesite	0.790276	0.022278	2.064504	0	0.015831	0.002874	0.03674	0
m5	Magnesite	0.361908	0.02268	5.584555	0	0.115744	0.019651	0.044934	0
		Ba	La	Ce	Pr	Nd	Sm	Eu	Gd
		0.03	0.006	0.005	0.006	0.048	0.041	0.009	0.034
1c17	Mag/cal	4.649972	0.018521	0.004005	0.003245	0	0.072158	0.039191	0
1c9	Mag/cal	0.489623	0.074066	0.024624	0.041954	0.013122	0	0.035983	0.003094
2c12	Magnesite	0.608805	0.031873	0.009587	0.030313	0	0	0.022731	0
m5	Magnesite	3.279487	0.054538	0.014053	0.006727	0.01355	0.00532	0	0
		Tb	Dy	Ho	Er	Tm	Yb	Lu	Hf
		0.049	0.017	0.007	0.030	0.008	0.022	0.007	0.038
1c17	Mag/cal	0	0	0	0	0.064479	0.01886	0.005522	0.189722
1c9	Mag/cal	0	0	0	0.002463	0.10934	0.126028	0.025722	0
2c12	Magnesite	0	0.043097	0	0	0.056552	0	0	0.021963
m5	Magnesite	0	0	0.01541	0.050137	0.006816	0.031537	0.008877	0.138804

Magnesite nodule data normalised to chondrite (Taylor and McClelland, 1985).

		Ta	Tl	Pb	Bi	Th	U
		0.014	0.022	0.031	0.014	0.034	0.029
1c17	Mag/cal	-0.051698	0.057156	-0.000459	0.010244	0.389405	5.456899
1c9	Mag/cal	0.229934	0.04863	0.011663	0.134284	-0.178577	1.578911
2c12	Magnesite	-0.231106	-0.036656	0.008294	0.057657	0.159996	0.380302
m5	Magnesite	0.12313	-0.028179	0.011963	0.039191	0.07349	60.29867

APPENDIX V

Formation temperature calculations using oxygen isotope data.

Aharon (1986)

$$\text{FORMULA :- } 1000 \ln \alpha_{X,Y} = \delta^{18}\text{O}_X - \delta^{18}\text{O}_Y = (A * 10^6 / T^2) + B$$

Where A & B are constants and have values of 3.53 & -3.58 (for magnesite) respectively, and X & Y are mineral phases.

Average oxygen isotopic composition of solutions is assumed to be around -2‰ (SMOW)

a) Vein and stockwork calculation

Oxygen isotope values for veins and stockworks vary from 12.6‰ to 15.7‰ (SMOW). Three samples make up the vein field.

$$\delta^{18}\text{O}_X - \delta^{18}\text{O}_Y = (A * 10^6 / T^2) + B$$

$$12.6 - (-2) = (3.53 * 10^6 / T^2) - 3.58$$

$$14.6 + 3.58 = (3.53 * 10^6 / T^2)$$

$$18.18 (T^2) = 3.53 * 10^6$$

$$T = [(3.53 * 10^6) / 18.18]^{1/2}$$

$$T = 440.65\text{K}$$

$$\therefore T = \underline{167.65^\circ\text{C}}$$

b) Nodule Calculation

Oxygen isotope values for nodules vary from 24.3 ‰ to 30.5 ‰ (SMOW). Nine samples make up the nodule field. Three samples of calcite and one dolomite are also present within this field.

$$\delta^{18}\text{O}_m - \delta^{18}\text{O}_w = (A \cdot 10^6 / T^2) + B$$

$$30 - (-2) = (3.53 \cdot 10^6 / T^2) - 3.58$$

$$32 + 3.58 = (3.53 \cdot 10^6 / T^2)$$

$$35.58 (T^2) = 3.53 \cdot 10^6$$

$$T = [(3.53 \cdot 10^6) / 35.58]^{1/2}$$

$$T = 314.98\text{K}$$

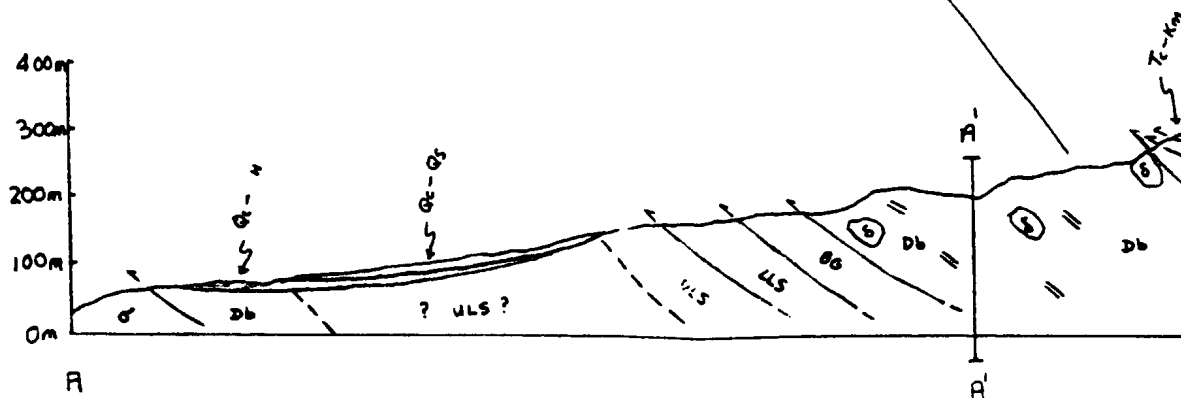
$$\therefore T = \underline{\underline{41.98^\circ\text{C}}}$$

Klippe of
Mamonía
sediments

**Zone I
magnesite
(veins and
stockworks)**

Vari-textured gabbro

**Sheeted diabase
dyke complex**

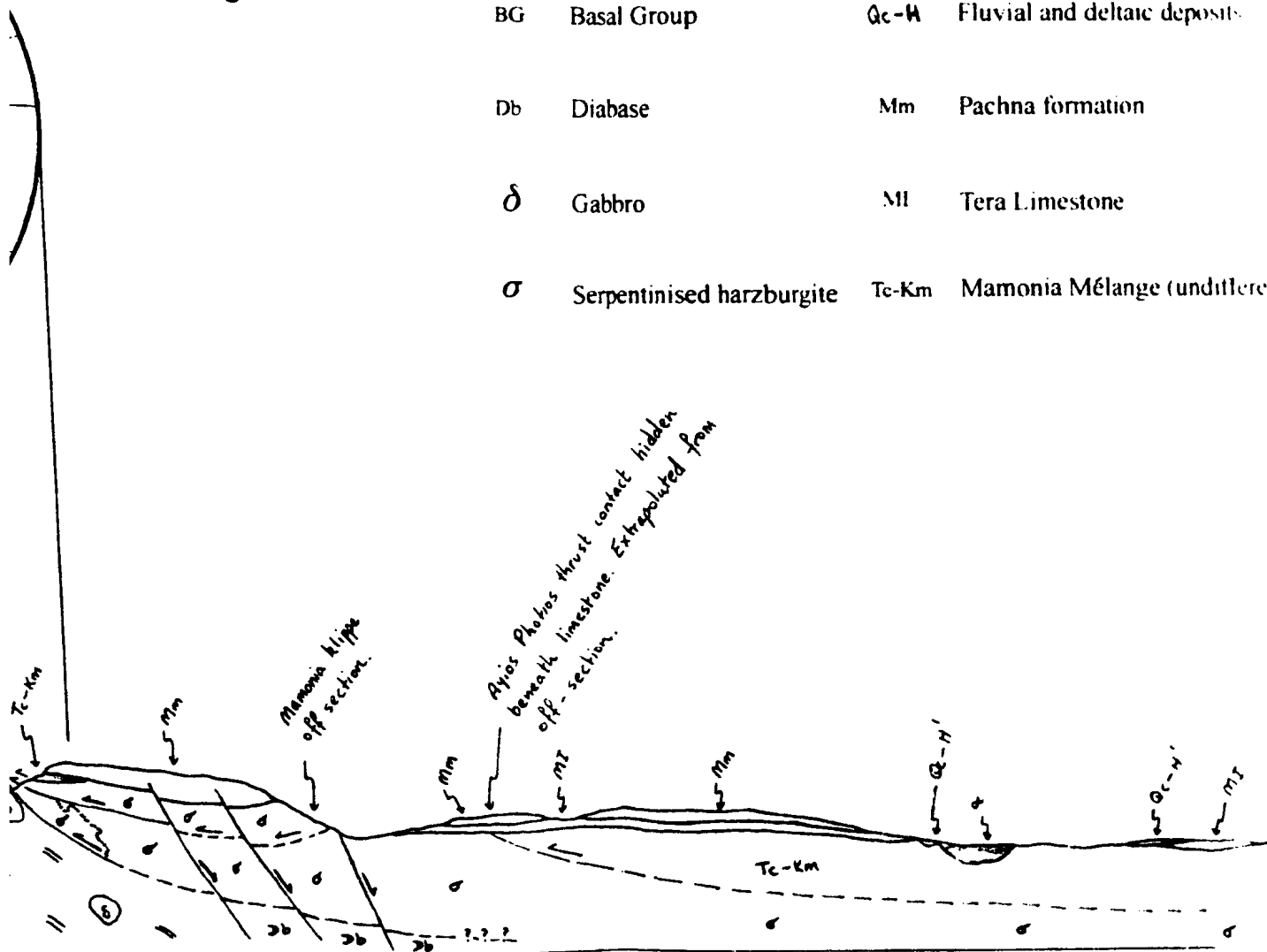


of
nia
nts

Key

ULS	Upper Lava Series	Qc-Qs	Fanglomerates
LLS	Lower Lava Series	Qc-H	Marine terrace deposits
BG	Basal Group	Qc-W	Fluvial and deltaic deposits
Db	Diabase	Mm	Pachna formation
δ	Gabbro	MI	Tera Limestone
σ	Serpentinised harzburgite	Tc-Km	Mamonia Mélange (undifferentiated)

Blocky serpentinised
harzburgite



Klippe of
Mamonia
sediments

Blocky serpentised
harzburgite

Key

ULS Upper Lava Series

LLS Lower Lava Series

BG Basal Group

Db Diabase

δ Gabbro

σ Serpentised harzburgite

Qc-Qs Fanglomerates

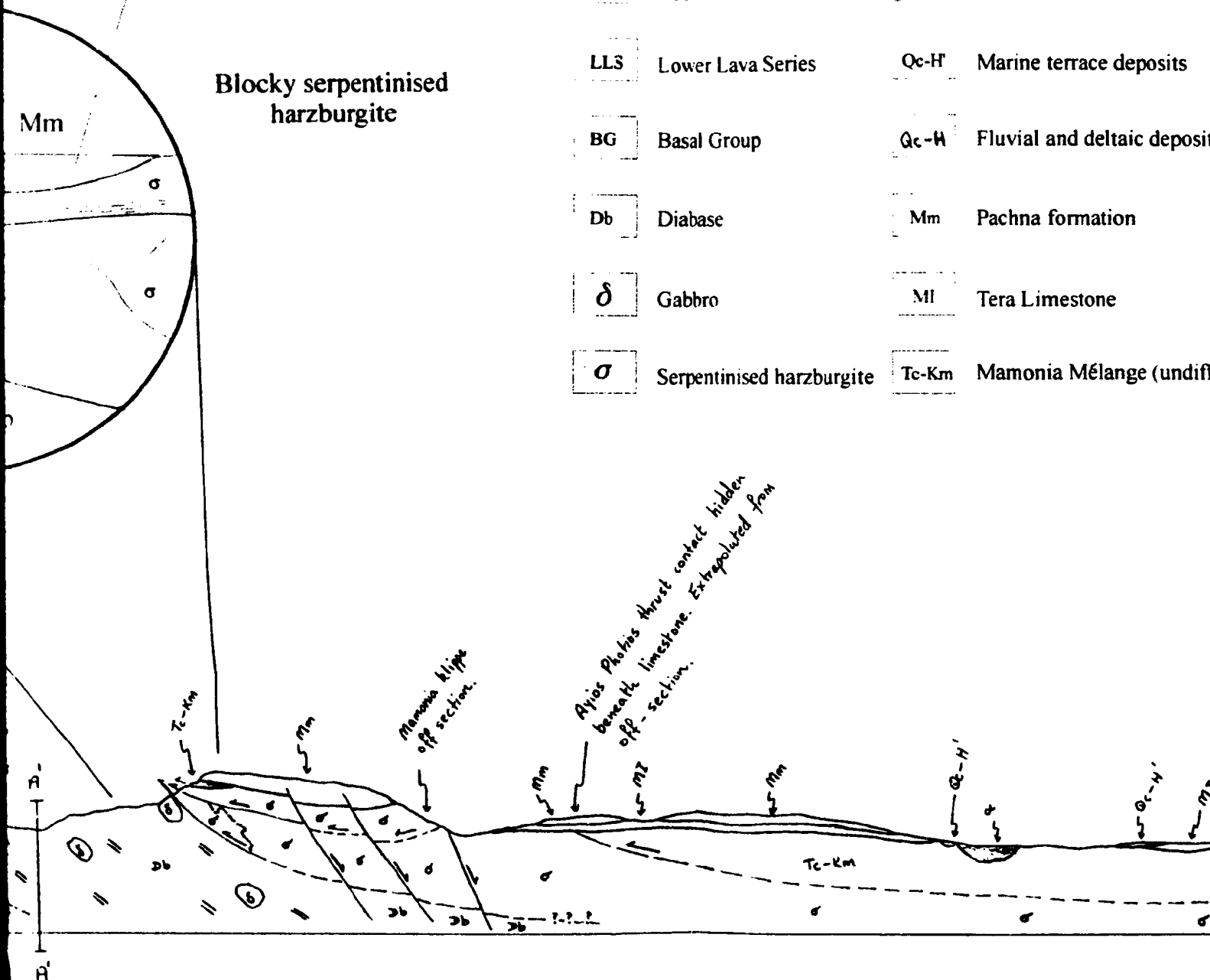
Qc-H' Marine terrace deposits

Qc-H Fluvial and deltaic deposits

Mm Pachna formation

MI Tera Limestone

Tc-Km Mamonia Mélange (undiff)





Thrust Fault



Normal Fault (tick indicates downthrown side)



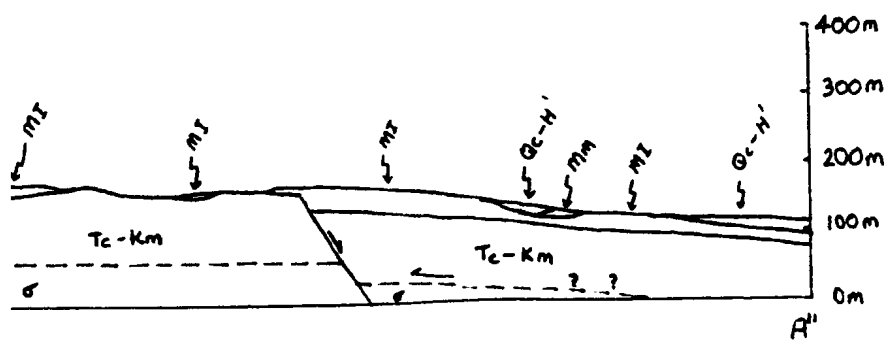
Diabase Dyke



Amphibolite

sits

lifferentiated)



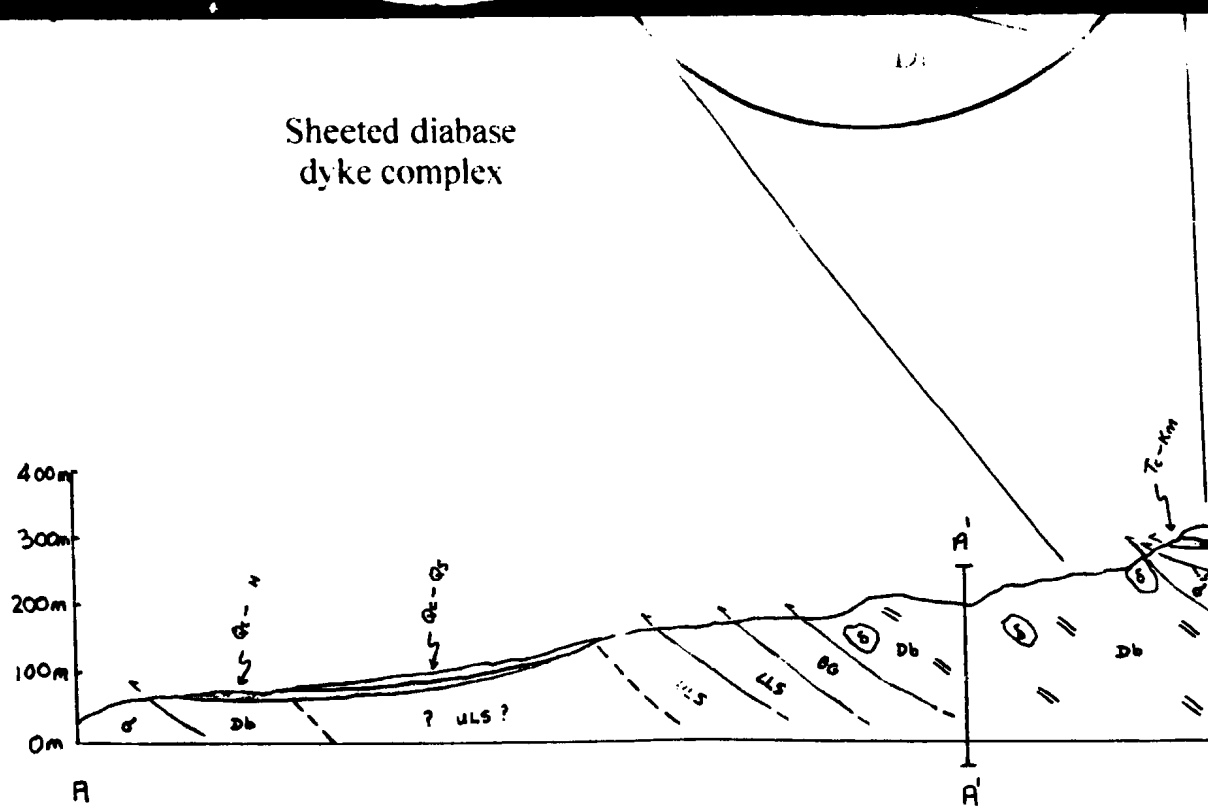
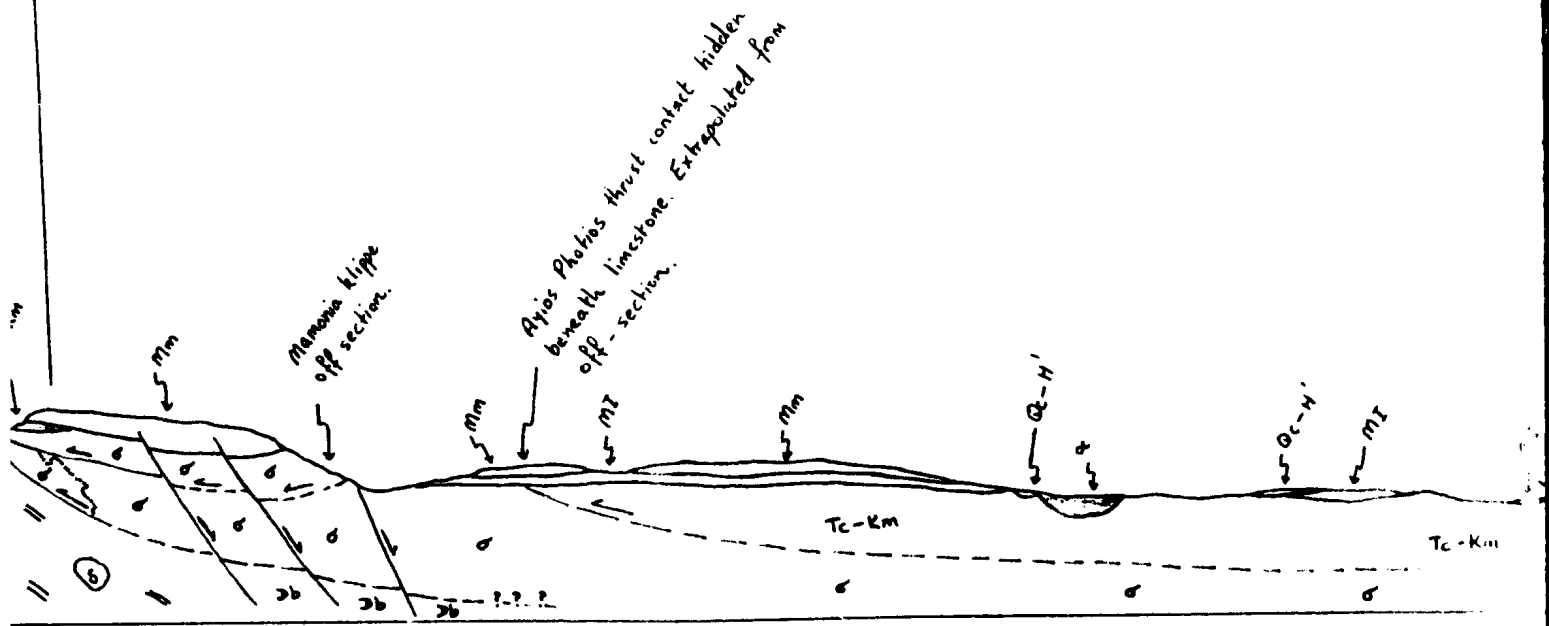
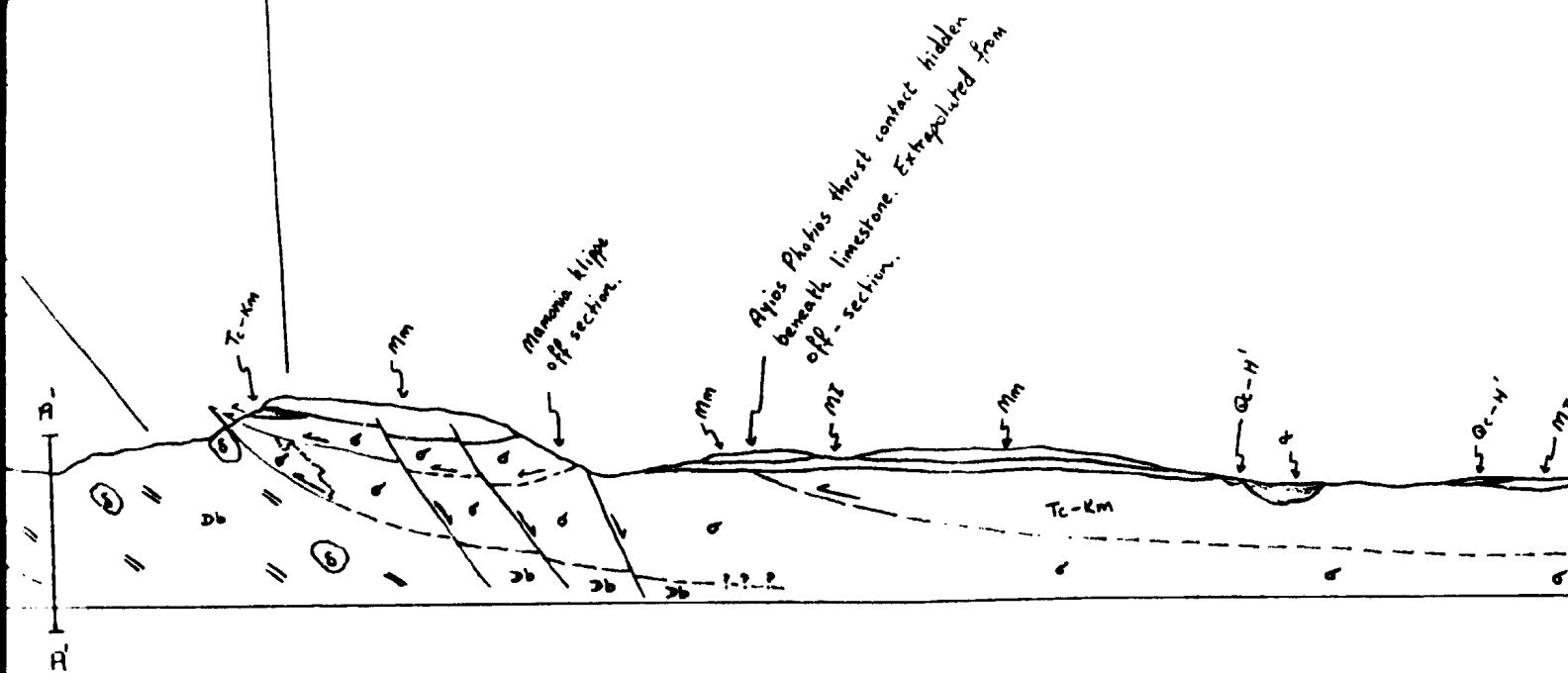


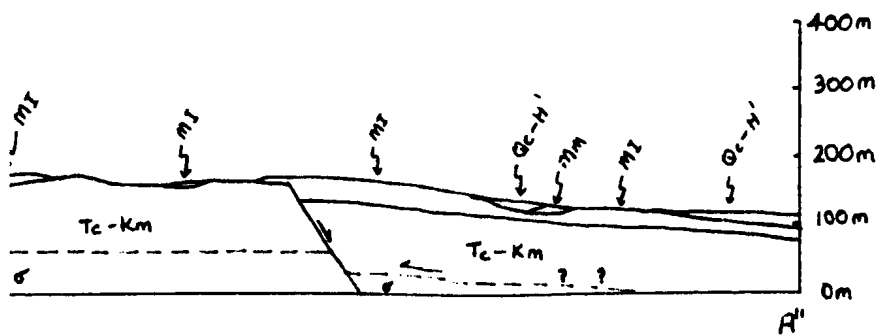
Figure 2.4b Cross section through the study area illustrating the structural position of the magnesite



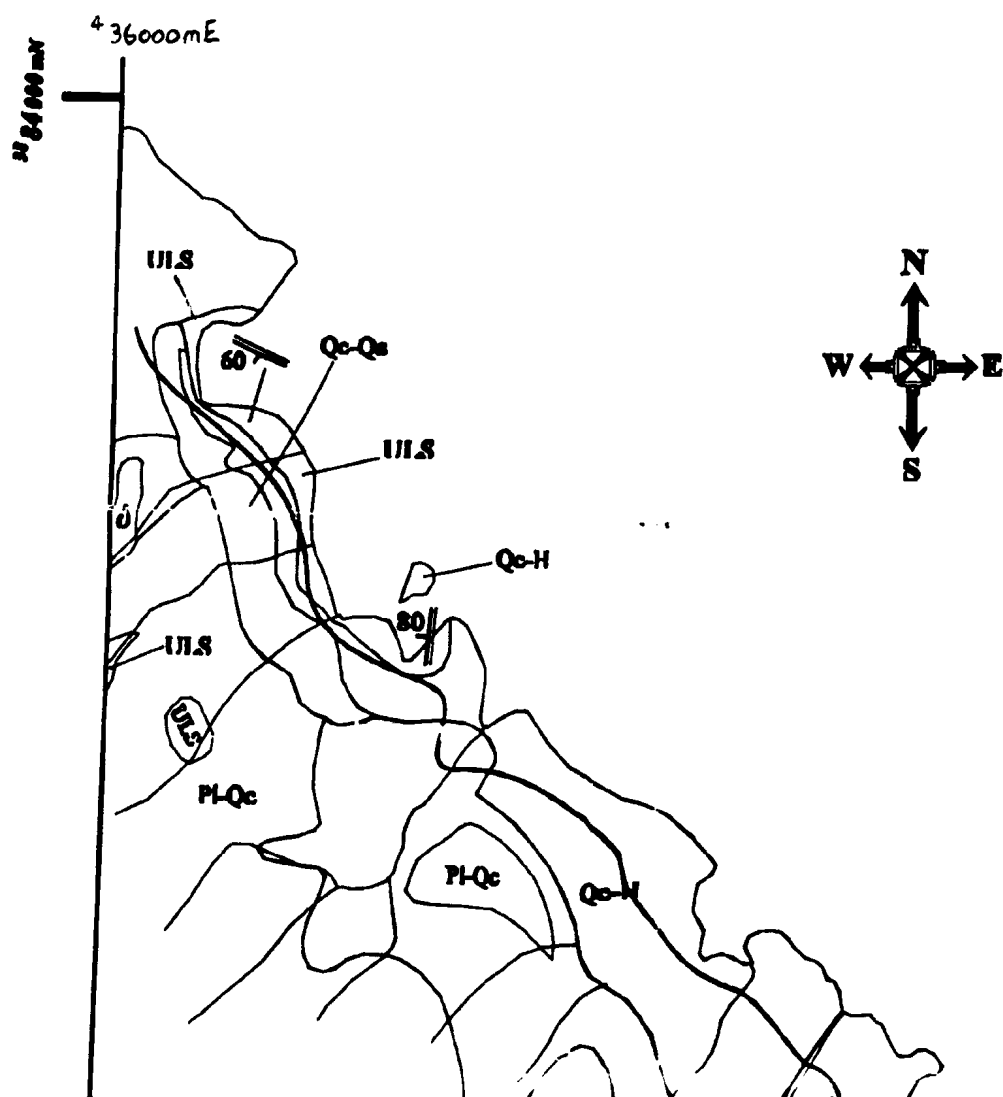
esite mineralisation.



position of the magnesite mineralisation.

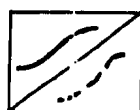


Geological Map of t

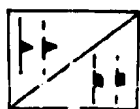


the Akamas Area.

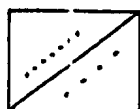
Geological Symbols



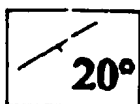
Geological boundary;
(defined, inferred)



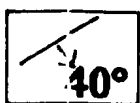
Thrust fault (defined, inferred)
Normal Fault (defined, inferred)



High angle fault, both dip-
slip and strike-slip (defined,
inferred)

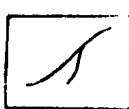


Strike & dip of bedding



Strike & dip of pillow lavas

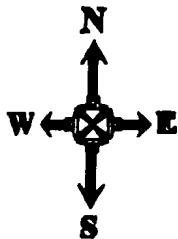
Topog



Agios
Georgios
Island



al Map of the Akamas Area.



**Agios
Georgios
Island**



Geological Symbols



**Geological boundary;
(defined, inferred)**



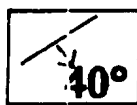
**Thrust fault (defined,
Normal Fault (defined)**



**High angle fault, both
slip and strike-slip (d
inferred)**



Strike & dip of bedding



Strike & dip of pillow



Strike-slip fault

1.

ools

dary;
d)

ined, inferred)
efined, inferred)

; both dip-
lip (defined,

edding

illow lavas

Topographic Symbols



Magnesite outcropping



Rivers

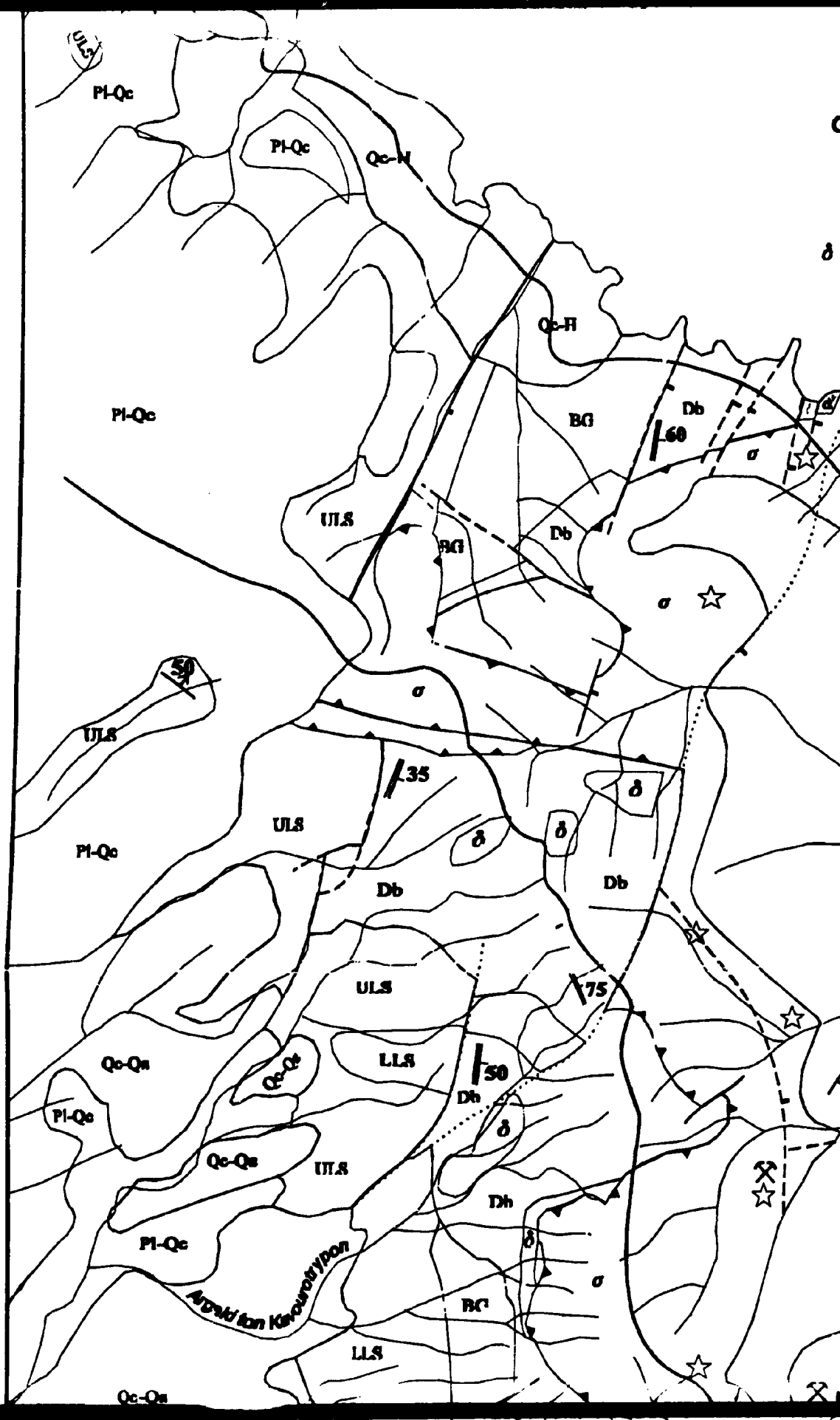


Asphalted road, non-
asphalted road



Settlement

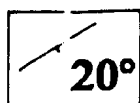
ination



**Agios
Georgios
Island**

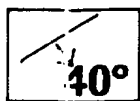


inferred)



20°

Strike & dip of bedding



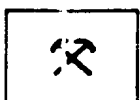
40°

Strike & dip of pillow lavas



60°

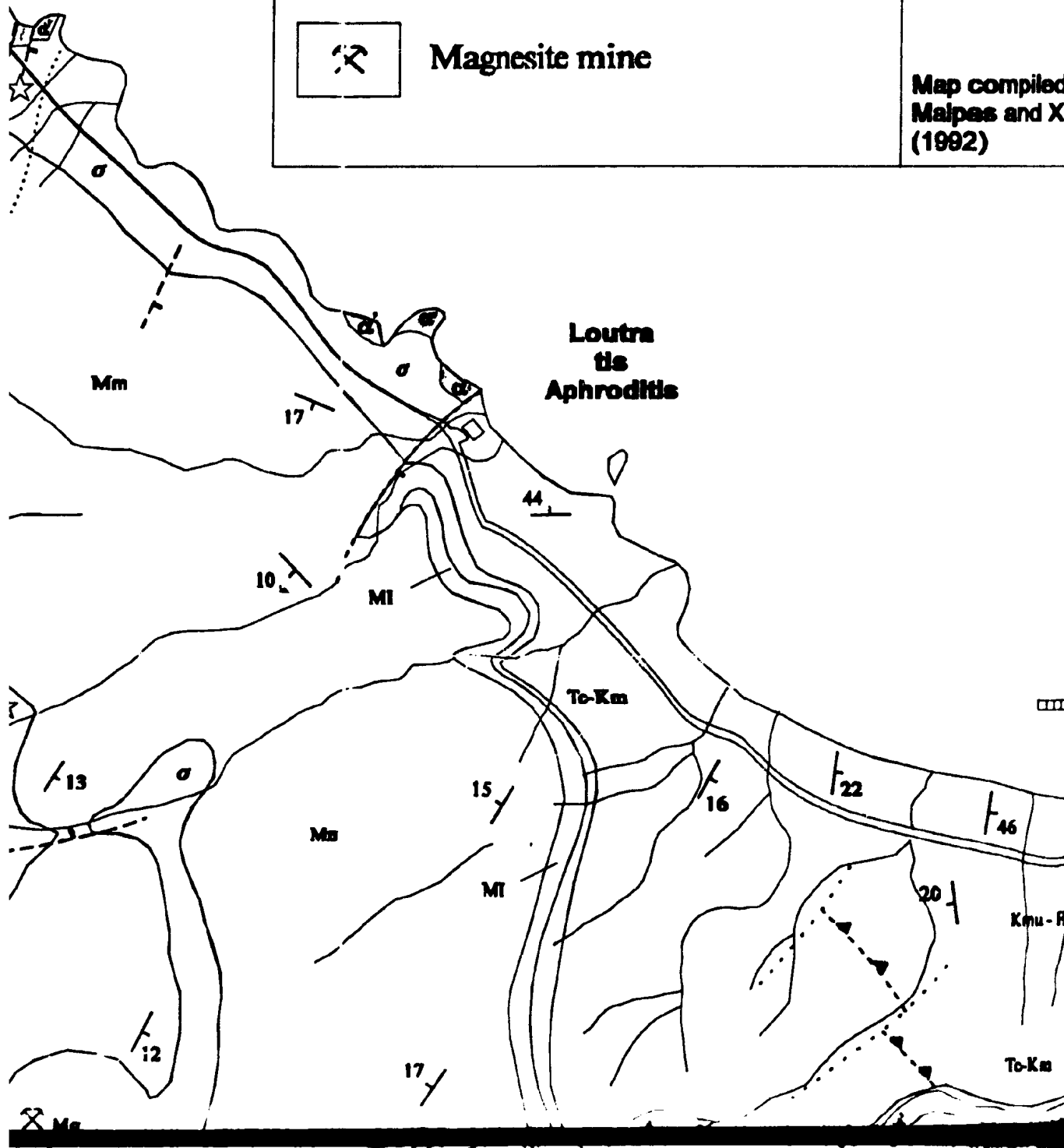
Diabase dyke orientation



Magnesite mine



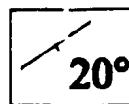
Map compiled
Malpas and Xe
(1992)



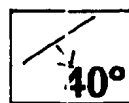
**Agios
Georgios
Island**



slip and strike slip (defined or inferred)



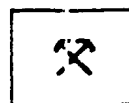
Strike & dip of bedding



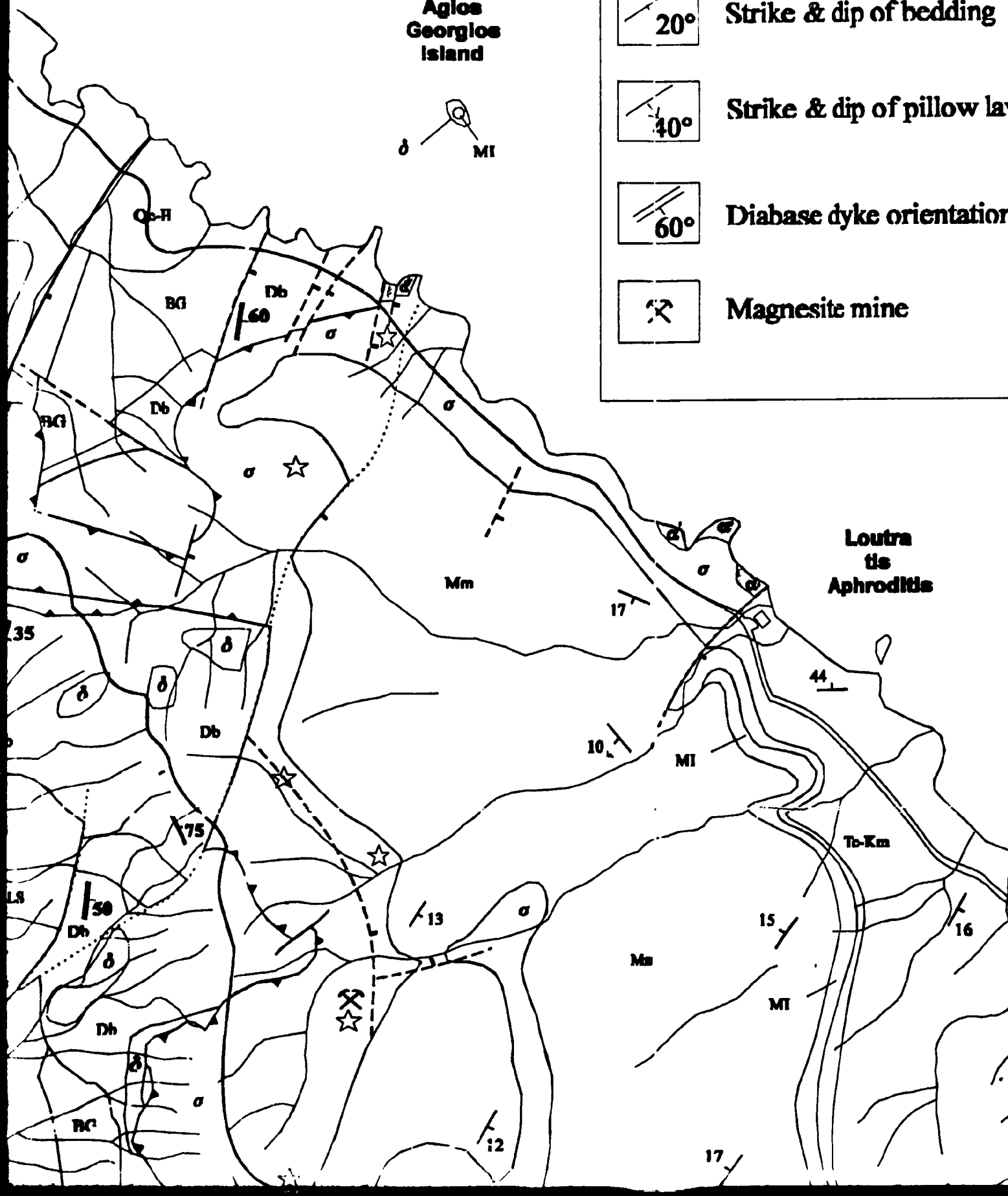
Strike & dip of pillow lavas



Diabase dyke orientation



Magnesite mine

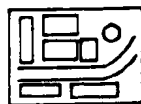


**Loutra
tis
Aphroditis**

ned



asphalted road



Settlement

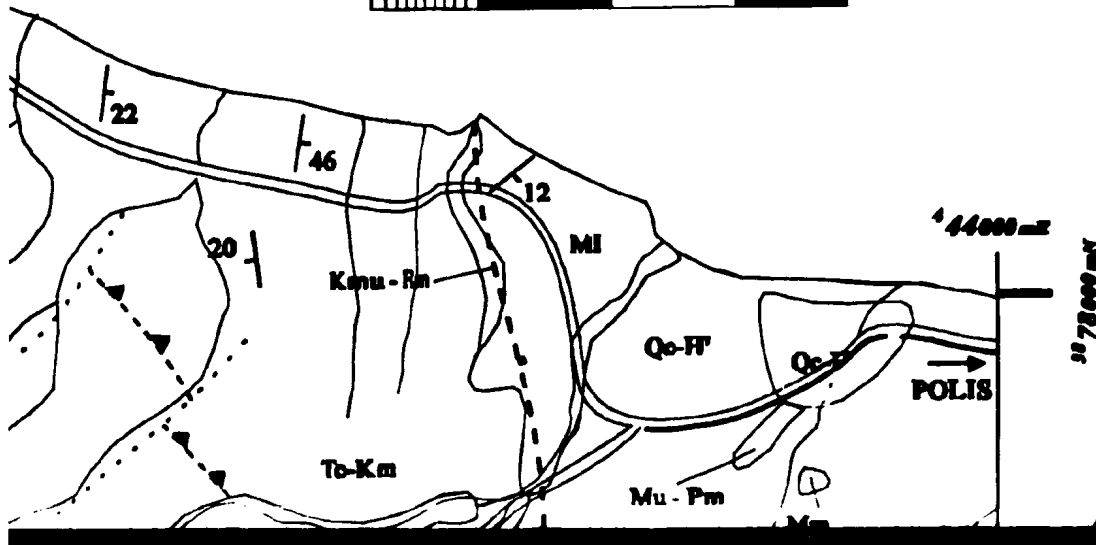
.vas

n

Map compiled and edited from
Malpas and Xenophon's
(1992)

James R Brydie
Dept of Earth Science
Memorial University.
St Johns
NF. 1994

0 1 2 3Km



PLEISTOCENE

HOLOCENE

SICILIAN

CALABRIAN

UPPER PLIOCENE

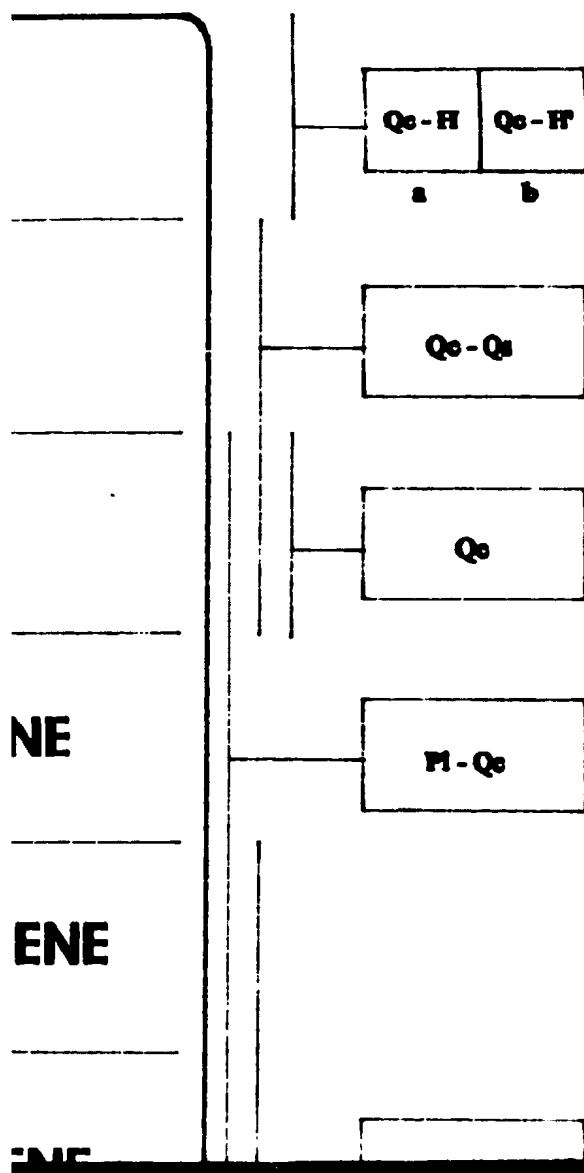
PLIOCENE

MIDDLE PLIOCENE

LOWER PLIOCENE

AGE RANGE

NEOAUTOCHTHONOUS ROCKS



Fluvial and deltaic Deposits

Sands and gravels with cobbles and boulders predominantly of igneous origin.

Fanglomerates

Alluvial cone and fan deposits consisting mainly of subangular sand and gravels and cobbles of igneous origin. Some fans contain significant quantities of carbonate detritus.

Marls, sandy marls and conglomerates

Green-grey marl, sandy marl with thin limestone beds and two metre thick beds of conglomerate.

Calcarenites with basal conglomerates

Coarse conglomerates at the base contain both igneous and sedimentary clasts and are overlain by calcarenites with some intraformational conglomerates or thin marly interbeds.

Marls, calcarenite, chalk and conglomerate

Grey to green-grey and buff-coloured marls in places interbedded with sandy marls and conglomerates.

LEGEND

IGNEOUS ROCKS

Deposits
and boulders

consisting mainly of subangular sands,
origin. Some fans contain significant

al conglomerates

with thin limestone beds
conglomerate.

al conglomerates

basal contain both igneous and
corals by calcarenites with
conglomerates or thin marly interbeds.

alk and conglomerate

coloured mud in places interbedded with
sandstone

AGE RANGE

UPPER TRIASSIC TO
UPPER CRETACEOUS

UPPER
CRETACEOUS

MIDDLE
CRETACEOUS

CARNIAN

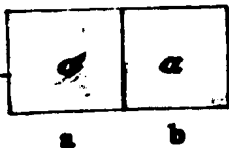
CRETACEOUS

MAASTRICHTIAN

ALLOCHTHONOUS ROCKS

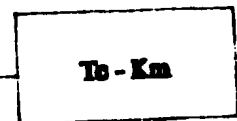
a) Serpentinite, b) Amphibolite

- a) Variably altered serpentinitised harzburgite with minor dunite
- b) Amphibolite-grade metavolcanics, metacherts and marbles



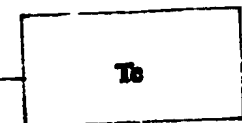
Mamonia Melange (undifferentiated)

Dismembered sandstone, red siltstone and radiolarite sequence containing variably sized blocks of Petra tou Romiou limestone which are spatially associated with blocks of alkaline volcanic rocks.



Petra tou Romiou Limestone

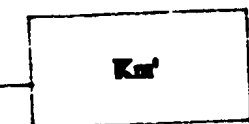
Partially recrystallized reefoidal limestone and limestone breccia occurring as large mappable blocks in Mamonia Melange.

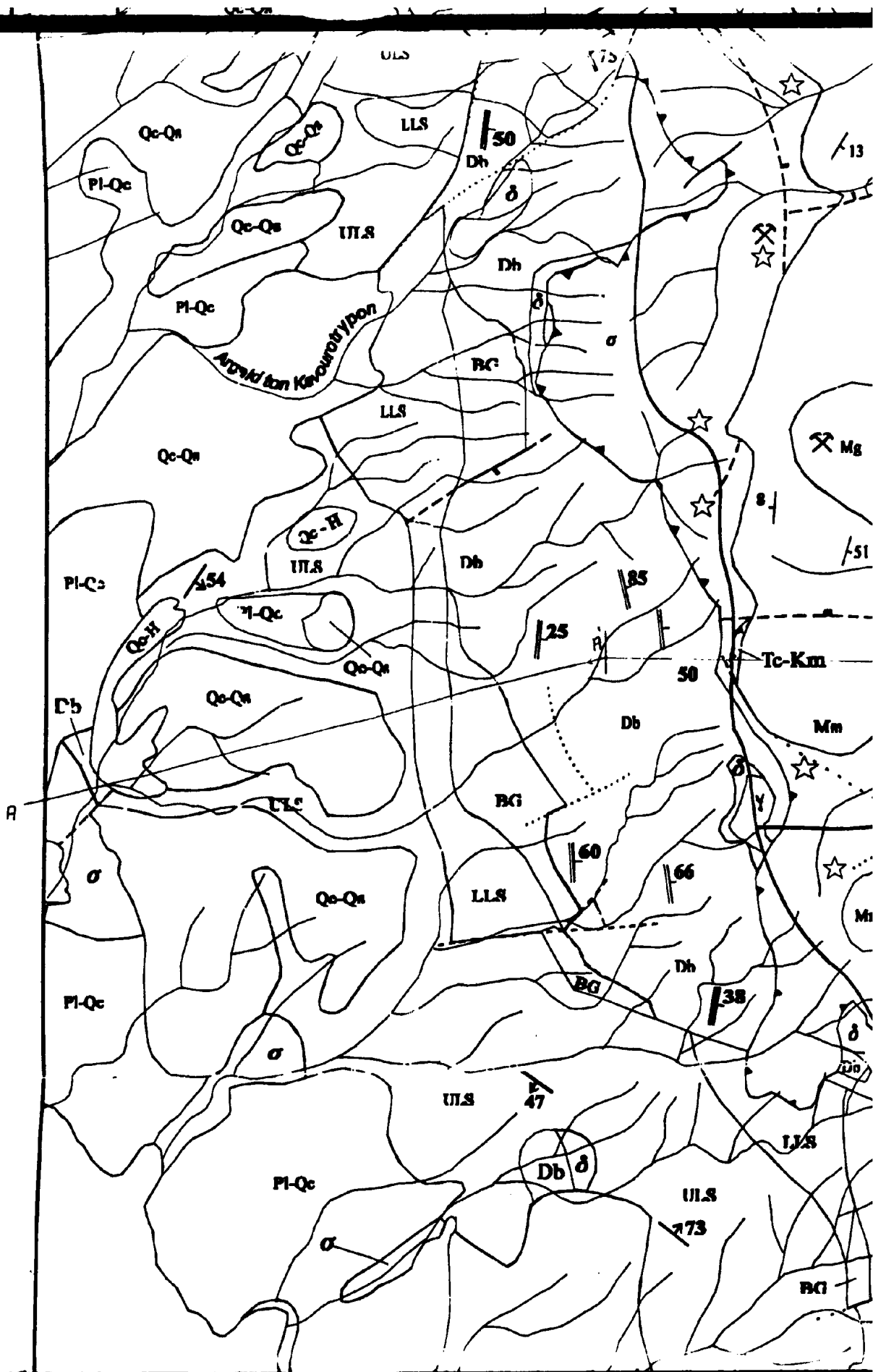


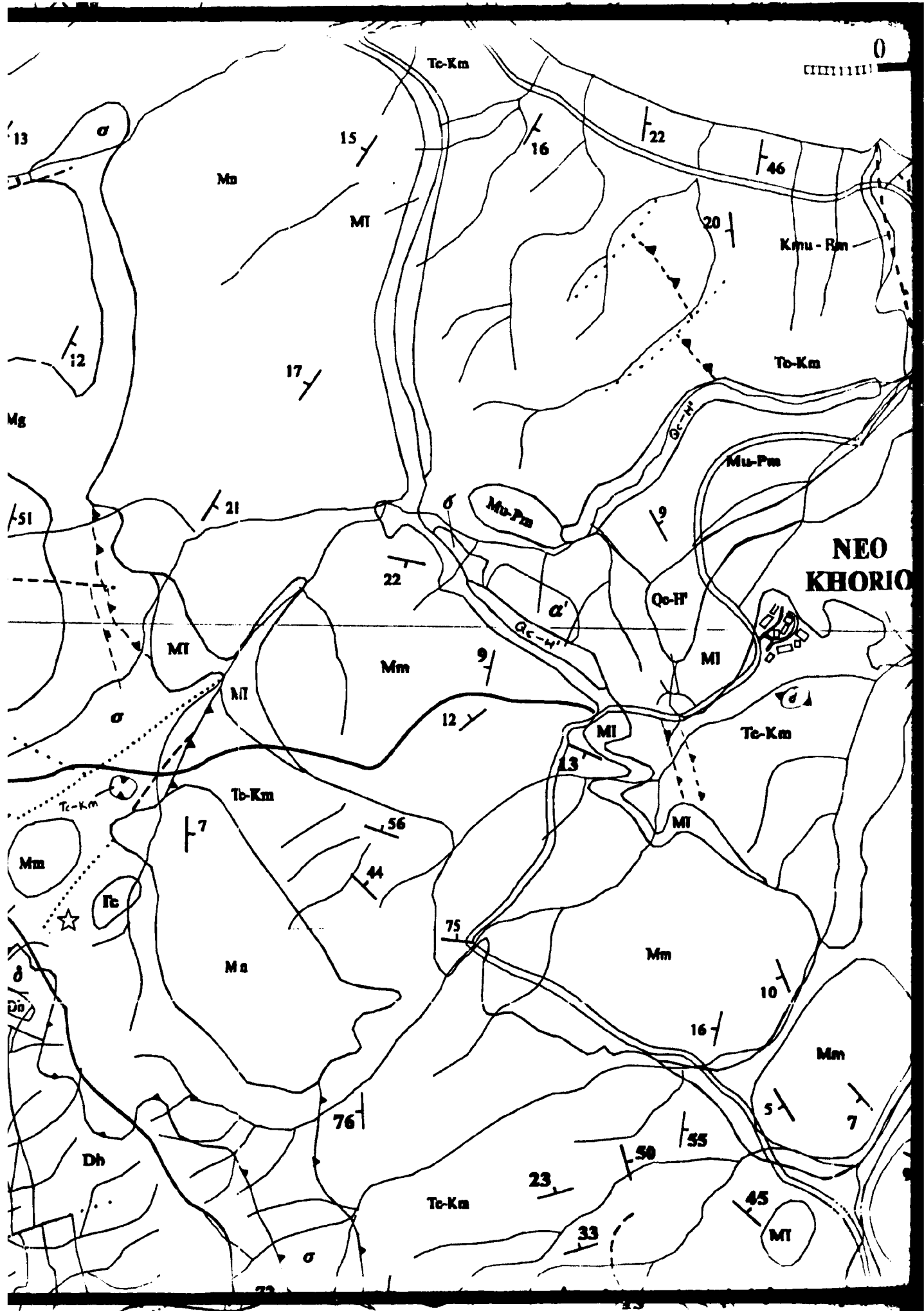
AUTOCHTHONOUS (?) ROCKS

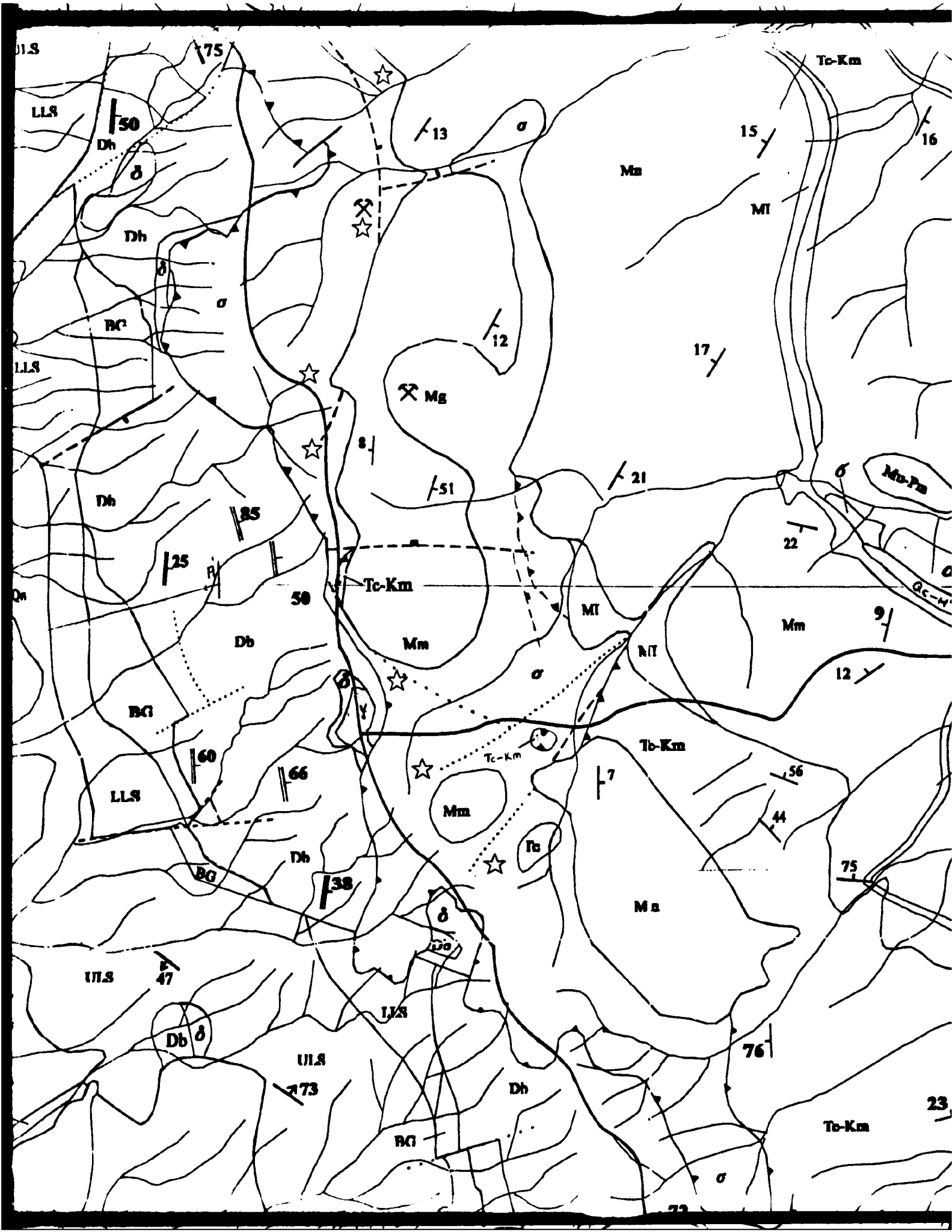
Kannavien Formation

Bentonitic clays interbedded with off-white volcanoclastic sandstones.

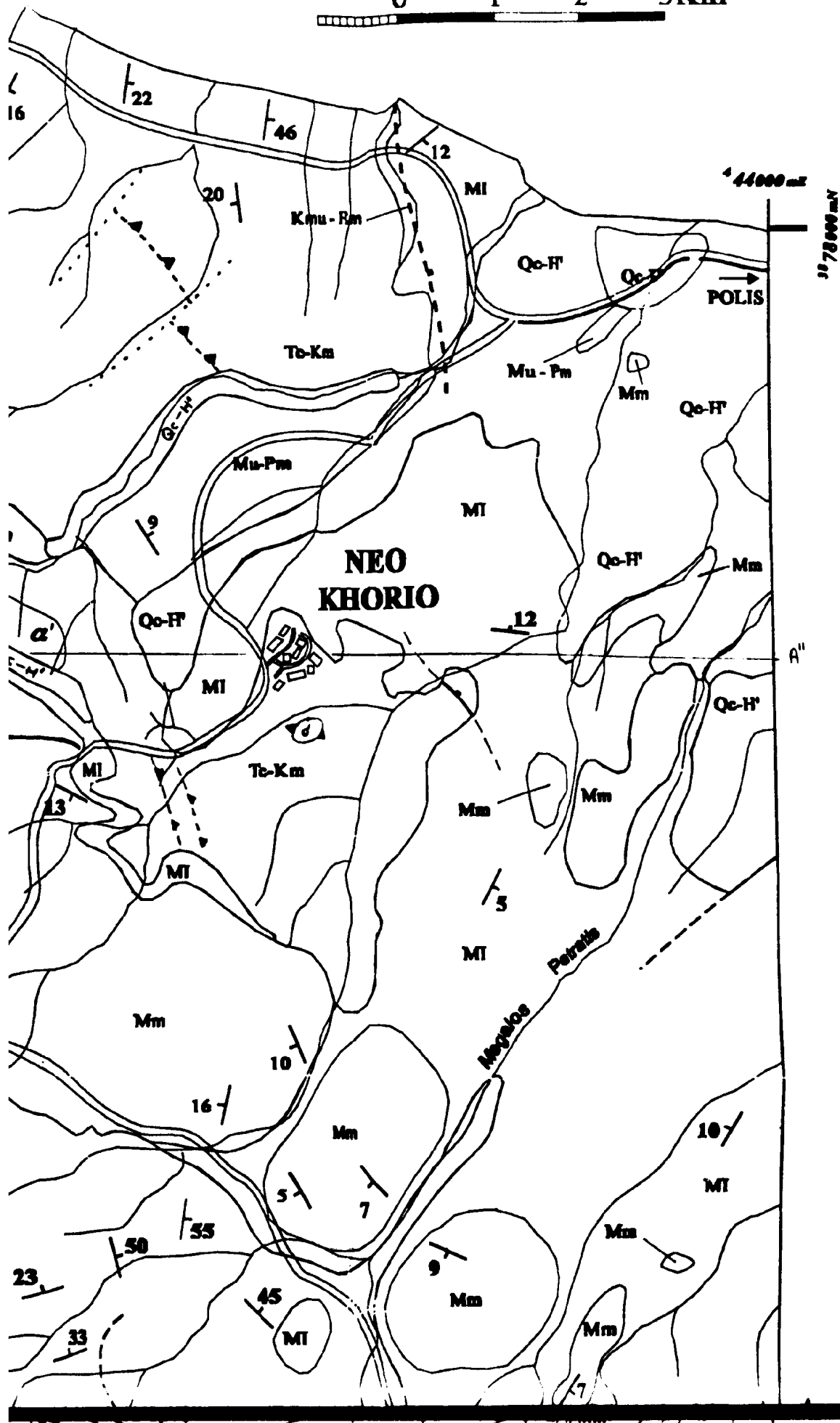








0 1 2 3Km



CALABRIAN

UPPER PLIOCENE

MIDDLE PLIOCENE

LOWER PLIOCENE

UPPER MIOCENE

MIDDLE MIOCENE

LOWER MIOCENE

MIDDLE EOCENE

LOWER EOCENE

PL

PLIOCENE

MIOCENE

EOCENE

Marls, sandy marls and conglomerates

Green-grey marl, sandy marl with thin limestone beds and two metre thick beds of conglomerate.

Calcarenites with basal conglomerates

Coarse conglomerates at the base contain both igneous and sedimentary clasts and are overlain by calcarenites with some intraformational conglomerates or thin marly interbeds.

Marls, calcarenite, chalk and conglomerate

Grey to green-grey and buff-coloured marls in places interbedded with gypsum, calcarenites or white chalk. Fluvio marine conglomerates are up to 70m thick.

Pachna Formation

Chalks with thin-bedded chalk-pebble conglomerates, marls and reef limestone (Koronia Limestone Member) and calcarenites.

Tera Limestone

Calcareous conglomerates, foraminiferous limestone with terrigenous detritus derived from Mameia lithologies; chalks and limestone breccias and limestones.

Leftara Chalks

Middle Leftara of Middle Eocene age : white chert-bearing thin bedded pelagic chalk, local thin-bedded grey crystalline limestones. Few thin beds of tephra. Lower Leftara of Late Maastrichtian age : thin- to medium bedded white chalk with thin greyish silty interbeds. Rare conchoidally fractured, fissile beds of siliceous shale and chert.

CARNIAN

MAASTRICHTIAN

TURONIAN

tan-grey and buff-coloured marls in places interbedded with calcarenites or white chalk. Fluvio marine conglomerates are thick.

th thin-bedded chalk-pebble conglomerates, marls and
tone (Koronia Limestone Member) and calcarenites.

as conglomerates, foraminiferal limestone with terrigenous
derived from Miocene lithologies; chalks and limestone
and limestones.

Lithars of Middle Eocene age : white chert-bearing thin bedded
chalk, local thin-bedded gray crystalline limestone. Few G.
ophra. Lower Lithars of Late Maastrichtian age : thin- to medium-
bedded, fossiliferous, micaceous, slightly conchoidal.

Petra ton Romieu Limestone

Partially recrystallized reefoidal limestone and limestone breccia occurring as large mappable blocks in Mamonia Melange.

Te

AUTOCHTHONOUS (?) ROCKS

Kannavien Formation

Bentonitic clays interbedded with off-white volcanoclastic sandstones.

Km'

Upper Lava Series

Olivine-phyric and aphyric pillow lavas and minor sheet flows.

ULS

Lower Lava Series

Plagioclase- and pyroxene-phyric pillow lavas and sheet flows.

LLS

Basal Group

Greater than 50% diabase dykes with screens of lower lava series.

BG

a) Sheeted Dyke Complex, b) Diabase Dykes

- a) 100% diabase dykes with characteristic dyke-in-dyke intrusions.
- b) Individual diabase dykes, with dip in degrees.

Db

72

a

b

a) Gabbro, b) Plagiogranite

- a) Varie textured gabbro and locally layered pyroxene gabbro.
- b) Quartz-diorite and plagiogranite, pegmatitic in places.

δ

Y

a

b

Wehrlite

Poikilitic with <1-2cm oikocrysts of clinopyroxene including <1mm chadacrysts of olivine. Minor intercumulate plagioclase.

W

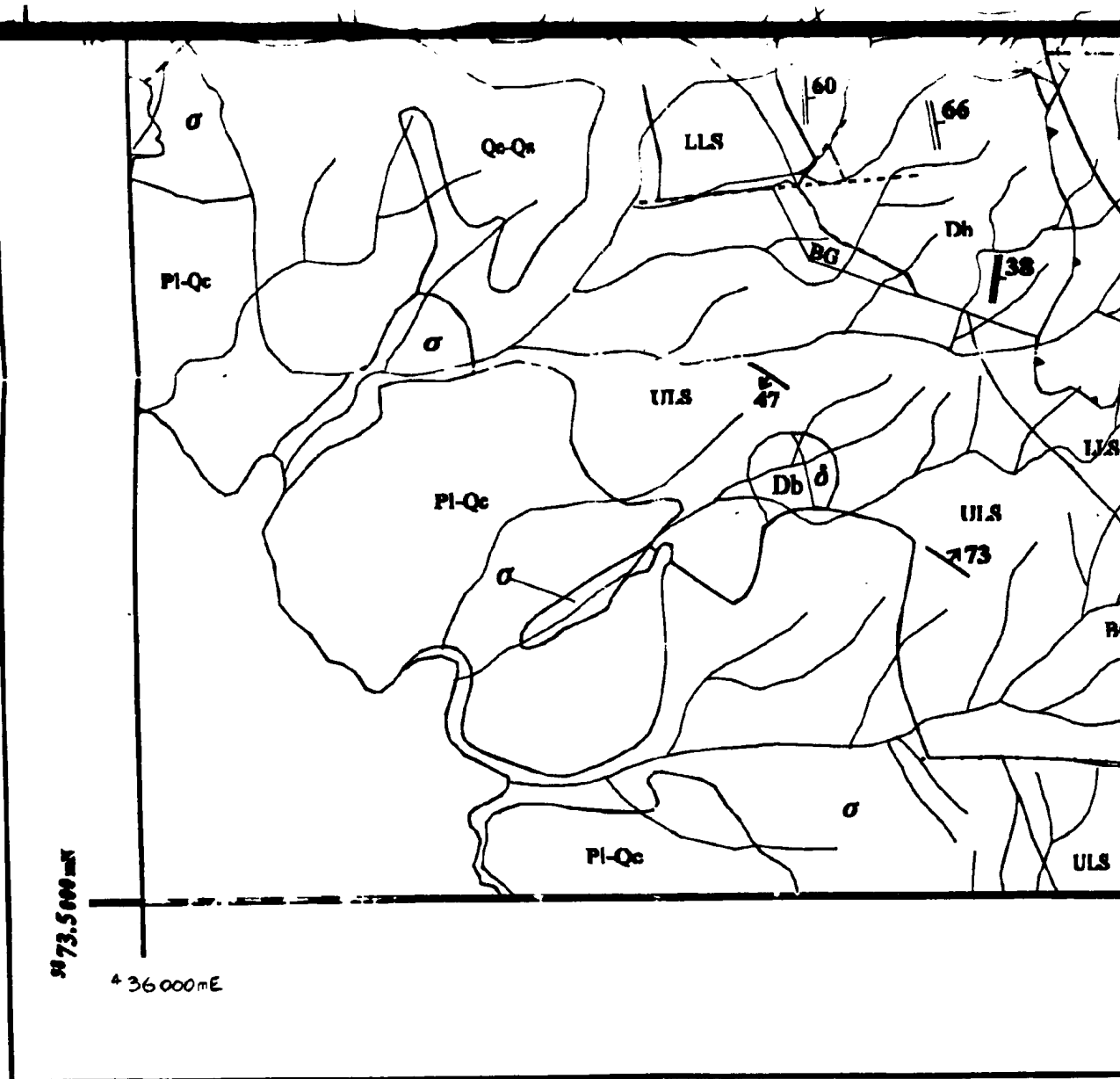
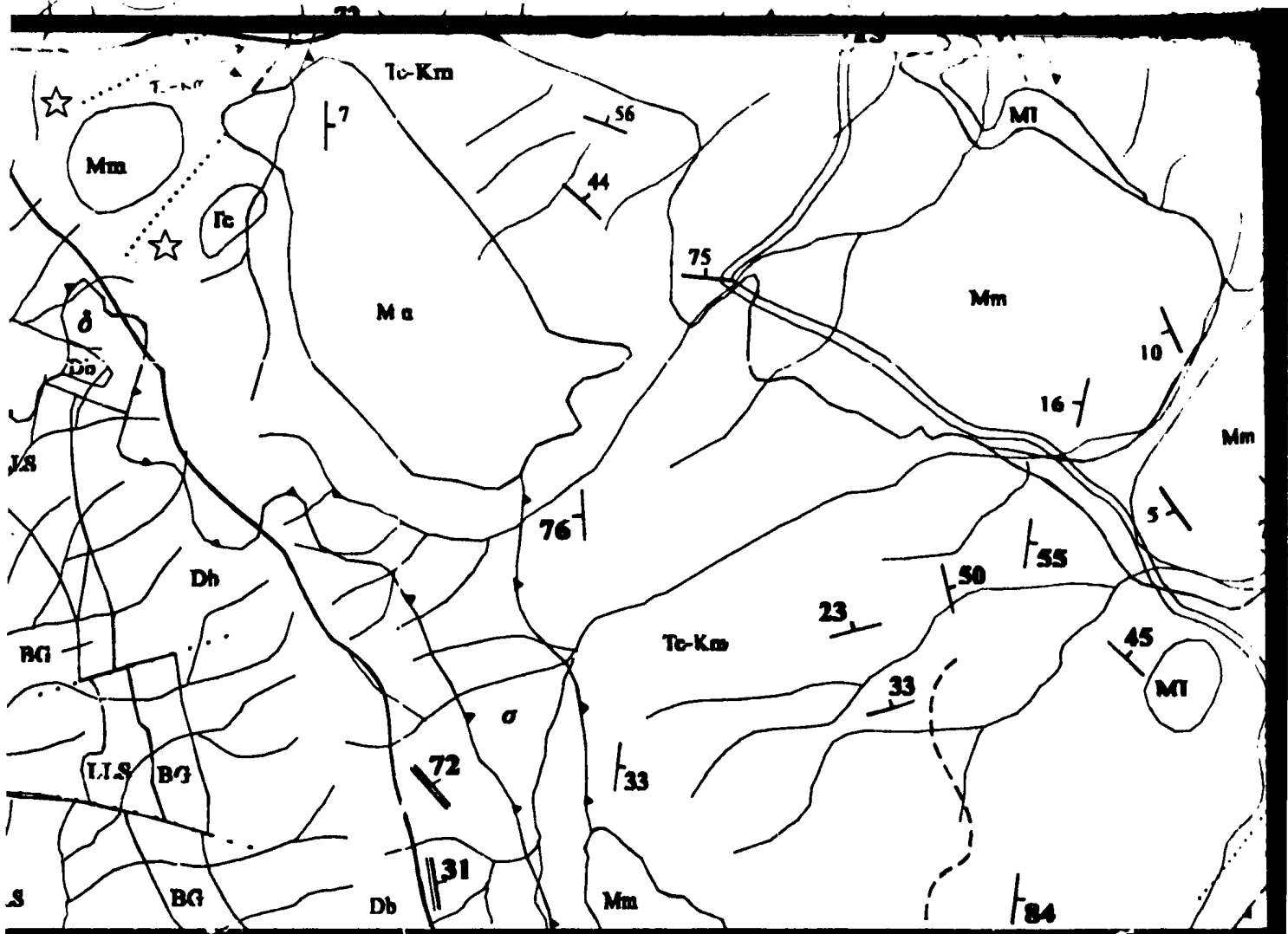
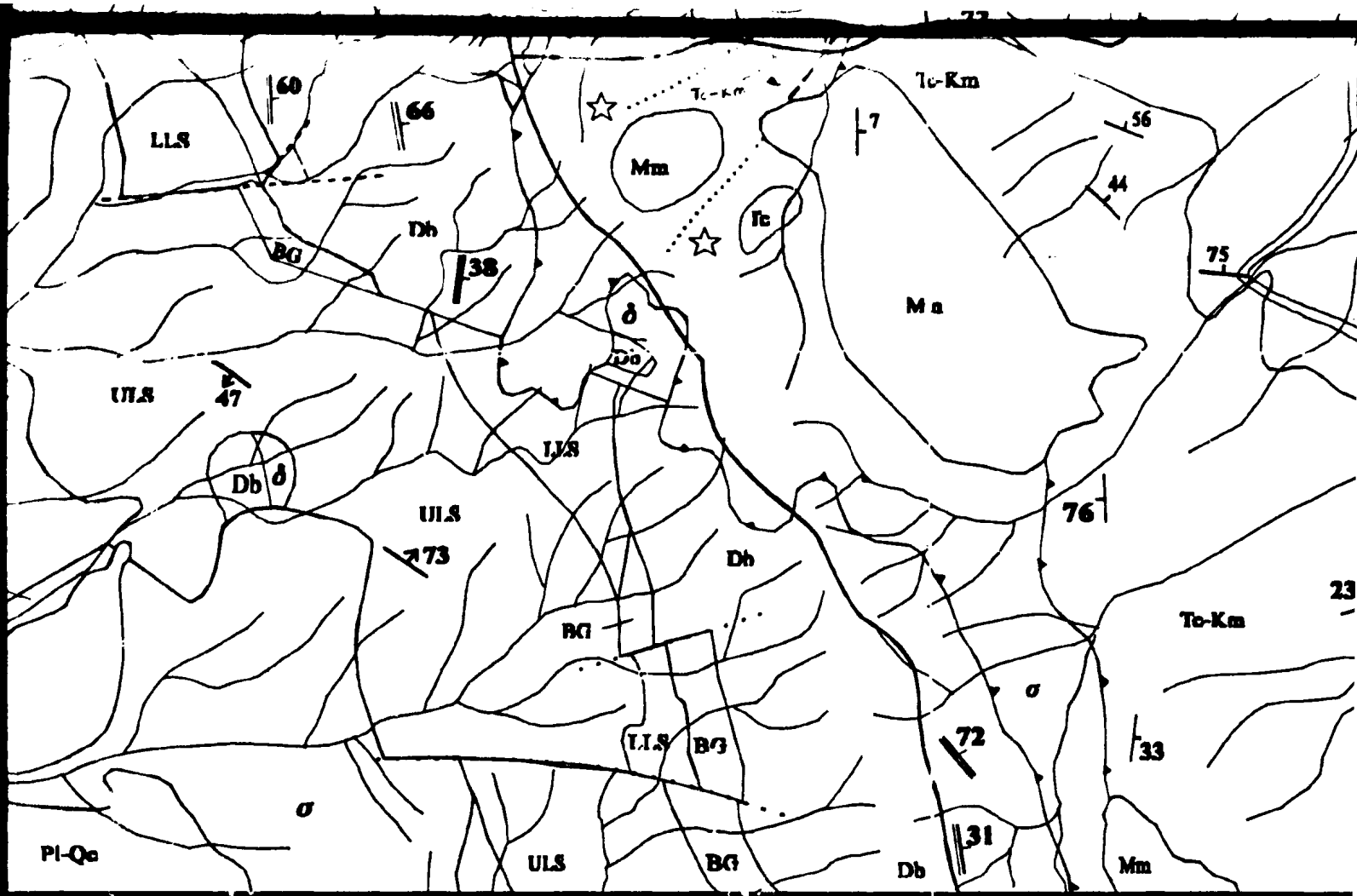
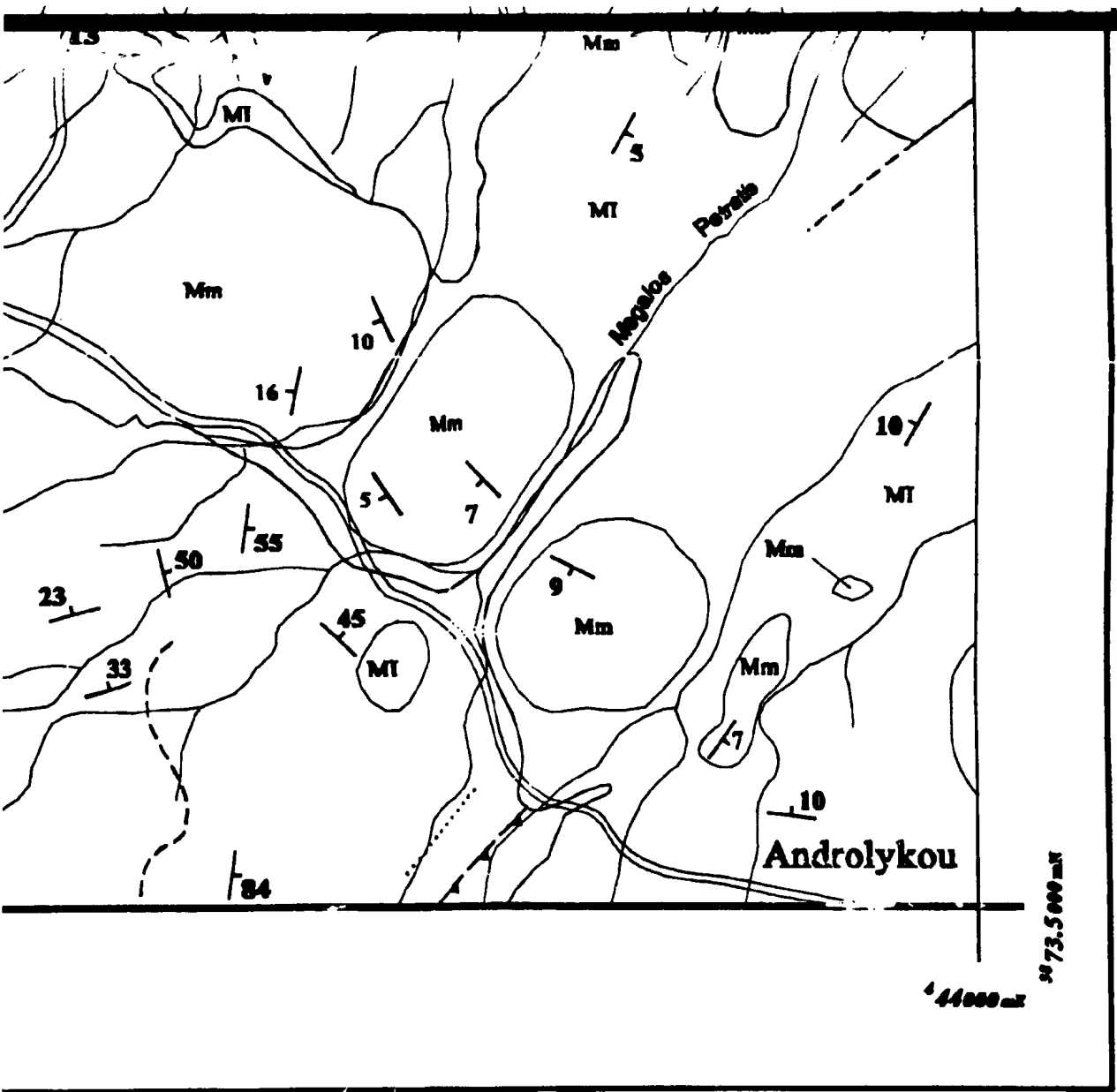
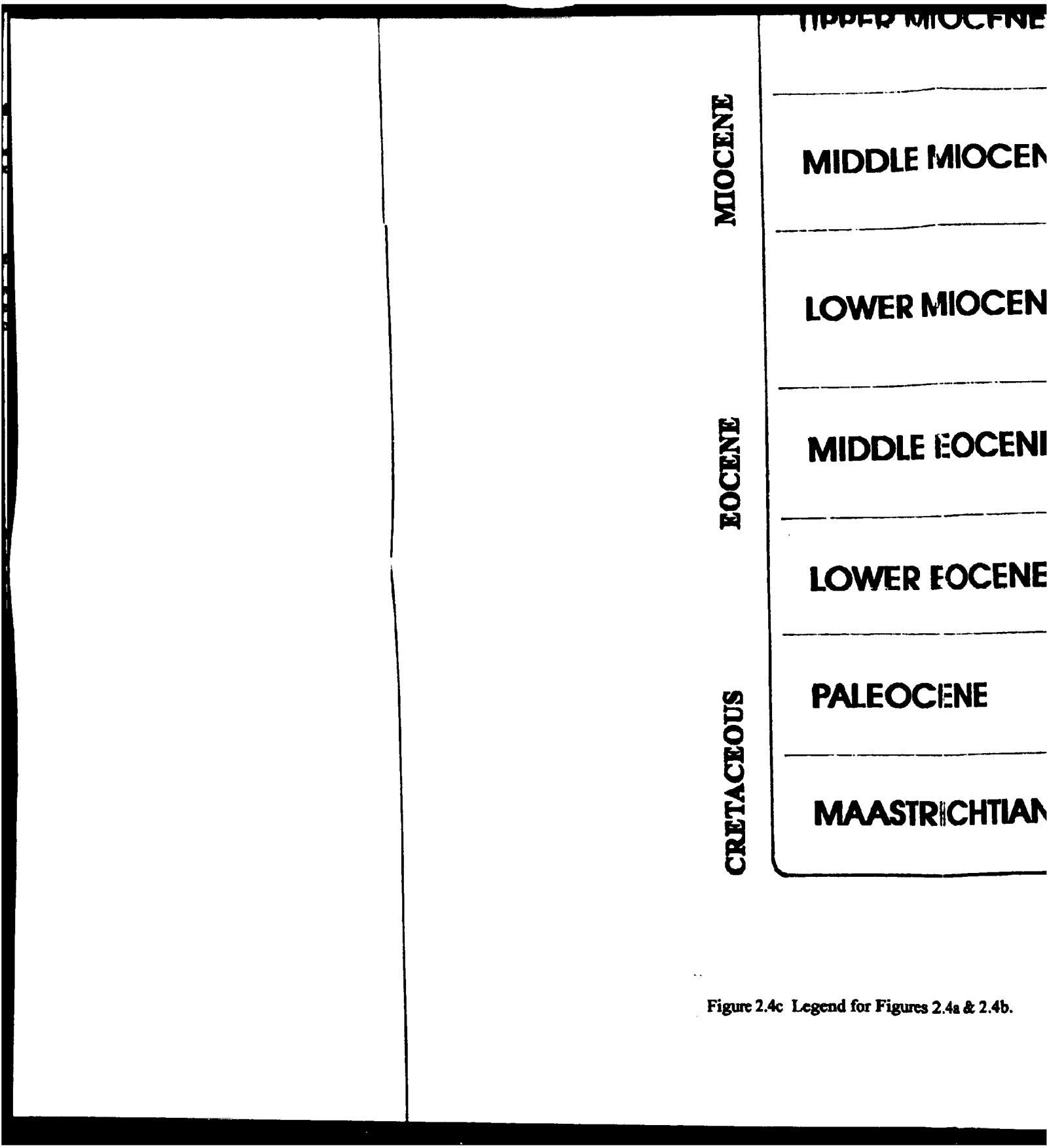


Figure 2.4a Geological map of the Akamas area.









MIOCENE

EOCENE

CRETACEOUS

UPPER MIOCENE

MIDDLE MIOCENE

LOWER MIOCENE

MIDDLE EOCENE

LOWER EOCENE

PALEOCENE

MAASTRICHTIAN

Figure 2.4c Legend for Figures 2.4a & 2.4b.

JE

Mm

Pachna Formation

Chalks with thin-bedded chalk-pebble conglomerates, marls and reef limestone (Koronia Limestone Member) and calcarenites.

E

MI

Tera Limestone

Calcareous conglomerates, foraminiferiferous limestone with terrigenous detritus derived from Mamonía lithologies; chalks and limestone breccias and limestones.

E

Kmu - Em

Leftara Chalks

Middle Leftara of Middle Eocene age : white chert-bearing thin bedded pelagic chalk, local thin-bedded grey crystalline limestone. Few thin beds of tephra. Lower Leftara of Late Maastrichtian age : thin- to medium-bedded white chalk with thin greyish silty interbeds. Rare conchoidal fractured, fissile beds of siliceous shale and chert.

I

Km

Kathikas Melange

Variably coloured, poorly sorted conglomerates with angular clasts up to boulder size in a sand and clay matrix. Most clasts are derived from the Mamonía Melange, but a smaller fraction are of ophiolite lithologies.

tion

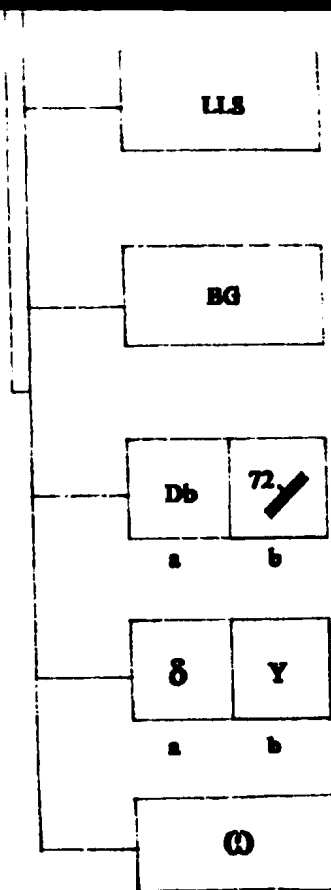
bedded chalk-pebble conglomerates, marls and
lonia Limestone Member) and calcarenites.

horates, foraminiferous limestone with terrigenous
in Mamonia lithologies; chalks and limestone
ones.

Middle Eocene age : white chert-bearing thin bedded
thin-bedded grey crystalline limestone. Few thin-
bedded Lofkara of Late Maastrichtian age : thin- to medium-
bedded with thin greyish silty interbeds. Rare conchoidally
bedded of siliceous shale and chert.

ange

poorly sorted conglomerate with angular clasts up to
sand and clay matrix. Most clasts are derived from
Maastrichtian, but a smaller fraction are of ophiolite lithologies.



Lower Lava Series

Plagioclase- and pyroxene-phyric pillow lavas and sheet flows.

Basal Group

Greater than 50% diabase dykes with saccos of lower lava series.

a) Sheeted Dyke Complex, b) Diabase Dykes

a) 100% diabase dykes with characteristic dyke-in-dyke intrusions,
b) Individual diabase dykes, with dip in degrees.

a) Gabbro, b) Plagiogranite

a) Varitextured gabbro and locally layered pyroxene gabbro,
b) Quartz-diorite and plagiogranite, pegmatite in places.

Wehrlite

Poikilitic with ≤ 2 cm oikocrysts of clinopyroxene including < 1 mm oikocrysts of olivine. Minor intercumulate plagioclase.

Legend text taken from Malpas and Xenophontos (1992).

